Construction and Testing of An Efficient Biophotonic Imaging (BPI) Reporter System to Study Pneumococcal Biology *In Vitro* and *In Vivo*

Thesis submitted for the degree of

Doctor of Philosophy

at the University of Leicester

by

Nada Alkhorayef

Department of Respiratory Science

University of Leicester

February 2021

Abstract

Streptococcus pneumoniae is a common nasopharyngeal resident in healthy persons, but it remains a major cause of pneumonia, bacteraemia and otitis media despite vaccines and effective antibiotics. There is an urgent need for novel therapeutic approaches, but such advances require a detailed knowledge of *S. pneumoniae* biology. To better understand pneumococcal biology and infections, we need sensitive *in vivo* imaging technologies. To this end, bioluminescence imaging can be used, for example, to evaluate anti-infectives, intraspecies interactions and pneumococcal virulence non-invasively. Pneumococcal strains containing click beetle luciferase (CBRluc) under the control of putative highly expressed pneumococcal promoters were constructed. The CBRluc constructs were integrated into known sites in the *S. pneumoniae* genome. The bioluminescent strains were compared to a *lux*-based system expressing bacterial luciferase using *in vitro* growth experiments and *in vivo* mouse model of pneumonia. The results revealed that CBRluc tagged bacteria showed robust activity of bioluminescence in exponential phase that is also maintained during stationary phase, whereas *lux*-expressing pneumococci emitted a light signal with high background that peaked during exponential phase and was significantly reduced in intensity during stationary phase. The presence of CBRluc did not affect the growth and virulence properties of the bioluminescent pneumococcal strains. *In vivo* bioluminescence activity obtained with CBRluc labelled bacteria was much higher than the *lux* containing strain under different promoters. This study also established that CBRluc reporter system can be used to study pneumococcal virulence in *G. mellonella* model.

The findings demonstrate that the CBRluc reporter system is more efficient than *lux*, providing a potential platform for utilization in understanding of the mechanisms of pneumococcal pathogenesis *in vivo*.

Acknowledgments

All praise and thanks to Allah who has helped me to achieve this work. Deep thanks go to my supervisors Prof. Hasan Yesilkaya, as well as to Prof. Peter Andrew, for their outstanding support and patience during the project. Great appreciation is due to my husband, Yousef Alsawi, my mother, Jawhara Alkhudairi, and my brother, Abdullah Alkorayef, for their enormous love and encouragement and for enabling me to study by dealing with family responsibilities for me. All regards and blessings to the lab team for their assistance during the lab work.

Although I cannot directly address my father, I will always remember and appreciate him. Finally, and most importantly, I would like to offer profound thanks to the best people in my life, my brothers, and sisters, for all their unconditional support.

Abbreviations

DNA Deoxyribonucleic acid
BHI Brain heart infusion
RNA Ribonucleic acid
bp Base pair
EDTA Ethylene diamine tetra acetic acid
CFU Colony Forming Unit
OD optical density
BHI Brain Heart Infusion
CDM Chemically Defined Medium
PBS Phosphate Buffered Saline
IVIS In Vivo Imaging System
BLI Bioluminescence imaging
BPI Biphotonic Imaging
RLU Relative Light Unit
CBRluc Click Beetle Red Luciferase
ATP Adenosine triphosphate
FMN Flavin Mononucleotide
µl Microliter
ml millilitre
mM millimolar
v/ v volume per volume
w/ v weight per volume

Table of Contents

Chapter 1. Introduction

1.1. *Streptococcus pneumoniae* characteristics

Streptococcus pneumoniae, known as pneumococcus, is a Gram positive aero-tolerant anaerobic bacterium, with lancet-shaped cocci; it is non-motile, non-spore forming and demonstrates α-haemolysis on blood agar by producing a green zone indicating incomplete haemolysis (Arbique et al., 2004). This green zone surrounding *S. pneumoniae* colonies results from the breakdown of haemoglobin by pneumolysin (Arbique et al., 2004). Pneumococcal cells are between 1 and 2 micrometres in diameter and grow optimally at 37 °C at a pH of 6.5 to 7.5. Horse blood is typically used in media preparation, and media containing a source of catalase are necessary for the growth of *S. pneumoniae* because it lacks this inherently (Taniai et al., 2008). More than 90 serotypes, based on varying polysaccharide capsules, have been identified, with fewer than 30 of these being observed to be virulent to humans (Cooper et al., 2011, Henrichsen, 1995).

The pneumococcus is distinguished from other streptococci by its ethyl hydrocupreine hydrochloride (optochin) sensitivity and bile (deoxycholic acid) solubility in 5% CO2. Carbon dioxide-rich environments may, however, lead to misidentification (Gardam and Miller, 1998). Although the emergence of resistant isolates to optochin have been reported in various geographical regions, this test remains a widely used tool for routine laboratory diagnostics (Marín et al., 2017). An agglutination test with capsular-specific antibodies is also frequently used to distinguish *S. pneumoniae*, although such tests may give negative results for pneumococcal cells without capsules (Arbique et al., 2004). Some studies have suggested the use of DNA-based differentiation methods to isolate pneumococcus from other streptococci, such as sequencing part of the *16S rRNA* gene or examination of the existence of pneumolysin gene, which is believed to act as a pneumococcal virulence factor (McAvin et al., 2001). These tests have, however, been reported to be ineffective due to the presence of the *ply* gene in other streptococci such as *S. mitis* and *S. oralis* and the resulting similarities in 16S rRNA sequencing between these groups and *S. pneumoniae* (Leegaard et al., 2010, Arbique et al., 2004). Although there are limitations to pneumococcal detection, pure isolation of pneumococci is not always required for clinical diagnostic work; however, it is extremely useful for

epidemiological studies seeking to formulate vaccine content (Kaltoft et al., 2008, Wyllie, 2016).

1.2. Epidemiology of pneumococcal diseases

Pneumococcus generally resides asymptomatically in the nasopharynx in healthy persons. However, it may invade different parts of the body if it gains entry to normally sterile parts of the airways, causing a broad spectrum of infections, particularly among young children, the elderly, and patients with compromised immune systems (JANOFF and RUBINS, 1997). Meningitis and pneumonia are examples of severe pneumococcal diseases caused by this microbe that may lead to high rates of morbidity and mortality (Janoff and Rubins, 2004). In 2000, approximately 14.5 million incidents of serious pneumococcal diseases were reported worldwide, leading to 826 000 deaths in children under the age of 5; most of these deaths were reported in developing countries (O'Brien et al., 2009, Melegaro et al., 2006). *S. pneumoniae* has also been identified as the main pathogen associated with pneumonia (Rudan et al., 2008, O'Brien et al., 2009). In England and Wales, 15,000 episodes of otitis media and nearly 40,000 cases of pneumonia are estimated to occur annually due to *S. pneumoniae* (Melegaro et al., 2006), while based on studies conducted in developing countries between 1969 and 1999, India is estimated to have the greatest number of pneumonia cases among children under 5 worldwide. According to estimates for 2000, Africa had the highest general incidence rate of pneumonia, though the greatest number of cases by country was still seen in India, which recorded 408,000 deaths. Nine further countries from Africa and Southeast Asia rounded out the 10 highest rates of death by country, with numbers ranging between 204,000 in Nigeria to 46,000 deaths in Niger (Rudan et al., 2008).

Increased risk of pneumococcal pneumonia and invasive pneumococcal diseases was generally observed in countries with high rates of HIV infection. The risk of invasive pneumococcal disease in South Africa was also greater in HIV infected persons as compared to in uninfected ones (Nunes et al., 2011). Age, genetic background, and immune status, are other factors associated with the incidence of invasive pneumococcal disease (van der Poll and Opal, 2009). Dworkin et al. (2001) conducted a study on patient data gathered between 1990 and 1998 that aimed identify the factors associated with pneumococcal disease; they found that black people were more at risk of developing pneumococcal disease, though their study did not determine

whether this was due to any form of genetic susceptibility or simply the generally lower socioeconomic status of such persons.

Pneumococcal meningitis is a severe disease, though it is less common than pneumonia; of 14.5 million pneumococcal disease cases in one study, only 0.7% were identified as meningitis (O'Brien et al., 2009). In 2000, Africa was seen to have the highest rate of pneumococcal meningitis cases by continent worldwide (O'Brien et al., 2009). Otitis media (ear infection) and sinusitis are less severe pneumococcal infections that are more common; these occur when pneumococcus spreads locally from the nasopharynx to the ears and sinuses, and *S. pneumoniae* has thus been reported as the most important cause of acute otitis media (Peltola et al., 2006). Generally, although by 2008 deaths among children aged under five had decreased globally, pneumococcal diseases continue to have a significant impact on mortality and morbidity rates (World Health Organization, 2012).

1.3. Prevalence of antimicrobial resistance in *S. pneumoniae* and the prevention of pneumococcal disease

Penicillin from the beta-lactam family (which includes the cephalosporin, carbapenem, and monobactam subfamilies), is the most commonly used drug for the treatment of pneumococcal infections. This treatment targets the enzymes known as penicillin-binding proteins (PBPs). PBPs, which are important for the synthesis of the peptidoglycan cell walls of bacteria, and which can thus be inactivated by antibiotics (Appelbaum, 2002, Hoban et al., 2001). Pneumococcal isolates were sensitive to all known antibiotics until the 1960s, at which time certain clinical isolates in the United States began to show decreased susceptibility to penicillin and several other antibiotics. The rate of resistance has since increased progressively among pneumococcal isolates, from 4.0% in 1980s to more than 25% in the 1990s, reaching 35% by 2002 (Jorgensen et al., 1990, Doern et al., 2005, Doern et al., 1996). The phenomenon of penicillin non-susceptibility had also been reported in other parts of the world by the early 1980s, such as Mexico, Japan, Saudi Arabia, Israel, Spain, France, Greece, Hungary, and the Slovak Republic (Felmingham, 2004). This increasing rate of resistance has been attributed to excessive use of antibiotics, and in Spain, for example, a direct relationship was observed between aminopenicillin consumption and penicillin resistance (Baquero et al., 1991). The emergence of resistance in pneumococcal isolates is commonly due to the development of altered PBPs that have reduced affinity to antibiotics. Acquisition of antimicrobial resistance

among *S. pneumoniae* is thus most likely associated with an exchange of genes from viridans streptococci by transposons (Appelbaum, 2002).

The proportion of penicillin-resistant strains varies by geographic location, with certain countries such as the Netherlands recording no resistance while others such as South Korea, South Africa, Hong Kong, and Taiwan report high percentages, exceeding 50% (Felmingham, 2004, Walsh and Amyes, 2004). In addition to resistance to penicillin, pneumococcal isolates have been reported to be resistant to other antibiotics, including erythromycin, clindamycin, tetracycline and chloramphenicol, all of which are otherwise used for the treatment of penicillin-resistant pneumococcal infections. In the United States, 20% of isolates were resistant to tetracyclines (Jacobs, 2004), while in Spain, 72.5% of 91 isolates recovered from children were tetracycline non-susceptible by the turn of the century (Charpentier and Tuomanen, 2000). Tetracyclines target ribosomal protein synthesis in bacteria, and alteration in the *tetM* gene thus leads to tetracycline resistance among *S. pneumoniae*. This gene also expresses a protein that interferes with inhibition of ribosomal protein synthesis (Appelbaum, 2002). Resistance to the macrolides family, which includes erythromycin, has also been observed globally since the late 1980s. In 1992, 27.5% of pneumococcal isolates were found to be resistant to erythromycin in France (Charpentier and Tuomanen, 2000), while in the United States by 1999, 30.7% of *S. pneumoniae* isolates were resistant to macrolides (Gay et al., 2000).

The emergence and increasing rates of resistance seen in *S. pneumoniae* present serious health threats and complicate the treatment of disease. Effective approaches to controlling pneumococcal disease have thus come to depend on more preventive strategies, such as vaccination. Vaccines have thus far been successful in reducing rates of pneumococcal diseases (Jacobs et al., 2008), and two main pneumococcal vaccines are available: the 23-valent-pneumococcal-polysaccharide vaccine (PPV 23) and the protein conjugated pneumococcal vaccine. The PPV 23 vaccine is composed of free capsular polysaccharides of the 23 most dominant serotypes among clinical isolates of *S. pneumoniae*, which cause 88% of cases of related invasive disease in adults (Jacobs et al., 2008). The efficacy of this vaccine is approximately 65% in terms of preventing invasive diseases in adults (Jacobs et al., 2008, Cadeddu et al., 2012); however, the limitations of this vaccine include a lack of protection against common upper respiratory diseases such as acute otitis media and sinusitis, and its lack of impact on pneumococcal carriage (Schrag et al., 2001). As such vaccines provoke T-cell-independent immune responses, they are also poor inducers of immunologic memory and, of

particular concern, this vaccine does not provide sufficient protection in children under 2 years of age, despite this group being most vulnerable to pneumococcal infection due to their immature immune systems that do not respond to PPV 23 (Cadeddu et al., 2012). Protein conjugated vaccines such as the heptavalent pneumococcal conjugate vaccine (PCV-7), which was introduced into the UK in 2002, are thus recommended for children under 2 years old. The protein conjugated vaccine contains capsular polysaccharides with a protein carrier: the presence of the protein stimulates a stronger immune response, as proteins can elicit T-cell dependent responses alongside the establishment of B-cell memory, thus facilitating the creation of immunological memory (Hayward et al., 2016, Golos et al., 2016). The PCV-7 thus provided protection against invasive pneumococcal disease caused by seven common serotypes, (4, 6B, 9V, 14, 18C, 19F, and 23F), some of which are paediatric serotypes, in a manner not found in 23 PPV (Balmer et al., 2007, Schrag et al., 2001). PCV-7 was replaced in 2010 by PCV 13, which targets a further six serotypes (Alari et al., 2016). The disadvantages of these vaccines include lower coverage of each pneumococcal serotype within the vaccine formulation, however, and although these conjugate vaccines have had an impact in preventing invasive pneumococcal disease, an increase in the carriage of non-vaccine serotypes has been observed in Gambia (Obaro, 1996). More effective new vaccines that can provide wider serotype coverage are thus required. However, generating wider serotype coverage increases the cost of preparation and thus the cost of such vaccines is likely to be higher (Schrag et al., 2001). Efficient technologies to study and understand the mechanisms of pneumococcal pathogens are therefore required to help develop and produce relatively inexpensive and effective vaccines.

1.4. Pneumococcal Colonisation

Transmission of *S. pneumoniae* occurs via respiratory droplets passing from persons carrying this bacteria in their upper respiratory tract (Kadioglu et al., 2008). The nasopharynx is colonised during the first months of life by multiple microorganisms, including *S. pneumoniae*, *Haemophilus influenzae*, *Neisseria meningitides*, and *Staphylococcus aureus* (Bogaert et al., 2004a), and although colonisation of the nasopharynx is generally asymptomatic, in some cases it can progress to the respiratory tract and thus trigger an array of systematic diseases. The factors effecting the transition from pneumococcal carriage to invasive disease are not completely understood; however, age and immune status are believed to pay major roles in this

process (Bogaert et al., 2004a). Pneumococcus can cause pneumonia when it spreads to the low respiratory tract; in addition, it can cause otitis media due to triggering inflammation of the middle ear (Weiser et al., 2018). The microbe can also invade the bloodstream, causing bacteraemia, or infects the tissues and fluids surrounding the brain and spinal cord, leading to meningitis (Weiser et al., 2018). Colonisation is thus a prerequisite for both transmission to new hosts and the precipitation of invasive disease in the carrier (Figure 1.1). Airway colonisers must avoid host challenges, penetrate into the mucous barrier, and obtain nutrients (Bogaert et al., 2004a). These challenges are summarised in the steps of colonisation, which include adherence to the nasopharynx (the epithelial lining), interaction with the nasopharyngeal microbiota, and evasion of the host immune system.

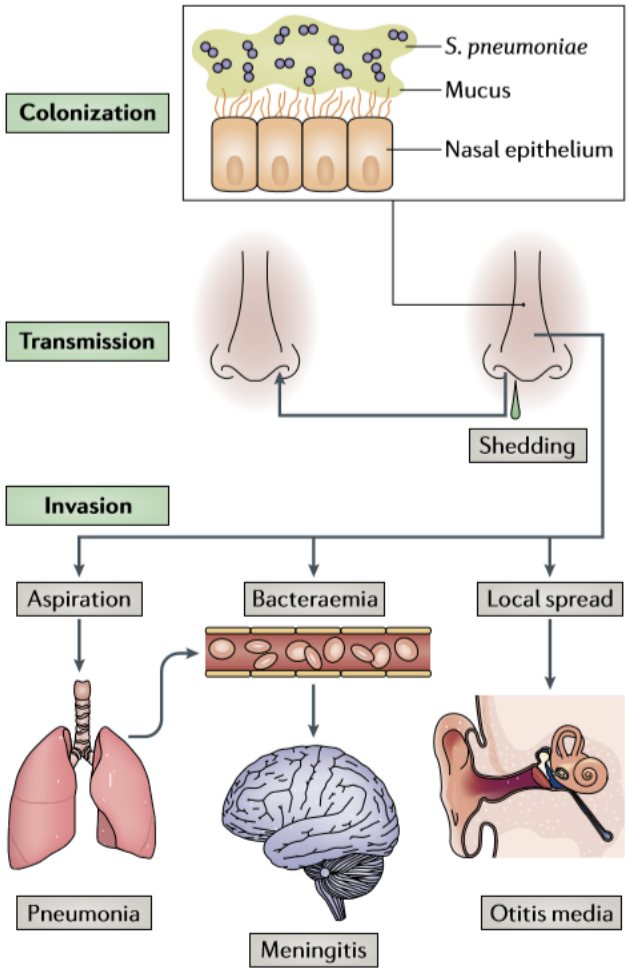

Figure 1.1. Pathogenesis of *Streptococcus pneumoniae*. The diagram illustrates the dissemination of pneumococci through the host tissues. The microbe begins by colonising the nasopharynx, as this is an initial step for both transmission to new hosts via nasal secretions and the triggering of invasive disease in the carrier. Pneumococcus can then spread beyond the

nasal epithelium by aspiration, bacteraemia, or local spread, causing inflammatory diseases such as otitis media or invasive disease such as meningitis and pneumonia (Weiser et al., 2018).

1.4.1. Adherence to the nasopharynx

Establishing stable adherence to the mucosal surfaces of the upper respiratory tract (Fahy and Dickey, 2010) is required for the establishment of effective colonisation. This is achieved by avoiding mucosal clearance, which is the first layer of defence in the nasopharynx. A 0.5 to 10 μm thick mucus layer covers the ciliated epithelial cells in the nasopharynx. The principal constituent of this mucus is a glycoprotein known as mucin, which is secreted by the goblet cells present within the epithelial layer, and which contains antimicrobial peptides and immunoglobulins (Fahy and Dickey, 2010). These features are facilitated by the negatively charged N-acetylneuraminic acid (sialic acid) found at the terminal end of the polysaccharide chains within the mucin molecules and sialic acid that bind to particles that are positively charged, such as standard bacteria, preventing them from passing the mucosal barrier and facilitating mucociliary clearance (Fahy and Dickey, 2010, Weiser et al., 2018). To overcome this barrier, *S. pneumoniae* produces negatively charged capsular polysaccharides to increase adherence to epithelial cells and help establish colonisation. *S. pneumoniae* also produces exoglycosidases such as a neuraminidase, known as NanA, and a β-galactosidase, BgaA. These enzymes further facilitate adherence and minimise the viscosity of the mucus by cleaving sialic acid residues, thus providing receptors for adherence and a carbon source for pneumococcal growth (Short and Diavatopoulos, 2015). After these encapsulated polysaccharides have facilitated escape from the mucosal barrier, however, the pneumococcus rapidly reduces encapsulation once it is covalently attached. Hammerschmidt et al. (2005) recovered invasive pneumococci from epithelial cells and visualised these using electron microscopy to observe this loss of capsular polysaccharides in pneumococcus recovered from such cells. This has been attributed to attempts at evasion of anticapsular immune responses, and probably enhances the adherence of pneumococcus to host receptors on epithelial cells. The ability to invade epithelial cells can thus be seen as the initial phase of invasive disease.

The pneumococcus produces several other molecules to encourage adhesion. Pneumococcal choline binding proteins, such as CbpA (also known as PspC), bind to the human secretory components of IgA and interact with the complement pathway, thus interfering with the host immune response and enhancing pneumococcal adhesion to host epithelia (Weiser et al., 2018).

In addition, some pneumococcal strains produce pilus-like structures on the bacterial cell surface, which facilitate adherence to epithelial cells, promoting colonisation of the nasopharynx (Barocchi et al., 2006). The pneumococcus frequently colonises asymptomatically in hosts with healthy immune systems, though poor mucosal immune response can facilitate persistent colonisation, which may then lead to infection. The effectiveness of the immune system is linked to age, and infants and the elderly are at high risk of contracting pneumococcal diseases due to their weaker immune systems. The incidence of pneumococcal colonisation was observed to be particularly high among children under 3 years old, with colonisation rates then declining to 8% among 10 year olds (Bogaert et al., 2004a), which may at least partially explain the high incidence of deaths among children younger than 5 due to pneumococcal disease.

1.4.2. Interactions with nasopharyngeal microbiota

Once it has established a stable presence on the mucosal surface, *S. pneumoniae* must compete for resources such as nutrients and space with other colonising microbiota. This interaction may be cooperative or competitive and may occur with other colonising bacterial species or with different serotypes of *S. pneumoniae*. A mouse model of *S. pneumoniae* intranasal carriage showed that mice colonised with a serotype 6B strain as a resident strain experienced reduced colonisation by a 23F strain prone to "super-colonisation" when challenged intranasally (Lipsitch et al., 2000), suggesting that normal flora can affect novel pneumococcal colonisation. Colonisation of the nasopharynx by *Haemophilus influenzae*, *Staphylococcus aureus*, and *S. pneumoniae* was also shown to be disrupted by various α-haemolytic streptococci (Ghaffar et al., 1999). The association of pneumococcal colonisation with colonisation by other bacterial species was investigated in children in Botswana, and children colonised with *S. pneumoniae* demonstrated substantial alterations in nasopharyngeal microbial composition (Kelly et al., 2017). It was also observed that changes in the nasopharyngeal microbiota (*Staphylococcus* and *Corynebacterium*), and lower relative abundances of *Corynebacterium* and *Staphylococcus* in children colonised with *S. pneumoniae*, could be attributed to the actions of hydrogen peroxide as produced by *S. pneumoniae* (Kelly et al., 2017). Pneumococcus produces a large amount of hydrogen peroxide as a by-product of

its pyruvate metabolism, and while pneumococcus can tolerate high peroxide production, many other colonising bacteria cannot, providing a competitive advantage for the pneumococcus.

Co-infection with a respiratory virus can also affect *S. pneumoniae* loads positively. Infection with an influenza virus in particular can facilitate the adherence of *S. pneumoniae,* as the neuraminidase activity of such viruses damages the epithelial cell layer within the respiratory tract, leading to greater exposure of receptors to pneumococcal adherence (Short and Diavatopoulos, 2015).

1.4.3. Evasion of the host immune system.

Following acquisition and colonisation, *S. pneumoniae* must continue to evade the host immune system to spread within the tissues of susceptible hosts. Encapsulation is well known for its role in limiting opsonisation by complements and antibodies; it also contributes to the evasion of mucus mediated clearance (Roche et al., 2014). *S. pneumoniae* has developed further mechanisms to minimise the effectiveness of host humoral response on mucosal surfaces, however, such as the production of zinc metalloprotease, ZmpA (also known as IgA1 protease). This protease is produced by bacteria specific to human immunoglobulin A (IgA), and IgA1 protease may interfere with host immunity on the mucosal surfaces that cover the upper respiratory tract by eliminating the agglutinating activity of human immunoglobulin A (Roche et al., 2014). This occurs by means of the cleavage of opsonising IgA, which leads to a change in bacterium surface charge that increases the likelihood of interaction between pneumococcal cell-wall choline and platelet-activating factor receptors.

C-reactive protein (CRP) is another host defence factor that interacts with the opsonisation activity of the complement. The concentration of this protein is elevated in response to infection and inflammation, and CRP then binds to cell-surface phosphorylcholine (ChoP), blocking the adherence of bacteria to epithelial cells and minimising bacterial colonisation (Gould and Weiser, 2002). Phosphorylcholine (ChoP) on bacterial surfaces (teichoic acid) mimics host platelet-activating factor (PAF) and allows binding to a major epithelial receptor (rPAF). This mechanism increases adherence and invasion of host epithelial cells; the molecular mimicry of PAF has thus been proposed as a factor promoting colonisation (Kadioglu et al., 2008).

The toll-like receptor 2 (TlR2) is another host factor required for the effective clearance of *S. pneumoniae*, being a major mammalian TLR that can recognise lipoproteins derived from bacteria and other organisms (Weiser et al., 2018). Another factor that greatly accelerates cellular immune responses to *S. pneumoniae* is the pore-forming cytotoxin pneumolysin, Ply; however, although this mechanism may contribute to activation of the complement system, enhancing pneumococcal clearance, it has recently been suggested that the expression of pneumococcal Ply might contribute to depletion of the complement component, minimising the binding of the complement to bacteria (Andre et al., 2017).

1.5. Pneumococcal virulence determinants

In order to evade complement attack, pneumococcus has developed multiple virulence factors that contribute to complement resistance and thus to phagocytosis. Major pneumococcal virulence factors include pneumococcal encapsulation, pneumolysin, and pneumococcal cell-surface proteins (Kadioglu et al., 2008, Andre et al., 2017). A combination of all these factors is required for the virulence of *S. pneumoniae* during an infection to increase significantly.

The pneumococcal polysaccharide capsule (CPS) is around 200 to 400 nm thick, and it plays a significant role in determining virulence levels during infection. More than 90 serotypes of *S. pneumoniae* have also been identified based on the chemical components of their capsules (Cooper et al., 2011). The thickness of the polysaccharide capsule is the main factor controlling the anti-phagocytic properties of *S. pneumoniae*, and a lack of capsule reduces virulence, as observed in pneumococcal mutants. In addition, the capacity to cause invasive disease varies depending on the capsular serotype (Hyams et al., 2010). This effect of encapsulation on virulence is believed to be related to the inhibition of the complement system in the host, which results in resistance to phagocytosis in pneumococcus (Hyams et al., 2010).

A further factor affecting pneumococcal virulence is pneumolysin, which contributes to virulence due to its ability to interact with the complement system, limiting complement clearance. Other functions have also been attributed to pneumolysin, such as a contribution to the cytolytic properties of pneumococcus, which leads to pore formation in different cells (Andre et al., 2017). The neuronal damage caused by apoptosis has also been associated with

the pneumococcal production of pneumolysin, and this leads to neuronal cell death in the central nervous system (Tuomanen, 1996).

Pneumococcal cell-surface proteins are classified into three groups: lipoproteins, choline-binding proteins, and proteins that bind covalently to the peptidoglycan of pneumococcus. More than 40 lipoproteins have been identified and described, such as pneumococcal iron acquisition A (PiaA), pneumococcal iron uptake A (PiuA), and pneumococcal surface adhesin A (PsaA), all of which have been shown to be implicated in pneumococcal virulence. PiuA and PiaA are reported to have importance in murine systemic infection, and immunisation of mice with recombinant PiuA and PiaA conferred immunity towards systemic challenges with *S. pneumoniae.* Further, PiuA and PiaA may take on a role in iron uptake, as culturing the bacteria in media without iron resulted in a reduction in growth and virulence (Brown et al., 2001). Mutation, as in *psaA,* can result in failure of pneumococcal adherence to host cells *in vitro*, which highlights the significance of PsaA in pneumococcal virulence. The role of PsaA in manganese uptake was also observed, withe *psaA* mutants requiring additional manganese to support a standard growth rate (Dintilhac et al., 1997).
Ten to fifteen choline-binding proteins have been identified in pneumococcus, including PspA and PspC (Kadioglu et al., 2008). It has also been suggested that PspA should be included in vaccines, as antibodies against PspA provide protective immunity against various serotypes. Its role in minimising complement activity appears to be most likely due to its inhibition of the binding of CRP to the phosphocholine moieties on the pneumococcal surface. The PspA mutant improves the pneumococcal surface binding for CRP (Mukerji et al., 2012) as compared to the wild type, PspC mutant, which showed reduced adherence to the target cells *in vitro*, highlighting its function as a virulence factor. PspC, also known as CbpA and SpsA, has the ability to bind to secretory components such as IgA, an action which limits the opsonization of macrophages and aids in microbial adherence. PspC can also bind to factor H (Al-Bayati et al., 2017), a complement control protein that helps microbes to evade the host immune response (Dave et al., 2004).

LPXTG-containing anchored proteins are the final group of pneumococcal cell-surface proteins, and these are covalently anchored to the pneumococcal cell wall by sortase enzymes. LPXTG-containing proteins have an N-terminal signal peptide and a conserved C-terminal sorting signal composed of a conserved LPXTG motif (Kadioglu et al., 2008). This motif is required for the attachment of a protein to the pneumococcal cell wall by sortase, as encoded

by the *srtA* gene. Mutation of *srtA* results in reduction in pneumococcal adherence to nasopharyngeal cells *ex vivo*, reflecting the importance of this enzyme in nasopharyngeal colonisation (Paterson and Mitchell, 2006). *S. pneumoniae* is known to express twenty LPXTG motif anchored proteins, including neuraminidases. These enzymes, encoded by *nanA*, *nanB*, and *nanC*, cleave sialic acids from host complex carbohydrates, providing binding receptors for adherence and carbon sources for pneumococcus (Short and Diavatopoulos, 2015). NanA, β-galactosidase (BgaA) and N-acetylglucosaminidas (StrH) have been observed to interact with complement components where such components have multiple glycosylation sites that are important for various functions. The ability of NanA, BgaA, and StrH to facilitate the sequential removal of sugars of host glycoconjugates has also been demonstrated, and they also deglycosylate complement components, thus inhibiting complement activity (Dalia et al., 2010).

Although pneumococcal virulence determinants have been extensively studied, however, these are often selected based on their *in vitro* relevance rather than *in vivo* work. Further, resistance to penicillin and other antibiotics remains challenging for the treatment of pneumococcal infections, while currently available vaccines are predominantly protective for only the serotypes represented in their formulation (Bogaert et al., 2004b). This leads to an urgent need for a tool that can be used to identify the *S. pneumoniae* genes essential during infection, and thus to determine potential protein vaccine targets *in vivo.*

1.6. Studying the *in vivo* biology of pneumococcus

Studying the biology of pneumococcus *in vivo* has already revealed important information related to the role of pneumococcal proteins in pathogenesis that can be exploited to identify possible targets for treatment or vaccination. Studying *in vivo* gene expression can be achieved by quantitative reverse transcriptase PCR (qRT-PCR) and microarrays, though each approach has its own limitations. Microarrays, for example, offer high throughput analysis, but require high abundance mRNAs for detection and evaluation of gene expression (Fu et al., 2009). Similarly, qRT-PCR attracts high costs and involves recovery of pneumococci from infected tissue for mRNA extraction and cDNA synthesis, thus necessitating many steps that may affect RNA integrity, and expression pattern. The level of bacterial RNA, generally 1%, found in the

background of host RNA means that the yield of bacterial RNA extracted from the infected tissues is often very low, while reverse transcriptase introduces biases due to template switching and primer-independent cDNA synthesis (Wang et al., 2009).

Nanostring nCounter is another technology that can be used to circumvent the limitations of microarrays based on its ability to detect low abundance mRNAs with high levels of sensitivity. The technology also overcomes the challenges of mRNA recovery and cDNA synthesis, as the complete nucleic acid is used on the Nanostring chip, eliminating the DNase and cDNA synthesis steps while still providing robust, highly sensitive enumeration of mRNA at a similar accuracy to RT-PCR (Brumbaugh et al., 2011). The nCounter assay enables digital quantification of any nucleic acid, but it is particularly useful for mRNA molecules.

Using this assay, up to 800 genes within a single reaction can be profiled using 10 ng of RNA or bacterial lysate, avoiding the need for nucleic acid purification and the enzymatic reaction steps. The assay begins with a hybridisation reaction using two probes composed of color-coded barcodes, with up to 50 base target-specific sequences for each gene of interest. The first probe is a biotin-labelled capture probe that immobilises the complex for data collection, while the second is a reporter probe labelled with a fluorescent barcode for the detection of signal. The hybridisation is performed by incubation for 12 hours at 65°C, which creates a range of colour code barcodes for the capture and reporter probes for each gene of interest. The probes and target complexes are purified by washing excess probes away by adding oligonucleotides complementary to the 5'-repeat sequence on the 5'-ends of each complex (Geiss et al., 2008). The purified complexes are then placed into a cartridge for binding, and the voltage is turned on to immobilise the complexes on the surface; finally, the bound barcode is imaged by a fluorescent microscope and counted. The level of expression is determined by the number of codes for each mRNA (Geiss et al., 2008). Although this technology allows examination of expression of genes *in vivo*, it does not allow gene expression analysis during infection within the same animal, and the expression profile does not necessarily correlate with the fitness of bacteria, however.

1.7. Animal models for *in vivo* studies

Animals are often utilised to model human infections, and in traditional studies, animals are infected with microbes and, at predetermined time points, sacrificed to extract the target tissue to determine bacterial load (Andreu et al., 2011, Jenkins et al., 2003). Such approaches provide valuable information, yet they require large numbers of animals to be sacrificed at multiple predetermined time points in order to follow the progress of infection. They also involve processing animal tissues and plating tissue homogenates to identify viable microorganisms, thus being very time consuming (Demidova et al., 2005). The acquired data are further limited to those tissues and organs analysed and, importantly, these conventional methods do not allow researchers to follow the progression of disease in a given animal, leading to confounding of much of the data analysis (Andreu et al., 2011, Jenkins et al., 2003). Existing animal models only reveal whether a given pneumococcal protein contributes to virulence or not, based on measuring the bacterial counts in different tissues and their survival time. In terms of real time spatial or temporal virulence, determinant expression is more useful for the introduction of targeted therapies (Andreu et al., 2011), suggesting that a better animal model of infection is needed, which ideally should also reduce the number of animals needed for experimentation, refine existing techniques to minimise animal suffering, and increase the data output by allowing detailed study of both host response and microbes during the course of an infection.

Over the past decade, *in vivo* imaging based on visible light emissions from luciferase-expressing bacterial cells has emerged. This bioluminescence imaging has streamlined *in vivo* studies of infection models and refined several animal models (Andreu et al., 2011). The technology allows the progress of infection to be followed in real time within the same animals, based on the ability to image entire living animals without needing to sacrifice those animals, which is useful for accurate monitoring of infection and evaluation of various anti-infective therapies throughout a course of treatment (Jenkins et al., 2003).

Fluorescence is another *in vivo* optical imaging that generates light through chemical reactions; however, unlike bioluminescence, such light generation requires an external light source to produce light. These two *in vivo* imaging systems also differ in terms of signal intensity and signal-to-noise (S/N) ratios. Although fluorescent signals are usually brighter than bioluminescence, the level of fluorescent background *in vivo* is higher than the equivalent bioluminescence. This autofluorescence in tissue drives the background noise higher, which makes florescence imaging less sensitive (Troy et al., 2004). Bioluminescence imaging is much more sensitive than fluorescence imaging due to the extremely low background intensity of

bioluminescence, and its ensuing high signal-to-noise (S/N) ratio (Ozawa et al., 2013). In this study, bioluminescence-imaging system was thus applied to construct and test an efficient biophotonic imaging (BPI) reporter system to study pneumococcal biology.

1.8. Biology of Bioluminescence

Various organisms, including insects, various sea species, and some bacteria, emit natural bioluminescence. The generation of such bioluminescence is created by a luciferase catalysed oxidation reaction of a substrate often called luciferin. This reaction requires energy, in the form of $FMNH_2$, the reduced Flavin mononucleotide, and ATP; oxygen; and potentially cofactors such as Mg^{2+}, which are needed for some luciferases (Wilson and Hastings, 1998). Three luciferases are widely used in the laboratory: those extracted from the firefly *Photinus pyralis* and the click beetle *Pyrophorus plagiophtalamus*, those extracted from the sea pansy *Renilla reniformis* and jellyfish, and those drawn from luminous bacteria (*Photorhabdus luminescens* and *Vibrio sp*.) (Andreu et al., 2011).

Luciferases from fireflies and click beetles are approximately 62KDa, and these are encoded by a single gene (*luc*), which was characterised in 1978 (Deluca and McElroy, 1978). These luciferases use benzothiazole luciferin along with ATP and oxygen to generate oxyluciferin, Adenosine monophosphate (AMP), CO_2, and light (Hastings, 1996). Fireflies and their relatives have varying peak emissions, with *P. pyralis* showing a peak at 560 nm while the *P. plagiophtalamus* luciferase emission range is between 546 to 593 nm (Wood et al., 1989). Interestingly, the peak emission of such luciferases shows increased activity at elevated temperatures as compared to that seen at a room temperature of 25 °C. Fireflies display peaks ranging from 578 nm at 25 °C to 612 nm at 37 °C, making firefly luciferase (Fluc) (Steinhuber et al., 2008) more nearly equivalent to click beetle luciferase (CBRluc) (Zhao et al., 2005). Luciferin administration in animal models a few minutes before imaging is required when using these luciferases to produce bioluminescent signals; this substrate shows a lack of toxicity and is generally distributed rapidly through the animal body (Contag et al., 1997).

Luciferases from sea pansies *Renilla reniformis* (36 kDa) and jellyfish (19.9 kDa) are encoded by the genes *Rluc* and *Gluc*, respectively, and use a coelenterazine substrate to generate CO_2, oxidized luciferin (coelenteramide) and blue light (480 nm) (Waidmann et al., 2011). As with

luciferin, coelenterazine must be administered before imaging by an appropriate route, generally tail-vein injection (Andreu et al., 2010). Rluc is ATP independent in its bioluminescence (Badr, 2014). Although the light produced by Gluc lies in the blue part of spectrum (480 nm), it has a broad emission spectrum that extends to 600 nm. It has also been reported that Gluc produces stronger signals *in vivo* than Fluc, making the signal from Gluc less susceptible to tissue absorption. Further, Gluc is also resistant to heat and extreme pH and has been reported to be secreted from mammalian and bacterial cells (Tannous et al., 2005). The blue light emission, which has high absorbance by pigmented molecules, and the poor biodistribution of coelenterazine make these luciferases less attractive for *in vivo* imaging, however (Badr, 2014).

Bacterial luciferases are heterodimeric enzymes encoded by the *luxABCDE* operon that generate a blue-green light (emission peak at 490 nm) based on the oxidation of a long-chain aldehyde and reduced flavin mononucleotide ($FMNH_2$) to form oxidized Flavin (FMN), a long-chain fatty acid and light (Wilson and Hastings, 1998). Oxygen is a required component for bacterial luciferases, though this is readily available within the cell. Bacterial luciferase binds one molecule of $FMNH_2$, preventing the auto-oxidation of $FMNH_2$ (Waidmann et al., 2011). Interestingly, bacterial luciferases also produce biosynthetic enzymes for substrate synthesis, abolishing the need to provide an exogenous substrate (aldehyde) (Wilson and Hastings, 1998). Bacterial luciferases are 77kDa, being composed of an α and a β subunit encoded by the *luxA* and *luxB* genes. The *luxC*, *D,* and *E* genes encode the subunits of a multienzyme complex that is significant for regeneration of the aldehyde substrate from the fatty acid produced by the bacterial luciferase reaction. All five genes in the operon are thus important for generating light (Brock, 2011). The *P. luminescens lux* system is frequently used in mammalian cell lines and animal models because of its high thermal stability, while *Vibrio* luciferases have been observed to be inactivated at 45 °C. The *Vibrio* luciferases are thus more useful in non-mammalian animals, such as zebra fish and plants, which require lower temperatures (Waidmann et al., 2011, Szittner and Meighen, 1990).

1.9. Luciferase activity detection *in vitro*

Bioluminescence imaging is a powerful tool used for monitoring various biological processes in cultured cells, using a luminometer, and in living animals, using a sensitive charged coupled

device (CCD) camera. Some biological processes of interest, such as promoter activity, are monitored in culture *in vitro* first before more complex *in vivo* systems are examined (Sadikot and Blackwell, 2008). Light is produced from cells labelled with a luciferase gene when it is exposed to the appropriate luciferin substrate in the presence of ATP, which is generally readily available within a cell. Photon emissions produced from such cells can be detected and measured *in vitro* by means of a light-sensitive instrument such as a luminometer, which may then be connected to a computer and an appropriate software platform for data analysis (Sadikot and Blackwell, 2008). A luminometer consists of a sample chamber, detector, signal processing method, and signal output display (Berthold et al., 2000). Luminometers may be of either microplate or test tube design, depending on the type of sample container held by the sample chamber. A tube luminometer has a light-tight box into which a tube containing a sample may be placed, whereas plate reading luminometers use 96-well plates or plates with 384 wells for the measurement of luciferase activity in multiple samples simultaneously. In each case, the sample chamber presents the sample to the detector, which is the key part of the luminometer and which consists of several photomultiplier tubes (PMT) (Berthold et al., 2000). These are often positioned underneath the sample. The measurement process is then initiated by inserting the sample in the test tube or well plate along with the substrate (luciferin) before assessing luciferase activity. Computer software is then applied once the data from the sample is sent to a PC for further analysis (Sadikot and Blackwell, 2008). At this point, luciferase activity is normalised to the protein content of the sample. In terms of signal processing, luminometers utilise either photon counting or current measuring. In photon counter luminometers, single photons within a PMT are counted, while current luminometers measure the electrical current that results when photons strike the PMT, and it is thus expected that not all photons will be measured, as not all light emitted from sample is directed to the PMT. The light is expressed in photons per second by a photon luminometer, or in arbitrary light units, referred to as relative light units (RLUs), where the luminometer measures electrical current. These two systems thus give numerically different light outputs, n issue compounded by differences in sensitivity. Additionally, while photon counters can measure very low light levels (Mizuguchi, 1998), their maximum detection remains relatively low.

1.10. Biophotonic imaging technology (BPI) for *in vivo* studies

BPI is a nontoxic technique that relies on the sensitive detection of visible light within living animals based on the use of a sensitive CCD camera, set within a light-tight chamber, accompanied by appropriate computer software for image data acquisition and analysis (Rice et al., 2001). The camera detects the visible wavelengths of radiation, ranging from 400 nm (blue light) to 600 nm (red light) (Demidova et al., 2005). To carry out BPI, animals are infected and, at the selected time point, injected with a subcutaneous exogenous substrate (luciferin). The luciferin dose is determined according to animal weight (Doyle et al., 2004, Andreu et al., 2011). The animals infected with bioluminescent strains must then be anaesthetised by inhalation of gaseous anaesthetics or injectable agents before imaging. These animals are placed in an image acquisition box on a moveable heated stage, allowing up to five animals to be imaged simultaneously. The camera records images of the photonic emissions and a Living Image software analysis is produced, quantifying the data and generating pseudo-coloured images (Figure 1.2) of the acquired grayscale reference image to represent the light density. These range from dark blue, which is the least intense, to red, which is the most intense. This procedure may take anywhere from a few seconds to several minutes, based on the strength and the penetration of bioluminescence signal through the tissue (Doyle et al., 2004). BPI is a sensitive tool with a low background signal that allows it to detect relatively low levels of pathogens in animal models during infection (Hutchens and Luker, 2007).

BPI thus achieves two of the three Rs: refinement and reduction. This tool minimises the number of animals required and refines existing *in vivo* models by allowing the same groups of animals to be imaged at different time points in order to assess ongoing pathogen burden and location in real time noninvasively (Andreu et al., 2011). Further, because the entire body of the infected animal is imaged, the presence of microorganisms can be identified at any location. BPI also refines *in vivo* models of infectious disease by revealing at an early stage if the animal will survive or die. Observation of luminescent signals in mice that have been inoculated with luminescent *Bacillus anthracis* in the cervical lymph nodes, for example, is evidence of immune system failure that will permit distribution to other organs and thus lead to death (Loving et al., 2009). The observation of such signals therefore allows for humane euthanasia where appropriate. In addition, BLI can minimise the level of stress and pain in animals by removing the need for invasive sampling at multiple time points for the determination of pathogen burdens in blood or other tissues (Andreu et al., 2011). Overall, the required number of animals is reduced, the obtained data is more reliable, and counts of

microbial pathogens are possible for any part of the animal. Additionally, the spatiotemporal expression of any gene of interest may be observed, thus allowing determination of the genes most closely involved *in vivo* virulence. Significantly, the efficiency of various therapies and host responses can also be tracked (Doyle et al., 2004, Demidova et al., 2005).

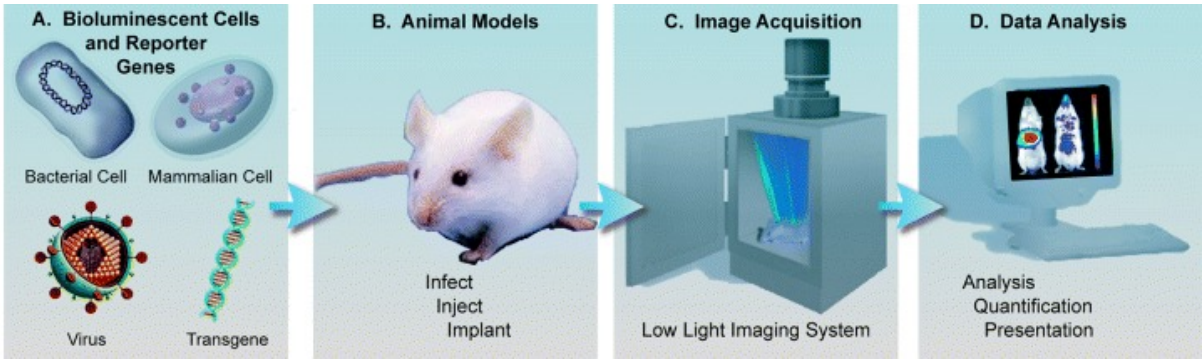

Figure 1.2. Bioluminescence imaging of infection. (A) Integration of reporter genes into the cells to emit bioluminescence. (B) Injection of mice with bioluminescent cells. (C) Recording photonic emissions in image acquisition box. (D) Living Image software analysing and quantifying the data (Doyle et al., 2004).

1.11. Bioluminescent imaging of bacterial infection

Bioluminescence applications in molecular imaging are generally referred to as BLI. The first study to use BPI for imagining infections in animal models was undertaken in 1995, utilising bacterial luciferase *lux* operon to examine *Salmonella* infections and the efficacy of antibiotic treatment in mice (Contag et al., 1995). Three strains of *Salmonella,* with different virulence levels, harbouring plasmid encoding *lux* operons were used to infect mice orally. That study concluded that luciferase gene integration did not affect the fitness of bacteria and that bioluminescence could be detected in animals infected with bioluminescent *Salmonella.* Further, the counts of bacteria were correlated to the intensity of this bioluminescence. Bioluminescent cells with bacterial luciferases emit blue light without the need for any addition of exogenous substrate. Further studies thus used the same system (*lux* operon) to examine different models of infectious disease. Francis et al. (2001) used the transposon-mediated integration of *lux* operon into the chromosome of Gram-positive bacteria, *S. pneumococcus,* after changing the gene order of the operon to *luxABCDE* for optimal expression in a murine lung infection model. The integration of luciferase operon into the

bacterial chromosome improved the stability of bioluminescent cells in the absence of antibiotic selection, a strategy that permits more robust correlation between the generation of light and bacterial cell counts; thus, any reduction of bioluminescence from sites of infection in animals treated in this way may be attributed to a reduction in bacterial numbers rather than any loss of plasmids.

The application of BLI provides new insights into the growth and dissemination of pathogenesis, thus facilitating the identification of virulence determinants, and potentially helping to develop new therapeutics. *Brucella melitensis* labelled with *lux* operon was used to monitor *Brucella* infections in mice, and imaging the progression of infection revealed novel sites of *Brucella* localisation and differences in tissue dissemination among *Brucella* mutants. *B. melitensis*, the most frequent cause of human brucellosis, was thus shown to progress to range of tissues, causing acute or chronic infections. Bioluminescence signals in infected mice were detected at the site of inoculation (peritoneum), in the inguinal lymph nodes, in the liver and spleen, and in two new sites, the testes and submandibular regions, reflecting the ability of *Brucella* to cause orchitis in humans. The utilisation of BLI can also provide insights into the *in vivo* role of microbial gene products based on identifying the dissemination and localisation of attenuated mutants in various tissues and comparing these to the infection dynamics of wild types (Rajashekara et al., 2005).

New insights into the *in vivo* patterns of growth and dissemination of *Bacillus anthracis*, which is responsible for causing anthrax, have also been observed by means of BLI. Mouse models of attenuated *B. anthracis* infection without capsulation have thus been developed, with the progression of nonencapsulated *B. anthracis* infection monitored in a cutaneous model of infection by BLI. The findings were then compared to those for encapsulated bacteria, and the BLI revealed that confinement to the site of inoculation for nonencapsulated bacteria was longer as compared to that seen in the wild type. Further, the dissemination of attenuated bacteria to the lungs and kidneys after progression to the draining lymph nodes was delayed (Glomski et al., 2007).

BLI has also provided improvements in study of biofilm biogenesis, which has previously been difficult to study *in vivo*. Biofilm formation is generally studied based on abiotic surface adherence, such as seen in prosthetic devices, followed by removal and quantification of the bacteria present. This conventional method does not allow for long observation of the

progression of infection, however. Monitoring of biofilm infection was, however, found to be possible in a mouse infection model based on imaging bioluminescent *Staphylococcus aureus* and *Pseudomonas aeruginosa* colonised on Teflon catheters. Significant bioluminescent signals for both *in vivo* models were observed, supporting the viability of BLI for studying the physiological state of biofilms. Recovery of bacteria from the catheters of infected animals also confirmed the correlation between light readings and the presence of viable cells (Kadurugamuwa et al., 2003).

The application of BLI may also accelerate testing and validation of antimicrobial agents and reduce the number of animals required for such studies. Rocchetta et al. (2001) used bioluminescent *Escherichia coli* to validate the antimicrobial efficacies of ceftazidime, tetracycline, and ciprofloxacin using a neutropenic-mouse thigh model of infection. A good correlation between the bioluminescence signal and the viable cells was observed, and the findings were compared favourably to traditional plate counting methods, revealing the viability of BLI for therapeutic testing.

BLI can be also used for studying gene expression. This process begins with the labelling of cells with reporter genes under promoter control of the gene of interest, then monitoring the resulting bioluminescent signals. This system has been used to determine the level and site of flagellin gene expression in Uropathogenic *Escherichia coli* (UPEC) during ascending infections, as this organism causes urinary tract infections (UTIs) in humans. Flagellum-mediated motility was observed to contribute to virulence by enabling UPEC to disseminate to the upper urinary tract. Lane et al. (2007) confirmed this observation *in vivo* by constructing luminescent cells with a *fliC* promoter to drive the expression of *lux*. The *fliC* showed flagellin-specific patterns *in vitro*, and the use of BLI enabled the researchers to monitor *in vivo fliC* expression to determine the involvement of *fliC* expression in migration to the upper urinary tract. Bioluminescence levels were found to be correlated with *in vivo fliC* expression as assessed *in vitro* using quantitative PCR, supporting the validity of BLI for gene expression studies.

In addition to studying pathogen biology, BPI can be applied to examine host responses during infection. This can be achieved by monitoring the bacterial loads in wild types and strains with altered immune systems infected with bioluminescent bacteria. Through such monitoring of gastrointestinal infections with bioluminescent *Citrobacter rodentium*, it was found that mice

lacking the p50 subunit of the transcription factor nuclear factor kappaB, are unable to clear such bacteria. The approach thus highlighted the importance of this transcription factor during infection (Dennis et al., 2008).

Finally, another very interesting study of mycobacterial infection showed further possible uses of two different bioluminescent systems for the simultaneous study of bacterial load and host response. Emission filters for the separation of bioluminescent signals were used in dual colour bioluminescence imaging to study two mycobacterial strains. These strains were labelled with CBRluc or Fluc, which emit distinct light wavelengths, permitting simultaneous imaging of two strains during infection in the same animal (Chang et al., 2014).

1.12. Factors that influence bioluminescent signals

Although BLI is an extremely useful technology, several factors may affect the sensitivity of bioluminescent signals. Signal quantification is one of these factors. Luciferase activity is measured by a luminometer or CCD camera and is recorded in relative light units (RLU). However, the RLU is not a standardised unit of measurement, and measuring specific luciferase activity, for example, with a different luminometer can result in the generation of totally distinct results. Bioluminescence sensitivity thus relies partly on the selected luminometer for *in vitro* measurement or the CCD camera for *in vivo* imaging (Badr, 2014). Background control is another factor that should be considered when designing any BLI experiment, as although bioluminescence imaging generates low background noise, including a control such as a media of the cell culture with addition of a substrate is recommended to minimise any background luminescence (Badr, 2014). Oxygen availability is another factor that may affect results, as it is required for all reactions using luciferase as a cofactor. It has thus been reported that bioluminescence cannot be detected under anaerobic conditions, such as in the necrotic cores of large tumours. However, bioluminescence can be detected when marine bioluminescent bacteria are used at O_2 concentrations as low as 10 nM (Bourgois et al., 2001).

The efficient delivery of exogenous substrate also affects the bioluminescence signal; substrate availability is thus very important in *in vivo* imaging. A sufficient amount of substrate must be administered to reach the reporter cells efficiently to generate a strong signal. The route of substrate administration may also have an effect on the emission of luminescent signals (Close

et al., 2011). The most commonly used route is intraperitoneal injection, due to its simplicity; however, the delivery of the luciferin requires absorption across the peritoneum and any variations in absorption can lead to changes in the luminescent signal. Although they are rare, injection failure, such as injections leading into the bowel, can also be confused with negative results (Inoue et al., 2009). Intravenous injection is another route for the rapid systemic profusion of luciferin; however, it has been observed that the uptake of luciferin by this route is slowed by the passage through gastrointestinal organs, pancreas, and spleen, affecting the duration of the emission of luminescent signals. A convenient alternative to these commonly used routes is subcutaneous injection, and Inoue et al. (2009) demonstrated that repeated subcutaneous injection of luciferin did not show local damage at the injection site in tumour model mice. Further, the peak time is shorter, and the peak signal larger than in intraperitoneal injections in mice tumour models (Inoue et al., 2009). The administration route of substrate for *in vivo* imaging should thus be chosen carefully to reflect the amount of substrate required and the solubility of the substrate (Close et al., 2011).

The efficiency and sensitivity of bioluminescent signals are influenced by further factors such as the depth of tissue. The distance that the light must travel through tissues affects the photon intensity significantly, decreasing it 10-fold for each centimetre of tissue depth (Signore et al., 2010). Small animals such as mice are thus recommended for BLI. Pigmentation of fur also affects photon intensity, though this can be minimised by shaving the fur (Demidova et al., 2005). The wavelength of light emissions produced by bioluminescent reporter proteins can also affect sensitivity to light intensity, with blue-green light at a wavelength of 400 nm being largely absorbed by tissues, while red light at wavelengths of 546 nm to 593 nm penetrates more deeply (Andreu et al., 2011). Haemoglobin, the primary absorber in the body, absorbs most significantly in the blue and green region of the visible spectrum, whereas its absorption of red wavelengths is lower. This allows red light to travel more easily through deeper tissue sites (Rice et al., 2001). Promoter activity, which drives luciferase expression, within the genes of interest also affects the sensitivity of the bioluminescent signal, as the reporter gene is expressed only when the relevant gene is activated (Waidmann et al., 2011).

1.13. Project overview

Francis et al. (2001) constructed bioluminescent pneumococcal strains using a system featuring a plasmid called pAUL-A Tn4001 *luxABCDE* Kmr. This cassette randomly integrates into the pneumococcal genome, allowing transposon mutants to be screened for their levels of bioluminescence using an ICCD camera. Bacteria with the highest levels of expression of light can then be tested in a pneumococcal lung infection model, with the resulting stable integration eliminating the need for antibiotics to maintain a plasmid expressing these genes. Several studies have since used this system, including bacterial *lux* operon *in vivo* localisation studies and analyses of microbial gene expression in *S. pneumoniae* (Beard et al., 2002, Orihuela et al., 2003, McCullers et al., 2007, Contag, 2008, Diavatopoulos et al., 2010, Henken et al., 2010, Short et al., 2011, Kong et al., 2013, Jensch et al., 2010). However, although this system has been exploited successfully in many cases, it lacks sensitivity and high doses of bioluminescent *S. pneumoniae* are required to initiate infection. This low sensitivity is probably related to the nature of the bioluminescence emitted by *lux*, which is blue, meaning that only a small part of the emitted light can travel through tissues due to absorption in animal tissues. In addition, it is NADPH dependent, requiring reducing agents of Flavin to initiate the bioluminescent reaction (Brodl et al., 2018). The random insertion of the transposon also causes mutations that may affect the virulence of the selected strain, and the strength of the promotor, which drives the *lux* expression, also affects the sensitivity of the system.

In the current study, a bioluminescence reporter system was thus created for use in *S. pneumoniae* based upon red- click beetle luciferase enzyme (CBRluc) instead; this was then compared with the previously described *lux* system. To properly assess the new system, a defined promoter at a defined site was used so that a direct comparison of different strains could be made. The first step, therefore, was *in vitro* optimisation of the use of CBRluc in *S. pneumoniae* under the control of a group of promoters predicted to be highly expressed *in vivo*.

1.14. Selection of an appropriate promoter to optimise CBRluc

This study aimed to construct a bioluminescent pneumococcal strain using CBRluc. Thus, this reporter gene was integrated into a known site in the *S. pneumoniae* genome under the control of various promoters predicted to be highly expressed *in vivo* using a pPP3 plasmid. The pPP3 CBRluc plasmid was kindly provided by Dr Andrew Ulijasz of Loyala University Chicago. Multiple features of pPP3 plasmid enable stable genomic integration of selected promoters that are fused to a promoterless click beetle *luc* gene. The pneumococcal insertion site, the *bgaA*

locus, has been previously shown not to affect virulence (Halfmann et al., 2007). The promoters in this study were selected because they have been reported to demonstrate high expression *in vivo*. Appropriate bioluminescent *S. pneumoniae* strains were thus constructed and tested *in vitro* to identify the most active promoters driving *luc* expression. The expression conditions were also optimised to achieve the highest possible expression levels both *in vitro* and *in vivo*.

The promoters tested in this study included pyruvate formate lyase B (*pflB*). PflB is essential for the metabolism of galactose, the most abundant sugar within the structure of respiratory mucin (Yesilkaya et al., 2009, Buis and Broderick, 2005), and *S. pneumoniae* is a microbe that depends on fermentative breakdown of sugars to generate energy. This microorganism thus resorts to fermentation processes for the generation of energy because it lacks a complete set of genes for respiration, and this ability to obtain and metabolise sugars is evidence for the *in vivo* fitness of this microbe. The fermentation process may take two alternative forms, depending on the environmental conditions; these are homolactic and mixed-acid fermentation. In the presence of sugars such as glucose, the preferred sugar for *S. pneumoniae* (Carvalho et al., 2011), homolactic fermentation occurs under aerobic conditions. In this route, pyruvate is converted to lactic acid by lactate dehydrogenase. In the presence of galactose, however, mixed-acid fermentation occurs, which generates acetyl-CoA and formate from pyruvate, under microaerobic and anaerobic conditions, by way of pyruvate formate lyase, which is coded *pflB* (Al-Bayati et al., 2017). The importance of this protein in galactose metabolism is an indication that it is highly expressed in *S. pneumoniae* (Karlin et al., 2004).

The *phrA* peptide signalling molecule in the TprA/PhrA quorum sensing (QS) system is another selected gene used for the construction of bioluminescent strains. It has also been reported that this gene is highly expressed in mouse tissues when using Nanostring technology (Cuevas et al., 2017). The TprA/PhrA QS system belongs to the RRNPP family of transcriptional regulators and has been suggested to be important in pathogenicity (Motib et al., 2019). Quorum sensing is a bacterial cell-to-cell signalling system that enables bacterial populations to synchronise their expression of genes at population level in a cell density-dependent manner in response to various environmental stimuli. The signals are based on secreted peptides used as autoinducers. When the density of these reaches a certain level, the autoinducers increase in concentration, which enables the bacteria to coordinate gene expression such as that seen in lantibiotic genes, which are important for competitive fitness during host infection (Miller and Bassler, 2001). It has also been observed that the TprA/PhrA system mediates quorum sensing,

and that the expression of *phrA* is induced in the presence of galactose (Hoover et al., 2015), consistent with activity in the upper respiratory track such as the human nasopharynx, where galactose is the main sugar (Yesilkaya et al., 2009, King, 2010). Hoover et al. (2015) further reported on the role of TprA/PhrA system in controlling the expression of genes known to process lantibiotic peptide. Galactose is the main sugar in the nasopharynx and being able to make use of this is thus important for pneumococcal colonisation of this tract (Yesilkaya et al., 2009). Lantibiotics are produced by the ribosomal machinery and generate antimicrobial activity during colonisation of the nasopharynx, which protects against other organisms. (Motib et al., 2019) thus concluded that PhrA plays a significant role in pneumococcal cells' colonisation of the human nasopharynx.

The promoter of pneumococcal surface protein A (*pspA*) is another selected target, as this plays a role in the inhibition of complement-mediated opsonisation (Kadioglu et al., 2008) by interfering with the fixation of complement component, C3, of the host during pneumococcal infection. C3 plays a central role in the activation of the complement system, while PspA has the ability to bind lactoferrin, an iron-sequestering glycoprotein, at respiratory mucosal sites. This binding of lactoferrin to pneumococci interferes with host immune functions during pneumococcal infection (LeMessurier et al., 2006). Immunisation with PspA provides protection in mice against invasive infection (Shaper et al., 2004), yet the *pspA* mutant showed no effect on colonisation of the human nasopharynx (McCool et al., 2002). The expression of *pspA* in bacteria from the nasopharynx and blood was highest as compared to *cps2A, piaA, ply, nanA,* and *spxB* during the progression of the disease from colonisation of the nasopharynx to systemic in mice. This is consistent with its function of inhibiting complement-mediated opsonisation (LeMessurier et al., 2006). As with *phrA,* virulence peptide (*vp1*) is a regulatory peptide that controls pneumococcal biofilm formation. The formation of biofilms plays an essential role in drug resistance, and cells in such formations show particular resistance to antibiotics. Generally, *vp1* was shown to be most highly expressed during middle ear infections (Cuevas et al., 2017).

The promoter of high temperature requirement A (*htrA*), one of the serine proteases, is important in terms of resistance to elevated temperature and oxidative stress, and thus this was also included in this study. Further, *htrA* mutant strains showed attenuation in both pneumonia and bacteraemia models of infection, underscoring the role played by HtrA in virulence (Ibrahim et al., 2004). Due to the importance of HtrA, it is expected to be highly expressed.

The promoter of *16S rRNA*, a major component of the small ribosomal subunit with 1,500 ribonucleotides, was also included alongside selected genes, as the *16S rRNA* gene promoter can be used as an internal control due to constitutive expression (Scholz et al., 2012).

Due to the importance of the selected gene promoters in pneumococcal pathogenesis, they are all predicted to be expressed significantly *in vivo*. For this study, the putative promoters of the selected genes were cloned to construct bioluminescence reporter strains containing CBRluc, which emits long light wavelengths ranging from 546 nm to 593 nm, to enhance whole-body imaging in murine infection models. By using a defined promoter and integration at a defined site, a direct comparison of different strains is hypothesised to be possible.

1.15. Aims and objectives

The basic hypothesis is that expression of different genes varies *in vivo*. The objective of this study is thus to identify the most highly induced gene promoters to support construction of an efficient bioluminescent *S. pneumoniae* that allows sensitive *in vivo* detection of microbes within intact living animals. A sensitive bioluminescent pneumococcal strain thus needed to be constructed that demonstrated luminescence at the highest level with a standard dose of *S. pneumoniae* in order to facilitate the study of pneumococcal gene function *in vivo* and *in vitro* and thus promote understanding of pneumococcal biology. The aim of this project is therefore to develop and refine current bioluminescent methodologies by using a biophotonic system (CBRluc) to minimise the limitations of the most common existing biophotonic system (bacterial luciferase) used to study the pathogenesis of *S. pneumoniae* during *in vivo* infections. This process began with identifying those *in vivo* genes predicted to be most highly expressed, based on literature searches and Nanostring technology. The relevant bioluminescent strains were then created and assessed *in vitro* and *in vivo*, after which the CBRluc candidate strain constructed in this study was compared with the existing strain containing pAUL- A Tn4001 *luxABCDE* Kmr. Finally, the bioluminescence of the CBRluc system was compared to that of the *lux* system under the same promoter

Chapter 2. Materials and Methods

2.1. Biological and chemical materials

Unless otherwise stated, all chemicals used in this project were purchased from Sigma Aldrich (Germany), New England Biolabs (UK), Fisher (UK), Oxoid (Thermo Scientific, UK) or Promega (UK). The bacterial strains and plasmids used in this study are all listed in Table 2.1

Strains/Plasmids	Description	
S. pneumoniae D39	Wild type of *Streptococcus pneumoniae* D39 (virulent serotype 2)	Laboratory stock
pPP3 CBRluc-wt	D39 :: pPP3 plasmid; Tet^R	Created for this study
P*pflB::luc*-wt	D39, pPP3- PpflB promoter region of *pflB* integrated to *luc*; Tet^R	This study
P*phrA::luc*-wt	D39, pPP3- PphrA promoter region of *phrA* integrated to *luc*; Tet^R	This study
P*rrna::luc*-wt	D39, pPP3- P16S *rrna* promoter region of *16S rrna* integrated to *luc*; Tet^R	This study
P*pspA::luc*-wt	D39, pPP3- PpspA promoter region of *pspA* integrated to *luc*; Tet^R	This study
P*vp1::luc*-wt	D39, pPP3- Pvp1 promoter region of *vp1* integrated to *luc*; Tet^R	This study
P*htrA::luc*-wt	D39, pPP3- PhtrA promoter region of *htrA* integrated to *luc*; Tet^R	This study
S.pneumoniae Tn4001 luxABCDE	D39:*lux*ABCDE ;Km^R	Francis et al. (2001)
P*spd1717::lux*-wt	D39, a genome of *S.pneumoniae Tn4001 luxABCDE* integrated into D39	This study
Ppp4::*lux*-wt	D39, promoterless pPP4 plasmid carrying *luxABCDE*	This study
pPP4::P*phrA::lux*-wt	D39, pPP4-PphrA promoter region of *phrA* integrated to l*ux*;Tet^R	This study
pPP3 CBRluc plasmid	Promoterless BagA for transcriptional fusions; Amp^R Tet^R	Dr Andrew Ulijasz, Loyala University Chicago

Escherichia coli strain Top10	Plasmid propagation, Amp^R	Thermo Fisher, UK

2.2. Bacterial growth conditions and media

Escherichia coli strain Top10 competent cells (Thermo Fisher, UK) were grown on Luria broth (LB) or Luria agar (LA) (LB: 10 g/ l of NaCl, 5 g/l of yeast extract and 10 g/l trypticase peptone; LA: LB with the addition of 1.5 % w/v bacteriological agar, Oxoid, UK) supplemented with ampicillin (100 µg/ml) (Sigma, UK) at 37 °C in a shaking incubator (220 rpm).

Streptococcus pneumoniae strain D39 was obtained from the laboratory stock of Dr Hasan Yesilkaya and grown at 37 °C either in brain heart infusion broth (BHI) or on a blood agar base supplemented with 5% (v/v) horse blood in a candle jar to encourage best growth. Bacterial stock in glycerol was prepared by means of a suspension of an overnight grown culture pellet in BHI containing 15% glycerol (v/v); this stock was then kept at -80 °C until use.

All media were prepared according to manufacturer's instructions, including sterilised by autoclaving at 121 °C for 15 min. When necessary, growth media were supplemented with antibiotics (kanamycin 400 µg/ml (Francis et al., 2001) or tetracycline 15 µg/ml, Sigma, UK). *S. pneumoniae* D39 was also grown in chemically defined media (CDM) supplemented with either 55 mM glucose or galactose. The full compositions of these media are listed in Table 2.2. CDM were prepared by mixing 870 ml Basal solution, 10 ml Vitamins, 80 ml Amino acids, 10 ml Micronutrients, 10 ml Nitrogenous bases, 1 ml Pyruvate, and 4 ml Choline-HCl (Kloosterman et al., 2006). The resulting medium was sterilised by filtration through a 0.22 µm pore membrane and stored at 4 °C until use.

Table 2.2. Compositions of chemically defined media (CDM)

Components	g l-1	Components	g l-1
Buffers/Salts		**Amino acids**	
Na_2-βglycerophosphate	26	Alanine	0.24
$(NH_4)_3$ citrate	0.6	Arginine	0.124
KH_2PO_4	1.0	Asparagine	0.352
Na-acetate	1.0	Aspartate	0.4
Na-pyruvate	0.1	Cysteine-HCl	0.4
Vitamins		Glutamate	0.5
Choline-HCl	10	Glutamine	0.392
Na-p-aminobenzoate	5.0	Glycine	0.176
D-Biotin	2.5	Histidine	0.152
Folic acid	1.0	Isoleucine	0.212
Nicotinic acid	1.0	Leucine	0.456
Ca (D+) Pantothenate	1.0	Lysine	0.44
Pyridoxamine-HCL	2.5	Methionine	0.124
Pyridoxine-HCl	2.0	Phenylalanine	0.276
Riboflavin	1.0	Proline	0.676
Thiamine-HCl	1.0	Serine	0.34
DL-6,8-Thioctic acid	1.5	Threonine	0.224
Vitamin B_{12}	1.0	Tryptophane	0.052
Nitrogenous bases		Valine	0.324
Adenine	1.0	**Micronutrients**	
Uracil	1.0	$MgCl_2$	20
Xanthine	1.0	$CaCl_2$	3.8
Guanine	1.0	$ZnSO_4$	0.5

2.3. Viable counts of bacterial aliquot

Bacterial colony forming units (CFU) were determined according to the Miles and Misra method (Miles et al., 1938). An aliquot (20 µl) of each bacterial culture was mixed with 180 µl

of Phosphate Buffered Saline (PBS) at pH 7.0 in a 96 well microtiter plate and then serially diluted. Forty microliters of each dilution were thus plated out, then these plates were dried and incubated overnight at 37 °C in a candle jar. Viable colonies were counted in sections, allowing 30 to 300 colonies to be observed. Bacterial colony forming units per ml were thus calculated using the following formula: CFU/ml= (Number of colonies x dilution factor) x (1000/40).

2.4. Bacterial growth studies in BHI and CDM

Growth studies in BHI and CDM supplemented with 55 mM of glucose or galactose were conducted using a MultiskanTM GO Microplate Spectrophotometer (Thermo Scientific, UK). A flat bottom microtiter plate was used for these growth studies, which were initiated by addition of 2 µl of bacterial suspension containing ~5 x 10^7 CFU/ ml to 198 µl of BHI or CDM. The relevant microtiter plate was then placed into the MultiskanTM GO Microplate Spectrophotometer, which was set to run 24 h readings at 37 °C at OD_{600}.The bacterial growth was measured then by colony counting as described in section 2.3 at various time points, with bacterial growth rates (μ) calculated based on the exponential phase of growth using the following equation:

$(\mu)\ h^{-1} = \ln OD_2 - \ln OD_1 / t_2 - t_1$

where ln refers to the natural logarithm of a quantity, t= time, and OD_2 and OD_1 are the optical densities at t2 and t1, respectively. The growth yield was thus calculated by measuring the highest value of optical density during the bacterial growth.

2.5. *Streptococcus pneumoniae* DNA extraction

DNA was extracted per Saito and Miura (1963). *S. pneumoniae* D39 was then grown overnight at 37 °C in BHI broth before being centrifuged at 3,500 rpm for 10 min; the supernatant was discarded at that point. The resulting pellet was then re-suspended in 400 µl TE buffer containing 25 % (w/v) sucrose, 60 µl of 500 mM EDTA, 40 µl of 10% (w/v) sodium dodecyl sulphate (SDS) (1 g in 10 ml dH_2O), and 2 µl of Proteinase K (12.5 mg/ml). This was followed by incubation at 37 °C for 1 to 2 h to obtain a clear cell lysate, which was then centrifuged using a microfuge (Sigma) at 13,000 rpm for 5 min. The supernatant was then transferred to a fresh tube and equal volumes of phenol: chloroform: isoamyl alcohol added prior to gentle

mixing to obtain a white emulsion. The lysate was then centrifuged again, at 13,000 rpm, for 10 min. The upper aqueous phase was transferred to a fresh tube without the white protein layer, and phenol: chloroform: isoamyl alcohol was added again before further centrifugation at 13,000 rpm for 10 min. At that point, 500 µl of the clear upper phase was mixed with 2.5ml of 100% ethanol (v/v) and 20 µl of 0.1X volume of 3 M sodium acetate (pH 5.2), with this mixture centrifuged at 13,000 rpm for 5 min. The supernatant was again discarded, and the pellet washed with 500 µl of 70% (v/v) ethanol. Finally, the tube was centrifuged at 13,000 rpm for 5 min and the ethanol discarded. The pellet was then allowed to dry before being re-suspended in 250 µl of TE buffer at pH 7.0.

2.6. Primer design and preparation

Oligonucleotide primers must be specifically designed for DNA amplification. The required primers were designed to have BamHI and SphI restriction sites in order to obtain a cleavable SphI - BamHI fragment, and these were manufactured by Eurofins. BPROM-softberry was used for promoter identification, and the stock primer solutions were diluted to 100 pM/µl using nuclease free water.

Table 2.3. Primers used in this study. Bold typeface indicates incorporated restriction sites.

Primers	Sequence (5'–3')
pPP3-F	CCACTATCGACTACGCGATC
pPP3-R	CTGTGGTAAGTGGCTGTGCT
PpflB -F+SphI	CG**GCATGC**GAAAAAAGGACTTTATTTTT
PpflB-R+BamH	CG**GGATCC**GTGCTTCAACAACTGTCTTA
PphrA-F+SphI	CG**GCATGC**TAAAGATAATAAACCTTCCT
PphrA-R+BamH	CG**GGATCC**ATTTTTTAATTCCACGTTTT
PrrnA-F+SphI	CC**GCATGC**GTATGTTGCGTCAGGAGCAC
PrrnA-R+BamHI	CG**GGATCC**TTCGTCCTGAGCCAGGATC
PpspA-F+SphI	GAC**GCATGC**TCGAAAGGATATCTTTATGTGA
PpspA-R+BamHI	ACG**GGATCC**TTGTTAAAATCATTTTTTTCT
Pvp1-F+SphI	GAC**GCATGC**TTAAAAATGGAATGACAATAAC
Pvp1-R+BamHI	ACG**GGATCC**TTGTTTCTGCAAATTGTAAAT
PhtrA-F+SphI	GAC**GCATGC**GACTCTATTCTAACATATTCTC
PhtrA-R+BamHI	ACG**GGATCC** TTTTGTAAAATGTTTTTAGATG
Lux-F+NcoI	GCG **CCATGG** AGGAGGACTCTCTATGAAATTTG
Lux-R+SalI	AGC**GTCGAC**GATATCAACTATCAAACGCTTCG
pPP3-R3	ATTTTTCCGGTTACGTTCCG
lux-R2	CCTCTGTCATGCCATTCTTT

2.7. Polymerase chain reaction

A HotStarTaq reaction mix (Qiagen, UK) was used for cloning confirmation and PCR amplification, with a PCR mixture composed of 2X 10 µl of HotStarTaq, 2 µl template (20 ng/ µl), 6 µl of nuclease-free water, and 2 µl primer mix (F/R, 1 pmol each/reaction). The PCR reaction was set to run for 30 cycles for amplification under set conditions of initial denaturation at 95 °C for 10 sec, annealing at 55 °C for 5 sec, extension at 72 °C for 1 min/1000 bp, and a hold set at 4 °C.

A PrimSTAR reaction was performed for DNA sequencing and PCR amplification. PCR mixture contained 10 µl of PrimSTAR HS premix, 2 µl template (20 ng/ µl) and 6 µl of nuclease-free water, 2 µl primer mix (1 pmol each/reaction). The reaction was set to run for 30 cycles for amplification under the set conditions of initial denaturation at 98 °C for 10 sec, annealing at 55 °C for 5 sec, extension at 72 °C for 1 min/1000 bp, and a hold set at 4 °C.

2.8. Agarose gel electrophoresis

The integrity of the DNA/PCR products was assessed using agarose gel electrophoresis. The DNA samples were routinely analysed on a 1% (w/ v) agarose gel prepared in 1X TAE buffer (40 mM Tris-acetate and 1 mM EDTA, with a pH of 8.0), with 0.2 µg/ml ethidium bromide used for DNA staining. The DNA samples were mixed with5 µl of 6 X gel loading dye (NEB, UK) before being loaded into the wells of the agarose gel. A 1 kb or 100 bp DNA ladder (NEB, UK) was also loaded as a control in each case to measure the approximate concentration and size of the DNA samples. Electrophoresis was conducted at 120 volts for approximately 25 min, and all DNA samples were then visualised under UV light.

2.9. DNA purification from agarose

DNA was purified from the agarose gel according to the manufacturer's instructions (Promega). This process began with cutting the required DNA band from the gel and transferring it into a 1.5 ml Eppendorf tube. After that,10 µl of membrane binding solution was added per 10 mg of gel slice, and the mixture was incubated at 50 to 65 °C to dissolve the gel

slice before an equal volume of membrane binding solution was added to the DNA solution and the entire mix was transferred to the minicolumn assembly. The sample was then centrifuged at 13,000 rpm for 1 min to discard any flowthrough and the DNA was washed twice by adding first 700 µl, and then 500 µl of membrane wash solution; this was followed by centrifugation at 13,000 rpm for 1 min. The minicolumn was carefully transferred to a new 1.5 ml Eppendorf tube, and 30 µl of nuclease free water was added to the centre of the minicolumn, which was then incubated at room temperature for 1 min. Finally, the sample was centrifuged at 13000 rpm for 1 min to elute the DNA, and the extracted DNA was stored at -20 °C.

2.10. Restriction digestion

To clone the inserts into pPP3 (Figure 2.1), the putative promotor regions for the target genes of *Streptococcus pneumoniae* DNA were amplified by PCR using the primers listed in Table 2.3, which had been modified to have the appropriate SphI and BamHI sites. The inserts and plasmids were double digested with BamHI and SphI enzymes to obtain cleavable SphI - BamHI fragments.

For the *lux* cloning, the *lux* cassette was amplified using the primers listed in Table 2.3 that incorporate NcoI and SalI recognition sites, and the pPP3 was also digested using both NcoI and SalI to remove the *luc* gene. The digestion reaction utilised 1 µg of each plasmid/ insert, 3 µl (10 U/ µl) restriction endonuclease (BamHI/ SphI) or (NcoI/ SalI), and 5 µl CutSmart™ buffer , made up to 50 µl with nuclease-free water. This was incubated in a water bath at 37 °C for 4 h before the digested plasmids and inserts were purified using the QIAquick PCR purification kit. The pPP3 CBRluc plasmid was kindly provided by Dr Andrew Ulijasz of Loyala University, Chicago, being derived from pPP2 (Halfmann et al., 2007) with replacement with a *luc* gene. The nucleotide sequence for pPP2 is available from GenBank (EF061139).

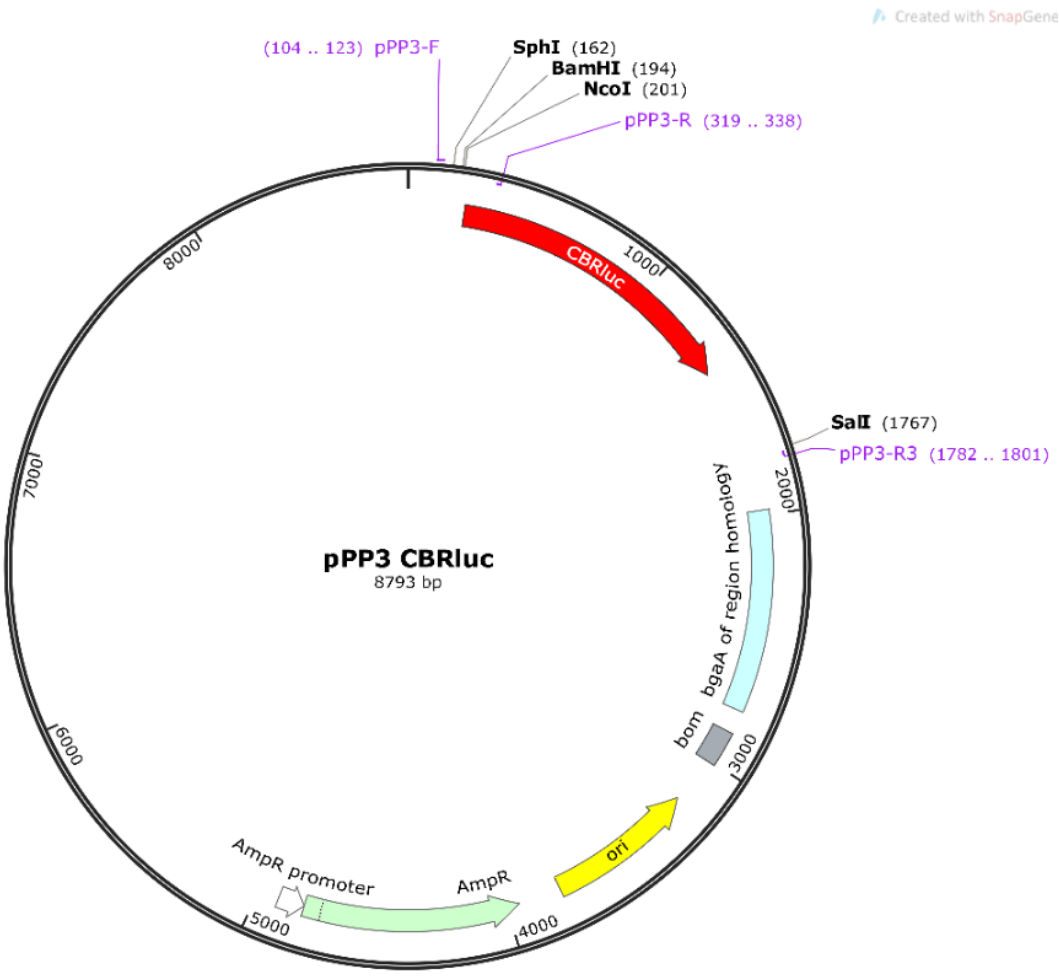

Figure 2.1. A diagram of the pPP3 CBRluc plasmid. AmpR: ampicillin resistance gene, bom: basis of mobility region. MCS: the multi cloning site in the pPP3 plasmid consists of SphI, BamHI, NcoI, and SalI restriction sites. pPP3-F/R/R3 indicates the pPP3 primers. The *bgaA* region of homology for plasmid integration into bgaA (SPD_0562) of NC_008533.2 of the pneumococcal chromosome is also shown.

2.11. DNA clean up after digestion

DNA fragments of interest were extracted and purified using Wizard® SV Gel and the PCR Clean-Up System (Promega, UK). The resulting DNA fragments were transferred to a 1.5 ml Eppendorf tube, and an equal volume of Membrane Binding Solution was added to the DNA fragments. The mixture was transferred into an SV Minicolumn assembly and incubated for 1 min at room temperature. The SV Minicolumn assembly was then centrifuged for 1 min at 14,000 rpm (Microfuge, Sigma) and the resulting supernatant discarded. The column was then washed with 700 µl of Membrane Wash Solution and centrifuged for 1 min at 14,000 rpm. The

supernatant was again discarded, and the washing process repeated with 500 µl of Membrane Wash Solution. The tube was cleaned, and the column assembly re-centrifuged for a further minute with the microcentrifuge lid open to allow evaporation of any residual ethanol before the SV Minicolumn was transferred to a clean 1.5 ml Eppendorf tube and 30 µl of nuclease-free water was applied directly to the centre of the column. The column was incubated at room temperature for 1 min, and then centrifuged at 14,000 rpm for 1 min. The SV Minicolumn was discarded and the Eppendorf tube containing the eluted DNA stored at -20 °C.

2.12. Ligation of DNA fragments

Ligation reactions were conducted in a 20 µl mix including T4 DNA Ligase (NEB, UK) by incubating at 16 °C for 16 h. The mixture included 1 µl (400 U/ µl) of T4 DNA Ligase (NEB, UK), 2 µl of 10 X T4 DNA ligase reaction buffer, a 1:3 molar ratio of plasmid to insert, and nuclease-free water of up to 10 µl.

2.13. Transformation into *E. coli*

The *E. coli* competent cells TOP10 (Thermo Fisher, UK) were used for propagation of recombinant plasmids. An aliquot of ligation mixture was transferred to an aliquot of competent cells, which was then placed in a pre-chilled Falcon tube and incubated on ice for 30 min. The mixture was then incubated in a water bath set at 42 °C for 45 sec before being immediately placed back on ice for 2 min. Finally, 500 µl of Luria broth was added to the transformation reaction and incubated at 37 °C for 90 min in a shaking incubator. The transformation mixture (250 µl) was then plated out on LB agar containing ampicillin before being incubated at 37 °C overnight. The transformation was confirmed by PCR using an empty plasmid as a control. The result was then analysed using electrophoresis with 1% (w/ v) agarose gel.

2.14. Plasmid extraction

The recombinant plasmid was extracted using a QIAprep spin Miniprep kit (Qiagen, UK) on a 10 ml culture that had been inoculated with *E. coli* containing the recombinant plasmid and then incubated overnight at 37 °C for 16 h. The overnight culture was centrifuged at 3,500 rpm for 10 min, and the supernatant was discarded so that the pellet could be re-suspended with 250 µl of Buffer P1 containing RNase A, to which 250 µl of Buffer P2 was added; this was mixed by inverting the tube four times before 350 µl of Buffer N3 was added. The tube was mixed by inverting it a further 4 to 6 times until a cloudy solution was formed, and the mixture was then centrifuged for 10 min at 13,000 rpm. The supernatant was applied to a QIAprep spin column and centrifuged for a further 60 seconds at 13,000 rpm before the flow-through was discarded. The QIAprep spin column was then washed with 500 µl Buffer PB to eliminate any nucleases, then centrifuged for 60 seconds, with the flow-through discarded. The column was washed with 750 µl Buffer PE and then centrifuged twice for 60 seconds each time to remove any residual buffers; all flow-through was discarded. Finally, the QIAprep column was placed in a clean Eppendorf tube and the plasmid was eluted by adding 30 µl Buffer EB (elution buffer), allowing it to stand for 1 min, and then centrifuging it at 13,000 rpm for 1 min. The resulting plasmid DNA was stored at -20 °C until needed.

2.15. DNA Sequencing of pPP4 plasmid

Genetic transformation of the *lux* cassette was also confirmed by DNA sequencing. The extracted recombinant plasmid was amplified using a PrimSTAR reaction, as previously described; this was then purified using the QIAquick PCR purification kit. The samples were sequenced at Eurofins Genomics, Germany, using plasmid specific primers pPP3-F /R3 (Table 2.3).

2.16. Transformation into *S. pneumoniae* D39

The recombinant plasmid was transformed following the procedure described by Bricker and Camilli (1999). The overnight *S. pneumoniae* D39 cultures in BHI at 37 °C were diluted in 10 ml of BHI broth (1:50) then incubated at 37 °C until the OD_{600} was between 0.06 and 0.08. At this stage, 860 µl of bacterial culture was mixed with 100 µl of 100 mM NaOH, 10 µl of 20 %

(w/v) BSA, 10 µl of 100 mM $CaCl_2$, 2 µl of 50 ng/µl competence stimulating peptide (CSP), and ~1 µg of extracted plasmid. This mixture was incubated at 37 °C for 3 h on a standing platform, and every hour, 330 µl of the reaction mixture was plated out on blood agar plates containing tetracycline. The plates were incubated overnight at 37 °C. The resulting recombinant plasmids were screened using PCR with pPP3 primers, (pPP3-F/ R) for promoter construct transformation or pPP3-F/R3 or luxR2 for *lux* cassette transformation; an empty plasmid was also used as a control.

2.17. Biochemical assays

Neuraminidase was assessed using 2-O-(p-Nitrophenyl)-α-D-N-acetylneuraminic acid and pneumolysin activity was assessed by means of a haemolytic assay. The procedures were conducted using crude cell lysates, as described below.

2.17.1. Cell free lysate preparation

A cell free lysate is required for biochemical assays. Overnight cultures of *S. pneumoniae*, grown in 10 ml BHI were thus centrifuged at 3,500 rpm for 10 min. The resulting pellet was re-suspended in 2 ml of PBS, and then, without any addition of protease or protease inhibitors, the re-suspended pellet was sonicated using a sonicator (Sanyo soniprep 150, Japan) at an amplitude of 8 microns for 15 sec at 45 sec intervals on ice to avoid denaturation due to overheating. This sonication process was repeated at least six times. The cell lysate was then transferred to a sterile Eppendorf tube and centrifuged at maximum speed for 15 min at 4 °C using a microfuge. The resulting supernatant was transferred to a sterile Eppendorf tube and stored at -80 °C.

2.17.2. Haemolytic assay

Pneumolysin activity was assessed by means of a haemolytic assay of pneumococcal lysates, as described by Owen et al. (1994). Thus, 5ml PBS and 5ml of defibrinated sheep blood were transferred to universal tubes and centrifuged in a Beckman Coulter AllegraTm X-22R centrifuge at 3,000 RPM at 4 °C for 15 min. The supernatant was discarded from the blood and

4,800 µl of PBS and 200 µl of blood cell pellet were mixed to make a 4% (v/ v) RBC solution. Initially, 50µl PBS was added to each well in a 96 well round bottom microtiter plate, leaving the first wells empty. Then, 100 µl of cell lysate from the strains was taken and put it in the first wells and homogenized, before a two-fold serial dilution was performed across row B; samples were mixed well after each addition. The 50 µl from the last well was discarded, then 50 µl of 4% (v/ v) red blood cells in PBS was added to each well in rows A and B. The plate was then incubated at 37 °C for 30 minutes. Haemolysis was observable directly by eye, with the wells in row B showing around 50% more haemolysis than comparable wells in row A at the point identified as the end of haemolysis.

2.17.3. Neuraminidase activity assay

Neuraminidase activity was assayed using 2-O-(p-Nitrophenyl)-α-D-N-acetylneuraminic acid (pNP-NANA; Sigma, UK) as described by Manco et al. (2006). To initiate the assay, 25 µl of pneumococcal cell lysate was added in triplicate to each well of a 96-well plate and mixed with 25 µl of 0.3 mM pNP-NANA. The plate was then incubated for 2 h at 37 °C. The reaction was stopped by the addition of 100 µl ice-cold 0.5 M Na_2CO_3 to each well. The activity of the NanA was then measured based on readings of the absorbance of released p-nitrophenol at 405 nm in a micro-plate reader (Bio-Rad, United Kingdom), with 25 µl of PBS added to a blank reaction well serving as a control. p-nitrophenyl (Sigma) was used to create a standard curve to measure the activity of neuraminidase in the samples in units that were then expressed as nmol pNP released per minute per microgram of protein under standard assay conditions.

2.18. Bioluminescence studies

2.18.1. *In vitro* bioluminescence quantification

The bioluminescence signal intensity of bioluminescent *S. pneumoniae* strains was quantified as described by Daniel et al. (2013). The procedure was initiated by inoculating an OD_{600} 0.05 dilution of reporter strains from -80 °C (OD_{600} at 0.5) stocks into BHI broth. *S. pneumoniae* type 2 D39 strain (wt) both with a plasmid but lacking promoter and without plasmid were also included in these experiments to verify that the luciferin and luciferase dis not affect the growth of bacteria. After the first stage, 3 x 200 µl aliquots of stock culture were transferred to white, clear bottomed 96-well plates and 0.1 mM click beetle luciferin (from 2 mM stock diluted in

water and stored at -80 °C) (Promega, UK) was added to the wells; 3 x 200 µl aliquots of the same strains without added luciferin were also included. The plate was then placed into a 37 °C 5% CO_2 incubator, with OD_{600} and luminescence readings (611 nm) taken every hour on a luminometer plate reader (Fluostar Omega). The plate reader was set at a gain of 3750 with a setting time of 0.2 seconds, an interval reading of 5 seconds, and a shake of 500 rpm set 10 s before each reading. Sterile BHI broth (3 x 200µl) was used as a negative control for the measurement of bioluminescence, and luciferase and optical density readings were obtained over 8 hours. Maximum growth rates (µ) were calculated during the exponential phase of growth, as described in section 2.4. The luminometer provided light measurements in relative light units (RLU), which are proportional to light intensity (photons/s).

2.18.2. *In vitro* bioluminescence signals versus viable cell numbers using a luminometer

Viable counts of cells and luminescence readings were determined simultaneously at selected time points (0, 2, 4, 6, and 8h). Light emission was quantified as described in section 2.18.1, while viable counts during bioluminescence growth were determined for the populations of culturable cells for all strains as described in section 2.3. The CFU/ml was determined after incubation at 37 °C for 24 h, and the CFU of the mid-log cultures of the bioluminescent strains was used to determine the relative bioluminescence intensity per cell.

2.18.3. Bioluminescent imaging

Light emissions from the colonies were imaged with a highly sensitive, cooled CCD camera mounted in a light-tight specimen box (IVIS). Imaging and quantification of signals was controlled by Living Image software. To initiate this imaging, bioluminescent cells were diluted to OD_{600} 0.05 in appropriate cell culture media on 96-well plates. The substrate luciferin (Promega, UK) was added to all wells with CBRluc strains according to the manufacturer's instructions 10 minutes prior to imaging. Imaging then lasted for 20h. *S. pneumoniae* D39 (wt) with and without empty plasmids were included as controls.

2.18.4. *In vitro* normalisation of bioluminescence signal with colony forming units using IVIS

P*phrA::luc*-wt and Pspd*1717::lux*-wt strains were grown until their mid-log phase. A 200 µl of each culture was then transferred to a 96-well plate and serially diluted. Each dilution was imaged using an IVIS camera and plated for CFU counts, as described in section 2.3. The CFU/ml of each representative dilution was calculated according to section 2.3 to determine relationship of total flux/CFU.

2.19. *In vivo* studies

2.19.1. Pneumococcal dose preparation

An aliquot of pneumococcal strain stock was streaked onto blood agar plates and incubated overnight at 37 °C in a candle jar, then 10 ml of BHI was inoculated with a sweep of colonies from these overnight cultures and incubated at 37 °C until OD_{600} 1.4 to 1.6. The cultures were then centrifuged at 3,000 rpm for 15 min to collect a cell pellet, which was re-suspended with 1 ml of fresh BHI serum broth (80 % v/v BHI and 20 % v/v filtered foetal calf serum). A 700 µl dose of the re-suspended culture was added into 10 ml of fresh BHI-serum medium, and this was incubated to OD_{500} 1.6. The dose was then divided into 500 µl aliquots and stored at -80 °C. After 24h, the cell number of a representative aliquot was determined by thawing the stock and the CFU/ml was checked, as described in section 2.3.

2.19.2. Animal passage of pneumococci and intranasal administration to mice

The bioluminescent strains underwent animal passage in order to prepare a standardised inoculum (Canvin et al., 1995). Non-passaged pneumococci stock was thawed and centrifuged at 13,000 rpm for 3 mins, and the pellet was then re-suspended with PBS to obtain approximately $2x10^7$ CFU/ml. Female CD1 mice aged 7 to 8 weeks old were used, housed in individually ventilated cages. All animal experiments were performed at Leicester University. Mice were infected intranasally with 50 µl of pneumococcal suspension and at predetermined time points post infection, infected mice were anesthetized with 2.5% isoflurane (v/v) over

oxygen (1.5 to 2 litres/ min) and imaged using an IVIS camera, as described in section 2.19.3, or culled for the collection of tissues. Approximately, 50 µl of blood was collected by cardiac puncture using 2 ml syringe, and the collected blood was transferred into 10 ml of fresh BHI and incubated overnight at 37 °C. The next day, the upper section of the bacterial culture was transferred into new universal tubes without disturbing the pelleted blood at the bottom. This culture was then centrifuged at 3,500 rpm for 10 min and re-suspended with 1 ml BHI containing 20% (v/v) of foetal calf serum. A 700 µl dose of re-suspended culture was then added to 10 ml of fresh BHI-serum medium and adjusted to OD_{500} 0.7. The culture was incubated until the OD_{500} reached 1.6, and the culture was then aliquoted into 500 µl fresh tubes that were kept at -80 °C until required. The viable bacteria counts were determined by thawing an aliquot and checking the CFU/ml as described in section 2.3.

2.19.3. *In vivo* mice imaging

Bioluminescence imaging was performed using a IVIS Lumina imaging system (Xenogen Corporation) as described in Daniel et al. (2013). The mice were anesthetised with isoflurane and shaved to optimise signal gain. Luciferin (150 mg/kg) was administered to the mice subcutaneously 15 min before each imaging timeslot. The luciferin was prepared at 15mg/mL in DPBS and the injection amount was determined at 10 µL/g of body weight. Each mouse thus received 150 mg luciferin/kg body weight. All mice were then placed into the specimen chamber of the IVIS imaging system, where a controlled flow of 1.5% isoflurane was administered through a nose cone via a gas anaesthesia system. Light emission was then quantified, with a pseudo colour image representing detected light intensity generated using Living Image software. After this whole body imaging, all mice were sacrificed to determine the bacterial count in their lungs. Dr Hasan Yesilkaya's research group at the University of Leicester performed this infection of mice stage.

2.19.4. Infection of *G. mellonella* with P*phrA::luc*-wt

*G. mellonella (*the wax moth larva), as a non-mammalian animal, is not subject to the ethical limitations of mammalian models. The insects were obtained from Live food, UK, and stored at 12 °C in incubator. Larvae between 0.25 and 0.3 g in weight were used, and ten randomly

chosen insects of the required weight were selected for each group. An inoculation was prepared as described in section 2.19.1, and a 10-µl Hamilton syringe was used to inject 10 µl of the bacterial suspension via the last left proleg in each insect. Larvae were infected with $1x10^4$, $5x10^4$, $1x10^6$ or $2x10^7$ CFU/larvae, at 10 larvae per group. The control group was injected with 10 µL phosphate buffered saline (PBS.) Following the injections, the larvae were incubated at 37 °C to facilitate the progression of the pneumococcal infection. Larvae were then scored as dead or alive at selected time points (8, 24, and 48h): larvae were determined to be dead when they displayed no movement in response to touch and when they showed dark pigmentation due to melanisation. An uninfected group inoculated with 10 µl PBS was included as a control. Three independent replicates of each infection experiment were performed, with average survival results recorded at 8, 24, and 48 h. The bacterial suspension was diluted and plated to determine the CFU/ml, as described in section 2.3, for each inoculation.

2.19.5. Determination of bacterial burden in *G. mellonella*

After larvae were infected with 10 µl doses of different dilutions as described in section 2.19.4 and assessed at selected time points. The live larvae at each time-point (no melanisation) were individually surface sterilized using 70% ethanol before haemolymph was collected into 1.5mL micro centrifuge tubes (Eppendorf, UK), each containing 50 µl of a saturated solution of N-phenylthiourea (Sigma) in distilled water to prevent external melanisation;15µl of haemolymph was thus collected from each larva. Haemolymph samples from four larvae in the same batch were pooled and serially diluted and plated to determine the CFU/ml, as described in section 2.3.

2.19.6. Studying the luciferin effect on the viability of *S. pneumoniae* in *G. mellonella*

Three concentrations of luciferin were used (15 mg/larva, 30 mg/larva, and 60 mg/ larva), creating three groups of larvae infected with the $1x10^7$ CFU/ml *S. pneumoniae* tagged CBRluc system. The first group (n=4) was injected with 3µl of 15 mg/larva luciferin (based on the manufacturer's recommendations for mice) prior to imaging. The second group (n=4) was

injected with 30 mg/larva of luciferin prior to imaging, while the third group received 60 mg/larva luciferin prior to imaging. Every group also included uninfected larvae as a control. Each larva was placed into a 0.5 micro centrifuge tube (Eppendorf, UK) for imaging using IVIS microscopy.

2.19.7. Imaging *S. pneumoniae* P*phrA::luc*-wt to assess *in vivo* bioluminescence intensity and bacterial load

G. mellonella larvae of 25 to 30 mg were injected with different doses of *S. pneumoniae* P*phrA::luc*-wt in 10 µl PBS using a Hamilton syringe, while a control group received just PBS. Larvae were incubated for 2 h at 37 °C in Petri-dishes, then 15 mg/larva luciferin in 10 µl of PBS was injected into each larva. Each insect was then placed into a 0.5 micro centrifuge tube (Eppendorf, UK), and scanned using IVIS, with light production quantified using the Living Image programme. After imaging, haemolymph was collected from the larvae and pooled as described in section 2.19.5 in order to determine and calculate the CFU/ml, as described in section 2.3.

2.19.8. Statistical analysis

Graphpad Prism software (Graphpad, California, USA) was used for all statistical analysis. Where appropriate, one-way or two-way analysis of variance (ANOVA) were used to compare the groups in the studies. A t-test was also used to determine statistical significance for each set f results. The results were expressed as means ± the standard error of the mean (SEM), while significance was defined as * $p < 0.05$, ** $p < 0.01$, *** $p < 0.001$ and **** $p < 0.0001$.

Chapter 3. Results

3.1. Selection and genetic analysis of promoter regions

This study aimed to develop improved reporter strains for enhanced bioluminescence imaging of *S. pneumoniae* during infection of experimental animal models. To achieve this, bioluminescent pneumococcal strains using CBRluc were constructed. CBRluc (click beetle luciferase) is a reporter encoded by a single gene (*luc*), which was characterised in 1978 by (Deluca and McElroy, 1978). This luciferase uses benzothiazole luciferin, along with ATP and oxygen, to generate oxyluciferin, adenosine monophosphate (AMP), CO_2, and light (Hastings, 1996). These constructs were integrated into a known site in the *S. pneumoniae* genome, under the control of promoters predicted to be highly expressed *in vivo,* using pPP3 plasmid kindly provided by Dr Andrew Ulijasz of Loyala University Chicago. This pPP3 plasmid enables stable genomic integration of the promoters with the click beetle *luc* gene. The selected insertion site, *bgaA* locus (codes for ß-galactodisase), is deleted upon such integration; however, *bgaA* deletion is known not to affect virulence (Halfmann et al., 2007). The promoters for the study were selected based on previous reports which indicated a high level of *in vivo* expression as detected by various gene expression assessment tools such as quantitative real time reverse transcriptase assay or Nanostring technology, a reproducible method for detecting the expression of up to 800 genes within a single assay (Geiss et al., 2008). Subsequently, appropriate bioluminescent *S. pneumoniae* strains were constructed and phenotypic characterisation of these completed. Their bioluminescence expression was then tested to identify the most active promoters driving *luc* expression.

The most efficient bioluminescent *S. pneumoniae* strain constructed in this study was then compared with a previously described *lux* system (Francis et al., 2001, Jensch et al., 2010) in terms of bioluminescence expression. To do this, both reporter genes were put under the same promoter, the *phrA* gene, which generated the highest level of bioluminescent induction as determined in this study. Finally, to validate *in vitro* results, *in vivo* experiments were carried out.

3.1.1. Analysis of pPP3 CBRluc plasmid

In order to construct the required bioluminescent strains, several experiments were performed. The initial experiment involved verification of pPP3 CBRluc, in which the plasmid was restriction digested and analysed by means of PCR to confirm its identity. An aliquot of plasmid was digested using NcoI restriction endonuclease, which linearised the plasmid, producing an expected size of approximately 9 kb of product, as shown in lane 2, Figure 3.1. The undigested plasmid appears to migrate faster than the linearised plasmid, potentially because the supercoiled plasmid is smaller in size, and hence may experiences less frictional resistance from the gel, allowing it to migrate more rapidly. In addition to restriction endonuclease analysis, the identity of the plasmid was confirmed by means of PCR using the specific primers (pPP3-F/ R) listed in Table 2.3 that target the cloning site. The reaction amplified approximately 234bp product, as shown in lane 2, Figure 3.2, which was consonant with the expected product size. Genetic analysis also proved the presumptive identity of pPP3 CBRluc.

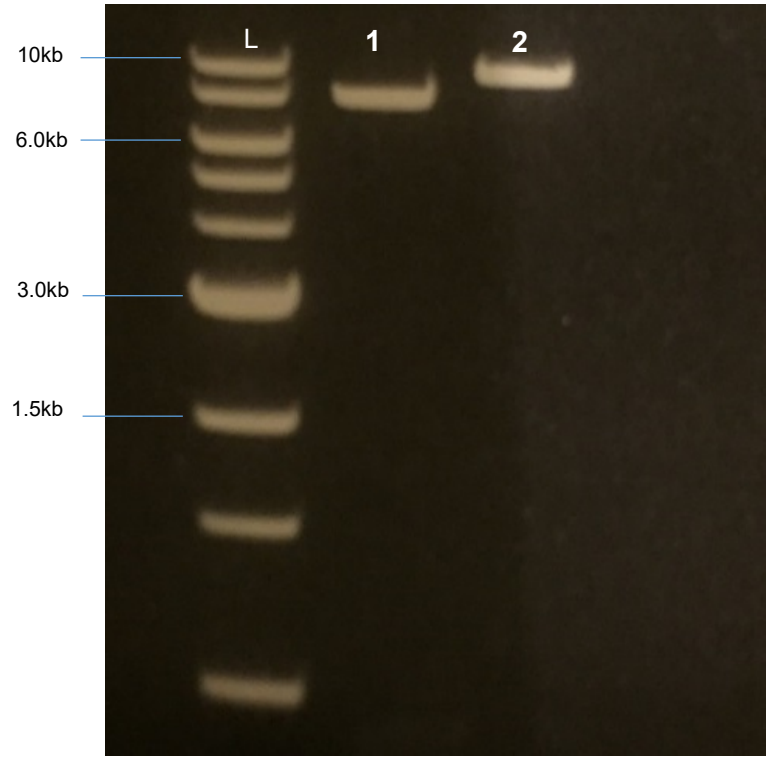

Figure 3.1. Gel electrophoresis showing digested and undigested pPP3 CBRluc. Lane (1) shows undigested plasmid, and lane (2) shows an approximately correct size of NcoI digested plasmid, 9kb. L: 500 ng of 1Kb DNA ladder.

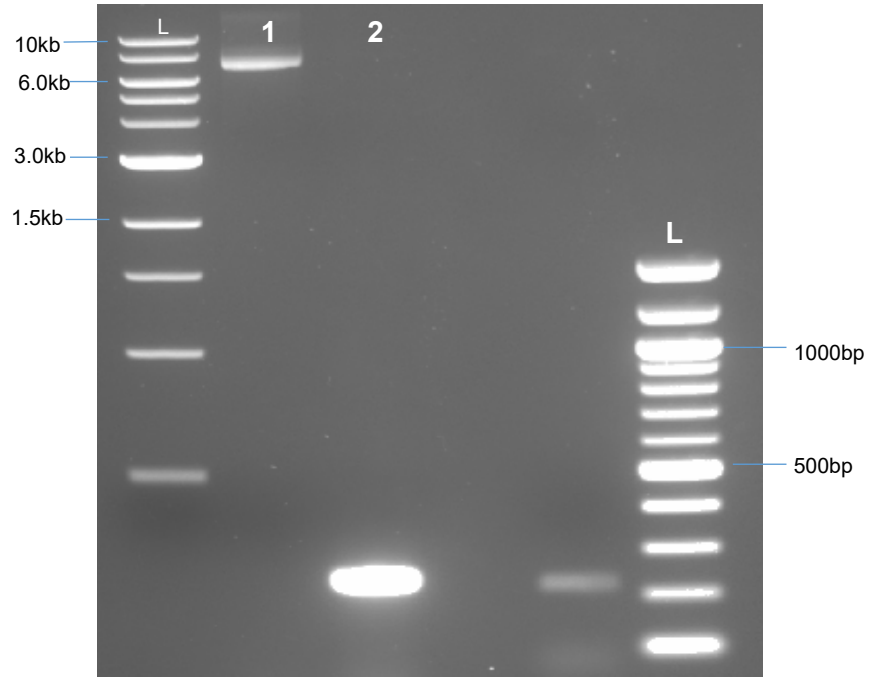

Figure 3.2. Agarose gel electrophoresis analysis showing the extracted plasmid (lane 1) as a control and the amplicons (lane 2), for a product of about 234 bp at the expected size. L: 500 ng of 1 kb DNA ladder.

3.1.2. Construction of a Click Beetle Red Luciferase Reporter System (CBRluc)

The main objective of this project was to construct a bioluminescent pneumococcal strain by integrating the reporter *luc* into a known site in the *S. pneumoniae* genome, under the control of promoters predicted to highly express within these genes. Bioluminescent *S. pneumoniae* were thus constructed with five different promoters of genes that have been reported to demonstrate high levels of expression *in vivo*.

The selected genes included pyruvate formate lyase, *pflB,* which is essential for galactose metabolism, as this is the most abundant sugar within the structure of respiratory mucin (Yesilkaya et al., 2009). The fermentation process is important for *S. pneumoniae*'s generation of energy, which occurs in two ways: homolactic and mixed-acid fermentation (Al-Bayati et al., 2017, Carvalho et al., 2011). In the presence of galactose, mixed-acid fermentation occurs, which generates acetyl-CoA and formate from pyruvate under microaerobic and anaerobic conditions by means of pyruvate formate lyase, which is coded by *pflB* (Al-Bayati et al., 2017). One of the Phr-peptide signalling systems, *phrA*, also plays a role in quorum sensing and is thus important in terms of pathogenicity (Motib et al., 2019). Quorum sensing is a bacterial cell-to-cell signalling system that enables bacterial populations to coordinate gene expression in response to various environmental stimuli (Miller and Bassler, 2001). PspA (pneumococcal surface protein A) promotes inhibition of the complement system during pneumococcal infection (LeMessurier et al., 2006), while *vp1* (virulence peptide) controls the pneumococcal biofilm (Cuevas et al., 2017) and *htrA* (high temperature requirement A) is important in developing resistance to elevated temperatures and oxidative stress (Ibrahim et al., 2004). The *16S rRNA* gene was used as internal control due to its stability of expression (Scholz et al., 2012) .

3.1.2.1 Amplification of putative promoter regions

The amplification of putative promoter regions was performed to clone them into the pPP3 CBRluc. The putative promoter regions (represented by "P") of *pflB* (205bp) (P*pflB*), *phrA* (191bp) (P*phrA*), *16S rRNA* (295bp) (P*rrnA*), *pspA (*571bp) (P*pspA*), *vp1* (318bp) (P*vp1*), and *htrA* (210bp) (P*htrA)* were amplified by means of primers incorporating SphI and BamHI recognition sites. PCR was then performed using HotStarTaq (Section 2.6), and the amplified

PCR products were purified using a DNA purification kit (Section 2.11). Successful amplification of putative promoters is shown in Figure 3.3.

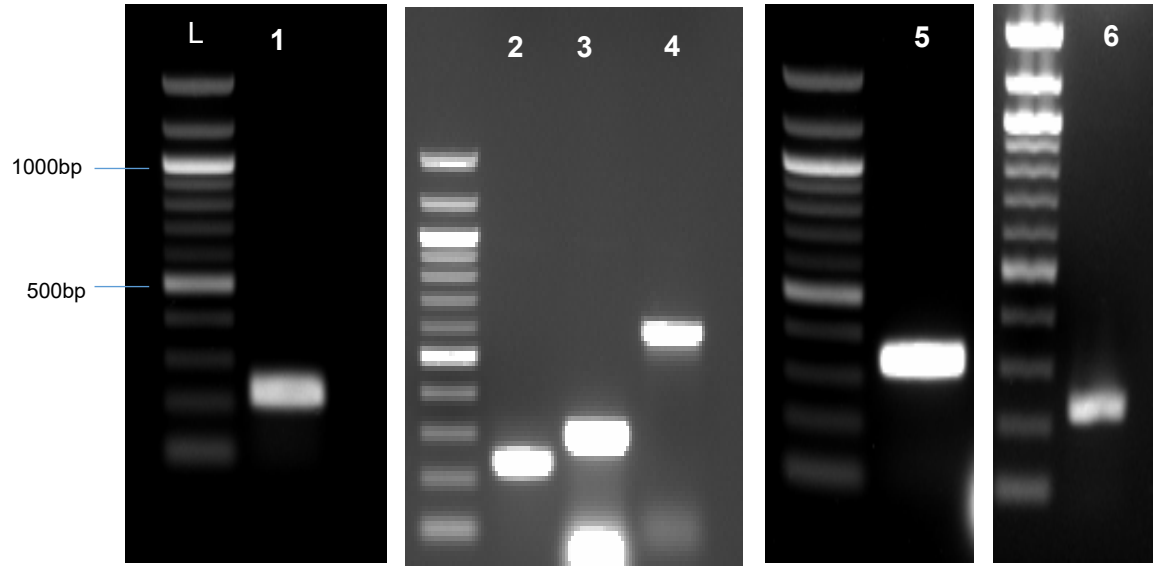

Figure 3.3. Agarose gel electrophoresis analysis confirming the successful amplification of putative promoter fragments belonging to P*pflB* (205bp), P*phrA* (191), P*rrnA* (295bp), P*pspA* (571bp), P*vp1*(318bp), and P*htrA* (210bp) in lanes 1, 2, 3, 4, 5, and 6, respectively. L: 100bp DNA ladder.

3.1.2.2. Construction of recombinant pPP3 CBRluc and its transformation into *E. coli*

The putative promoter regions of *pflB* (205bp), *phrA* (191bp), *16S rRNA* (295bp), *pspA* (571bp), *vp1*(318bp), and *htrA* (210bp) were amplified by primers incorporating SphI and BamHI recognition sites (Table 2.3). The amplified PCR products were then purified using a DNA purification kit (Section 2.11), and the restriction enzymes SphI and BamHI were used to digest the inserts. The plasmid and those inserts with compatible ends were ligated as described in section 2.12; these ligation mixtures were then transformed into *E. coli* TOP10.

The results were analysed using PCR; the empty plasmid was also included, acting as a control to show the expected size with and without promoters. The results are shown in Figures 3.4, 3.5, 3.6, 3.7, 3.8, and 3.9, and these confirm the success of the cloning into pPP3 CBRluc. The amplicons, of an expected size of approximately 437bp for P*pflB,* are shown in

Figure 3.4 in lanes 2, 3, 5, 6 and 7, while the other lanes (1, 4, 8, 9, 10 and 11) contain the amplicons from the empty plasmid. Amplified products of approximately 232bp show correspondence with the multiple cloning site regions in pPP3 CBRluc. The successful cloning of *PphrA* into the pPP3 CBRluc is thus confirmed in Figure 3.5 in lanes 1, 2 and 3, which display amplicons of about 423bp in size, while the amplicons in lane 4 represent the cloning site region in empty pPP3. The successful cloning of P*rrnA* into CBRluc is shown in lane 1 of Figure 3.6, which contains amplicons of 527bp in size, including the putative promoter region (295bp) and a 232 bp region of a vector sequence, while the amplicons representing the empty plasmid (232 bp) are shown in lane 2.

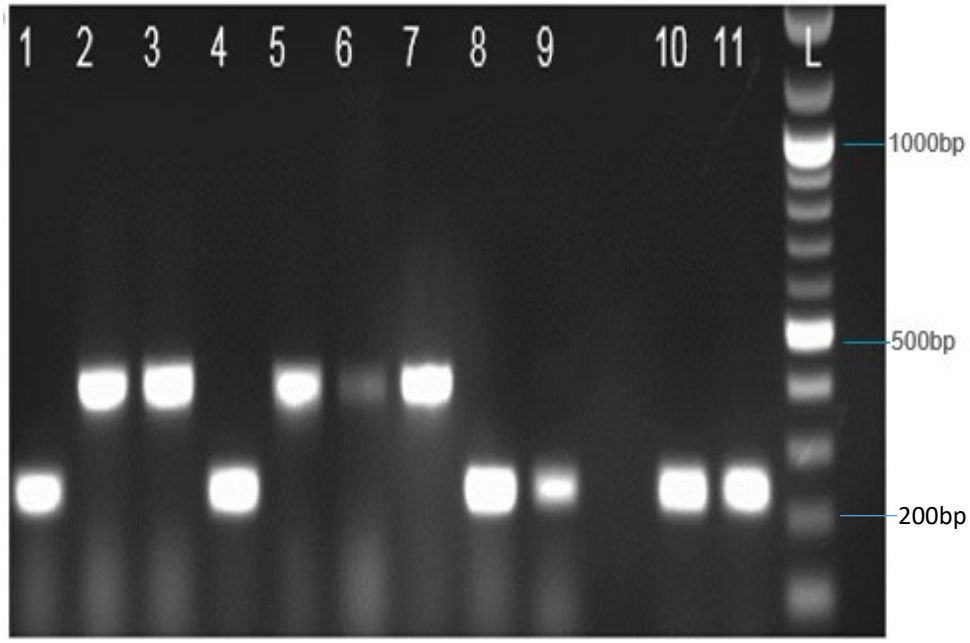

Figure 3.4. Agarose gel electrophoresis confirming the cloning of P*pflB* into pPP3 CBRluc. The amplicons in lanes 2, 3, 5, 6, and 7, at about 437 bp, represent the putative promoter region (205bp) with 232 bp is the region around the multiple cloning sites in pPP3; the clones in lanes 1, 4, 8, 9, 10 and 11 did not have an insert. L: 100bp DNA ladder.

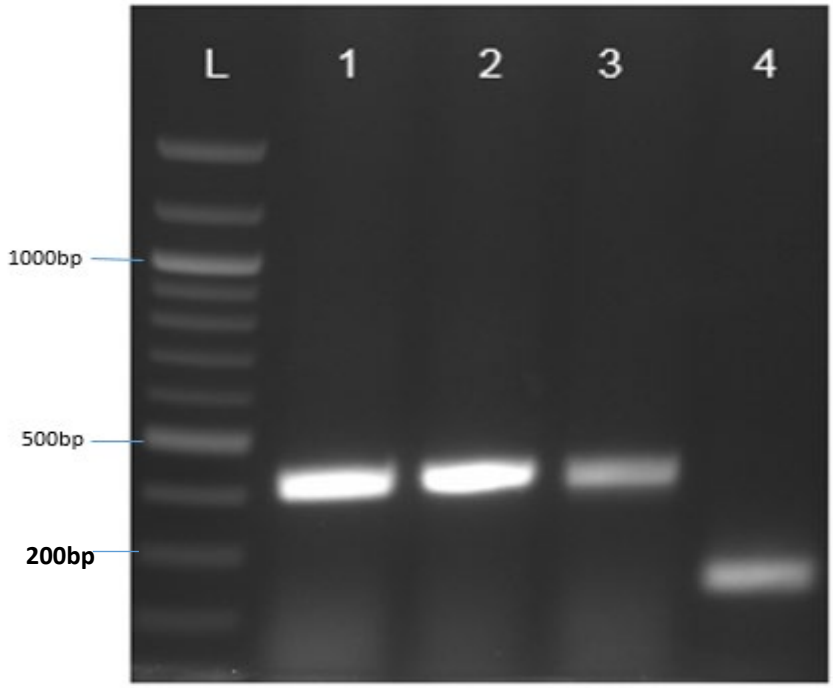

Figure 3.5. Agarose gel electrophoresis confirming the cloning of P*phrA* into pPP3 CBRluc. The amplicons in lanes 1, 2 and 3 are at about 423bp, including the putative promoter region (191 bp), with the 232 bp region representing the region surrounding the cloning site. L: 500 ng of 100bp DNA ladder.

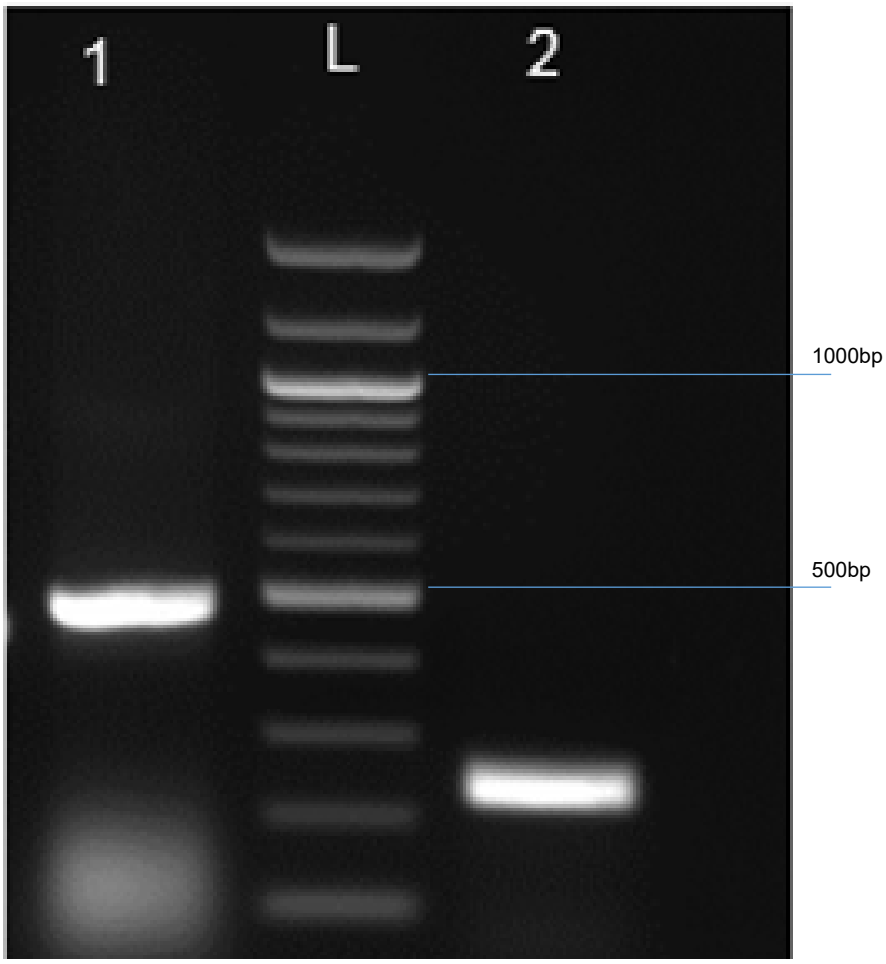

Figure 3.6. Agarose gel electrophoresis confirming the cloning of P*rrnA* into pPP3CBRluc plasmid. The amplicons in lane 1 are at about 527bp, including the putative promoter region (295bp), with 232 bp being the region of the vector sequence; the empty plasmid (235bp) is used as the control in lane2. L: 500 ng of 100bp DNA ladder.

P*pspA* cloning into pPP3CBRluc plasmid was confirmed, as shown in Figure 3.7, lane 1, with amplicons at about 803 bp, including the putative promoter region (571bp) and the 232 bp region of the vector sequence; the amplicons from the empty plasmid (235bp) are shown in in lane 2. Figure 3.8 demonstrates the successful cloning of P*vp1* into pPP3 CBRluc. Lanes 1, 3, 4, 5, 6 and 8 show positive results, with approximately 550 bp product, including the putative promoter region (318bp), with the 232 bp region representing the cloning site; the amplicons from the empty plasmid (approximately 235 bp) are shown in lanes 9 and 10. P*htrA* cloning into pPP3 CBRluc plasmid was also confirmed in Figure 3.9, in lanes 1 to 6, by successful amplification of approximately 442 bp; the amplicon is constructed of the putative promoter region (210bp), with the 232 bp region representing the cloning site. The amplicons from the empty plasmid are depicted in lane 7.

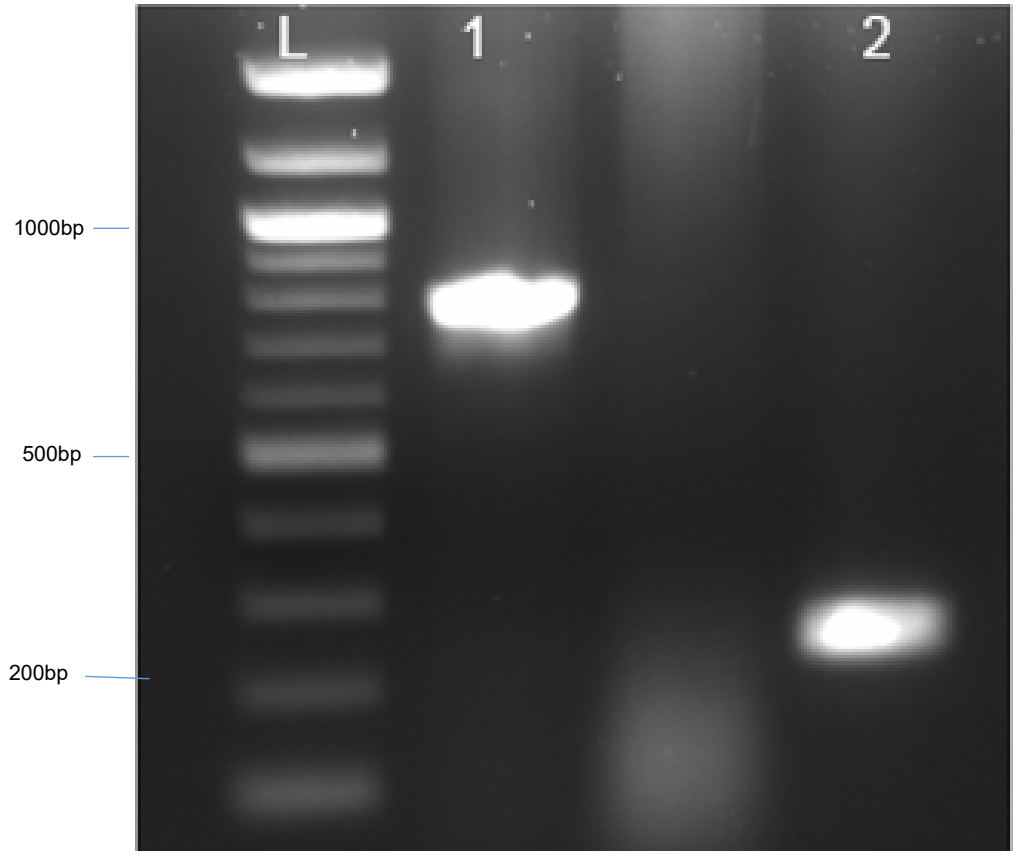

Figure 3.7. Agarose gel electrophoresis confirming the cloning of P*pspA* into pPP3CBRluc. Amplicons in lane 1 are at about 803bp, including the putative promoter region (571bp), with the 232 bp region representing the cloning site. The amplicons from the empty plasmid are shown in lane 2 (235bp). L: 500 ng of 100bp DNA ladder.

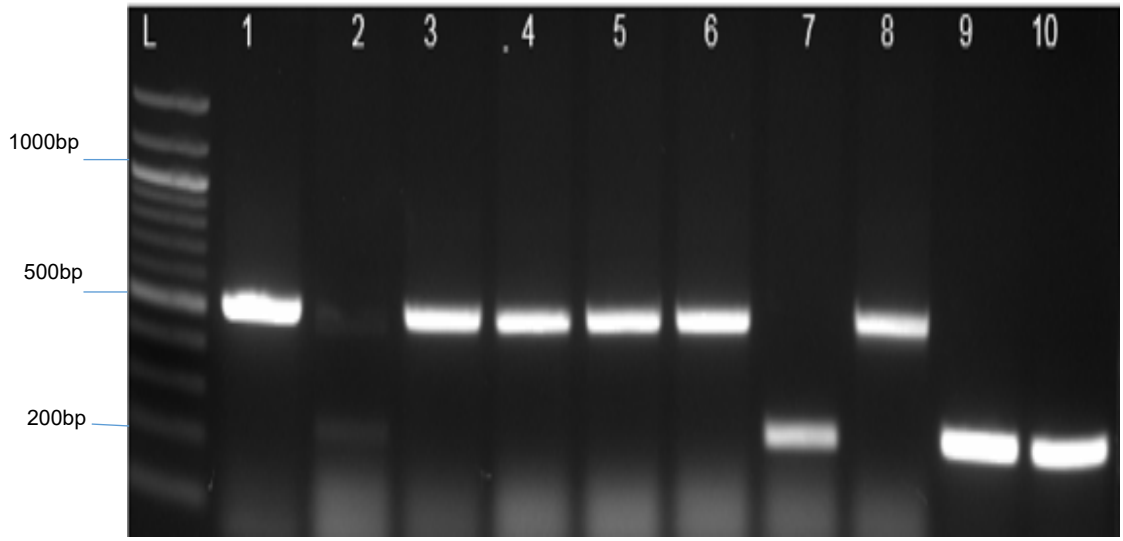

Figure 3.8. Agarose gel electrophoresis confirming the cloning of P*vp1* into pPP3CBRluc. Lanes 1, 3, 4, 5, 6 and 8 show positive results with ~550 bp product. The amplicons from the empty plasmid generated approximately 235 bp product (lanes 7, 9, and 10). L: 100bp DNA ladder.

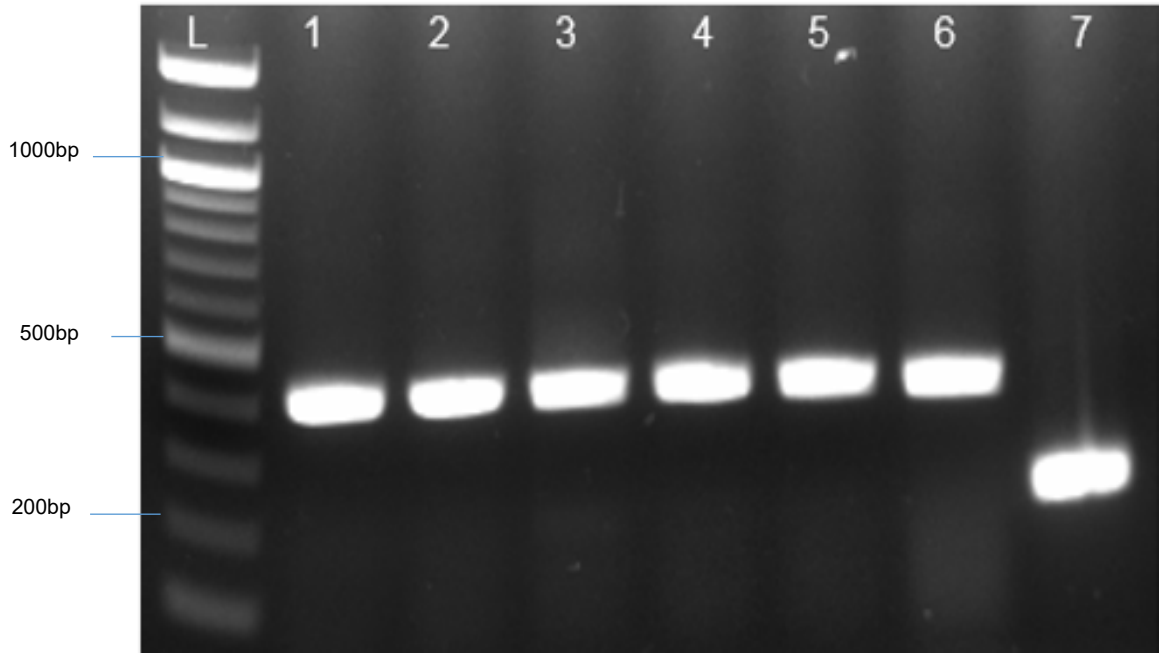

Figure 3.9. Agarose gel electrophoresis confirming the cloning of P*htrA* into pPP3CBR*luc.* Amplicons in lanes 1-6 at ~ 442bp contained the putative promoter region (210bp), with the 232 bp region representing the cloning site. The empty plasmid (lane7) generated 235bp. L: 500 ng of 100bp DNA ladder.

3.1.2.3 Integration of CBRluc constructs into *S. pneumoniae* D39 and confirmation by PCR

To integrate CBRluc constructs into the *S. pneumoniae* genome in a single copy, an aliquot of recombinant pPP3 CBRluc plasmid was transformed into an *S. pneumoniae* D39 strain. The transformants were selected on a blood agar containing 15 µg/ml tetracycline, and the selected transformants were analysed by PCR using pPP3-F/R primers; an empty plasmid was included as a control.

As indicated in Figures 3.10, 3.11, 3.12, 3.13, 3.14, and 3.15, the successful transformation was confirmed by 1% (w/v) agarose gel electrophoresis. Amplified products of 437bp for P*pflB* (Figure 3.10) are shown in lanes 3 and 4, while the 423bp band for P*phrA* (Figure 3.11) appears in lanes 1 to 5 . A product of 527 bp for P*rrnA* is depicted in lanes 1, 2 and 3 in Figure 3.12, while a 550 bp product represents the amplicons for P*vp1* as seen in lanes 1 to 4 of Figure 3.13. An 803 bp band for P*pspA* is shown in lanes 1 to 3 in Figure 3.14, while lanes 1 to 9 in Figure 3.15 include the 442 bp product for P*htrA*. An empty plasmid was used as a control for all transformation reactions, generating a product at 235bp when pPP3-F/ R primers were used.

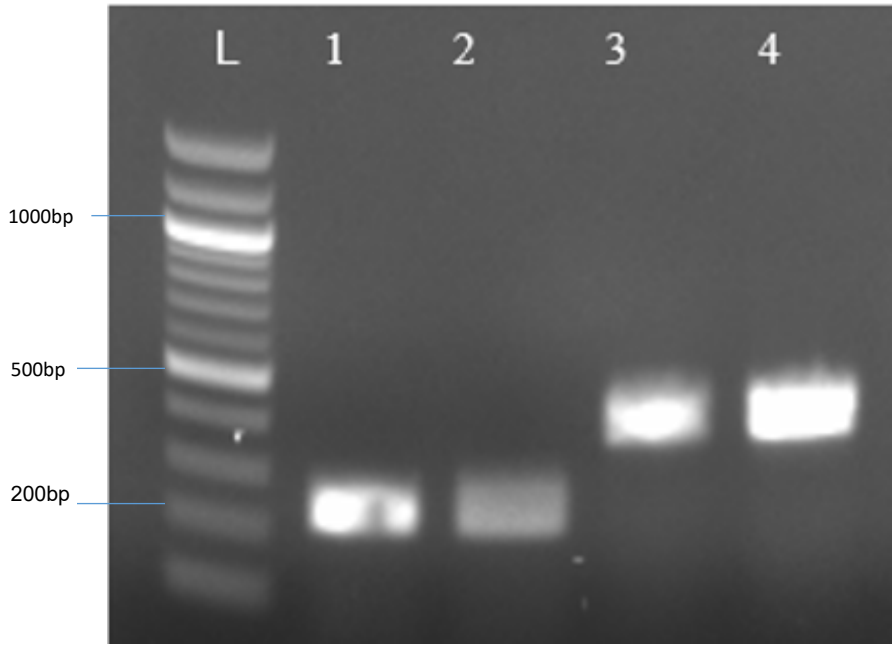

Figure 3.10. Agarose gel analysis of selected transformants for integration of P*pflB::luc* to *S. pneumoniae*. Lanes 3 and 4 show positive results, with a 437 bp product. The empty plasmid

generates an approximately 235 bp product, when pPP3-F/R primers are used, (lanes 1 and 2) as a control. L: 100bp DNA ladder.

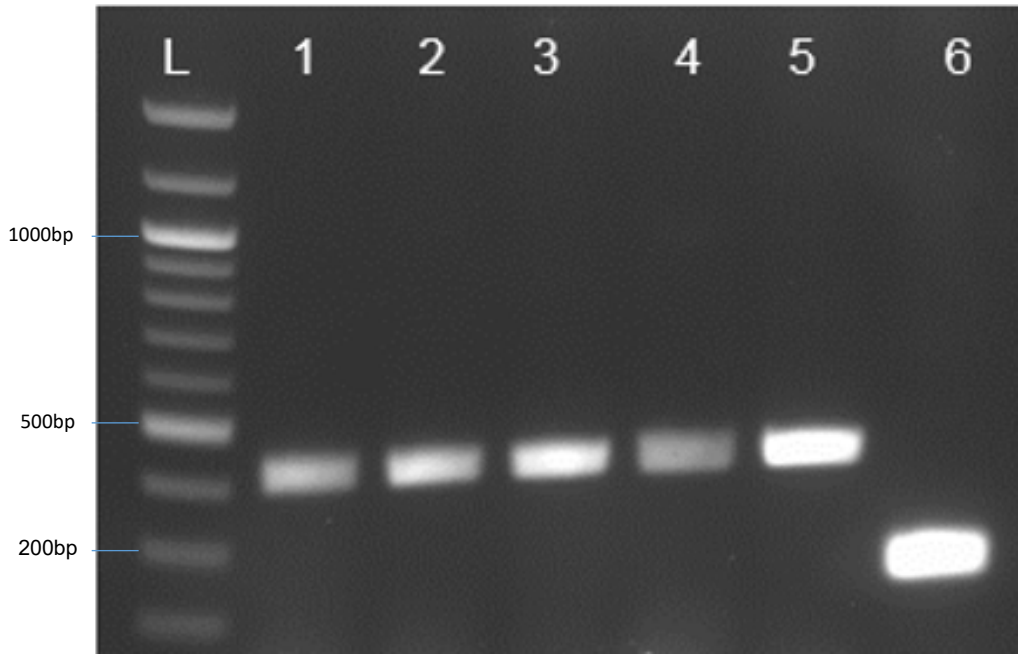

Figure 3.11. Agarose gel analysis of selected transformants for integration of P*phrA::luc* to *S. pneumoniae.* Lanes 1, 2, 3, 4 and 5 show positive results with 423 bp product. The empty plasmid generates approximately 235 bp product when pPP3-F/ R primers are used (lane 6) as a control. L: 100 bp DNA ladder.

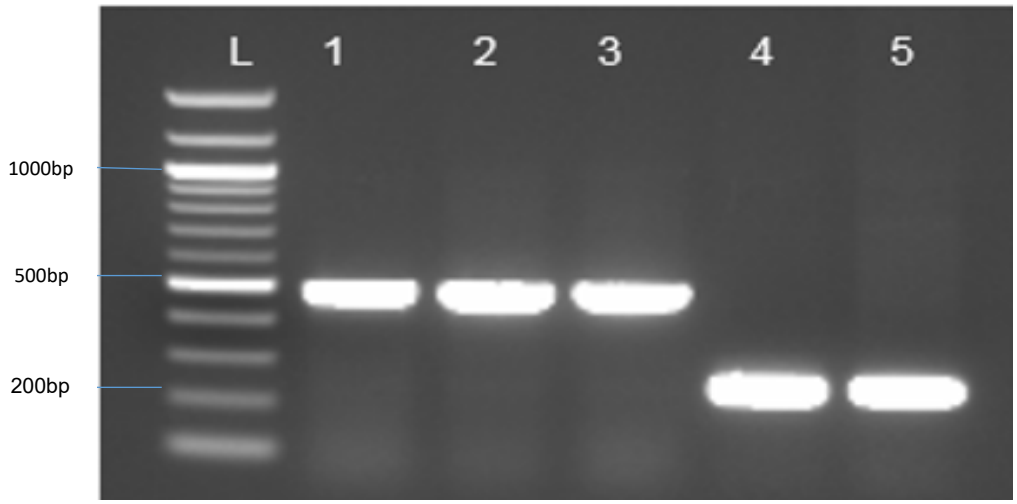

Figure 3.12. Agarose gel analysis of selected transformants for integration of P*rrnA::luc* to S. pneumoniae. Lanes 1, 2 and 3 show positive results with 527 bp product. The empty plasmid generates approximately 235 bp product when pPP3-F and pPP3-R primers are used, (lanes 4 and 5) as a control. L: 100bp DNA ladder.

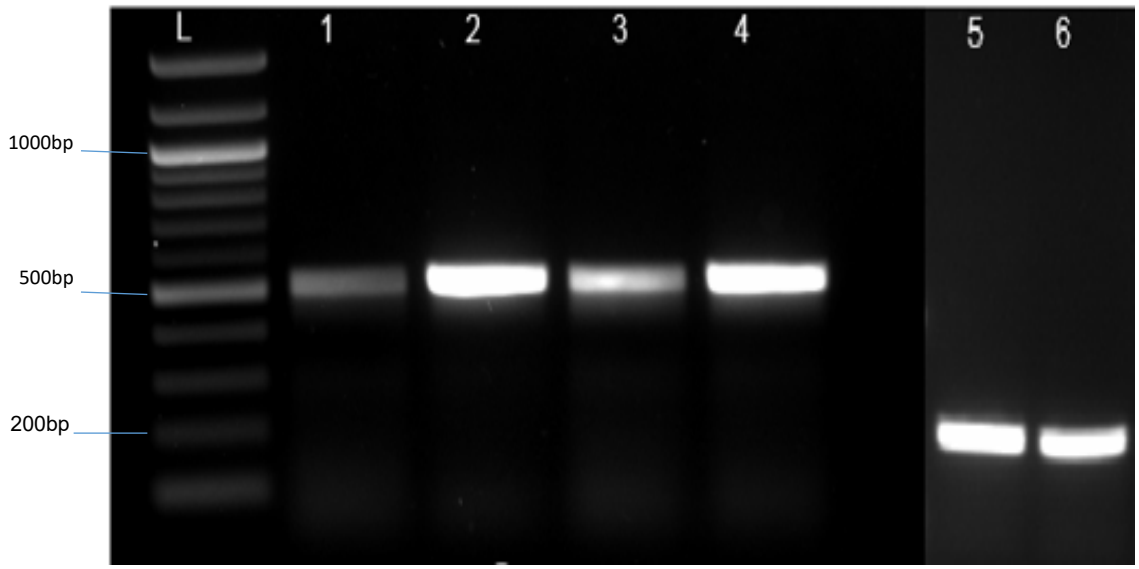

Figure 3.13. Agarose gel analysis of selected transformants for integration of P*vp1::luc* to *S. pneumoniae*. Lanes 1, 2, 3 and 4 show positive results with 550 bp product. The empty plasmid used as a control generates approximately 235 bp product as seen in lanes 5 and 6. L: 100 bp DNA ladder.

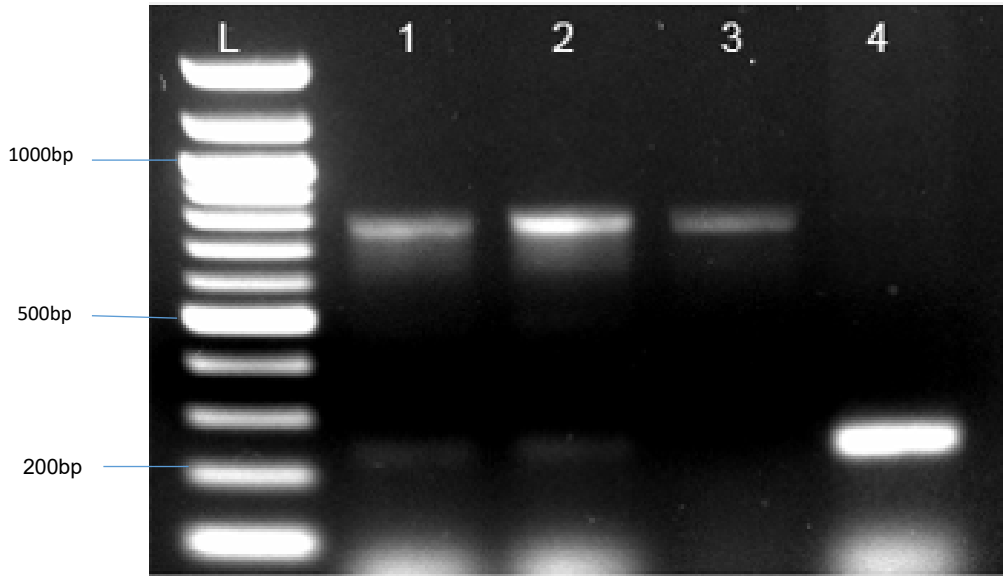

Figure 3.14. Agarose gel analysis of selected transformants for integration of P*pspA::luc* to *S. pneumoniae*. Lanes 1, 2 and 3 show positive results, with 803 bp product. The empty plasmid used as a control generates approximately 235 bp product in lane 4. L: 100bp DNA ladder.

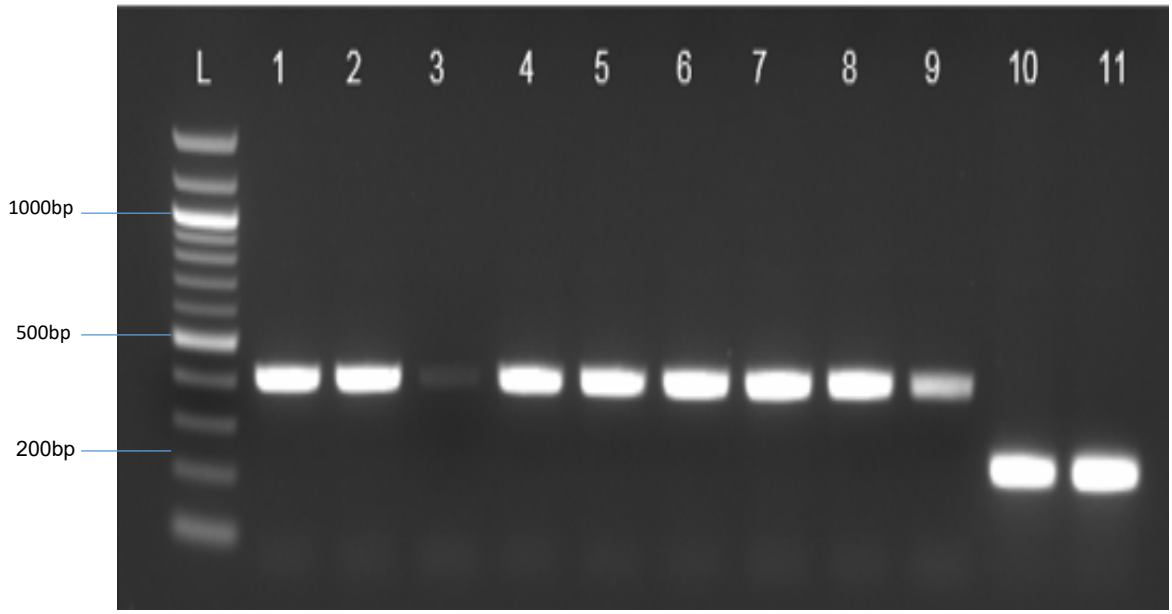

Figure 3.15. Agarose gel analysis of selected transformants for integration of P*htrA*::*luc* to *S. pneumoniae*. Lanes 1 to 9 show positive results, with 442 bp product. The empty plasmid generates approximately 235 bp product when pPP3-F/ R primers are used (lanes 10 and 11) as a control. L: 100bp DNA ladder.

3.2. Phenotypic characterisation of *S. pneumoniae* bioluminescent strains

To check the growth behaviour of the produced bioluminescent strains as compared to the wild type, the strains were grown in BHI, with additional reporter strains grown in CDM supplemented with 55 mM glucose or galactose as the sole carbon source at 37 °C, as described in section 2.4, used to determine whether any effects on sugar metabolism arise from reporter gene integration. *S. pneumoniae* requires a carbon source to generate energy to grow in the respiratory tract, yet the ability of bacteria to grow with only limited requirements for carbon sources most likely mimics the "natural" growth of pneumococcus in the respiratory tract and blood. The wild type D39 and a strain containing pPP3 CBRluc, in the form of an empty plasmid without a promoter, were included as controls for the phenotypic analysis.

The effect of reporter gene integration on the production of virulence factors was then determined by measuring various important virulence determinants of *S. pneumoniae*, including neuraminidase and pneumolysin. All experiments were undertaken both with and without luciferin in order to examine the effects of luciferin on both the growth phenotype and expression of virulence proteins.

3.2.1. Growth of pneumococcal strains in Brain Heart Fusion (BHI)

CBRluc strains were grown in BHI media both with and without substrate (luciferin), with growth recorded at 8 h at OD_{600}. No significant differences in growth rate and yield were observed for any of the pneumococcal strains (Figure 3.16 A, B), suggesting that neither plasmid nor the addition of luciferin impede pneumococcal growth profiles. The growth rates and yield were calculated as described in section 2.4, and application of a one-way ANOVA and a Dunnett's multiple comparison test revealed no significant differences in the growth profiles between strains ($p > 0.05$).

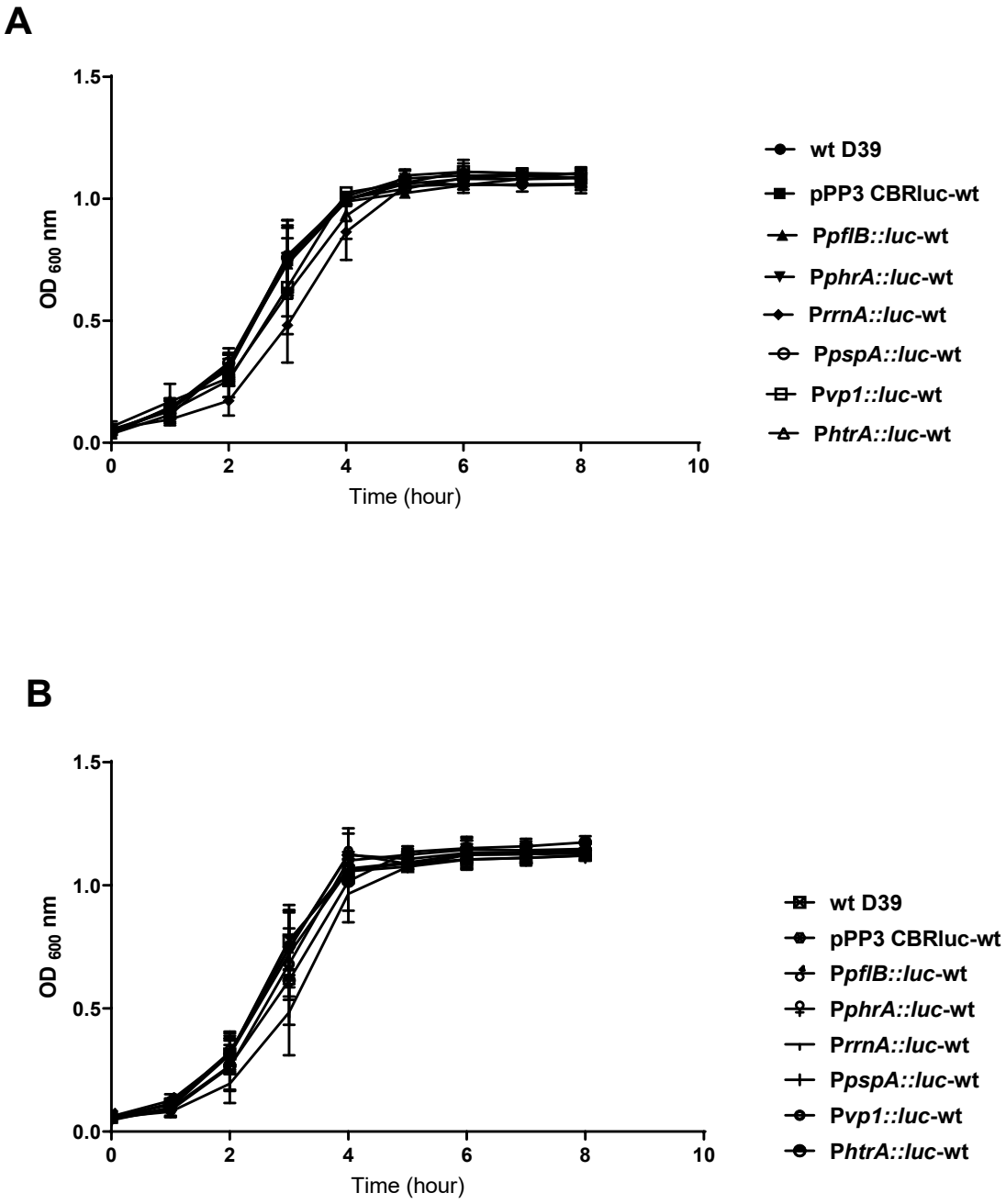

Figure 3.16. Growth profiles of the CBRluc strains and D39 wild type in BHI media with (A) and without (B) luciferin. No significant difference in the growth profiles of the strains was observed as assessed by one-way ANOVA and Dunnett's multiple comparison testing ($p > 0.05$). The experiment was repeated four times for each strain; the vertical line represents the standard error of the mean.

Table 3.1. Growth rate (μ) and growth yield (Max OD_{600}) of pneumococcal strains grown with (+) and without luciferin in BHI. Values are the average of three replicates of four experiments. (±) indicates standard errors of mean (SEM).

Strains	Growth rate μ (h^{-1}) specific Growth rate during the exponential phase (h^{-1})	Growth yield (Max OD_{600})
wt D39+	0.34±0.01	1.08± 0.029
wt D39	0.37±0.03	1.138±0.034
pPP3 CBRluc-wt +	0.34±0.03	1.103±0.022
pPP3 CBRluc-wt	0.4±0.07	1.167± 0.049
P*pflB::luc*-wt+	0.33±0.01	1.104±0.015
P*pflB::luc*-wt	0.37±0.04	1.156± 0.051
P*phrA::luc*-wt +	0.35±0.02	1.110± 0.026
P*phrA::luc*-wt	0.4±0.07	1.131± 0.026
P*rrnA::luc*-wt +	0.34±0.04	1.085±0.012
P*rrnA::luc*-wt	0.38±0.05	1.145± 0.028
P*pspA::luc*-wt +	0.33±0.02	1.12±0.020
P*pspA::luc*-wt	0.37±0.04	1.165± 0.032
P*vp1::luc*-wt +	0.38±0.03	1.145±0.038
P*vp1::luc*-wt	0.42±0.05	1.167±0.032
P*htrA::luc*-wt +	0.33±0.02	1.149±0.021
P*htrA::luc*-wt	0.37±0.057	1.188± 0.034

There were no significant differences among strains in terms of growth rate ($p > 0.05$).

3.2.2. Evaluation of growth of bioluminescent strains in CDM supplemented with glucose or galactose

To mimic the “natural” growth of pneumococcus in the respiratory tract, bioluminescent constructs were grown in chemical defined media (CDM) supplemented with 55 mM of either glucose or galactose. The resulting growth profiles were then compared to the wild type growth to assess effects on growth behaviour. Figures 3.17 A and B and 3.18 A and B show similar growth profiles in reporter and non-reporter strains (wt, pPP3 CBRluc-wt) with and without exogenous substrate (luciferin) in CDM. A Dunnett's multiple comparison test revealed no significant difference in growth among pneumococcal strains irrespective of luciferin additions.

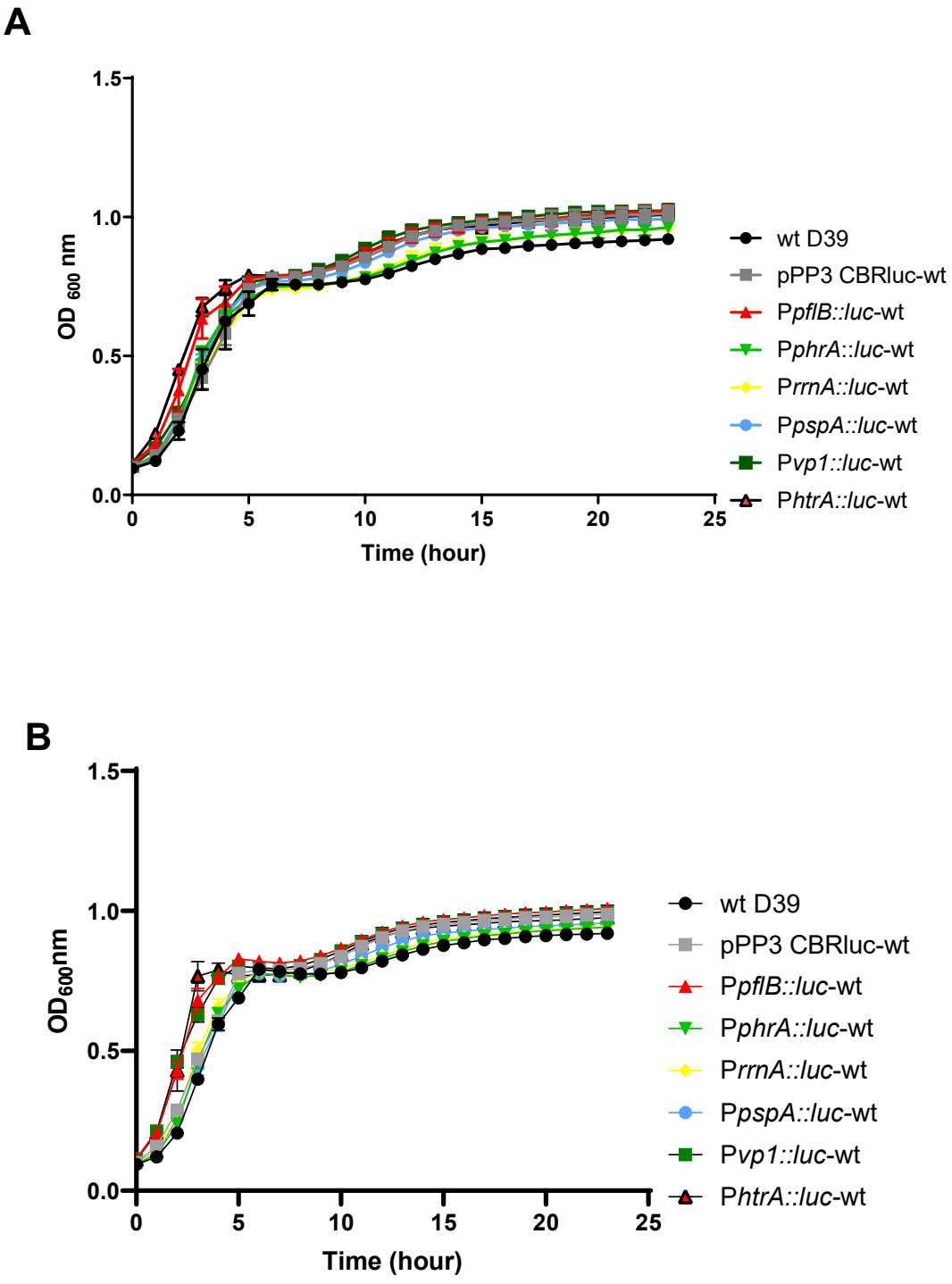

Figure 3.17. Growth profiles of pneumococcal strains with (A) and without the addition of luciferin (B) in CDM supplemented with 55 mM glucose. No significant difference in growth profiles was seen between strains as assessed by one-way ANOVA and Dunnett's multiple comparison testing ($p > 0.05$). Each datum point is the mean of three independent tests.

Table 3.2. Growth rate (μ) and yield (maximal OD_{600}) of pneumococcal strains grown with (+) or without luciferin in CDM supplemented with 55 mM glucose. Values are the averages of three replicates of experiments. (±) indicates the standard errors of means (SEM).

Strains	Growth rate μ (h^{-1}) specific Growth rate during the exponential phase (h^{-1})	Growth yield (Max OD_{600})
wt D39+	0.1416 ±0.006	0.921±0.005
wt D39	0.1421±0.003	0.929± 0.002
pPP3 CBRluc-wt+	0.1494±0.001	1.013±0.015
pPP3 CBRluc-wt	0.1543±0.0008	0.987± 0.012
P*pflB::luc*-wt+	0.1487 ±0.0007	1.021±0.013
P*pflB::luc*-wt	0.1555 ±0.002	1.008±0.011
P*phrA::luc*-wt+	0.1438 ±0.0008	0.962± 0.010
P*phrA::luc*-wt	0.14766±0.001	0.942±0.014
P*rrnA::luc*-wt+	0.1405±0.0009	0.960±0.011
P*rrnA::luc*-wt	0.1519±0.002	0.946± 0.010
P*pspA::luc*-wt+	0.1511±0.005	0.994±0.011
P*pspA::luc*-wt	0.1534 ±0.001	0.957± 0.012
P*vp1::luc*-wt+	0.1492±0.003	1.027±0.009
P*vp1::luc*-wt	0.1472±0.002	0.997± 0.025
P*htrA::luc*-wt+	0.1424±0.002	1.009± 0.012
P*htrA::luc*-wt	0.1403 ±0.0023	0.975±0.020

No significant difference was found among strains in terms of growth rate ($p > 0.05$).

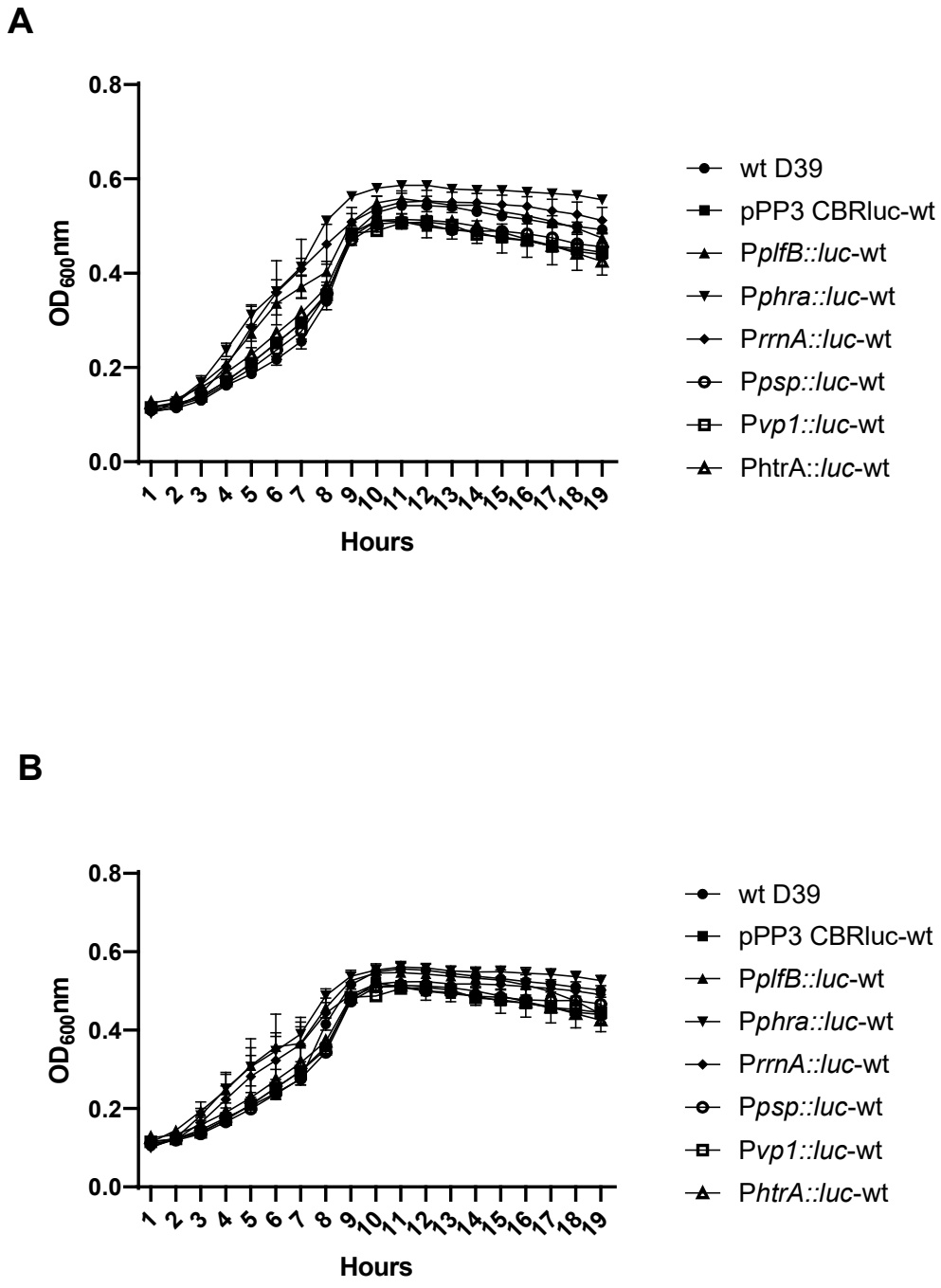

Figure 3.18. Growth profiles of pneumococcal strains with (A) or without (B) addition of luciferin grown in CDM supplemented with 55 mM galactose. There was no significant difference between the strains and wild type in terms of growth rate based on a Dunnett's multiple comparison test. Each point is the mean of three independent tests.

Table 3.3. Growth rate (μ) and yield (maximal OD_{600}) of pneumococcal strains grown in CDM supplemented with 55 mM galactose. Values are averaged across three experiments. (±) indicates the standard errors of means (SEM).

Strains	Growth rate μ (h^{-1}) specific Growth rate during the exponential phase (h^{-1})	Growth yield (Max OD_{600})
wt D39+	0.053±0.001, n=3	0.54±0.004
wt D39	0.056±1.71, n=3	0.55±0.001
pPP3 CBRluc-wt +	0.051±0.001, n=3	0.51±0.016
pPP3 CBRluc-wt	0.050±0.001, n=3	0.52±0.019
P*pflB::luc*-wt+	0.055±0.002, n=3	0.55±0.012
P*pflB::luc*-wt	0.054±0.003, n=3	0.54±0.024
P*phrA::luc*-wt+	0.062±0.001, n=3	0.586±0.003
P*phrA::luc*-wt	0.059±0.0017, n=3	0.55±0.013
P*rrnA::luc*-wt+	0.056±0.004, n=3	0.55±0.023
P*rrnA::luc*-wt	0.054±0.001, n=3	0.52±0.007
P*pspA::luc*-wt+	0.051±0.002, n=3	0.50±0.003
P*pspA::luc*-wt	0.051±0.001, n=3	0.51±0.012
P*vp1::luc*-wt+	0.052±0.001, n=3	0.506±0.008
P*vp1::luc*-wt	0.052±0.001, n=3	0.50±0.008
P*htrA::luc*-wt+	0.050±0.001, n=3	0.51±0.0034
P*htrA::luc*-wt	0.050±0.0007, n=3	0.514±0.003

There are no significant differences between the strains and wild type in terms of growth rate based on Dunnett's multiple comparison testing.

3.2.3 Assessing bioluminescent pneumococcal strains for the production of proteins involved in virulence

After testing CBRluc strains for growth behaviours, investigation of whether pPP3 CBRluc integration affects neuraminidase and pneumolysin production was undertaken, as these are critical factors for pneumococcal colonisation and virulence (Kadioglu et al., 2008), and as the

created strains are intended to eventually be used for virulence studies, it was important to assess their individual virulence properties.

3.2.3.1. Assessing neuraminidase activity

Neuraminidase is required for the efficient cleavage of terminal sialic acid residues in host glycans, where neuraminidase activity exposes potential binding receptors for pneumococcal adherence (Short and Diavatopoulos, 2015). In addition, this enzyme provides a source of carbon by cleaving sugars in mucosal surfaces for bacterial metabolism (Parker et al., 2009). Pneumococcal neuraminidase activity is encoded by *nanA, nanB*, and *nanC*, and neuraminidase A (NanA) takes on major roles in pneumococcal adherence to mucosa and pneumococcal colonisation (Parker et al., 2009, Kadioglu et al., 2008). To examine the neuraminidase expression of bioluminescent strains as compared to those seen in the wild type, enzyme activity was assayed, with and without the addition of luciferin, using pneumococcal cell extracts prepared after growth in BHI. Figure 3.19 shows similar activity in reporter strains as in the wild type, and analysis reveals that no significance differences exist between the strains in terms of neuraminidase activity. The mean values of the neuraminidase activity of the wild type and reporter strains are shown in Table.3.4. The results indicate that bioluminescence expression does not impair bacterial fitness and virulence.

Table 3.4. Neuraminidase activity of pneumococcal strains. Values are averaged over three experiments. (±) indicates the standard error of means (SEM).

Strain	Mean ± SEM
wt D39	44.39±0.78
pPP3 CBRluc-wt	45.34±0.89
P*pflB::luc*-wt	44.51±0.49
P*phrA::luc*-wt	41.39±0.76
P*rrnA::luc*-wt	47.2±0.29
P*pspA::luc*-wt	44.22±0.85
P*vp1::luc*-wt	43.323±0.76
P*htrA::luc*-wt	44.32±1.4
wt D39+	46.6±0.87
pPP3 CBRluc-wt+	45.004±1.07
P*pflB::luc*-wt+	45.7±1.185
P*phrA::luc*-wt+	48.9± 2.12
P*rrnA::luc*-wt+	48.6± 2.13
P*pspA::luc*-wt+	45.48±0.78
P*vp1::luc*-wt+	45.17±0.2
P*htrA::luc*-wt+	48.35±1.4

There is no significant difference between any strains and the wild type in terms of neuraminidase activity, based on Dunnett's multiple comparison test.

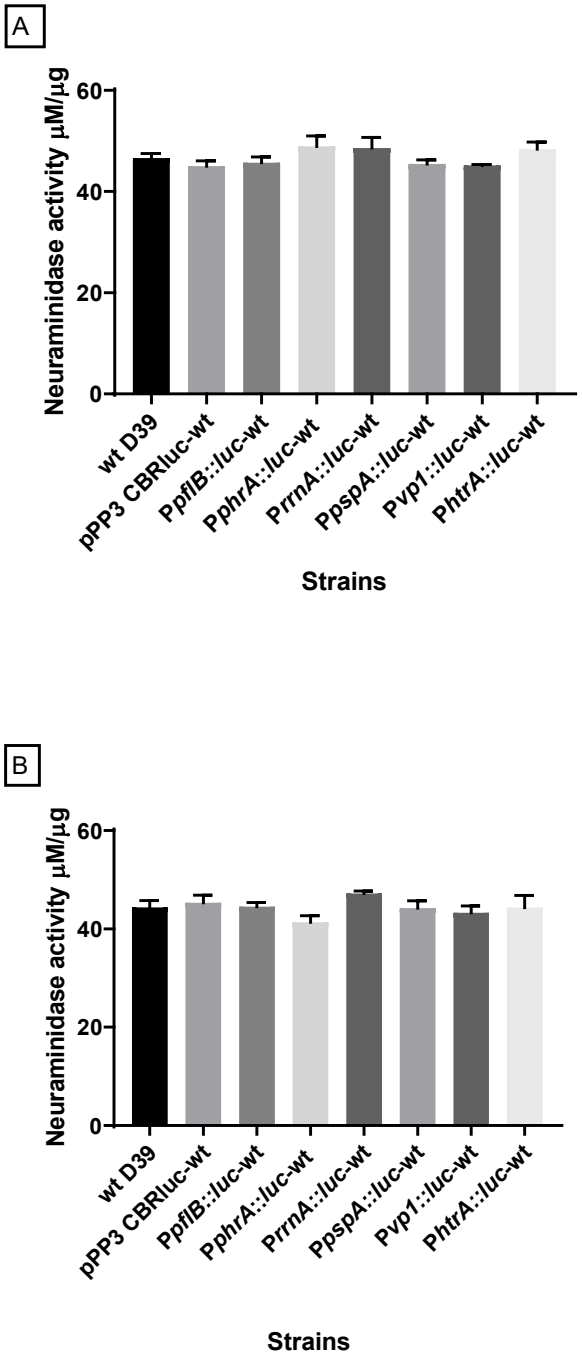

Figure 3.19. Neuraminidase activity of pneumococcal bioluminescent and non-bioluminescent strains using p-NPA as a substrate. (A) Neuraminidase activity of strains with luciferin. (B) Neuraminidase activity of strains without luciferin. Enzyme activity was expressed as micromoles of p-nitrophenol released from the substrate per microgram of the protein. The results were generated from three independent experiments, and analysis revealed that no significant differences could be detected among the strains in terms of neuraminidase activity based on Dunnett's multiple comparison test.

3.2.3.2. Assessing haemolytic activity

Haemolytic activity is attributed to the pneumolysin enzyme, a protein toxic to host cells that causes cell lysis and tissue damage and which may also modulate the immune system and plays a role in the activation of the complement (Rai et al., 2016). Haemolytic activity was tested in the cell lysates of pneumococcal strains grown in BHI (Figure 3.20) by means of sheep erythrocytes, and the results were compared to the haemolytic activity of the wild type (D39). Figure 3.20 shows the similarity of haemolytic activity among all pneumococcal strains ($p > 0.05$).

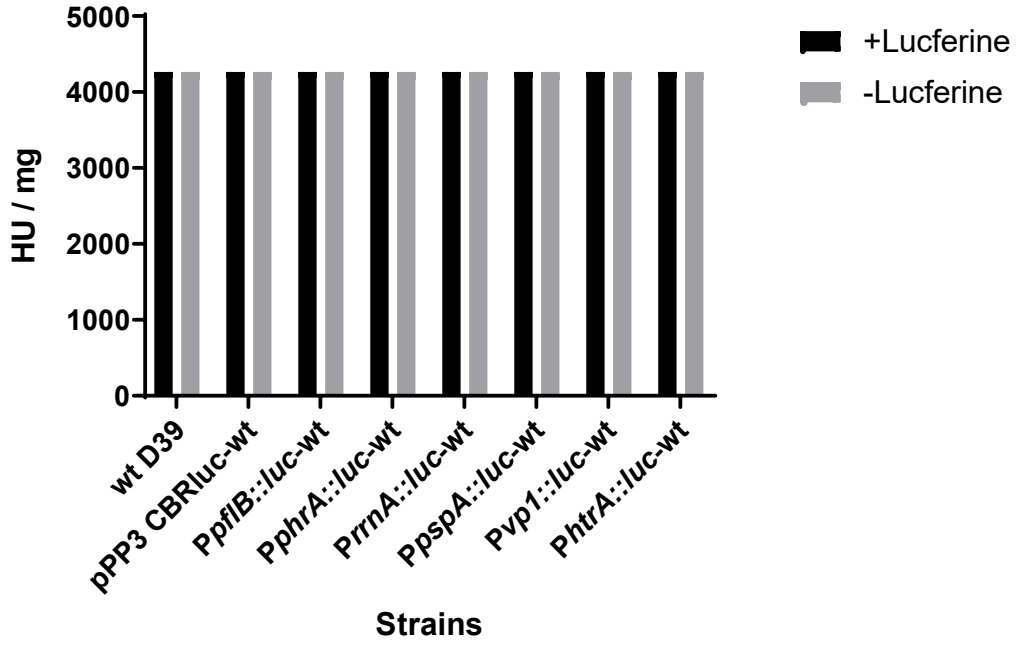

Figure 3.20. Haemolytic activity in the cell lysates of CBRluc-containing strains, comparing promoterless strains with and without luciferin grown in BHI. The haemolytic assay was done using 4% v/v defibrinated sheep blood. No significant difference among strains relative to the wild type was observed ($p > 0.05$). Experiments were repeated in three replicates of eight independent biological samples both in the presence and the absence of luciferin.

3.3. Bioluminescent imaging systems in CBRluc strains

Bioluminescent imaging systems in animal models require microbial strains featuring constructs that produce light. For this purpose, pPP3, which expresses click beetle red luciferases, were used in this work. CBR luciferases are coded by the *luc* gene and require access to an exogenous substrate, luciferin, to produce a visible light. The reporter also gene requires an active promoter to drive *luc* expression. Five reporter strains that were expected to offer high expression *in vivo* were selected. Prior to *in vivo* evaluation, however, the bioluminescent constructs under the selected promoters were tested for light expression to evaluate each promoter's strength *in vitro*.

3.3.1. Evaluation of promoter strength in bioluminescence profiles using a luminometer *in vitro*

Different reporter strains expressing *luc* under the influence of different promoters were tested with regard to promoter strength. Samples were created both with and without substrate (luciferin), and the kinetics of light production and optical density $OD_{600\ nm}$ were measured for CBRluc tagged bacteria in order to assess the levels of bioluminescence during growth in the BHI medium. *S. pneumoniae* D39 with empty pPP3 and without plasmid were also included as controls to determine background bioluminescence. Readings were recorded for 8 hours using a Fluostar Omega Luminometer with light output integrated over a 5 s period with continuous mixing prior to reading. All light output was expressed as relative light units. As Figure 3.21 indicates, no activity was seen for the parent strain without any constructs or for the wild type with promoterless pPP3 CBRluc. In addition, the reporter strains without the addition of luciferin did not show any emissions, highlighting the importance of this substrate for the emission of light. Emission of light was thus recorded only from reporter strains in the presence of the oxidation substrate (luciferin), where the selected promoters successfully induced *luc* gene expression resulting in light production due to the luciferase activity. The signal intensity differed depending on the promoter used, however.

The photon emission data (Figure 3.21) shows that maximum intensity of light emission occurred during the exponential phase and that the photon counts (the emitted light) for P*phrA::luc*-wt strain were superior to those recorded for the other CBRluc strains. The

bioluminescent signal quantified for P*phrA::luc*-wt strain was 11872±772, whereas the values for P*pflB::luc*-wt, P*psp::luc*-wt, P*vp1::luc*-wt, and P*htrA::luc*-wt were 5288±164, 985±76, 254±51, and 1129±205, all in RLU, respectively. Promoter strength in terms of emitted light decreased in the order P*phrA*> P*pflB*> P*pspA* > P*htrA* > P*vp1* during the exponential phase. The promoter of the *16SRNA* gene was not assessed for promoter strength, however, as it was constructed to be used as a control to normalise RLU expression for other strains due to its constitutive expression.

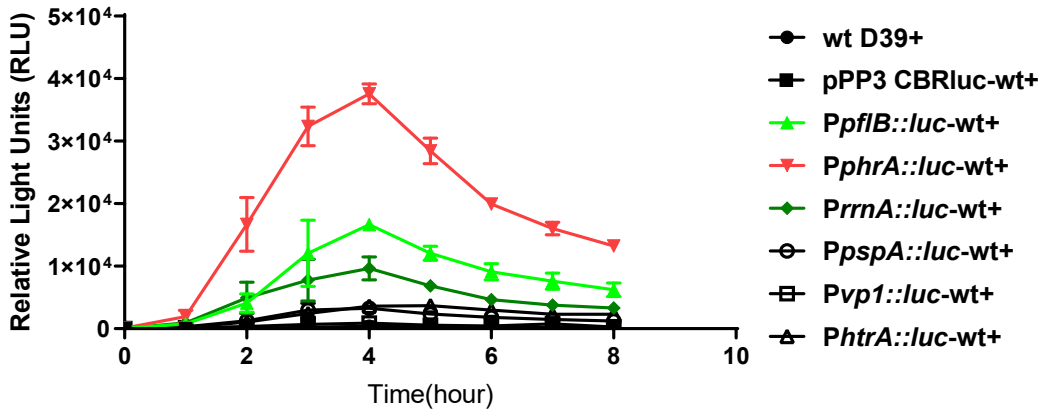

Figure 3.21. RLU emitted by bioluminescent and non-reporter pneumococcal strains (wildtypeD39 and pPP3CBRluc-wt) with (+) and without (-) luciferin in BHI during *in vitro* growth. Strains without luciferin showed no bioluminescence. The experiment was repeated four times for each strain. There was a significant difference between the means of reporter strains in terms of light expression as compared to P*phrA*::*luc*-wt based on a one-way ANOVA. **** $p < 0.0001$.

Table 3.5. RLU emitted by bioluminescent and non-reporter *S. pneumoniae strains* (D39 and pPP3 CBRluc-wt) with (+) luciferin. Values are averaged over three experiments. (±) indicates the standard errors of means (SEM).

Strains	**Mean ±SEM**
wt D39	134±10
pPP3 CBRluc-wt	85±16
P*pflB::luc*-wt	5288±164
P*phrA::luc*-wt	11872±772
P*rrnA::luc*-wt	2909±652
P*pspA::luc*-wt	985±76

P*vp1::luc*-wt	254±51
P*htrA::luc*-wt	1129.08±205.8

There is a significant difference among the resulting means in terms of RLU ($p < 0.0001$).

3.3.2. Bioluminescence profiles normalised to CFU

To examine whether bioluminescence production is influenced by colony forming units (CFU), all light intensities were normalised against the CFU. CBRluc tagged *S. pneumoniae* were grown in BHI and the relative light units (RLU) and bacterial CFU were determined at given time points (0, 2, 4, 6, and 8). The results indicated that luminescence levels are correlated with cell density during the exponential growth phase for all reporter strains. Wildtype D39, with and without pPP3 CBRluc, was also included as a control. Figure 3.22 shows the luminescence emissions during the growth of the luciferase-producing strains. CFUs for all strains were approximately 10^7 CFU/ml for the first 2 h, indicating a lag phase, after which the CFU/ml increased up to ~10^9 CFU/ml within 4 hours. Bioluminescence intensity increased proportionally with CFU counts up to the 4 h point, after which no further increases in bioluminescence and CFU were observed. Instead, there was a slight decline in CFU/ml from 4 to 8 h.

The positive correlation between colony forming units (CFU) and luminescence during the exponential phase allowed mid-log cultures to be used to determine the bioluminescence intensity per cell. The first and last points of exponential growth were selected for the calculation of the relative light units per 1x10^8 cell. The RLU values per 1x10^8 declined in the order P*phrA*> P*pflB*> P*pspA* > P*htrA* > P*vp1* during the exponential phase (Figure.3.23). The values of RLU per 1x10^8 CFU are shown more clearly in Table 3.6, and these indicate that P*phrA::luc*-wt with 15258 RLU±3858 displayed the greatest bioluminescence during the exponential phase.

Table 3.6. Relative light units per cell of *luc* containing strains during exponential growth. Values are averages of three experiments. (±) indicates the standard errors of means (SEM).

Strains	**Mean±SEM**
P*phrA::luc*-wt	15258±3858
P*pflB::luc*-wt	7054 ±1827.9
P*rrnA::luc*-wt	5293 ±2257.9

P*psp::luc*-wt	1777±593.9
P*vp1::luc*-wt	185±57.57
P*htrA::luc*-wt	1056±415.5

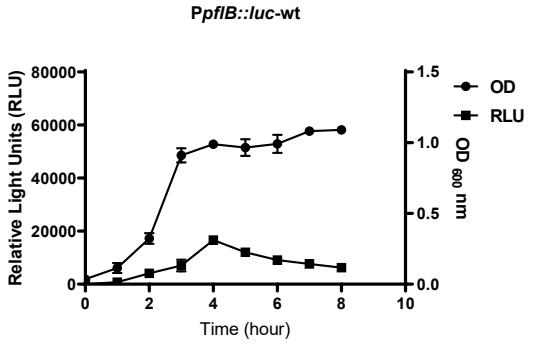

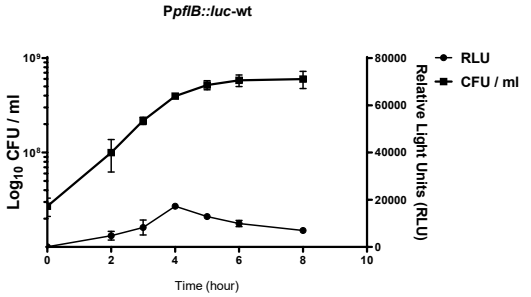

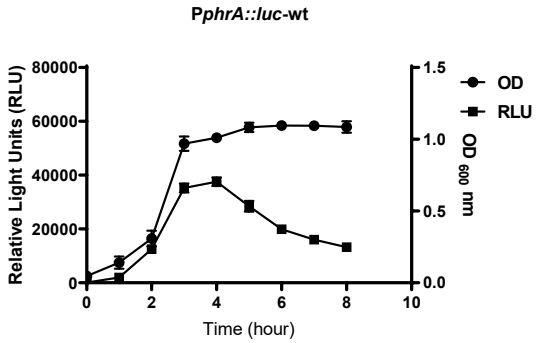

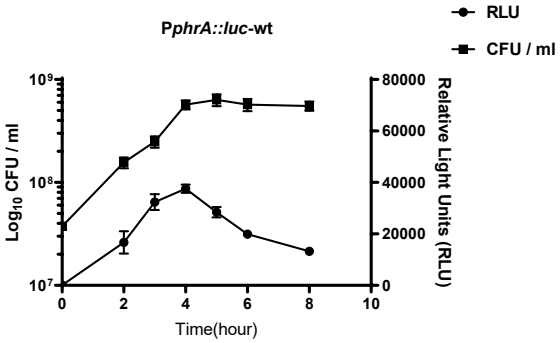

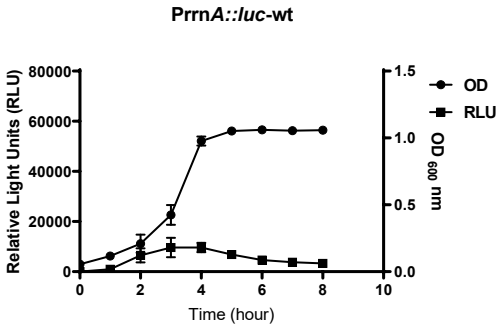

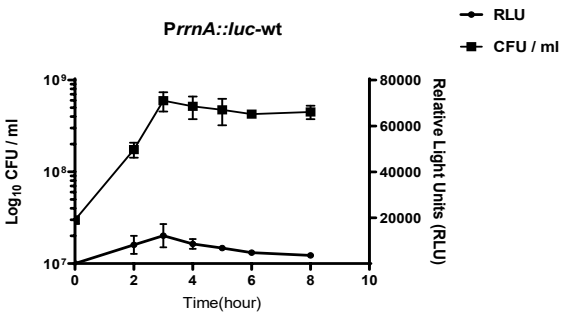

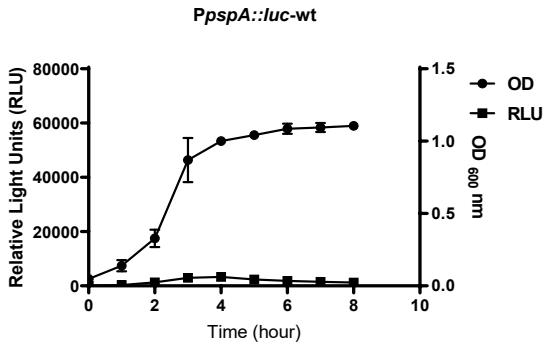

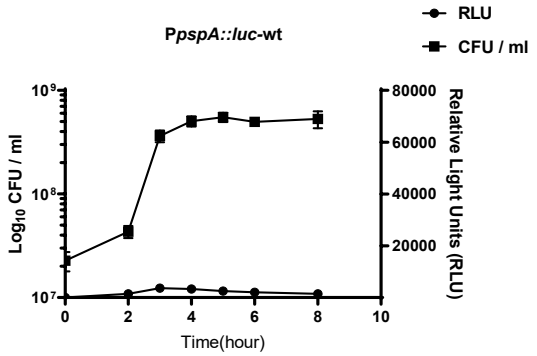

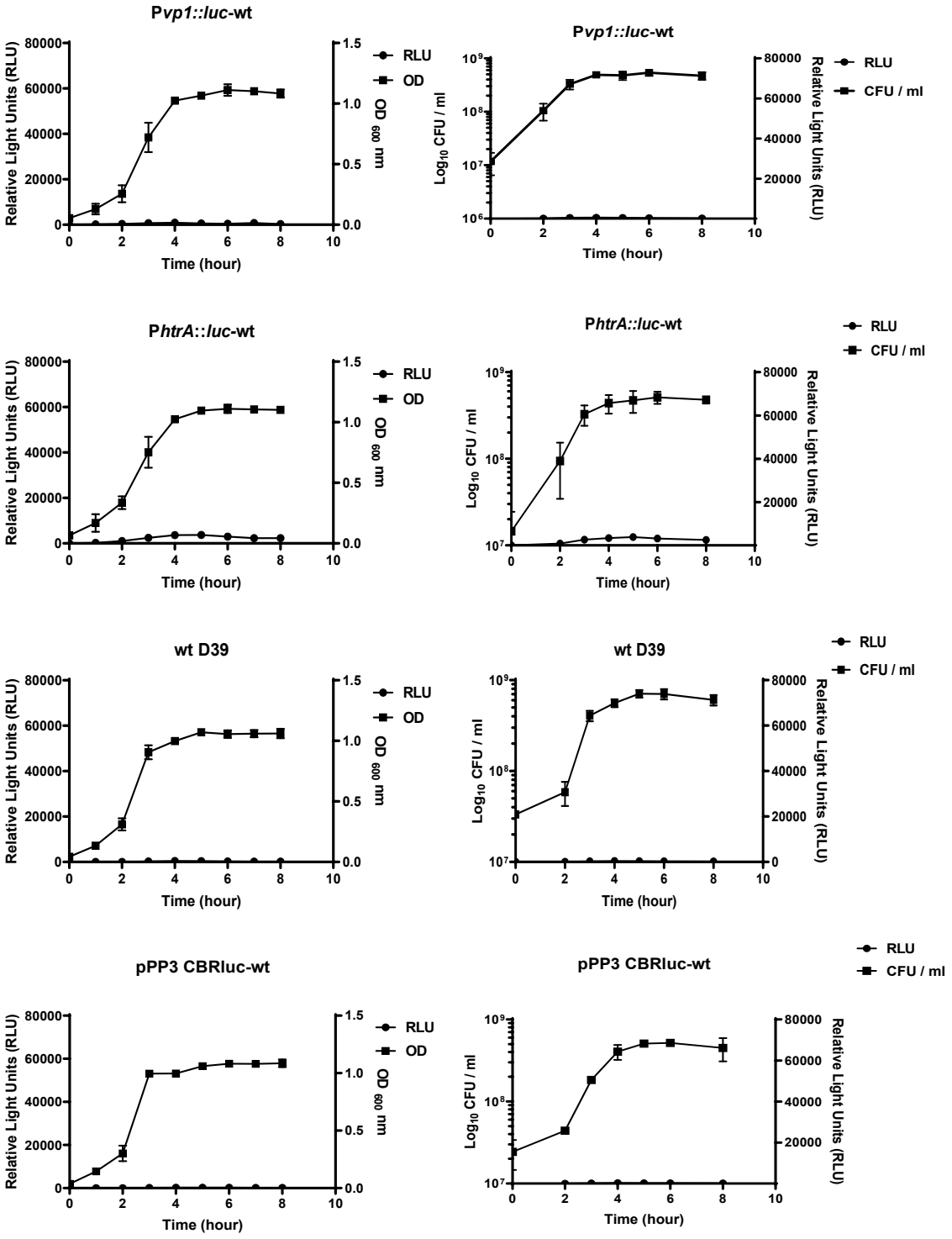

Figure 3.22. Bioluminescence correlated with cell density during exponential growth *in vitro*. Cultures of *S. pneumoniae* were inoculated to an OD $_{600}$ nm of 0.05, and the OD and the luminescence were given as relative light units (RLU) measured over 8 h. Each datum point is the mean of three to four independent tests, while the vertical line represents the standard error of the mean.

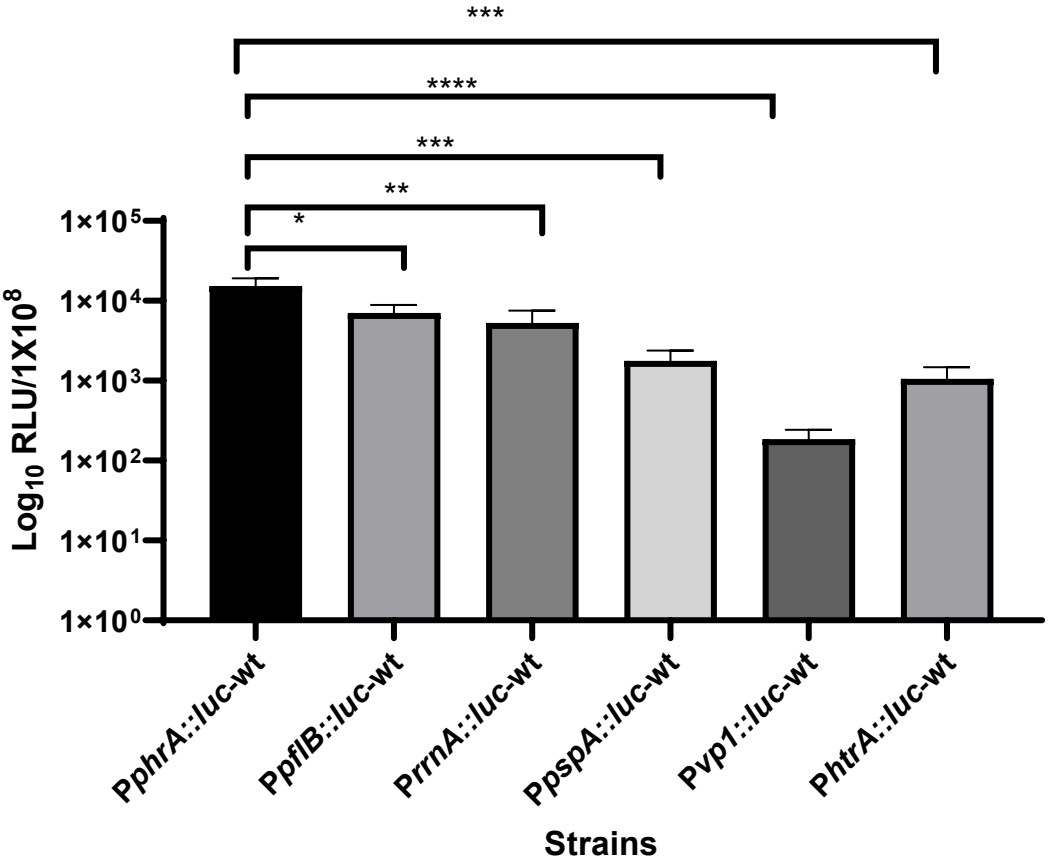

Figure 3.23. Relative light units per cell during exponential growth. The values represented correspond to the relative light units per $1x10^8$ during the exponential phase. There is a significant difference among means based on a one-way ANOVA and Dunnett's multiple comparison testing ($p < 0.0001$). The experiment was repeated three times for each strain and the vertical line represents the standard error of the means.

3.3.3. Bioluminescence imaging of luminescent bacteria growth using IVIS microscopy.

In addition, the RLU values of the strains being measured using a luminometer, the bioluminescence profiles of CBRluc *S. pneumoniae* were also monitored and imaged over time. Strains were grown in BHI broth for 24 h and imaged using an IVIS microscope, and the wild type and pPP3 CBRluc-wt were included as controls to ascertain the background luminescence. The appropriate oxidation substrate was also added to the CBRluc strains. Luminescent images were taken using a highly sensitive cooled CCD camera mounted in a

light-tight specimen box (IVIS) over a 24 h period, with imaging and quantification of signals controlled by Living Image (Xenogen Corporation) acquisition and analysis software.

Figures 3.24 A and B indicate no activity among the non-reporter strains because of the lack of promoters driving *luc* gene expression. The bioluminescence was observed only in reporter strains due to *luc* expression induction by the promoters. Additionally, no emission of light was detected at the initial stages of growth. The data in Figure.3.24 A show the photon flux expressing strongly in actively growing cultures (logarithmic phase) and the maximum intensity of light emission thus occurs during this phase. The photon flux increases as bacteria grow. Once bacteria enter the stationary phase, within 4 h, the strains show a reduction in both photon emissions (Figure.3.24B) and flux (Figure.3.24A). This reduction in bioluminescence expression was also observed in previous studies (Andreu et al., 2011, Daniel et al., 2015), and most likely occurs due to a decrease in the metabolic activity linked in turn to a decrease in the availability of the ATP required for luciferin oxidation. The results for growth rate calculations indicated that the maximum bioluminescence is obtained with P*phrA::luc*-wt with a peak signal of 7371833 RLU±1609790 (n=3), whereas Pp*flB::luc*-wt , P*psp::luc*-wt, P*vp1::luc*-wt, and P*htrA::luc*-wt achieved 5076666 RLU±1310166.4 (n=3), 1729833 RLU±254919 (n=3), 200500RLU±98072 (n=3), and 2638333 RLU±553340 (n=3), respectively (Table 3.7, Figure 3.24 A). The signal intensity thus differs depending on the promoter used. Dunnett's multiple comparison testing revealed that, with the exception of P*pflB::luc-wt,* P*phrA::luc*-wt generated the most bioluminescence. Consequently, P*phrA*::*luc*-wt was selected for further testing *in vivo*.

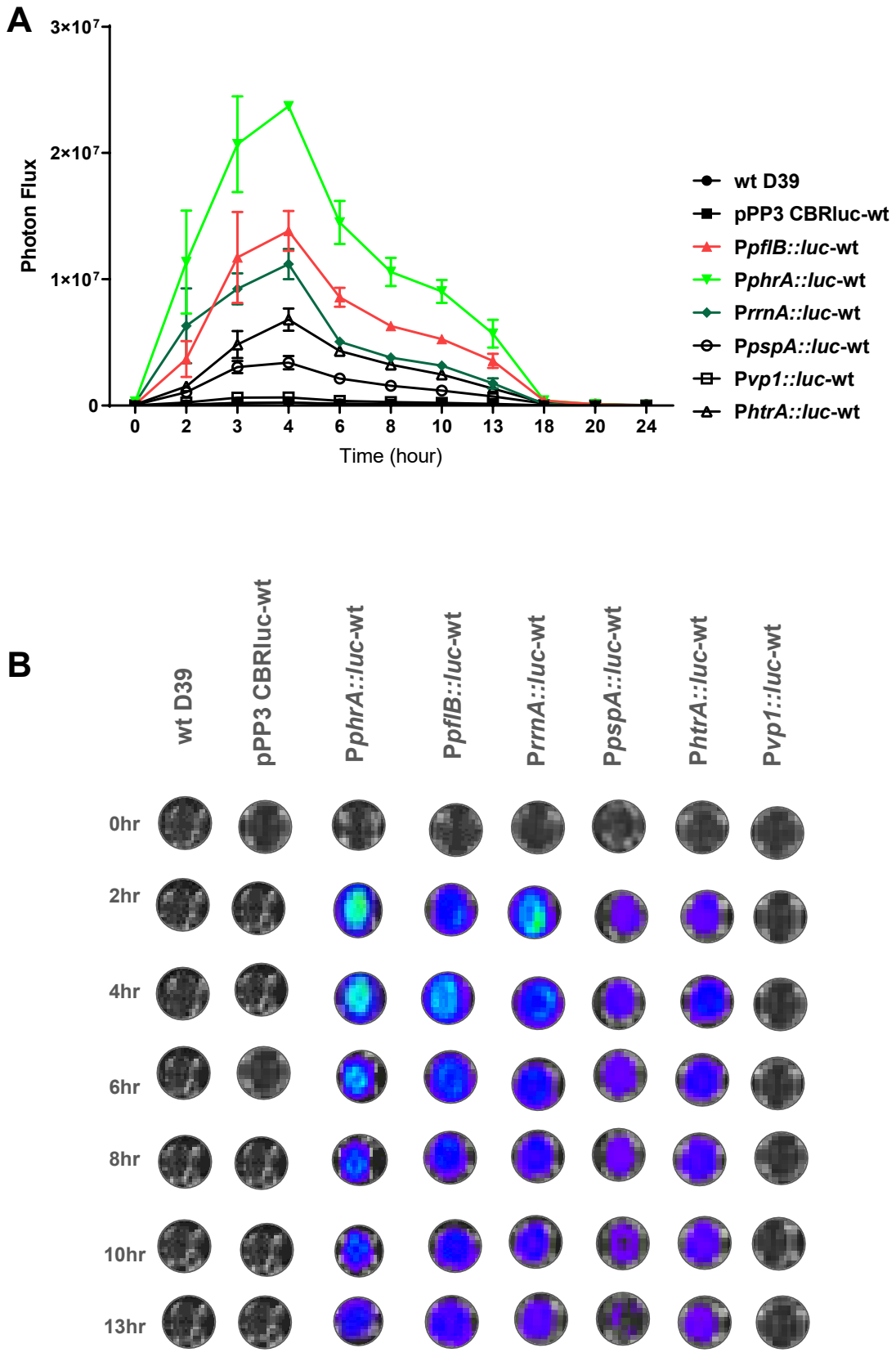

Figure 3.24. Luminescence of CBRluc tagged *S. pneumoniae* during growth. **(A)** Luminescence (flux) of luciferase-tagged *S. pneumoniae* strains during *in vitro* growth in BHI

broth as measured by IVIS. Each datum point is the mean of three independent tests, while the vertical line represents the standard error of the means. **** $p < 0.0001$. **(B)** Luminescence imaging of luciferase-tagged *S. pneumoniae* strains over 24 h. Strains were grown in BHI broth for 24 h to monitor bioluminescence. Light was then detected for up to 13 h. Luminescent images were taken using the IVIS Lumina II system and processed using Living Image software (Xenogen Corporation).

Table 3.7. Relative light units (photon flux) of pneumococcal strains during exponential growth using an IVIS microscope. Values are averaged over three experiments. (±) indicates the standard errors of means (SEM).

Strains	**Mean±SEM**
wt D39	80800±29136.5
pPP3 CBRluc-wt	72900±38984.2
P*pflB::luc*-wt	5076666.6±1310166.4
P*phrA::luc*-wt	7371833.3±1609790.3
P*rrnA::luc*-wt	4596500±700588.8
P*pspA::luc*-wt	1729833.3±254919.9
P*vp1::luc*-wt	200500±98072.6
P*htrA::luc*-wt	2638333.3±553340.8

There is a significant difference between the reporter strains, with the exception of P*pflB::luc-wt,* in terms of light expression in RLU based on Dunnett's multiple comparison testing as compared to P*phrA::luc*-wt, which generated significantly more bioluminescence.

3.4. Comparing CBRluc to a lux-based system for bioluminescence imaging

3.4.1. Construction and integration of pPP4-*lux* constructs into *S. pneumoniae* D39 and confirmation using PCR

After construction and *in vitro* testing of the CBRluc based bioluminescent reporter strains, the *luc* and *lux* systems were compared, having both been placed under the transcriptional control of P*phrA*; this was selected as being the most inducible promoter. The *lux* system bacterial luciferase, which generates light at a wavelength of 490nm, was constructed under the SPD_1717 promoter (Francis et al., 2001, Jensch et al., 2010) and transferred to the wild type D39 to enable comparison with the D39 strain containing P*phrA::luc* also constructed in this study. While the reporter genes and the promoter genes are different in P*phrA*::*luc* and P*spd1717*:: *lux*, it was important to compare P*phrA::luc* with P*spd1717:: lux*, as well as to make a direct comparison of bioluminescence expression in the *lux* cassette and CBRluc, for which the *lux* cassette was integrated into pPP3 under the putative promoter P*phrA*, which offered the greatest bioluminescence induction among the tested promoters (Figure 3.25).

The QIAprep spin Miniprep kit was used to extract pSB2035 containing the *lux* cassette (Qazi et al., 2001). This *lux* cassette was amplified using primers incorporating NcoI and SalI recognition sites (Table 2.3), and the amplified PCR products were purified using a DNA purification kit (Section 2.11). The amplicons were then analysed by agarose gel electrophoresis, which confirmed the expected 5636 bp product size of the *lux* cassette (Figure 3.27).

The QIAprep spin Miniprep kit was also used to extract pPP3, while to release the *luc* fragment, the plasmid was digested using both NcoI and SalI, as described in section 2.10. Agarose gel electrophoresis was then used to visualise the successful digestion of pPP3 for the removal of the *luc* gene (Figure 3.26). In Figure 3.26, lane1 shows the digested plasmid, at approximately at 7221 bp for empty plasmid (without P*phrA* promoter) and lanes 2 to 4 show the digested plasmid at 7409 bp for pPP3::P*phrA* , excluding the *luc* gene, which gives a product size of 1572bp (1184 bp for *luc*, plus the sequence representing upstream and downstream of the cloning site). The digested plasmid was extracted using the Wizard® SV Gel and PCR Clean-Up System (section 2.9), and the restriction enzymes NcoI and SalI were used to digest the inserts. The plasmid and the inserts with compatible ends were ligated as

described in section 2.12, and the ligation mixture was transformed into *E. coli* TOP10. The empty plasmid without a putative promoter was then constructed as a control, giving pPP4::*lux*. The results were analysed by means of PCR, and these are shown in Figure 3.28, confirming the successful cloning of the *lux* cassette into pPP3::P*phrA*::*luc* in place of *luc* to create pPP4::P*phrA*::*lux.* Using ppp3-F/ R3 primers and the recombinant plasmid as a template, a product of 5962 bp was obtained, representing 5636 bp of *lux* cassette, consisting of *phrA* promoter region (191bp) and a 135 bp region surrounding the multiple cloning sites. The cloning also was further confirmed by the use of primers inside the *lux* gene to produce a product of 753 bp. The result was analysed by agarose gel electrophoresis, which confirmed the cloning success of the *lux* cassette using ppp3-F/lux-R2 (Figure 3.29).

The recombinant pPP4::*lux and* pPP4::P*phrA::lux* constructs were then integrated into the *S. pneumoniae* D39 genome separately, as described in section 2.16. The transformants were selected on a blood agar containing 15 µg/ml tetracycline, and selected transformants were then analysed by means of PCR using pPP3-F/R3 primers, with pPP4::P*phrA::lux* and pPP4::*lux* used as templates. As indicated in Figure 3.30, successful transformation was confirmed by 1% (w/v) agarose gel electrophoresis, which showed amplified products of 5962 bp for pPP4::P*phrA::lux* and 5774 bp for pPP4::*lux*.

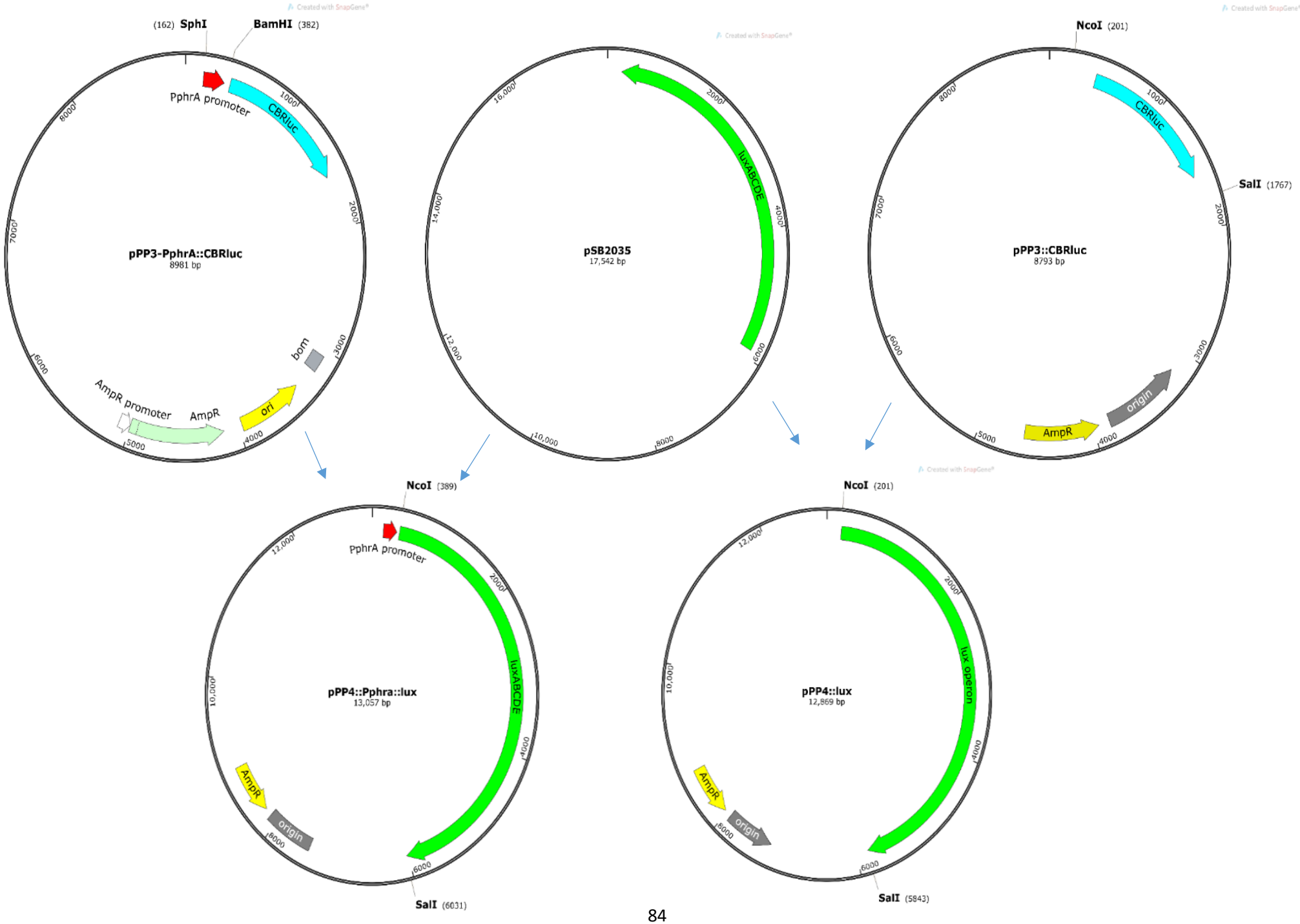
(162) SphI
BamHI (382)
PphrA promoter
CBRluc
pPP3-PphrA::CBRluc
8981 bp
bom
AmpR promoter
AmpR
ori
pSB2035
17,542 bp
luxABCDE
NcoI (201)
CBRluc
SalI (1767)
pPP3::CBRluc
8793 bp
AmpR
origin
NcoI (389)
PphrA promoter
luxABCDE
pPP4::Pphra::lux
13,057 bp
AmpR
origin
SalI (6031)
NcoI (201)
lux operon
pPP4::lux
12,869 bp
AmpR
origin
SalI (5843)

Figure 3.25. Construction of pPP4::P*phrA*::*lux* and pPP4::*lux*. The lux operon was amplified from pSB2035 using primers lux-R+SalI (AGC **GTCGAC** GATATC AACTATCAAA CGCTTCG) and lux-F+NcoI (GCG**CCATGG**AGGAGGACTCTCTAT GAAATTTG); the underlined sequences correspond to the SalI and NcoI restriction enzyme sites in the lux-R and lux-F primers, respectively. The amplified gene (5636 bp) was digested with SalI and NcoI and ligated into the same sites in pPP3::P*phrA::luc* and pPP3 CBRluc after removal of luc.

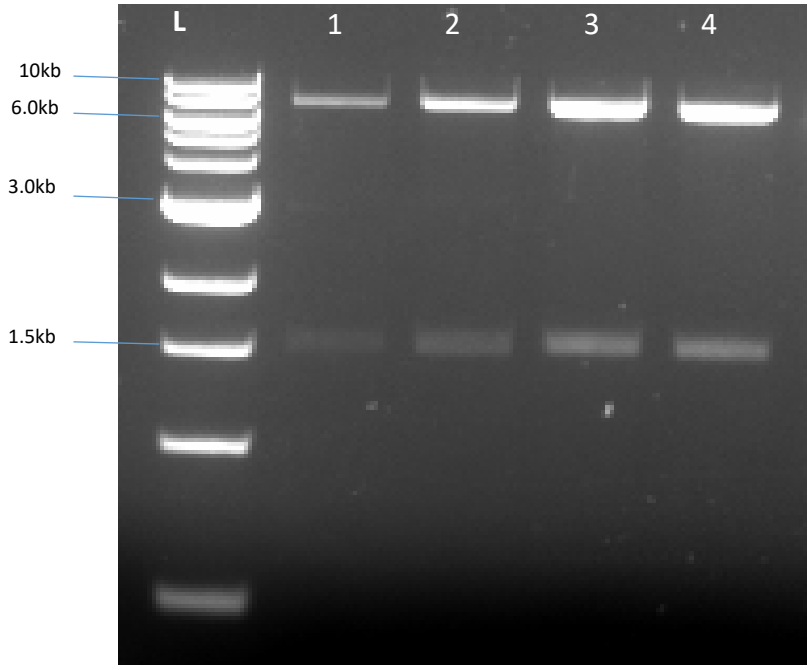

Figure 3.26. Agarose gel electrophoresis showing the digested pPP3 CBRluc and pPP3::P*phrA*::*luc.* NcoI and SalI digested *luc gene* (1572bp). Lane 1 shows digested plasmid of approximately 7221 bp for the empty plasmid and lanes 2 to 4 show a product at 7409 bp for pPP3::P*phrA::luc*. L: 1Kb DNA ladder.

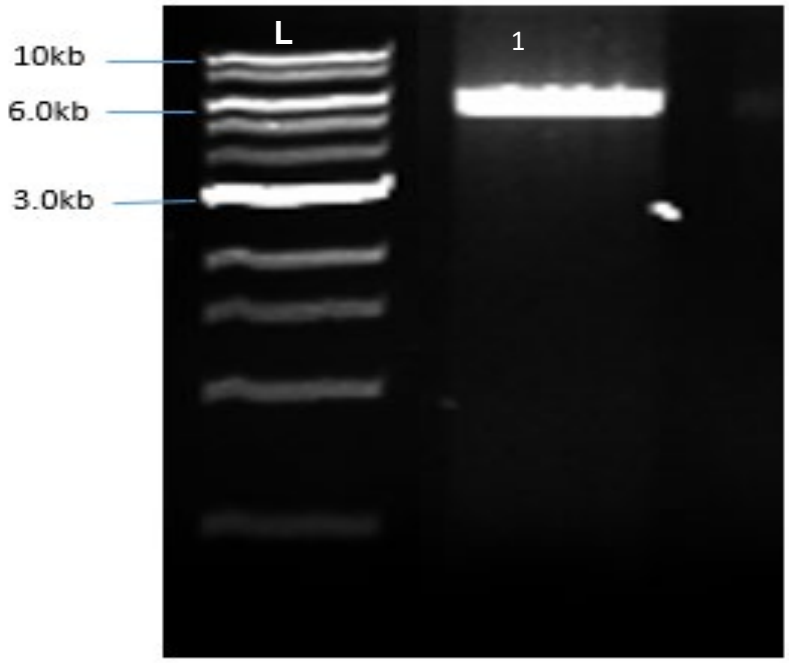

Figure 3.27. Agarose gel electrophoresis analysis showing the expected size of the *lux* cassette at 5636 bp using lux-F/R primers Table 1. L: 1kb DNA ladder.

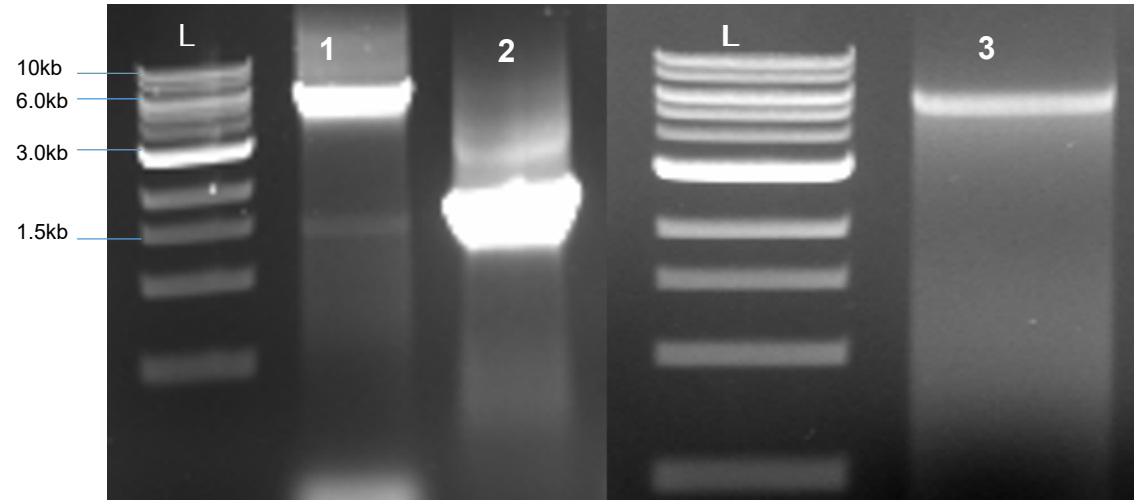

Figure 3.28. Agarose gel electrophoresis confirming the cloning of *lux* cassette using ppp3-F/R3 primers, which amplify the product of 5962 bp from pPP4::P*phrA::lux* in lane 3, which includes the *lux* cassette, and the putative promoter region of *phrA* (191 bp), with the 135 bp region representing the cloning site. An amplicon of 5774 bp (5636 bp plus a 138 bp region representing the cloning site) for pPP4::*lux* in lane 1, and a product of 1572 bp for pPP3 CBRluc in lane 2 were also obtained. L: 1kb DNA ladder.

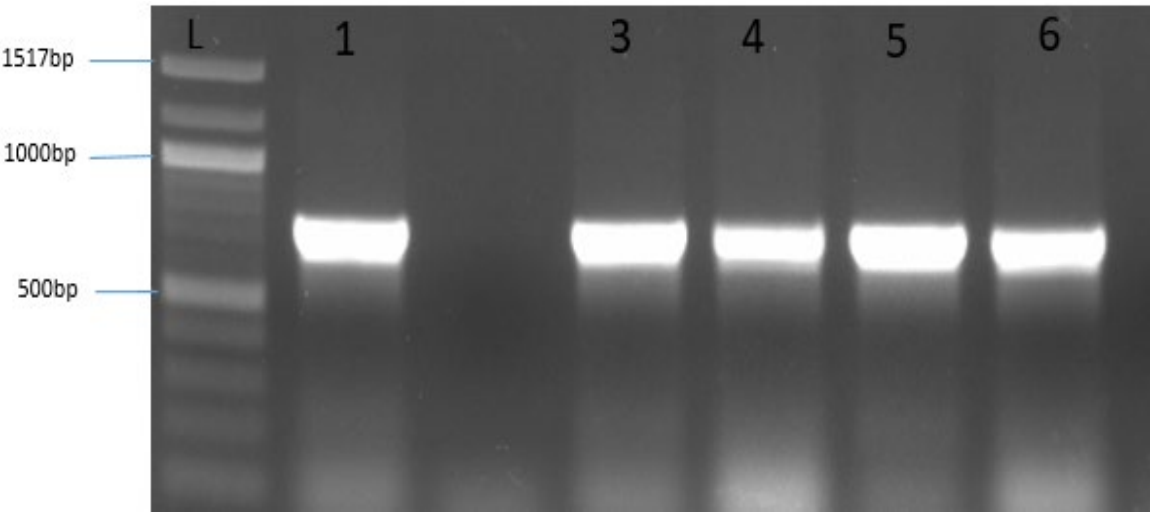

Figure 3.29. Agarose gel electrophoresis confirming the cloning of lux cassette into pPP4 plasmid using ppp3-F/lux-R2 primers, which have annealing sites inside the lux cassette. A product of 753 bp was obtained, as shown in lanes 1, 3, 4, 5 and 6. L: 100bp DNA ladder.

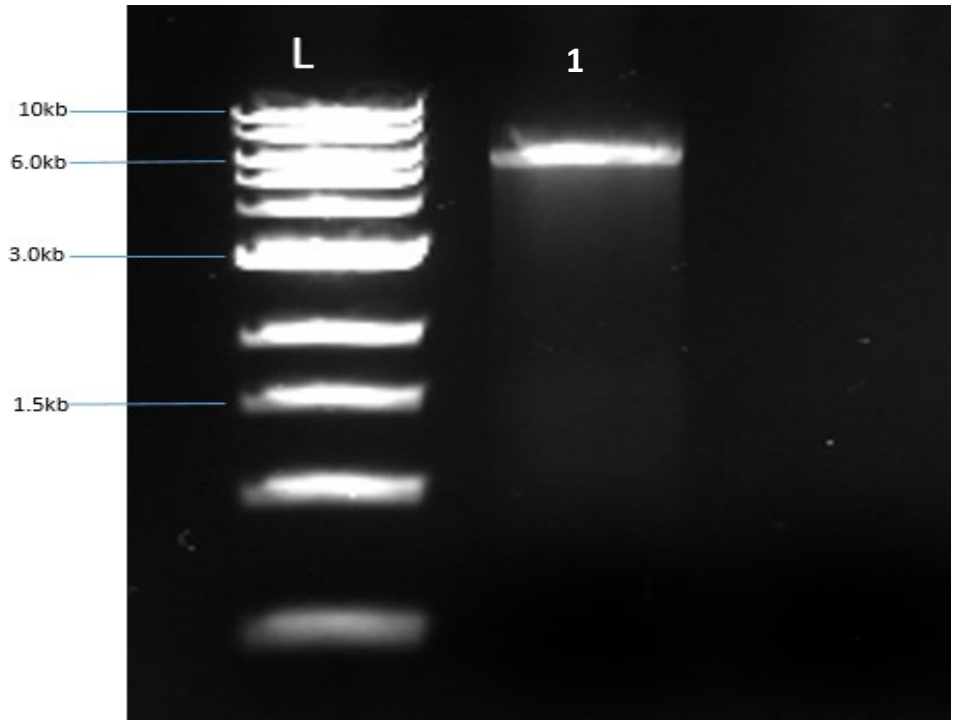

Figure 3.30. Agarose gel analysis of a selected transformant for integration of pPP4::P*phrA*::*lux* to *S. pneumoniae*. Lane1 shows a positive result, with a 5962 bp product. L: 1kb DNA ladder.

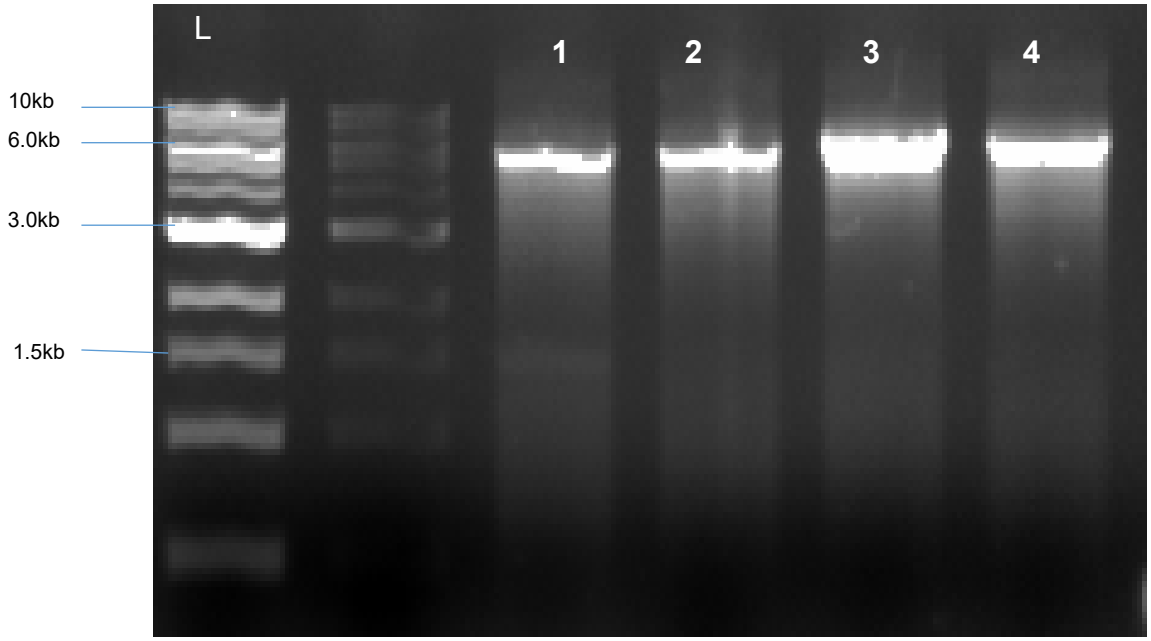

Figure 3.31. Agarose gel analysis of selected transformants for integration of pPP4::*lux* to *S. pneumoniae*. Lanes 1 to 4 show positive results, with a 5774 bp product. L: 1kb DNA ladder.

3.4.2. DNA sequence analysis of pPP4

DNA sequencing was used for further confirmation of the successful *lux* operon cloning. The recombinant plasmid, pPP4::P*phrA::lux,* was purified and extracted from an overnight *E. coli* culture. The target genes were then sequenced using pPP3-F/R3, and an aliquot of recombinant plasmid was sent for DNA sequencing to Eurofins Genomics, Germany. The sequence results were analysed by BLAST, hosted at the National Centre for Biotechnology Information (NCBI). The results showed successful cloning, and the insertion site of the lux cassette into the ppp3 sequence is shown in Appendix 1.

3.4.3. Phenotypic characterisation of pPP4::P*phrA::lux*-wt

To test the background phenotypic characterisation of the *lux*-based reporter strain and to assess whether there is any effect from *lux* integration on growth behaviour, growth studies were also completed in BHI. In addition, strains were grown in CDM supplemented with 55 mM glucose or galactose as the sole carbon source at 37 °C, as described in section 2.4, to determine whether there is any effect from reporter gene integration on pneumococcal growth in minimal media. The wild type D39 and pPP4::*lux*-wt were included as controls. The effect of *lux* integration on the production of virulence factors was also determined by measuring certain important virulence factors for *S. pneumoniae*.

3.4.3.1. Growth profiles of S. pneumoniae tagged with lux in Brain Heart Fusion (BHI)

The *lux*-based reporter strains, P*spd1717::lux*-wt, pPP4::*lux*-wt and pPP4::*phrA::lux*-wt, and the wild type D39 were grown in BHI medium at 37 °C; the optical density was recorded for 8h using a Multiskan TM GO Microplate Spectrophotometer (Thermo Scientific, UK). The growth rates and yields were calculated as described in section 2.4, and no significant differences in growth rates were observed for any of the *lux*-based reporter strains (Figure 3.32) as compared to the wild type *S. pneumoniae* D39 based on one-way ANOVA and Dunnett's multiple comparison testing ($p > 0.05$). These results suggest that the plasmid does not impede the growth rate.

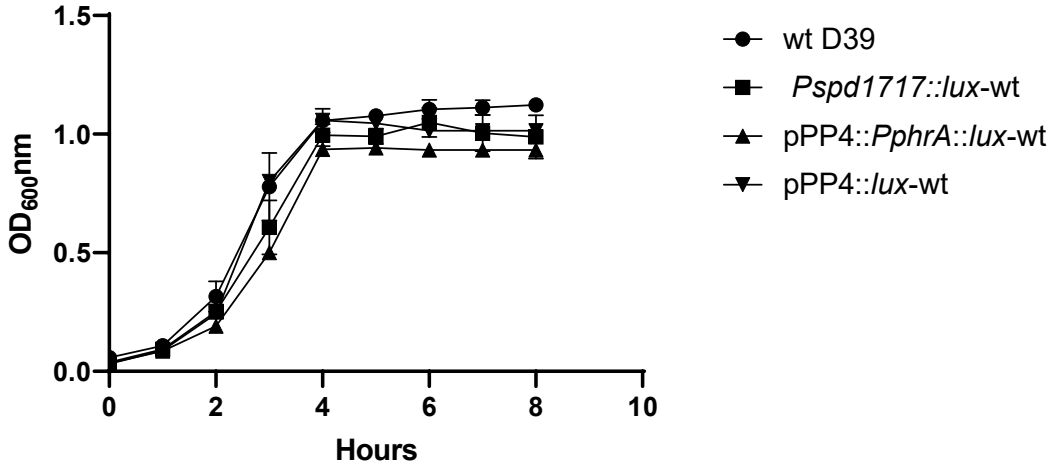

Figure 3.32. Growth profiles of the *lux*-based reporter strains and D39 wild type in BHI. No significant differences could be detected among the strains in terms of growth rate using one-way ANOVA and Dunnett's multiple comparison testing ($p > 0.05$). The experiment was repeated 3 to 4 times for each strain, and the vertical line represents the standard error of the means.

Table 3.8. The growth rates (μ) and yields ($MaxOD_{600}$) of pneumococcal reporter strains in BHI. Values are averages of three replicates of three to four experiments. ± indicates the standard errors of means (SEM).

Strains	Growth rate μ (h^{-1}) specific Growth rate during the exponential phase (h^{-1})	Growth yield (Max OD_{600})
wt D39	0.37±0.036, n=4	1.13±0.034
P*spd1717::lux*-wt	0.37±0.038, n=4	1.059±0.057
pPP4::*PphrA*::*lux*-wt	0.37±0.001, n=3	0.94±0.015
pPP4::*lux*-wt	0.40±0.002, n=3	1.05±0.008

3.4.3.2. Growth profiles of lux reporter strains in CDM

Bacteria were grown in media supplemented with 55 mM glucose or galactose to examine their growth behaviour in nutrient limited conditions. The wild type D39 and Ppp4::*lux*-wt were included as controls. The results showed similar growth profiles in *lux*-based reporter

strains as in the wild type control (Figure 3.33), which suggests that the presence of *lux* does not affect growth profiles on glucose or galactose.

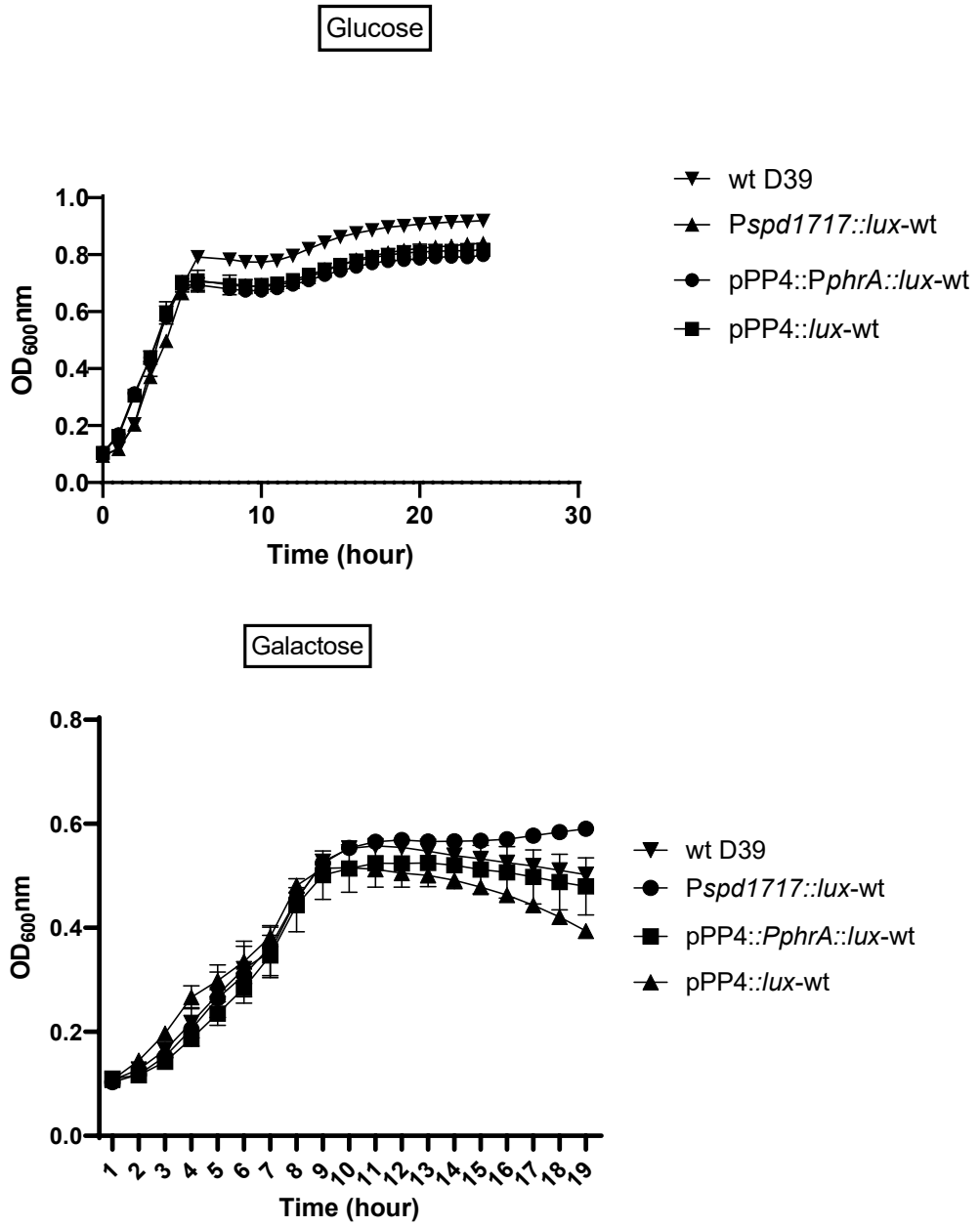

Figure 3.33. Growth profiles of *lux*-based reporter strains grown in CDM supplemented with 55 mM glucose or galactose. No significant differences were determined among the strains in terms of growth rate using one-way ANOVA ($p > 0.05$). Each point is the mean of three independent tests.

Table 3.9. Growth rates (μ) and yields (maximal OD_{600}) of pneumococcal strains grown in CDM supplemented with 55mM glucose. Values are the average of three replicates of experiments. ± indicates the standard errors of means (SEM).

Strains	Growth rate μ (h^{-1}) specific Growth rate during the exponential phase (h^{-1})	Growth yield (Max OD_{600})
wt D39	0.14±0.003	0.91±0.0016
P*spd1717::lux*-wt	0.136±0.0018	0.84±0.005
pPP4::*PphrA*::*lux*-wt	0.131±0.004	0.8±0.010
pPP4::*lux*-wt	0.134±0.003	0.82±0.012

Table 3.10. Growth rates (μ) and yields (maximal OD_{600}) of pneumococcal strains grown in CDM supplemented with 55mM galactose. Values are the average of three replicates of experiments. ± indicates the standard errors of means (SEM).

Strains	Growth rate μ (h^{-1}) specific Growth rate during the exponential phase ($h^{-1)}$	Growth yield (Max OD_{600})
wt D39	0.057±0.0006, n=6	0.56±0.003
P*spd1717::lux*-wt	0.058±0.0007, n=6	0.58±0.002
pPP4::*PphrA*::*lux*-wt	0.055±0.006, n=3	0.52±0.045
pPP4::*lux*-wt	0.054± 4.78, n=3	0.53±0.002

3.4.3.3. Assessing lux-based pneumococcal strains in the production of neuraminidase

Neuraminidase activity, a critical factor for pneumococcal colonisation and virulence (Kadioglu et al., 2008), was tested in the pneumococcal strains. Neuraminidase activity was assayed in *lux* reporter strains using the pneumococcal cell extracts prepared after growth in BHI. Figure 3.34 shows similar neuraminidase activity in both the *lux* reporter strains and the wild type. The mean values for neuraminidase activity were 44.4 U ± 0.78 for the wildtype, 47.5 U ± 1.9 for P*spd1717::lux*-wt, 44.7 U ± 0.75 for pPP4::P*phrA::lux*-wt, and 45.19 U ±

0.92 for pPP4::*lux*-wt. These results indicate that bioluminescence expression does not impair bacterial fitness and virulence.

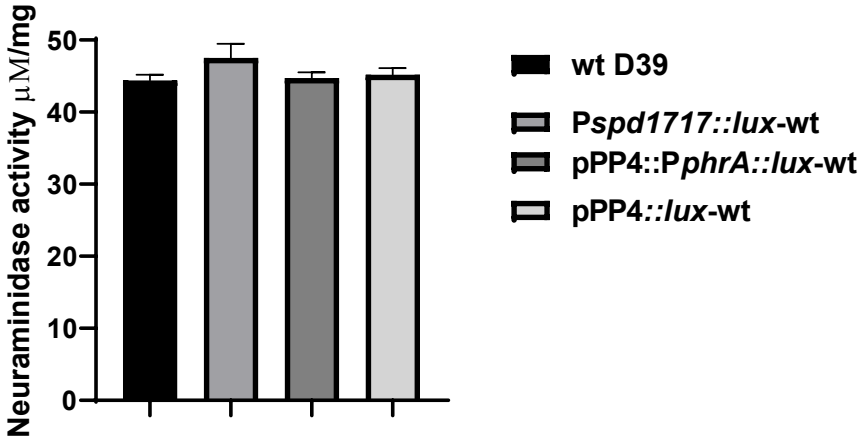

Figure 3.34. Neuraminidase activity in pneumococcal cell lysate for *lux*-tagged bacteria and wild type using p-NPA as a substrate. The enzyme activity was expressed in terms of micromoles of p-nitrophenol released from the substrate per microgram of protein. Testing was done in three independent experiments, and analysis revealed no significant differences among the new strains in terms of neuraminidase activity relative to the wild type ($p > 0.05$).

3.4.4. Bioluminescent imaging of *lux*-based reporter strains

3.4.4.1. Evaluation of bioluminescence profiles of *S. pneumoniae* tagged with P*spd1717::lux*-wt and P*phrA::luc*-wt, and the wild type D39 *in vitro* using IVIS and a luminometer

To assess the bioluminescence profiles of P*spd*1717::*lux*-wt, P*phrA::luc*-wt, and the wild type D39 (control for background bioluminescence) *in vitro,* a cooled CCD camera mounted in a light-tight specimen box (IVIS) was used, with the imaging and quantification of signals, controlled by means of Living Image (Xenogen corporation) acquisition and analysis software. Strains were grown in BHI broth for 24 h to monitor bioluminescence using an IVIS microscope. the wild type D39 was included as a control, and oxidation substrate was added for the CBRluc strain. The resulting luminescent images are shown in Figure 3.35B, and the analysis of these images is shown in Figure.3.35A.

As expected, no bioluminescence was detected for the wild type because it lacks plasmid. Bioluminescence production was recorded only for the reporter strains, based on reporter gene expression induced by the promoter. The light output for the reporter strains increased as the bacteria grew, and the bioluminescence reached a peak following 4 h of bacterial growth remaining relatively high during the stationary phase for P*phrA::luc*-wt. The *lux* system under the spd1717 promoter, on the other hand, showed higher signal induction during the initial growth, yet the bioluminescence signal from this *lux*-containing strain P*spd1717::lux*-wt diminished rapidly as the bacteria entered the stationary phase. This may be related to a reduction in the metabolic activity of the bacteria, and therefore in the availability of $FMNH_2$, a bacterial cofactor required by *lux* for light production (Andreu et al., 2010). The growth rate of the peak signal for P*spd1717*:: *lux*-wt was recorded as 7398333 RLU± 253316 (n=3), whereas for P*phrA*::*luc*-wt, it was 5970000 RLU ± 2999205 (n=3) (Figure.3.36). Both systems showed a reduction in photon emissions (Figure 3.35B) and flux (Figure 3.35A), most likely a consequence of the growth phase of the bacteria. The control wild type D39 was included to measure the background luminescence, which was 80800 RLU ± 29136 (n=3). No significance difference in peak bioluminescence production was detected among the reporter-strains based on one-way ANOVA and Dunnett's multiple comparison testing.

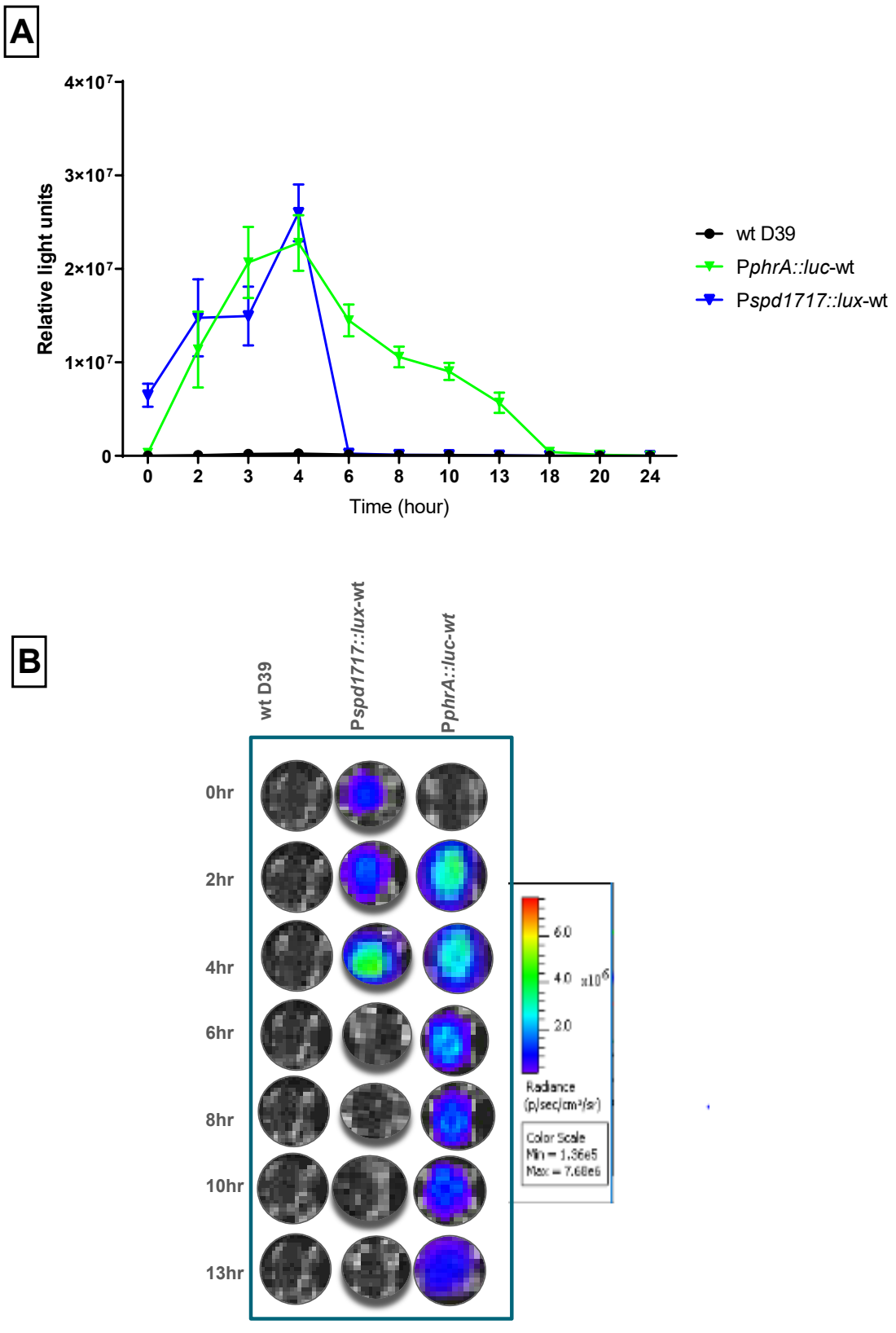

Figure 3.35. Luminescence of luciferase-tagged *S. pneumoniae* containing P*phrA::luc* and P*spd1717*:: *lux* over 24h in BHI media. Wild type D39 (Wt D39) was included to assess background bioluminescence. (A) Luminescence (flux) of luciferase-tagged *S. pneumoniae*

strains during *in vitro* growth in BHI broth. Data and error bars represent the mean and standard error of triplicate samples for each time point. One-way ANOVA and Dunnett's multiple comparison testing were used to compare groups ($P > 0.05$). (B) Luminescence imaging of luciferase-tagged *S. pneumoniae*. Strain was grown in BHI broth for 24 h to allow monitoring of bioluminescence. Luminescent images were taken using an IVIS Lumina II system and processed using Living Image software. The coloured bar represents bioluminescent signal intensity in terms of photon counts.

The light outputs for P*phrA::luc*-wt and P*spd1717*::*lux*-wt were also measured using a plate luminometer to facilitate further *in vitro* testing. Following the addition of luciferin to P*phrA::luc*-wt , the kinetics of the ensuing light production were measured during the growth phase in the BHI medium. The readings were recorded over 8 hours using Fluostar Omega. As Figure 3.36 indicates, the maximum intensity of light emission occurred during the exponential phase. The maximal light signals recorded for the P*phrA::luc*-wt strain, with mean values of 37562.7 RLU, and 57909.5 RLU, were recorded in P*spd1717*:: *lux*-wt. The growth rate of the peak signal for P*phrA::luc*-wt was 11872 RLU± 772, whereas the P*spd1717*:: *lux*-wt strain recorded up to 18995 RLU ± 5344. These results show that the signal intensity differs depending on promoter used and on the reporter gene. This experiment also revealed the difference in sensitivity in terms of light detection between the ICCD camera system used by IVIS and the luminometer, with the detection range of the luminometer being relatively limited. The lower limit of RLU detected by the luminometer was 10^2, whereas the ICCD camera in IVIS can utilise 10^7. A similar observation on sensitivity differences between the two systems was also reported by Rocchetta et al. (2001).

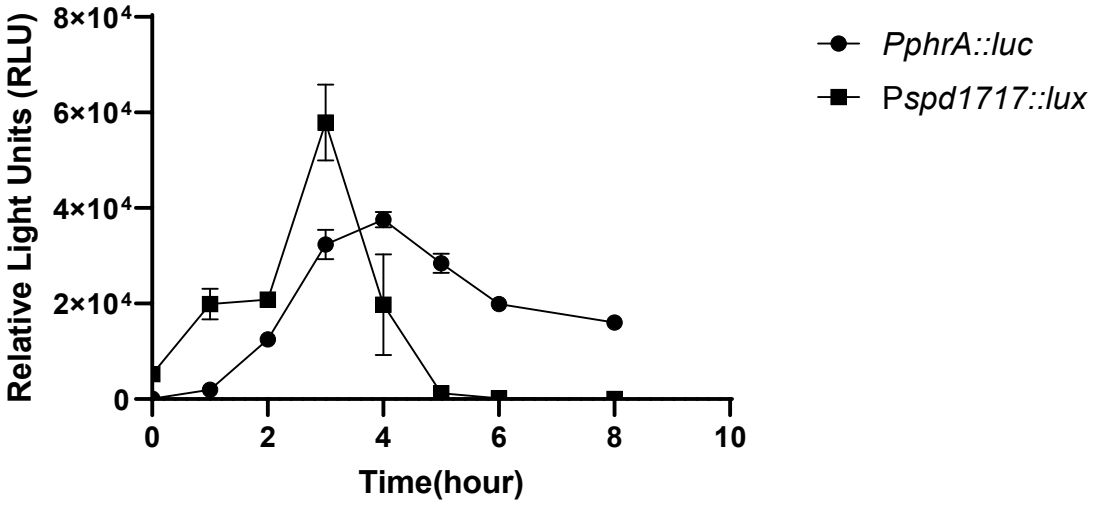

Figure 3.36. RLU emitted by bioluminescent pneumococcal strains (P*phrA::luc*-wt and P *spd1717::lux*-wt) in BHI during *in vitro* growth. Each datum point is the mean of four independent tests in replicates and the vertical line represents the standard error of the means. No significant differences in the means of RLUs were found between the strains using a t-test or one-way ANOVA.

3.4.4.2. Bioluminescence intensity dependence on the number of bioluminescent bacteria

In this experiment, an IVIS microscope was used to show the correlation of light to CFU for P*phrA::luc*-wt and Pspd1717::*lux*-wt strains. In addition, this test allowed determination of the limits of photonic detection in the absence of mammalian cells. Each luminescent strain was serially diluted in a 96-well plate until no luminescence signals were detectable; the CFU/ml of each representative dilution was then calculated in order to determine the relationship between total flux and CFU (Figure 3.37A, B). The wild type D39 was included as a control for CFU, and no bioluminescence was observed for the wild type, as expected (Figure 3.37C). The bioluminescence profiles of both the *lux* and CBRluc luciferase reporters were indeed dependent on the number of luminescent bacteria (Figure 3.37C), with bioluminescence intensity correlated linearly with the number of bioluminescent bacteria (Figure.3.37A and B). The most diluted samples in which photons were detectable contained between 1 and $3x10^7$ CFU/ml

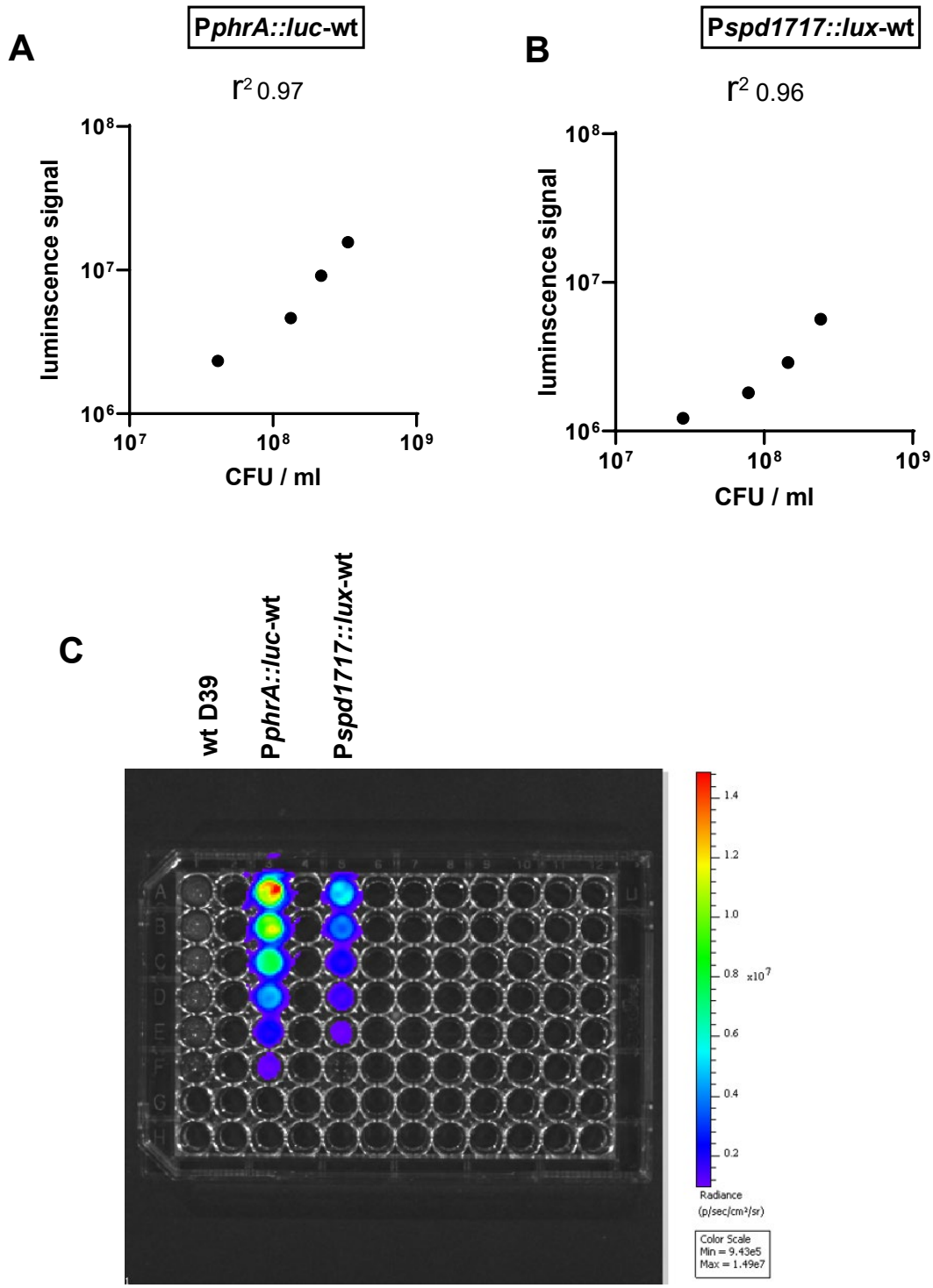

Figure 3.37. Luminescent images from an IVIS microscope of CBRluc tagged *S. pneumoniae* under the control of P*phrA* (P*phrA::luc*-wt), and *lux* tagged *S. pneumoniae* under the control of *1717 promoter (* P*spd1717*::*lux*-wt*)* (C) Serial dilutions in a 96-well plate were imaged for the bioluminescent strains. P*phrA::luc*-wt and P1717::*lux*-wt were grown to mid-log phase, and wild type D39 was included as a control for CFU. A 200 µl dose of culture was then transferred to a 96-well plate and serially diluted. Each dilution was imaged and

plated for CFU assessment. The data obtained was then analysed, and a good correlation between CFU and luminescence was observed when linear regression analysis was used to determine the relationship between flux and CFU values (A and B).

3.4.4.3. Bioluminescence profile normalised to CFU for lux tagged strains

To normalise the light to viable bacteria, and to highlight the dependence of light on CFU, *lux* tagged *S. pneumoniae* was grown in BHI and, at predetermined time points (0, 2, 4, 6, and 8 h), the viable numbers of bacteria were determined. Figure 3.38 shows that the luminescence level correlated well with cell density during the exponential growth phase for the reporter strains. However, the light faded quickly during late exponential and stationary phases (Figure 3.38). This reduction was attributed to decreased metabolic recycling of FMN to $FMNH_2$, the essential cofactor for bacterial lux activity. While pPP4::*lux*-wt was included as a control for light emissions, no light was observed, as expected, from pPP4::*lux*-wt (a control) due to the lack of a promoter to induce *lux* expression (Figure 3.38).

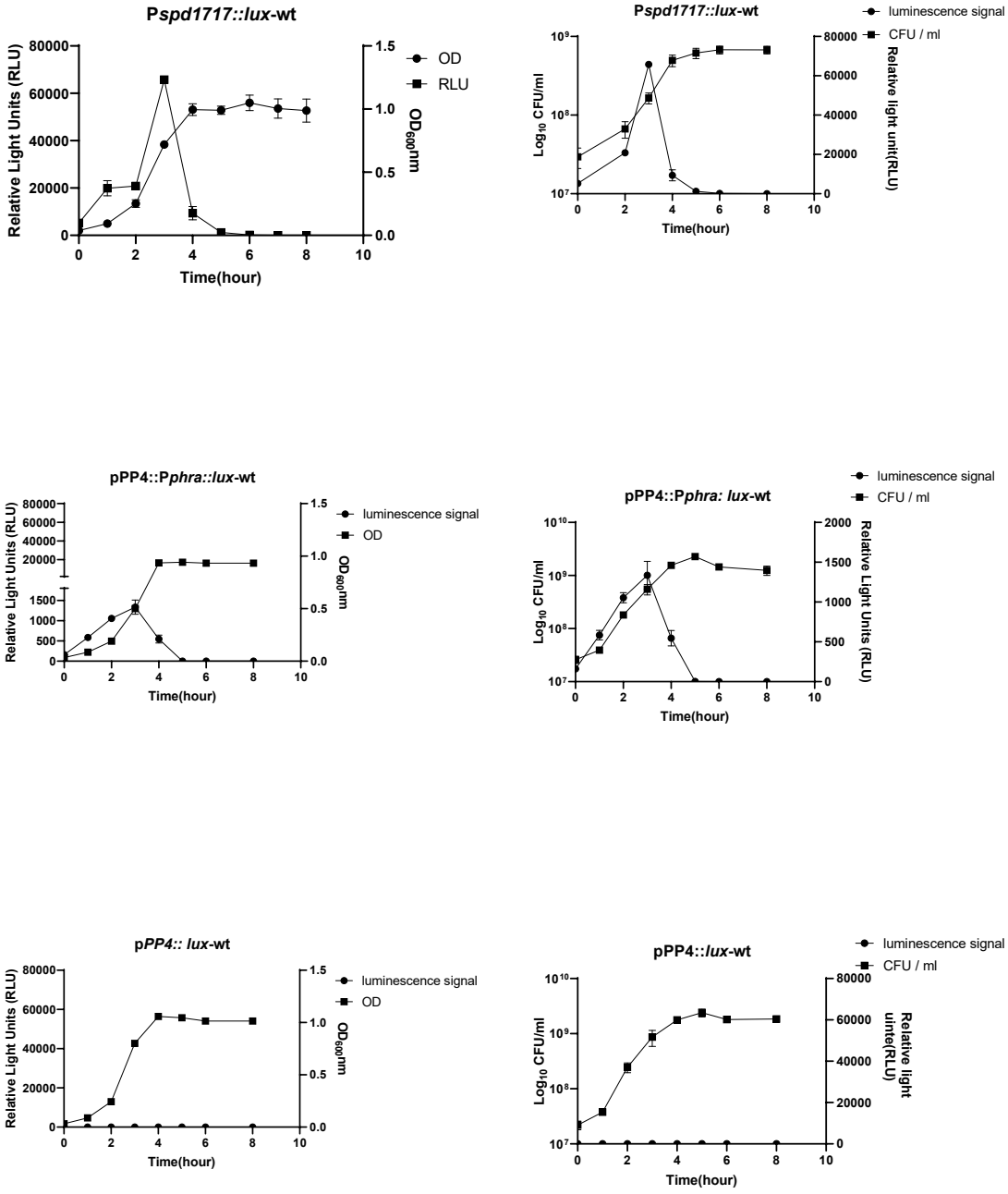

Figure 3.38. Bioluminescence correlations with the cell density during exponential growth *in vitro*. Cultures of *S. pneumoniae* were inoculated to an optical density of 600 nm and the OD and the luminescence given as relative light units (RLU) were measured over a period of 8 h. Each datum point is the mean of three to four independent replicate tests and the vertical lines represent the standard errors of the means.

3.4.4.4. CBRluc signals are brighter and produce greater flux than lux-based systems under the same promoters during *in vitro* growth

To allow for direct comparison between the bioluminescence production of CBRluc and that of the *lux* cassette, the *lux* cassette was integrated into pPP3 under the transcriptional control of the putative *phrA* promoter, P*phrA*, which produced the highest bioluminescence expression *in vitro* among the promoters examined in this project (section 3.3.1). Light production was measured during growth in BHI medium, with readings recorded for 8 hours using a luminometer. A t-test analysis of this data then revealed significant differences between the two reporter systems ($p < 0.0001$). Figure 3.39 shows that, under the same promoter, the CBRluc system generates more light than the *lux* system; the maximum recorded bioluminescence signal for P*phrA::luc*-wt was recorded as 37562.7 RLU, while 1335.08 RLU was recorded at maximum for P*phrA::lux*-wt. The growth rate of the peak light signal for P*phrA::luc*-wt was 11872 RLU ± 772, while the equivalent was 375 RLU ± 68 for P*phrA::lux*-wt. As the CBRluc system produces stronger bioluminescence, this system may be more useful when lower numbers of bacteria are used as a way to improve imaging.

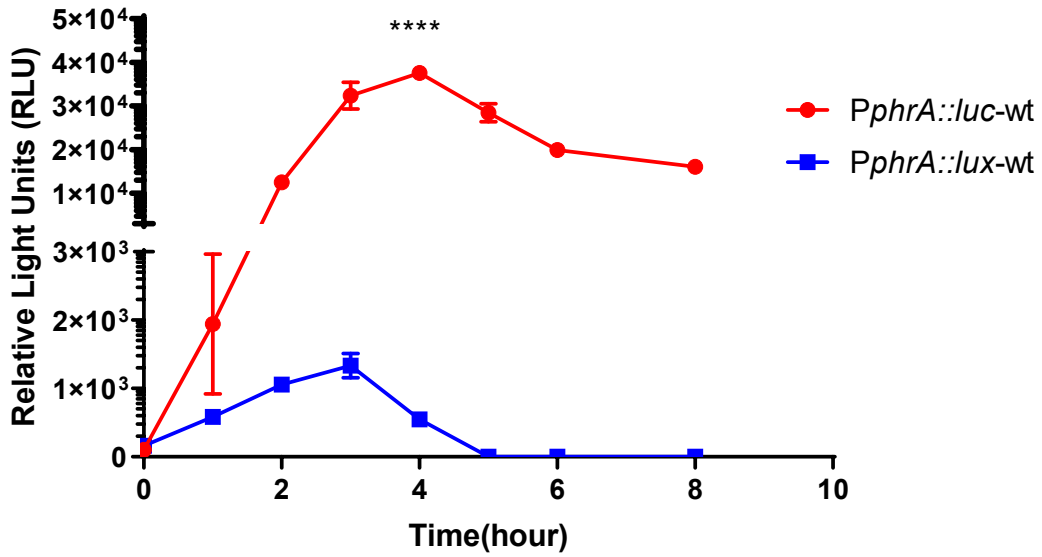

Figure 3.39. RLU emitted by bioluminescent pneumococcal strains P*phrA::luc*-wt and *PphrA::lux*-wt in BHI media during *in vitro* growth. The experiment was repeated four times

for each strain. Each datum point is thus the mean of four independent tests and the vertical lines represents the standard error of the mean. **** p <0.0001.

3.5. *In vivo* testing of reporter strains

3.5.1. Testing of bioluminescent strains in mouse infection models

Animal models are widely used for studying infections disease; however, in traditional formats, large number of animals are required to obtain quantitative data by means of tissue sampling, and the tests do not provide data in real time regarding spatial or temporal distribution of pathogens during an infection (Rocchetta et al., 2001). Contag et al. (1995) showed that labelling bacteria with luciferase proteins streamlined the real-time study of infection processes noninvasively in studies using *Salmonella* infection of mice, thus demonstrating the efficacy of this technology for monitoring bacterial growth in living host tissues. In the search for improved whole-body images in murine infection models, many bacterial species such as *Listeria monocytogenes* (Ur Rahman et al., 2017), and Lactobacillus have been tagged with CBRluc (Daniel et al., 2015). These studies have observed that CBRluc is more sensitive and expresses greater bioluminescence than bacterial luciferase *lux* systems (Ur Rahman et al., 2017) and green click beetle luciferase (CBGluc) (Daniel et al., 2015), with CBR luciferases showing peak emissions ranging from 546 to 593nm (Wood et al., 1989).

To validate *in vitro* results gathered for P*phrA::luc*-wt and P*spd1717::lux*-wt, a mouse model of pneumococcal pneumonia was used in this research, based on the model established by Dr Hasan Yesilkaya's research group at the University of Leicester. This is initiated by the administration of inoculum through the nostrils of anesthetised mice, and it has previously been used to understand the contribution of pneumococcal proteins to virulence, making it the ideal tool for probing host response to pneumococcal infection (Kadioglu and Andrew, 2005). It allows the measurement of virulence parameters in the form of survival time, bacterial load in lungs and blood, and levels of inflammation (Chiavolini et al., 2008), and the mice may be challenged by intranasal, intravenous, or intraperitoneal routes. While the intraperitoneal route allows the largest dose of inoculum to be delivered, however, the intranasal route mimics the natural means of infection in humans more closely (Chiavolini et al., 2008).

In the current study, outbred female CD1 mice aged 7 to 8 weeks old were used. These mice were infected intranasally with the bioluminescent bacteria to validate the light signals.

3.5.1.1. Validation of luminescence signals of P*phrA::luc*-wt and P*spd1717:: lux*-wt in mice

Female CD1 mice were used for developing and validating *in vitro* results for P*phrA::luc*-wt and P*spd1717::lux*-wt. The two reporter strains were subjected to animal passage to standardise the inoculum, with separate groups of 5 mice infected with pneumococcal strains in doses of approximately 1.2×10^6 CFU/mouse for P*phrA::luc*-wt and $9x10^5$ for P*spd1717::lux*-wt.. External monitoring of transmitted photons at 6 and 24 h post-infection by means of an IVIS imaging system followed such infection. The bioluminescent signals were quantified in anesthetised mice, and no detectable light emission from either group of mice infected with a pneumococcal strain was seen at 6 h post-infection, most likely due to the low bacterial counts at this stage. However, light emission was detectable at 24 h post-infection, though from only two mice in each group (Figure 3.40). At the 24 h examination those mice displaying light emission were sacrificed and the bacteria recovered from their lungs and blood enumerated after serial dilution. There was no difference in bacterial counts recovered from lungs or blood in either strain (Figure 3.41 B, C): he bacterial loads in the blood of mice infected with P*phra::luc*-wt ($\log_{10}$ 7.30 CFU/ml) and those infected with P*spd1717::lux*-wt ($\log_{10}$ 7.32 CFU/ml) were substantially similar (Figure 3.41B). Bacteria counts recovered from the infected mice lungs were $\log_{10}$ 5.47 CFU/mg for P*phrA::luc*-wt and $\log_{10}$ 5.52 CFU/mg for P*spd1717::lux*-wt (Figure 3.41C). Although there was no difference in bacterial loads among the mice tissues infected with the various strains, the peak bioluminescent signals did differ between the strains. P*phrA::luc*-wt measurements reached $3.7x10^7$ RLU, whereas the scanned mice infected with P*spd1717::lux*-wt reached only $5.2x10^6$ RLU (Figure 3.41A), indicating that the light generated by lux was attenuated during whole body imaging, potentially as a consequence of the low penetrating power of the shorter wavelength light emitted by lux.

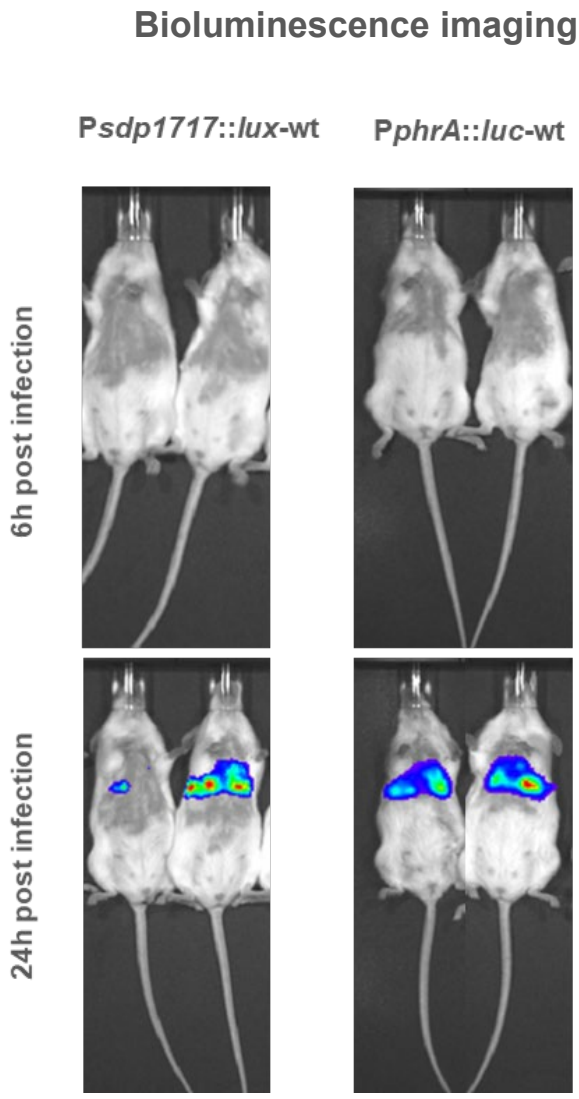

Figure 3.40. *In vivo* BLI of mice infected with *S. pneumoniae* tagged with either bacterial *lux* under *spd*1717 promoter or P*phrA::luc*. Each group of mice (n=5) was infected with *S. pneumoniae* at a dose of approximately 1.2×10^6 CFU/mouse for P*phrA::luc*-wt or with P*spd1717::lux*-wt at a dose of $9\text{x}10^5$ CFU/mouse. Two mice emitting light were detected for each system as infection was followed by IVIS microscope imaging over time, at 6 and 24 h post infection, after subcutaneous luciferin injection. Light emission was detectable at 24 h post-infection from only two infected mice in each group.

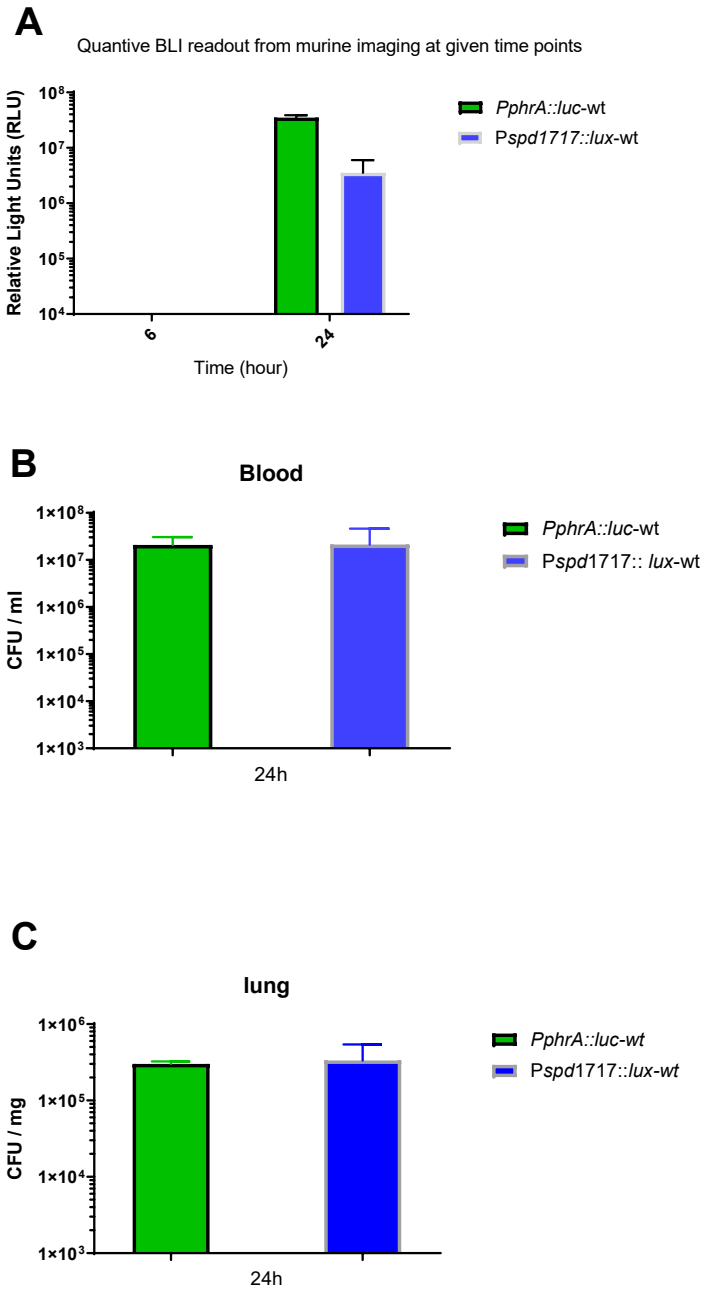

Figure 3.41. *In vivo* bioluminescence imaging. (A) Quantitative BLI readout from murine whole-body imaging at selected time points quantified using Living Image software. Luminescence is shown as relative light units (RLU). Bacterial counts of infected mice recovered from blood (B) and lungs (C) were determined from only positive mice (those emitting light) after plating serial dilutions of homogenate. Data and error bars represent means and standard means. The peak values of relative light units for the two system are thus seen to differ.

Table 3.11. RLU of mice (n=2) infected intranasally with P*phrA::luc*-wt and mice (n=2) infected with P*spd1717::lux*-wt, based on counts of pneumococcal strains recovered from lungs and blood for the two group. Bioluminescence observed 24 h post-infection and RLU data were different for the two groups.

Strains	RLU 6H	RLU 24H	Log10 CFU/ mg lung	Log10 CFU/ ml blood
P*phrA::luc*-wt	7.32E+05	3.23E+07	5.50	7.44
	5.97E+05	3.76E+07	5.45	7.13
P*spd1717::lux*-wt	5.29E+05	1.80E+06	5.27	6.56
	5.05E+05	5.29E+06	5.68	7.58

3.5.1.2. Assessment of bioluminescent signals from P*phrA::luc*-wt after passaging

P*phrA::luc*-wt was further tested in a larger group size, and imaged at 6, 24, and 30 h post-infection. Thirty mice were infected with approximately $2.4x10^5$ CFU/mouse with the P*phrA::luc*-wt strain. The bioluminescence was quantified at 6, 24, and 30 h post-infection by imaging 15 anesthetised mice at each point. The other fifteen mice were divided into three groups, with one such group sacrificed at each of 6, 24, and 30 h post-infection to correlate the RLU with the CFU results. The results of the whole body imaging of mice indicated no bioluminescence at 6h post infection, which is likely to be because, at this stage the bacterial counts were likely to be low and the metabolic state of the bacteria would be less likely to be adjusted for the generation of light (Figure 3.42). Light was detected from 5 of 15 mice at 24 h post-infection, and from 6 mice among the 15 at 30 h post-infection. One mouse died at 30 h post-infection, probably due to high bacterial counts, as the death of the mouse coincided with increased light signals at 24 h, with $9.5x10^7$ RLU was recorded. Analysis from this

experiment included only those mice with positive bioluminescence signals. The peak light signal at 24h post-infection was $5.14x10^7$ RLU, while at 30h, this reached up to $1.13x10^8$ RLU (Figure 3.43A). The bacterial loads from the lungs at 6, 24, and 30 h post-infection were $\log_{10}$ 2.16 ± 0.43 CFU/mg (n=5), $\log_{10}$ 2.29 ± 0.38 CFU/mg (n=5), and $\log_{10}$ 3.3 ± 0.33 CFU/mg (n=11), respectively (Figure 3.43 B).

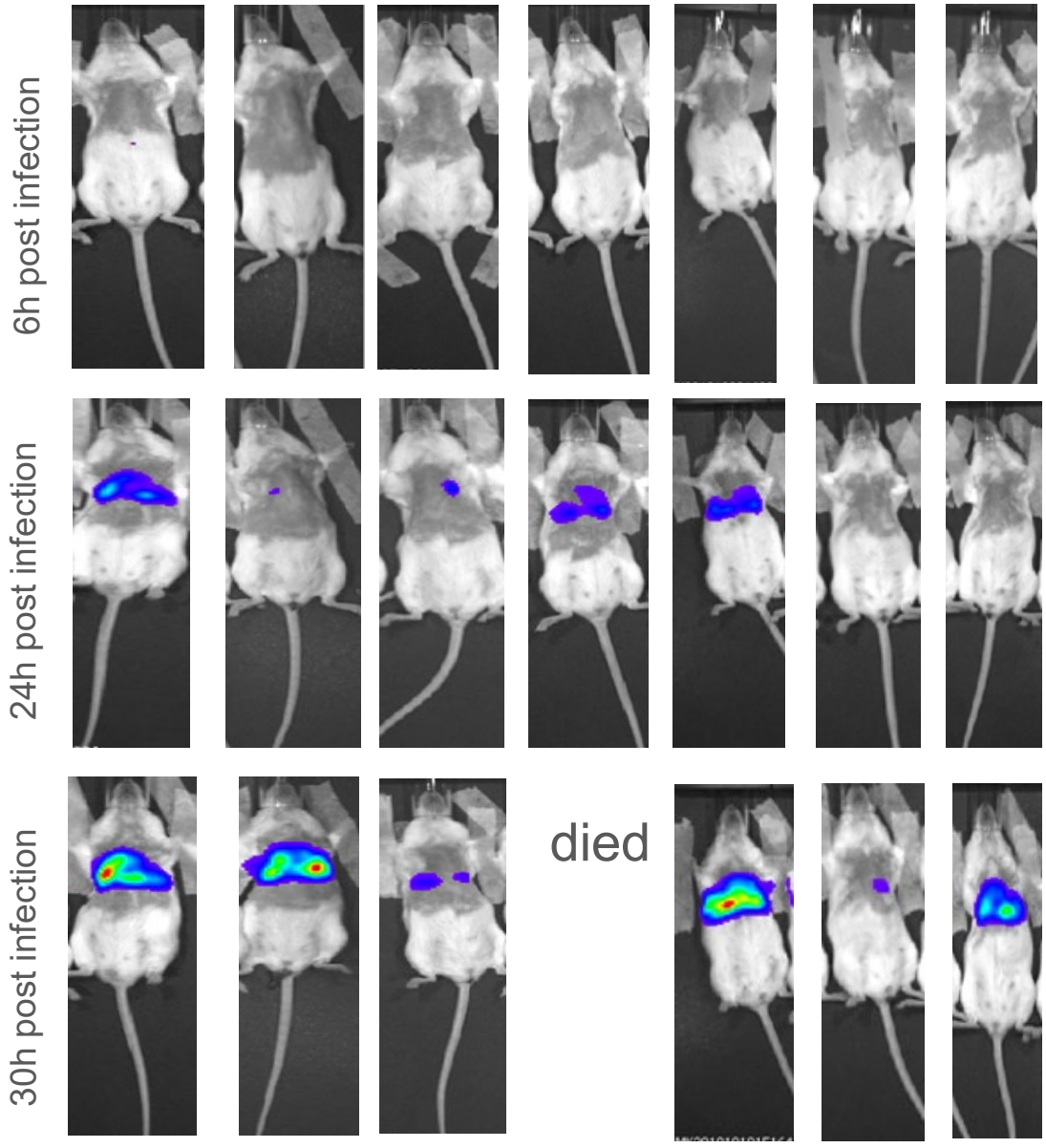

Figure 3.42. *In vivo* BLI of mice infected with *S. pneumoniae* tagged with P*phrA::luc*. Mice (n=15) were infected intranasally with *S. pneumoniae* with doses of approximately $2.4x10^5$ CFU/mouse. The infected mice were imaged using IVIS at 6, 24, and 30 h post-infection after subcutaneous luciferin administration. Light emission was detectable at 24 and 30 h post-infection in 6 mice.

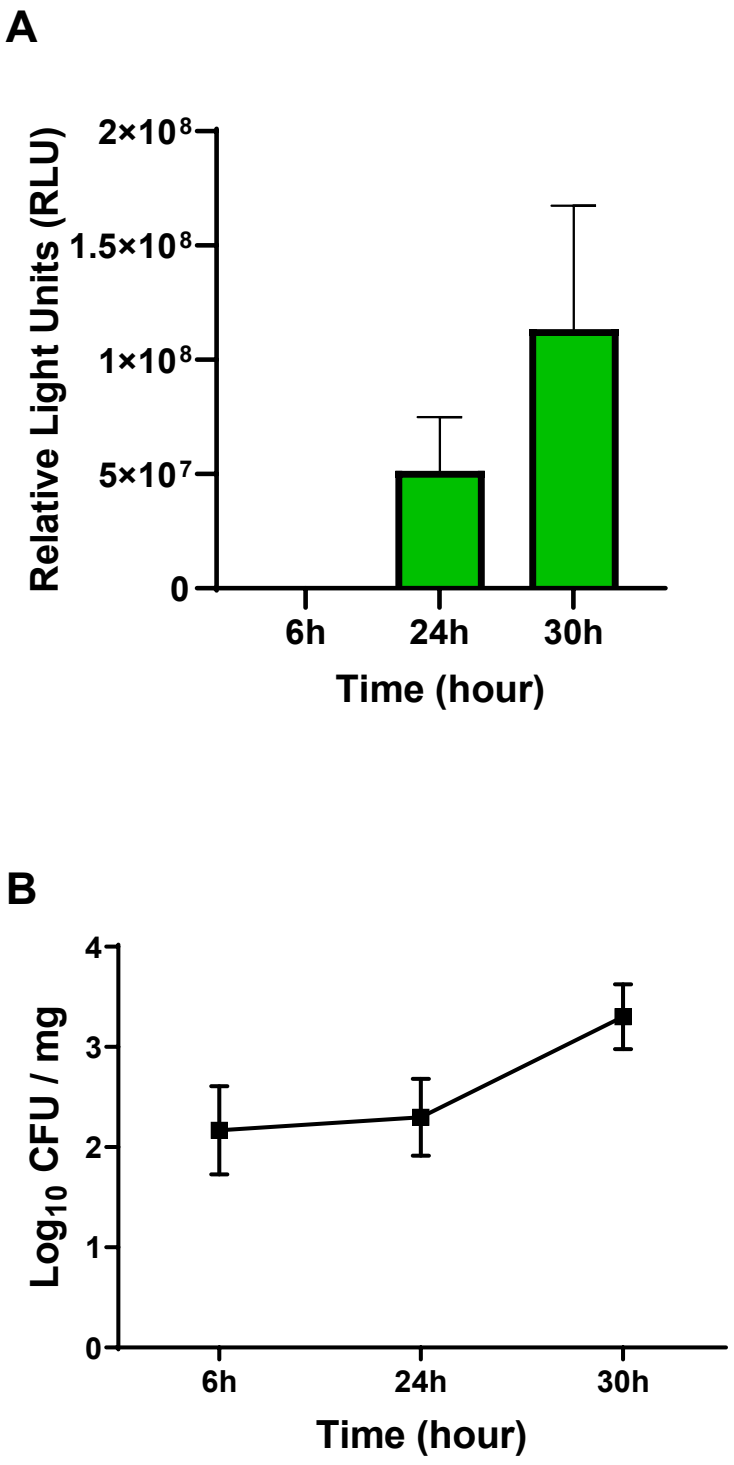

Figure 3.43. *In vivo* bioluminescence imaging of mice infected with P*phrA::luc*-wt. (A) Quantitative BLI readouts from murine whole-body imaging at various time points post-infection. Luminescence is shown in relative light units (RLU). (B) Bacterial count from infected mice recovered from lungs and determined after plating of the homogenate. Data and error bars represent the means and standard errors.

3.5.1.3. *In vivo* virulence test of luminescent P*phrA::luc*-wt strain.

To investigate whether pPP3::*luc* affected pumococcal virulence as compared to the wild type D39, a group of mice (n=15) was infected intranasally either with $2.4x10^5$ CFU/mouse P*phrA::luc*-wt or with $6x10^5$ CFU/mouse wild type D39. At 6, 24, and 30 h post infection, 5 mice in each group were sacrificed and the bacterial loads recovered from the lungs and blood were determined for each group. An unpaired t-test was used to compare the mean of each group for predetermined time points that revealed no diferrences between the two groups. P*phrA::luc*-wt was thus found to be as virulent as the wild type D39. Figure 3.44 shows the mean of bacterial loads recovered from lungs (A) and blood (B) at 6, 24, 30 h post-infection. The bacterial counts recovered from the lungs of mice infected with P*phrA::luc*-wt were $\log_{10}$ 2.16 CFU/mg ± 0.43 (n=5), with $\log_{10}$ 2.23 CFU/ mg ± 0.11 (n=5) retreived for mice infected with the wild type D39 at 6 h post-infection. At 24 h post-infection, the bacterial loads were $\log_{10}$ 2.29 CFU/mg ± 0.38 (n=5) for mice infected with P*phrA::luc*-wt and $\log_{10}$ 1.8 CFU/mg ± 0.37 (n=4) for mice infected with the wild type. At 30h post-infection, the bacterial loads of mice infected with P*phrA::luc*-wt ($\log_{10}$ 4.08 CFU/mg ± 0.81 n=4), and with wild type ($\log_{10}$ 3.45 CFU/mg ± 0.62, n=4) were not significantly different (Figure 3.44A). Negative results as found in mice with no bacteria identified in their lungs were excluded from this analysis.

No bacteria were recovered (Figure 3.44B) from blood for either group at 6 h post-infection. At 24 h post-infection, bacteria from blood was recoverd from only one mouse for each strain, making the results non-statistically comparable. At 30 h post-infection, the bacterial loads recovered from blood were $\log_{10}$ 4.47 CFU/ml ± 0.7 (n=4) for mice infected with P*phr::luc*-wt and $\log_{10}$ 5.89 CFU/ ml ± 0.65 (n=3) for mice infected with the wild type. This difference was not statistically significant ($p > 0.05$), allowing the conclusion that P*phrA::luc*-wt is as virulent as the wild type D39.

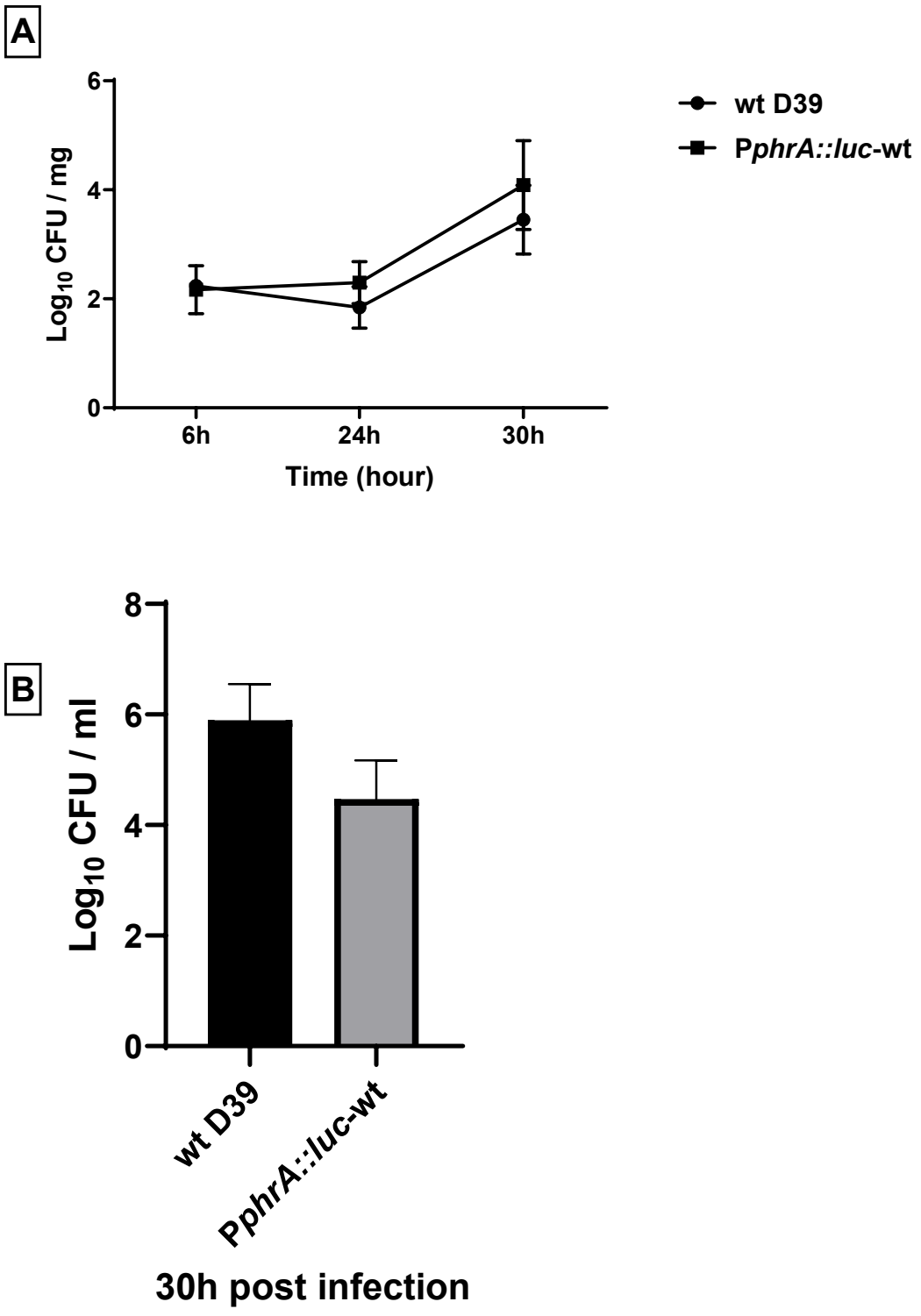

Figure 3.44. Bacterial load in mice tissues infected intranasally with D39 or P*phrA::luc*-wt strains. Bacteria were recovered from the lungs (A) and blood (B) and the colony counts in serially diluted samples determined by plating. Data and error bars represent the means and standard errors. An unpaired t-test revealed no differences between the two groups in terms of bacterial load recovered from the lungs or blood at 30 h post-infection.

3.5.2. Validation of *Galleria mellonella* as a novel model organism to test the bioluminescent P*phrA::luc*-wt strain

The cost ands ethics of using murine infection models must be carefully considered (Ignasiak and Maxwell, 2017), and researchers are thus working to develop alternative models. The features of *G. mellonella* (greater wax moth or honeycomb moth) make it attractive as an alternative infection model, and it is increasingly being used to study microbial infections. *G. mellonella* use is not subject to standard ethical restrictions on mammalian studies, and it is cheap and easy to handle and maintain, requiring no anesthesia or special training in use (Cools et al., 2019, Harding et al., 2013). Nevertheless, the innate immune system of *G. mellonella* shares a structural similarity and functional homology to the innate immune systems found in mammals. *G. mellonella* shows a powerful resistance to microbial infection, despite the absence of an adaptive immune system, based on cellular and humoral defenses (Tsai et al., 2016). This humoral immune system includes antimicrobial peptides, complement-like proteins, and melanin, all of which can kill pathogens. The celullar immune response is further mediated by cells known as hemocytes, which are similar to mammalian phagocytic cells, which are found within the hemolymph, a blood substitute (Tsai et al., 2016). Importantly, *G. mellonella* can also be incubated at 37 °C, which allows for the study of mesophilic bacteria important for human and animal health (Harding et al., 2013).

A number of studies have demonstrated that *G. mellonella* can acts as an *in vivo* infection model for *S. pneumoniae*. *G. mellonella* has been challanged with different isolates to test the virulence of *S. pneumoniae,* as determined by assessing survival time. Mortality was attributed to bacterial growth, while survival was assumed to be due to the clearance of batceria. The model can thus distingush between serotypes with different virulence properties (Evans and Rozen, 2012). *G.mellonella* has also been utilised for the evaluation of antibiotic efficacy. The insects werechallenged with different serotypes of pneumococcus, followed by treatment with amoxicillin and moxifloxacin. These antibiotics had an effect on survival time, proving the suitability of this model for evauating antibiotic efficacy against *S. pneumoniae* (Cools et al., 2019).

Although the *G. mellonella* model is easy to use as compared to mammalian models, it requires a range of additional steps, including larvae homogenization, serial dilution, and

plating, which are time consuming. These additional steps can also lead to errors and large experimental artefacts in results. The use of luminescent bacteria can help reduce the need for these steps and faciliate the follow-up of infection and treatment without the need for bacterial recovery. Using real-time bioluminescence imaging using a *lux* reporter system to track infection in the *G.mellonella* model has thus been reported. *Listeria monocytogenes* was tagged with *luxABCDE* to investigate the expression of virulence genes required for mice infection. This was examined by studying the expression of virulence gene promoter activity during infection in *G. mellonella* larvae at 37 °C. It was observed that virulence genes are expressed significatly in the *G. mellonella* model based on detection of bioluminscence levels indicating promoter activity (Joyce and Gahan, 2010). *In vivo* monitoring of *Mycobacterium abscessus* treatment was also validated in *G.mellonella*, with bioluminscence imaging used to assess the bacterial load of luminescent *M. abscessus* after treatment with various antibiotics. Various antimicrobial effects were thus demonstreted by means of applying this technolgy in the model (Meir et al., 2018).

3.5.2.1. *S. pneumoniae* proliferation kills *Galleria mellonella* larvae in a dose dependent manner.

To prove the susceptibility of *G. mellonella* to *S. pneumoniae* and to demonstrate that this could be used as an infection model, the impact of different inoculum sizes on *G. mellonella* were evaluated in the current work. The insects were divided into sets of 10 animals and infected with different inoculum doses, ranging from 5×10^3 to 1×10^6 CFU/larva. Survival levels were determined throughout the course of infection. Ten larvae were also injected with phosphate buffered saline (PBS) as an assay control. Larvae were kept at 37 °C and monitored over 48 h. After the initial experiment, the 1×10^8 CFU/ml dose was excluded, as the insects could not tolerate this high level of inoculum and died within 3 h. The mean survival percentage was recorded for every dilution after this, however. The results showed that by increasing the dose gradually, the mean survival percentage was decreased, demonstrating the pathogenicity of P*phrA::luc*-wt strain to *G. mellonella* and the ability of the model to respond appropriately to different inoculum sizes. The $1x10^5$ CFU/larva dilution killed most animals, while the $5x10^3$ CFU/larva dose had no effect on mortality, with no mortality recorded within 8 h after infection. The percentage mortality of the cohort that received 1×10^5 CFU/larva was 80% ± 7.0 at 24 h post infection, while the cohort that received $5x10^4$ CFU/larva had 13.3% ± 3.3 mortality, and the group infected with $1x10^4$ CFU/larva developed only 5% ± 5 mortality. No mortality was recorded in the group

challenged with $5x10^3$ CFU/larva. At 48 h post infection, the mean mortality value was 95% ± 2.8 for the group that received $1x10^5$ CFU/larva, while the groups infected with $5x10^4$ and $1x10^4$ CFU/larva had recorded mortalities of 43.3% ± 3.3 and 10% ± 0, respectively. No mortality was observed for the control group injected with PBS (Figure 3.45). These results demonstrated that *S. pneumoniae* is pathogenic to *G. mellonella*, and that mortality occurs not due to the procedure but rather due to the nature of the infectious agent.

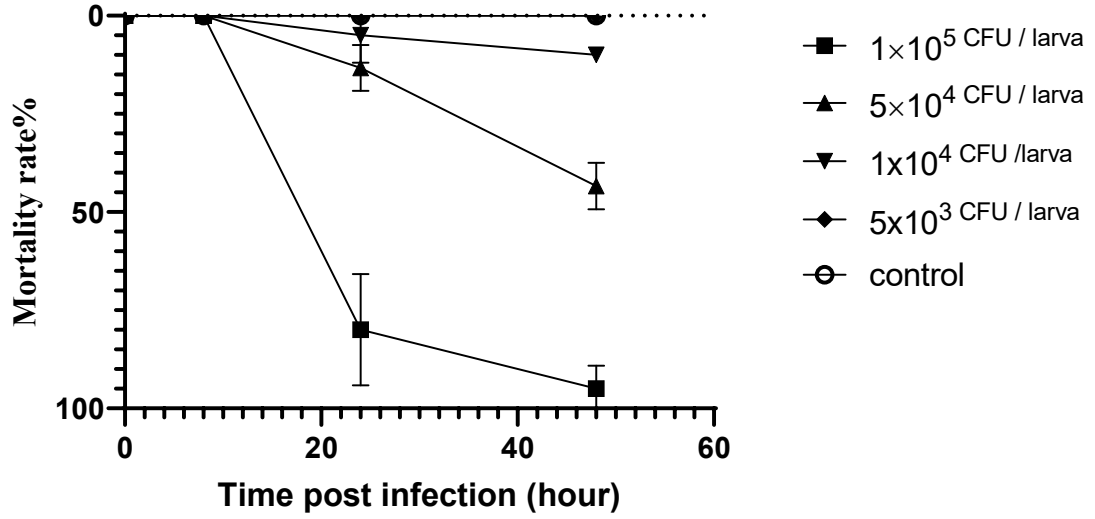

Figure 3.45. *S. pneumoniae* infection of *G. mellonella* to test dose-dependent mortality. Larvae survival after injection with the P*phrA::luc*-wt strain. Inocula of different sizes (~1×10^5,~5×10^4,~1×10^4, and~5×10^3 CFU/larva) were injected to groups of 10 insects and larvae survival was monitored every 8, 24, and 48 h post infection. A PBS injection was used as an assay control. Error bars show the standard errors of means for three individual experiments.

3.5.2.2. Assessment of the effect of luciferin on the viability of *S. pneumoniae* in *G. mellonella*

To facilitate the use and detection of bioluminescent bacteria tagged with CBRluc in living larvae, the impact of substrate concentration on the viability of bacteria was investigated. Three different concentrations of luciferin were used (15, 30, and 60 mg/larva). For each, a group of 5 insects was infected and imaged 2 h post-infection using IVIS, after luciferin injection. Another set of larvae was also included for the CFU assessment, as well as one for assay control which received only PBS. The experiment was repeated two to four times for

every concentration. No significant differences in the RLU were seen when different concentrations of luciferin were used ($p > 0.05$) (Figure 3.46 A, B, and C). Luciferin concentrations of 15 mg/larva, 30 mg/larva, and 60 mg/larva were recorded as giving 410685 ±83723.3, 414900 ±93127, and 426833 ± 111750 RLU, respectively (Figure 3.47A). The insects without luciferin did not generate any light due to the absence of oxidation substrate. Bacteria were recovered from the three larvae groups that received different concentration of luciferin by homogenization, and bacterial counts in the larvae homogenates were determined by plate counting, as described in section 2.19.5. The experiment was repeated three times. The peak values of bacterial load in larvae injected with 15 mg/larva, 30 mg/larva and 60 mg/larva luciferin were 2050 CFU/larvae ± 332.91, 1841.66 CFU/larvae ± 472.65, and 1583.33 CFU/larvae ± 356.00, respectively (Figure 3.47B). The analysis showed no significance differences in bacterial load between the groups that received different concentrations of larvae and the group without luciferin (1925 CFU/larvae ± 675). This experiment thus demonstrated that luciferin concentrations as used in this experiment do not affect either bioluminescence intensity or the viability of bacteria.

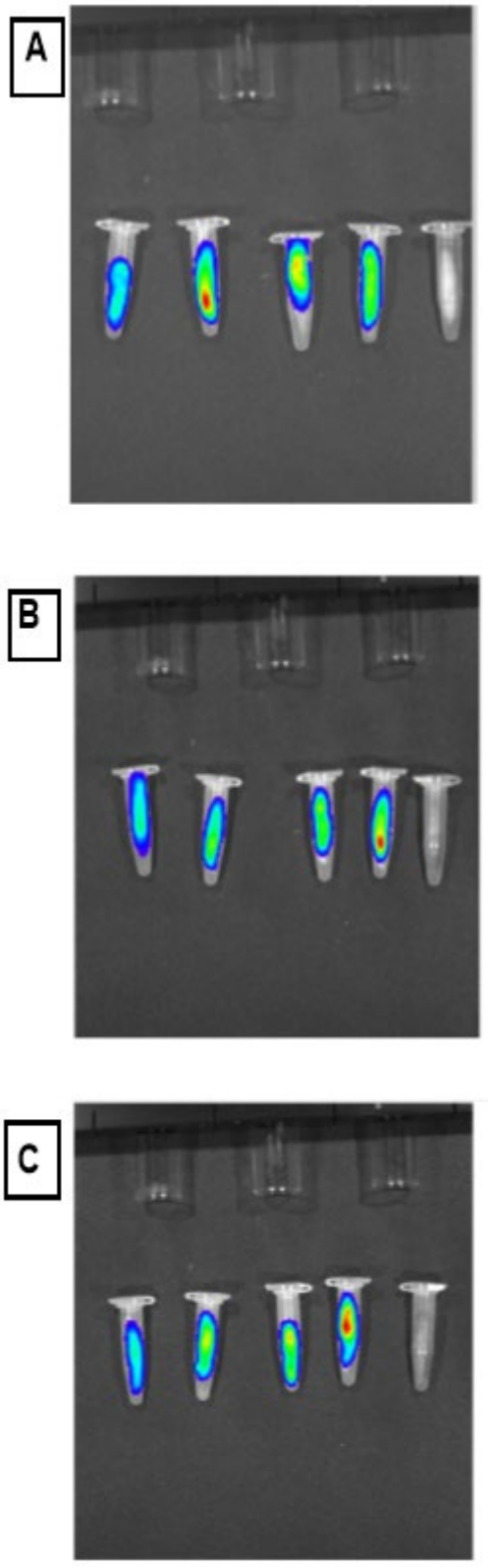

Figure 3.46. Bioluminescence imaging of larvae injected with different luciferin concentrations. Larvae (n=5) injected with the *S. pneumoniae* containing the P*phrA::luc*-wt system with 15 mg/larva (A), 30 mg/larva (B), or 60 mg/larva luciferin before imaging. In each group, one larva was used for CFU counts.

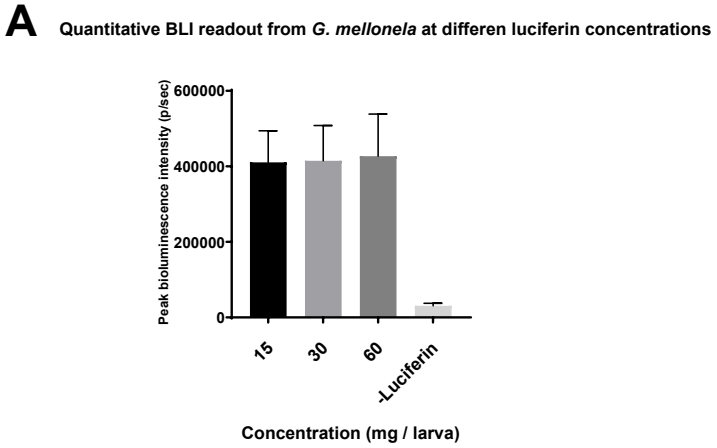

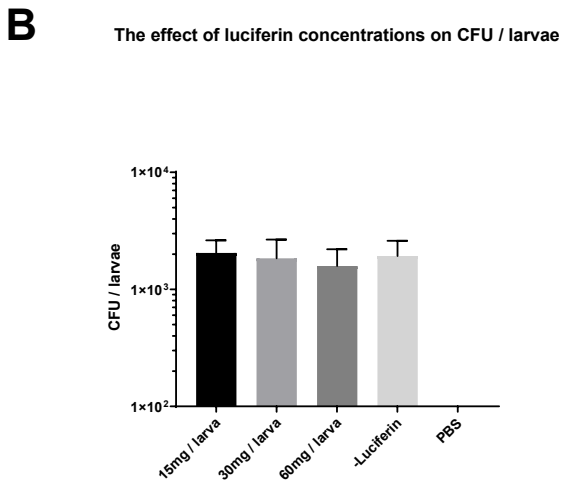

Figure 3.47. Luciferin concentrations do not affect bioluminescence intensity or viability of bacteria. Three inocula of luciferin were used (15 mg/larva, 30 mg/larva, and 60 mg/larva). (A) Peak bioluminescence intensity obtained after injecting all luciferin inocula showed considerable similarity ($p > 0.05$). (B) The viability of bacteria recovered from larvae injected with all different concentrations of luciferin (15 mg/larva, 30 mg/larva, or 60 mg/larva) and the larvae without luciferin showed no significant differences in bacterial load among the groups based on one-way ANOVA and Dunnett's multiple comparison testing.

3.5.2.3. *In vivo* bioluminescence level accompanied by bacterial growth

To validate the use of luminescence as a substitute for CFU counts and to prove the suitability of this model for following the course of an infection using IVIS, *G. mellonella* was infected with varying doses of P*phrA::luc*-wt ($1x10^4$, $5x10^4$, and $1x10^5$ CFU/larvae) in 10 µl. Two hours after injection, luciferin 15 mg/larva (in 10 µl of PBS) was given to the larvae and they were then scanned using IVIS. The bioluminescence was quantified for between 4 to 16 larvae in each case, with the number of pneumococci determined by recovering the haemolymph from infected larvae 2 h post-infection. Haemolymph were pooled (four for each experiment) and CFU/larva was calculated. Each point in Figure 3.48 represents CFU/larva from 2 to 4 independent experiments. The control was the larva injected with PBS. For this analysis, both bioluminescent positive and negative larvae were included. Figure 3.48 shows that, with the increasing dose, the bioluminescence gradually increased. The peak light signals recorded for infective doses containing $1x10^4$, $5x10^4$, and 10^5 CFU/larvae were 33050 RLU ± 7435, 77787 RLU ± 14376, and 181366 RLU ± 23661, respectively. No light was detected for the control due to the lack of bacteria. A linear regression revealed that the goodness of fit was 0.91, and the data thus demonstrate that the bacterial load is correlated with detectable light.

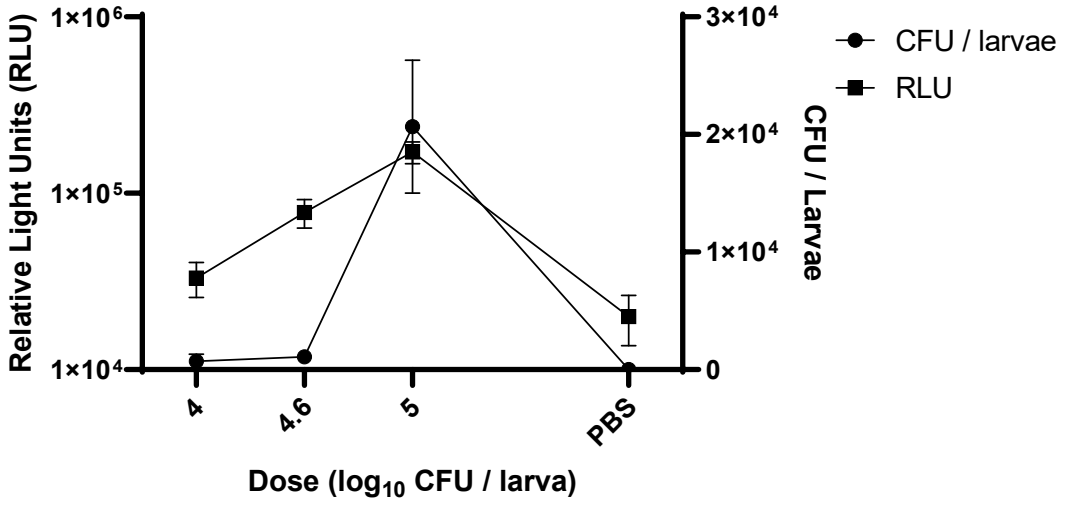

Figure 3.48. Effect of varying inocula doses of P*phrA::luc*-wt on RLU 2 h post infection. *G. mellonella* larvae of 25 to 30 mg were injected with different doses of P*phrA::luc*-wt in 10 µl PBS using a Hamilton syringe. Two hours after injection, 15mg/larva luciferin in 10 µl of

PBS was given to the larvae and they were scanned using IVIS. Each point represents the mean bioluminescence collected from between 4 to 16 *G. mellonella.* For the bioluminescence analysis, both positive and negative larvae were included. By increasing the dose gradually, the bioluminescence was seen to increase as a result. The number of pneumococci from larvae 2 h post infection was also determined. Haemolymph from larvae infected with different doses of P*phrA::luc*-wt were pooled (four for each experiment) and CFU/larva calculated. Each point represents CFU/larva from 2 to 4 independent experiments, while the control indicates the larva injected with PBS as a negative control for CFU.

Chapter 4. Discussion

4. Overview

Streptococcus pneumoniae is a frequent inhabitant of the nasopharynx in healthy hosts but it is also well known for its association with pneumonia and meningitis as well as uncommon diseases, such as sinusitis and otitis media (Bogaert et al., 2004a). Pneumonia is the most common cause of death from infection in developed countries (O'Brien et al., 2009). Resistance to penicillin and other antibiotics remains a challenge for the treatment of pneumococcal infections. In addition, the available vaccines are predominantly protective for the serotypes represented in their formulation (Bogaert et al., 2004b). It is essential, therefore, to study the pathogenesis of pneumococcal infections in detail to develop a better understanding of the mechanism of pneumococcal disease, which is a prerequisite for the development of effective vaccines.

Bioluminescence imaging has been shown to be a sensitive *in vivo* imaging tool and useful approach that streamlines *in vivo* studies of infection models (Demidova et al., 2005). Contag et al. (1995) were the first to report the bioluminescence detection of bacterial pathogens in living animals. Such techniques allow for a reduction in the number of animals required in experiments. An individual animal can be utilised to follow the infection through the entire experiment and thus acts as its own control. The same animal can be used to estimate the bacterial burdens with photonic imaging (Doyle et al., 2004, Andreu et al., 2011). Repeated tissue sampling in conventional methods is not applicable as death is the endpoint of tissue extraction, however with BLI, the same animal can be imaged repeatedly, non-invasively and rapidly. The animal is only sacrificed at main time points for more detailed analyses. Therefore, the use of *in vivo* BLI imaging provides longitudinal monitoring of the bacterial burden. Moreover, BLI provides a major impact on ethical, time and cost considerations (Andreu et al., 2011, Hutchens and Luker, 2007, Doyle et al., 2004). In addition to monitoring the bacterial infection (Orihuela et al., 2003, Henken et al., 2010), *in vivo* BLI with bioluminescent *S. pneumoniae* has been used to evaluate therapeutics and vaccines (Barman et al., 2011).

The aim of this study was to develop improved reporters for enhanced bioluminescence imaging of the pathogen in mouse models of infection. The study was initiated by the construction of the efficient bioluminescent pneumococcal strain to show luminescence in a highest level with a lowest dose of *S. pneumoniae*. Bioluminescent *S. pneumoniae* D39 was

initially successfully generated that allows BLI through expression of the bacterial *lux* operon (*Photorhabdus luminescens*). Francis et al. (2001) used Tn4001 transposon for a random integration of the *luxABCDE* and a kanamycin-resistant cassette, and the construct was transposed into *S. pneumoniae* D39 by plasmid pAUL-A. Light is produced only in a bacterial cell if this operon has transposed downstream of a promoter on the bacterium's chromosome. The resulting bacteria were screened for levels of bioluminescence using an ICCD camera and the most highly-expressing strain was selected and designated Xen7. Sequencing of the transposant's chromosome has revealed that the insertion site of the *lux* operon was the gene coding for a hypothetical protein of unknown function (Gene number SPD_1717). The genome of Xen7 was transferred into a panel of *S. pneumoniae* strains by transformation, and thus this mutation was transferred. This system has been used successfully in previous studies (Orihuela et al., 2003, Johnson et al., 2013, Orihuela et al., 2004, Henken et al., 2010, Barman et al., 2011); however, a decrease in light detection was associated with an increase in tissue depth because of the low penetrating power of the shorter wavelength light emitted by *lux* operon (peak 490 nm). In invasive bacterial infection, the surrounding tissue may attenuate BLI signals and thus this system can underestimate the actual *in vivo* bacterial load (Andreu et al., 2011). *In vivo* BLI with *lux*-expressing strains, therefore has been suggested to be more effective for determining the bacteria burden for superficial bacterial infections such as microbial infections of the skin (Miller et al., 2019).

Here I created a vector expressing click beetle (*Pyrophorus plagiophthalamus*) red luciferase (CBRluc), which emits longer wavelengths of light up to 593 nm with potential applications in deep tissue whole-body imaging (Andreu et al., 2011). CBRluc construct was stably integrated into a bacterial genome to maintain light production in all progeny and to make BLI signals highly correlated with the CFU. With CBRluc, the light production is generated only with the addition of the substrate, luciferin, at the bioluminescence measurement whereas *lux* operon continuously produces light and consumes ATP (Hakkila et al., 2002). Therefore, the bacteria harbouring *lux* operon are under constant metabolic stress. This has been observed in a bioluminescent strain of *Citrobacter rodentium,* where the bioluminescent strain showed a competitive disadvantage in a mouse model of infection, due to a constitutive expression of *lux* operon (Read et al., 2016). The random integration of the *luxABCDE* cassette into the genome may affect the virulence of the selected strain. This has been shown in a bioluminescent derivative of *S. pneumoniae* TIGR4, where expression of the *lux* operon resulted in reduced virulence compared to the parent TIGR4 in a mouse model of infection (Blue and Mitchell,

2003). Further to the impact on the virulence, the expression of *lux* genes led to down-regulation of the expression of the pneumococcal pilus (Herbert et al., 2018). Xen7 genome was transferred to TIGR4 to create Xen35, where the *lux* operon was inserted into SP_1914 (the TIGR4 equivalent of SPD_1717). These genes in Xen35 are, therefore, of a D39 (serotype 2) allele. Herbert et al. (2018) used genomic analysis for Xen35 and the parent TIGR4 to show the reason for the difference in virulence. They observed that there are many genomic changes that caused mutations, which are seemingly derived from Xen7. In addition, they found changes in gene expression levels of Xen35 compared to the parent TIGR4. Herbert et al. (2018) concluded that the expression of the *lux* operon in TIGR4 affects the expression level of known virulence factors, leading to a reduced virulence of TIGR4 similar to that observed with Xen35.

The impact of the expression of *lux* operon has been attributed to the disruption of carbon catabolism (Herbert et al., 2018). Production of light by *lux* genes relies on the recycling of FMN to $FMNH_2$. This recycling is catalysed by flavin reductase that is NADH dependent, resulting in the oxidation of NADH to NAD^+. The level of NAD^+ is, therefore, relative to NADH. These two factors are required for carbon catabolism and thus it is necessary to maintain the redox balance. Alteration in the redox balance has been observed to affect bacterial metabolism (Vemuri et al., 2006, Neves et al., 2002). Changes in carbon catabolism led to alterations in the regulation of some genes and thus regulation of virulence factors was influenced in *S. pneumoniae* (Iyer et al., 2005). Alteration in the redox balance of pneumococcus may also affect enzymes that need NADH, such as NADH oxidase. This enzyme has been implicated in the toxic effects of oxidative stress on the pneumococcal cell (Auzat et al., 1999). The deficiency of virulence may also be due to the need for ATP for production of the aldehyde substrate (RCHO) to generate the light. The aldehyde is oxidised to produce a long-chain fatty acid (RCOOH), which is required for bacterial luciferase reaction, *lux* operon (Wilson and Hastings, 1998). Utilisation of ATP in luciferase reaction may deplete the cellular levels of ATP, which is required for cellular metabolism. *S. pneumoniae* depends on the fermentative breakdown of sugars to generate energy (Al-Bayati et al., 2017). The central metabolism of pneumococcus consists primarily of glycolysis. Two molecules of ATP, two molecules of NADH and two molecules of pyruvate are generated by catabolising glucose and other sugars via glycolysis. Glycolysis is followed by pyruvate fermentation to generate lactic acid by lactate dehydrogenase (NADH dependant); simultaneously NAD+ regeneration, which is required for glycolysis, and under aerobic conditions, sugar limitation or other

conditions such as formate, acetate and ethanol, is generated (Figure 4.1) (Ramos-Montañez et al., 2010). Bioluminescence production via *lux* genes may, therefore, deplete the ATP and NADH (Herbert et al., 2018).

Unlike *lux* operon, CBRluc is non-NADH dependent, and in the present study a stable chromosomal integration of CBRluc in *S. pneumoniae* (using a defined site and under a defined promoter) was achieved. Transformation of large genetic entities, such as operons, in a single transformation may be associated with some genomic changes (Croucher et al., 2012). This suggestion was observed in Xen35, where mutations were shown outside of the *lux* gene recombination region (Herbert et al., 2018). The present work aimed to enhance the bioluminescence imaging of the pathogen in infection models by using a reporter gene that generates longer wavelength light. In addition, an attempt was made to overcome any mutation that may affect the virulence by using a defined site under a defined promoter.

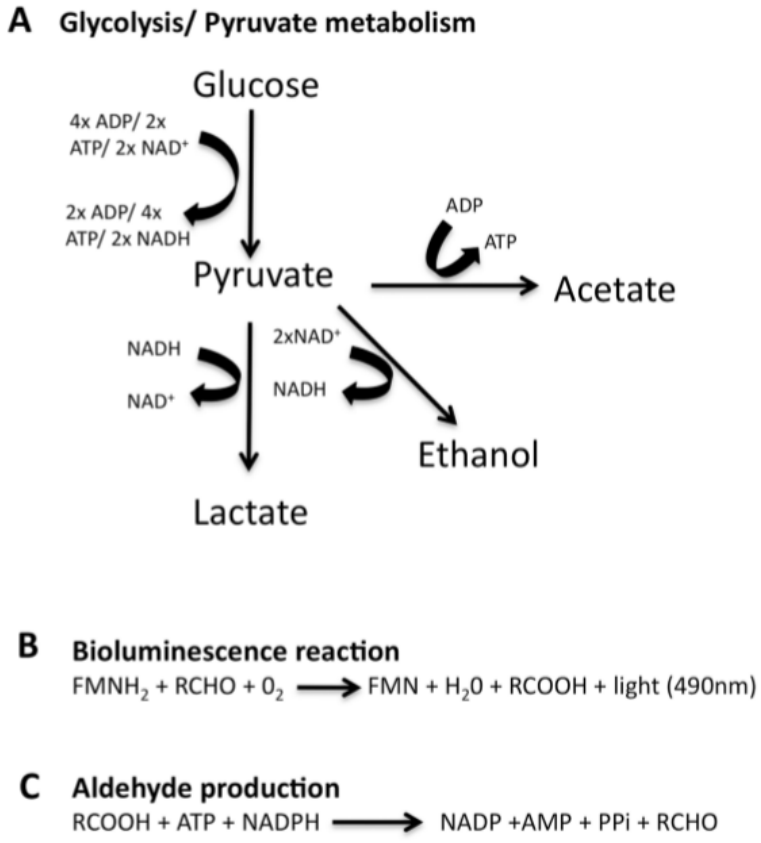

Figure 4.1. The diagram shows the generation and consumption of energy. (A) Glycolysis starts with a breakdown of glucose producing adenosine triphosphate ATP, reduced nicotinamide adenine dinucleotide (NADH), and pyruvate. The reaction requires ATP, adenosine diphosphate (ADP) and oxidised nicotinamide adenine dinucleotide (NAD+). The pyruvate metabolism generates further ATP. (B) Bacterial luciferase reaction. The reaction is

catalysed by luciferase enzyme for reduced riboflavin ($FMNH_2$), long-chain aldehyde (RCHO) and oxygen (O_2) producing flavin mononucleotide (FMN), water (H_2O), fatty acids (RCOOH) and generating light (490nm). (C) Aldehyde generation. Starting with long-chain fatty acid (RCOOH), energy (ATP), reduced nicotinamide adenine dinucleotide phosphate (NADPH), which is catalysed by the fatty acid reductase producing nicotinamide adenine dinucleotide phosphate (NADP), adenosine monophosphate (AMP), pyrophosphate (PPi) and RCHO (Herbert et al., 2018).

4.1. Manipulation of pneumococcal strains

To investigate the intensity of bioluminescence generated by CBRluc relative to *lux* genes, I created a CBRluc-expressing strain under a putative promoter that is highly expressed *in vivo*. The CBRluc gene was integrated into a known site in the *S. pneumoniae* genome using pPP3 plasmid. This plasmid enables a stable genomic integration of promoters. Five genes predicted to be highly expressed were selected in this study. The promoter sequences of these genes were obtained using the BPROM-softberry programme that detects the -10 and -35 nucleotides upstream of the transcription start site, which are essential for transcription initiation and the rate of transcription. The promoters were amplified to drive the expression of the CBRluc gene. Although the recombinant plasmid can directly be transferred to *S. pneumoniae*, *Escherichia coli* was used to propagate the recombinant plasmid DNA. The recombinant plasmid was then transformed into *S. pneumoniae*. The transformation is the uptake of naked DNA by the bacteria and the integration of the acquired DNA molecule into their genome. The ability to uptake DNA is called competence. *S. pneumoniae* was the first pathogen observed with a natural transformation system where cells acquire competence as they grow. The bacteria become competent when they are grown to a cell density of between 10^7 and 10^8 bacteria/ ml (LACKS, 1997).

To construct the bioluminescent strains, the recombinant plasmids were transformed into *S. pneumoniae* after isolating from *E. coli*. To confirm the success of the transformation, genetic analysis and bioluminescence measuring, via luminometer and IVIS microscope, were performed. Production of light from all the constructed strains confirmed the successful transformation, and the promoters were able to drive the CBRluc expression successfully. A *lux*-expressing strain was created herein using chromosomal DNA from the bioluminescent *S. pneumoniae* strain D39*lux* (Jensch et al., 2010). The strain D39*lux* was obtained by

transforming with the genomic DNA from the bioluminescent strain Xen10 (A66.1 serotype 3) (Francis et al., 2001).D39 Xen10 carries the Tn4001 *luxABCDE* Km^r cassette under the promoter of the SPD_1717 gene and shows the bright bioluminescence (Francis et al., 2001). In addition, to make a direct comparison for the bioluminescence expression of *lux* cassette and CBRluc, *lux* operon was integrated into pPP3 after the removal of the *luc* gene, under the putative *phrA* promoter, which has the greatest bioluminescence expression among the promoters. Production of luciferase and emission of light proved the successful transformation. DNA sequencing was used for further confirmation of *lux* operon cloning.

4.2. Growth and kinetics of *S. pneumoniae* wild-type and bioluminescent constructs *in vitro*

The growth assessment of bioluminescent *S. pneumoniae* in different media by monitoring the optical density at 600 nm (OD) and cell viability (CFU) did not show any difference relative to the wild-type growth, indicating the successful integration of CBRluc. The addition of the luciferin substrate did not impede the growth behaviour. This result was consistent with the results obtained with different bioluminescent bacteria, *Listeria monocytogenes* (Ur Rahman et al., 2017) and lactic acid bacteria (Daniel et al., 2013). It was suggested that the expression of CBRluc is affected by the metabolic state of bacterial cells because the luciferase reaction relies on bacterial metabolites, mainly ATP. This was illustrated by increasing the light output as bacteria grew and then the gradual decrease in the light was observed when *S. pneumoniae* entered the stationary phase, which reflects the slow decrease in the metabolic activity. This has been shown in previous studies with different bacteria (Ur Rahman et al., 2017, Daniel et al., 2015, Andreu et al., 2010, Marincs, 2000). Reliance on metabolic activity may be an advantageous tool in the detection of a microbial metabolic activity state. The *in vitro* growth rate of *lux*-expressing strains in BHI broth was not affected by the presence of the integrated plasmid in previous studies (Sandgren et al., 2005, Francis et al., 2001, Jensch et al., 2010).

In this study, the light output for the *lux* harbouring strains increased as the bacteria grew and a sharp decrease in the bioluminescence signal was observed when bacteria entered the stationary phase. The sharp reduction in light intensity was also reported previously (Herbert et al., 2018, Francis et al., 2001). This was attributed to a decreased metabolic recycling of FMN to $FMNH_2$, the essential co-factors for bacterial luciferase activity. This was investigated

by Szittner et al. (2003), where a 100-fold increase in light emission was observed when they cloned a gene encoding a NADPH-FMN oxidoreductase in a yeast model. The availability of $FMNH_2$ could be a limiting factor. However, as the mechanism of bioluminescence generation by CBRluc does not rely on the metabolic recycling of FMN to $FMNH_2$, efficacy, CBRluc containing strains exhibited robust activity in the lag and stationary phases in this study.
Neuraminidase and pneumolysin activities in bioluminescent constructs were tested compared to the wild-type (D39). Previous studies have focused on the role of neuraminidase and pneumolysin activities in their contribution to pneumococcal colonisation and pathogenesis. Brittan et al. (2012) reported that a deficiency of neuraminidase A led to a decrease in pneumococcal adherence to epithelial cells, and biofilm formation. The adherence failure of a mutant clarifies the role of neuraminidase in colonisation. The neuraminidase activity reveals receptors for adherence and releases monosaccharides from complex host glycans, providing a carbon source for pneumococcus. This observation is in accordance with what was shown about the role of NanA in mucin utilisation (Yesilkaya et al., 2008). The pneumolysin mutants showed decreased virulence for mice relative to the wild-type D39, as reported by Berry et al. (1989). Given the important role in pneumococcal pathogenesis, neuraminidase and pneumolysin activities were tested in this study. The results showed similar neuraminidase and pneumolysin activity levels in bioluminescent strains such as the wild-type, showing the integration of bioluminescent constructs did not influence the synthesis of two important determinants of pneumococcal virulence.

Luciferase production by the recombinant strains was measured *in vitro*, using IVIS microscope and luminometer, in parallel with the determination of the total number of viable pneumococci in this study. Comparing RLU to CFU in *S. pneumoniae* cultures showed that the peaking of photon emissions per CFU was observed for all promoter-containing constructs during the log phase following four hours of bacterial growth, and then decreased gradually when the bacterial cells entered the stationary phase. This phenomenon was similar to what has previously been reported for CBRluc (Miller et al., 2019, Ur Rahman et al., 2017, Daniel et al., 2015, Daniel et al., 2012); suggesting that a decrease in bioluminescence was very likely due to the impact of metabolic changes taking place during the stationary phase. As observed previously for CBRluc-producing strains of lactic acid bacteria (Daniel et al., 2012), there was a tight correlation between bioluminescence output and the colony-forming units during the log phase, and a positive correlation between the OD_{600} and light yield during the exponential

phase. These findings indicate that luminescence from CBRluc-tagged bacteria can successfully be used for the accurate quantification of bacterial numbers during growth.

4.3. *phrA* promoter provided the highest luciferase expression

Promoters of the five selected genes were generated and cloned into pPP3::CBRluc-wt. The resulting constructs were integrated into a pneumococcal genome. The promoter strength of the five selected promoters was investigated by determining the bioluminescence profile per cell count. Light was measured during growth in the BHI medium. The promoters drove the expression of CBRluc in *S. pneumoniae* successfully. The results demonstrated that the reporter strains are affected by the strength of the promoter. During the log phase, the promoter strength decreased in the order P*phrA* > P*pflB*> P*pspA* > P*htrA*> P*vp1*, as indicated from the RLU/ CFU data (Figure 3. 21). The data showed that photon counts for CBRluc strains under the *phrA* promoter yielded the highest bioluminescence per CFU relative to those recorded for the other CBRluc strains ($P < 0.0001$). The mean the values of RLU per $1x10^8$ cells for P*phrA::luc*-wt was 15258 RLU ± 3858 followed by P*pflB::luc*-wt with 7054 RLU ± 1827, P*psp::luc*-wt with 1777 RLU ± 593, P*htrA::luc*-wt with 1056 RLU ± 415 and the minimum value was recorded with P*vp1::luc*-wt with 185 RLU ± 57. The findings indicated that these genes are highly expressed in the growth conditions employed in this study.

The *phrA* promoter was found to be highly induced in this study which is consistent with a previous study, which showed that *phrA* in *S. pneumoniae* is highly expressed during the colonisation of the human host (Hoover et al., 2015). In a mouse model of pneumococcal pneumonia, the cohort challenged with *phrA* mutant showed a higher survival time compared to the wild-type, proving the significant role of PhrA in pneumococcal virulence (Motib et al., 2019). Due to its importance in pneumococcal infection, a high expression of *phrA* would be expected. Under the promoter of *pflB*, the expression was high but not stronger than P*phrA* in this study. *pflB* mutant was found to be attenuated in pneumococcal growth (Al-Bayati et al., 2017) due to the importance of *pflB* for galactose metabolism. It is, therefore, expected to be highly expressed and this was shown in the results of this study and is in agreement with the findings presented in an earlier study (Karlin et al., 2004). PspA is important for the colonisation of the nasopharynx, which provides a binding site for lactoferrin, an iron-sequestering glycoprotein, at respiratory mucosal sites. The binding of lactoferrin to

pneumococci interferes with host immune functions during pneumococcal infection (LeMessurier et al., 2006). However, *pspA* mutation had no effect on the colonisation of the human nasopharynx (McCool et al., 2002). Microarray analysis has shown that *pspA* transcription appears to be upregulated in the blood (Orihuela et al., 2004). *In vivo pspA* was reported to be highly expressed in bacteria recovered from the nasopharynx and blood, compared to *cps2A, piaA, ply, nanA* and *spxB* during the progression of the disease from the colonisation of the nasopharynx to systemic disease (LeMessurier et al., 2006). The *in vitro* expression results herein showed superiority of P*phrA* over P*pspA*.

HtrA is a member of the heat-shock proteins group which is a highly conserved group. These proteins are induced in bacteria when they are exposed to environmental stress conditions such as elevated temperature (Ibrahim et al., 2004). Deletion of *htrA* leads to reduced fitness of *S. pneumoniae* for colonisation and increased sensitivity to thermal, oxidative and osmotic stress (Sebert et al., 2002). Given the important role of *htrA* it was expected to be expressed highly. However, P*htrA* herein showed a similar light expression to P*pspA* and a weaker expression compared to P*phrA*.

Virulence peptide 1 (*vp1*) was notified to be a highly-expressed peptide in chinchilla middle-ear effusions. In addition, this peptide has been reported to be present in the vast majority of pneumococcal strains and is one of the most highly-expressed transcripts when pneumococci are exposed to host cells (Cuevas et al., 2017, Aprianto et al., 2018). *Vp1* promotes biofilm development and positively regulates a genomic locus responsible for processing, importing and the catabolism of hyaluronic acid (Marion et al., 2012, Yadav et al., 2013, Cuevas et al., 2019).In animal infection models, *vp1* has been reported as acting as a virulence factor that contributes to carriage, dissemination and mortality(Cuevas et al., 2019, Cuevas et al., 2017). The addition of synthetic *vp1* to the pneumococcal cultures enhanced the biofilm formation (Cuevas et al., 2017). The *in vitro* results herein of the reporter pneumococcal strain containing the *vp1* promoter on BHI did not show any light expression. It was thought that this could have been due to a technical error during the processing of the strain. However, when this reporter strain was tested for light expression on CDM media supplemented with galactose during *in vitro* growth (data not shown) to check if there was an induction, P*vp1::luc* containing pneumococcal strain showed a light expression close to the *pflB* expression but not higher than *phrA*. It seems that when CDM supplemented with galactose is used, the *vp1* promoter would be induced. Previously, it was reported that *vp1* is repressed in rich media (Kadam et al. 2017;

Cuevas et al. 2017). This finding suggests that galactose must have a major influence in the induction of the *vp1* promoter.

In this study, factors affecting the induction of selected promoters have not been studied. However, in future, the environmental factors important for the induction of these promotors can be studied quantitatively in the presence of, for example, different sugars, metals and acidity. Finally, the promoter of the *16SRNA* gene, a major component of the small ribosomal sub-unit with 1500 ribonucleotides, was constructed and can be used to normalise the RLU expression for other strains due to its constitutive expression (Saxena et al., 2008).

4.4. Stronger bioluminescence produced from CBRluc than *lux* operon *in vitro* under the same promoter

A strong expression of the *lux* cassette, placed under the promoter of P*SPD1717* but not under P*phrA* , was shown by IVIS imaging and luminometer in this study. Under different promoters, there was no significant difference between these two systems, *lux* and CBRluc. However, the light produced from *lux* operon under the *PSPD1717* promoter was higher during the exponential phase then faded quickly as bacteria entered the stationary phase. This observation was reported by Francis et al. (2001) study with the same strain Xen10. Likewise, previous studies with different bacteria, for example with *L. monocytogenes*, containing *lux* operon showed the sharp reduction of light at the stationary phase (Ur Rahman et al., 2017, Riedel et al., 2007). Furthermore, during the monitoring of gemifloxacin activity on *S. pneumoniae in vitro*, a sharp decline in light generation was shown before the peak of bacterial growth (Beard et al., 2002). The reduction was attributed to a decreased metabolic recycling of FMN to $FMNH_2$, the essential co-factors for bacterial luciferase activity (Duncan et al., 1994).
When both the *luc* and *lux* systems were placed under the P*phrA* promoter in this study, a significant difference was shown between the expression of CBRluc and *lux* operon. The CBRluc expression generated brighter light than *lux* operon under P*phrA*. The CBRluc expression was approximately 31 times brighter than the signal obtained with *lux* operon, very likely due to emitting longer wavelength light. I showed that the luminescence of CBRluc can be detected during pneumococcal infection in mice. This system can be useful when lower numbers of bacteria are used to initiate infection, and thus imaging can be more sensitive.

Previous studies compared the use of different bioluminescent reporters in the same host. The use of the firefly, Fluc, *Gaussia* Gluc and the bacterial luciferase *lux*, were optimised in mycobacteria (Andreu et al., 2010). This study concluded that Fluc produced the highest luminescence *in vitro* and *in vivo*, ten times brighter than that obtained with *lux*, and 100 times that of Gluc. These conclusions are in agreement with my results, except that I used CBRluc instead of Fluc; however, these two luciferases belong to the same luciferase system and both need a substrate for the production of the light and ATP. Another study also reported the same findings for CBRluc and the *lux* system in *Lactococcus lactis* (Daniel et al., 2012). The authors found that the bioluminescence signal obtained from *L. lactis*-CBRluc was ten times higher than in *L. lactis lux* reporter, indicating the suitability of CBRluc for *in vivo* bacterial detection. Snewin et al. (1999) reported that the *lux* system generates a brighter light than Fluc. However, this study used *luxAB* alone without *luxC*, *D* and *E* genes which are significant for the regeneration of the aldehyde substrate from the fatty acids produced by the bacterial luciferase reaction. Using *luxAB* alone requires the addition of an exogenous substrate (aldehyde) which may be in excess, thus the signal was higher. Andreu et al. (2010) tested this explanation by cloning an extra promoter in front of *luxCDE* to induce the substrate synthesis, which led to a six-fold higher signal intensity.

4.5. *In vivo* test of CBRluc and *lux* systems

Once the bioluminescent constructs were tested *in vitro*, where the signal intensity mediated by P*phrA*:: *luc* during *in vitro* growth was enhanced especially during the exponential phase, I proceeded to explore whether the bioluminescence signal obtained with the recombinant strain under P*phrA* was strong enough for the imaging of bacteria *in vivo* in host tissues. Different pathogens in previous studies have been tagged with CBRluc reporters generating enhanced whole-body images in a murine infection model (Daniel et al., 2015, Ur Rahman et al., 2017). Murine infection models are widely used for studying pneumococcal infections (Van Der Linden et al., 2009). These models allow studying many different parameters such as survival time, bacterial load in lung and blood, level of inflammation and the histological changes induced by the pathogens on tissues. They allow the generation of reproduceable data (Chiavolini et al., 2008).

In this study, mice were challenged intranasally to mimic the natural way of infection in humans. The infective dose can be administered in a controlled manner through an intranasal route. The *in vivo* imaging included P*phrA*::*luc*-wt and P*1717*::*lux*-wt reporter strains. CBRluc uses a non-toxic substrate (luciferin) that can be repeatedly administered for multiple time-points for image acquisition. This aspect of CBRluc can be an advantageous feature, where the light production is generated only when the substrate is added and not continuously. This means the cells are not under constant metabolic stress for the generation of light. Furthermore, luciferin is not expensive (Van Reet et al., 2014), it is well optimised for administration, and repeated subcutaneous injection of luciferin did not show local damage at the injection site (Inoue et al., 2009). In this study, the luciferin was administrated subcutaneously, which gave a stronger signal than that obtained with the intraperitoneal injection route in the mouse tumour model (Inoue et al., 2009). P*phrA*::*luc* or P*1717*::*lux*-expressing *S. pneumoniae* were subject to passaging in order to standardise the inoculum.

The signal producing *S. pneumoniae* in mice could be seen in the lungs of mice infected either with unpassaged P*phrA*::*luc* or P*1717*::*lux*-expressing *S. pneumoniae.* Analysis of the two-system revealed that the *in vitro* expression profile was not reflected *in vivo*. The two-system showed similar dynamics in the early phase of infection. No bioluminescence was generated within the six-hour post-infection time for either system (Francis et al., 2001). It is possible that bacteria did not reach a threshold concentration, hence no light was detected six hours post infection. Differences in the peak emission between the two strains were observed 24 hours post infection, with a higher bioluminescence signal for *S. pneumoniae* CBRluc. Although there was no difference in the bacterial load recovered from lungs, the peak emission was higher for P*phrA::luc*-wt. The signal had approximately a tenfold superiority to those of *S. pneumoniae-lux*. This probably is due to the nature of bioluminescence that is emitted by *lux*, which is the blue and small part of the emitted light that can travel through tissues. The signal attenuation was during the whole-body imaging, potentially because of the low penetrating power of the shorter wavelength light emitted by *lux* operon. Due to this aspect of *lux* operon, a high dose of bioluminescent *S. pneumoniae* was required to initiate and monitor pneumococcal infections (Johnson et al., 2013).

The bioluminescent pneumococcal strain Xen10 is a middle-ear adapted strain with the Xen7 genome that was developed by Francis et al. (2001). Xen10 was used for studying

pneumococcal otitis media in chinchillas. During the monitoring of the infection, Johnson et al. (2013) observed that bioluminescence cannot be detected with concentrations of less than 10^4 CFU/ mL, which is higher than the stated concentration to initiate the middle-ear infection (500 CFU/ mL) (Johnson et al., 2013). The use of a high inoculum dose, therefore, is not ideal for the capture of the important aspects of pathophysiology of a middle-ear infection. The authors concluded that this system with *lux* operon is unable to detect small concentrations of bacteria. Moreover, the bioluminescent signals were attenuated during passage through the tissues (Johnson et al., 2013). This limitation might hinder the use of a system harbouring *lux* operon. Similarly, dim signals generated from the *lux*-expressing *S. epidermidis in* biofilms was difficult to detect because this system is constrained with the microbial metabolic activity and *S. epidermidis* biofilms consist of metabolically-dormant cells (Miller et al., 2019, Vuong et al., 2008, Cerca et al., 2014). *In vivo* BLI signals of *lux*-expressing strains compared with the *lux* + *luc* expressing strain in the mouse model of *Staphylococcus aureus* bacteraemia showed that the latter strain gave considerably high levels of BLI signals from internal organs, such as the kidneys, relative to the expression of *lux* alone, improving the detection and imaging of the bacterial burden (Miller et al., 2019). Increasing the BLI signals with deeper penetration allowed an improvement in the *in vivo* BLI imaging of organ dissemination during bacterial infection in mice. The high photon emission of CBRluc is due to the longer wavelength ranging from 546 nm to 593 nm in the red-light spectrum, which exhibits better penetration (Wood et al., 1989, Andreu et al., 2011). The CBRluc luciferase gene is a single polypeptide, whereas *luxABCDE* operon has five polypeptides and thus there is a difference in the induction coefficients of both luciferases. This may explain the difference in the light production (Hakkila et al., 2002).

Unlike the *lux* system, the CBRluc system was able to generate light even with a low dose in this study. The dose was ten times less, between 1.8 to $2.4x10^5$ CFU/ mouse, and the light was generated in this number of bacteria in 36% of mice after passaging. The mice were sacrificed to determine the thresholds of detection and to correlate luminescence with the bacterial load. The lower limit of bacterial detection in case of CFU was $\log_{10}$ 2.16 CFU/ mg of the lungs whereas the lower limit of RLU detection was $\log_{10}$ 3.35 CFU/ mg in the lungs.
The effect of passaging on the production of microbial hemolysin and phospholipase in rabbits was investigated using unpassaged and passaged *Listeria monocytogenes* which showed similar activity levels (Vahidy et al., 1996). However, other studies suggested that passaging might impose selective pressure on *L. monocytogenes*, rendering the microbe to

respond more quickly with the up-regulation of virulence factors in response to the host immune system. This was supported by a study that investigated the effect of passaging on the immunogenicity of the recombinant vaccine vector *L. monocytogenes,* which showed to be enhanced after passaging even at a relatively low dose (Peters and Paterson, 2003). The effect of passaging on the detection of the bioluminescent strain was investigated herein using P*phrA*:: *luc*-wt. No bioluminescence was detected six hours post infection. The lack of light in six hours may indicate that the density of bacteria did not reach a threshold level to make *phrA* promoter be induced or alternatively, the microbe was not metabolically adapted to the *in vivo* environment at this stage for promoter induction. The low bacterial burden in tissues was also supported by the fact that no bacteria could be cultured from blood six hours post infection. At 24- and 30-hours post infection, increasing levels of bioluminescent signals could be observed and this was also consistent with the elevated CFU counts in the tissues. Passaged bacteria were able to effectively induce luciferase expression and produce light.

I must acknowledge that there was a variation in light detection among mice. This was very likely due to the use of low infective doses in this study. Routinely, in Leicester $1x10^6$ CFU/ mouse is used to achieve a 90-100% mortality. In this study, I used almost ten times less CFU/ mouse, approximately $2.4x10^5$. Another reason for the lack of bioluminescence in certain mice in this study could be due to the inaccurate administration of the dose. Henken et al. (2010) observed the effect of the selected mouse model on the detection of bioluminescence. *In vivo* bioluminescence imaging was used for two mouse strains, BALB/c, C57BL/6. Although the bioluminescence signals were detected in both models after infection with bioluminescent *S. pneumoniae,* weaker signals were shown in the C57BL/6 strain compared to BALB/c, demonstrating the effect of the selected mouse strain on bioluminescence imaging. Therefore, in future, the mouse experiments should be repeated with a high infective dose and different mouse strains.

A comparative study of *in vivo* bioluminescence imaging for CBRluc and Fluc expressing transfected cells revealed that the click beetle luciferases are superior over Fluc (Miloud et al., 2007). CBRluc has been shown to enhance the whole-body images in murine infection models with other microorganisms, including *Listeria monocytogenes*, and *Candida albicans* (Ur Rahman et al., 2017, Kapitan et al., 2016). This makes CBRluc more suited to detect such bacteria *in vivo*.

For the bacterial fitness, the *in vivo* results showed no significant difference between the wild-type and the bioluminescent pneumococcal strain containing the P*phrA*::*luc* construct, proving that the insertion site, *bgaA* locus, did not influence the bacterial virulence (Halfmann et al., 2007) and the luciferase production did not impede the fitness (Ur Rahman et al., 2017, Daniel et al., 2012).

Taken together, the *in vivo* BLI imaging findings indicated that this technology has several benefits over conventional methods for monitoring pneumococcal infection in mouse infection models rapidly. BLI imaging allows the detection of the spatial and temporal distribution of bacteria in the entire animal body, providing accurate information about the progression of disease. The development of CBRluc-expressing *S. pneumoniae* provided increased bioluminescent signals with deeper tissue penetration for improved *in vivo* BLI to study the development of pneumoniae in mice and in future, the system can be utilised to evaluate novel therapies and vaccines.

4.6. *Galleria mellonella* as an alternative model

The greater wax moth *Galleria mellonella* is increasingly being used as an alternative model to study microbial infections. Low cost, simple handling, simplified ethical considerations and a lack of adequate animal models for various infectious diseases make this model highly attractive. There is no need for specialised equipment to infect and house *G. mellonella* (Ignasiak and Maxwell, 2017). It can be housed in petri dishes and kept in an incubator. Larvae can be incubated in wide range of temperatures (from 25 to 37°C), allowing the mimicking of various physiologic conditions (Harding et al., 2013). In addition, larvae have a number of structural and functional similarities with the mammalian innate immune system, and consequently, these insects can be used to assess the antimicrobial effect (Cools et al., 2019). This model has cellular and humoral defences. The cellular immune response is mediated by immune cells, termed haemocytes. These are found within haemolymphs, which is analogous to blood in a mammalian host. These cells have the ability to phagocytose and kill pathogens through the production of a reactive oxygen species, such as superoxide (Harding et al., 2013). Six types of haemocytes have been identified in *G. mellonela*. These include prohemocytes, plasmatocytes, granular cells, coagulocytes, spherulocytes and oenocytoids (Tsai et al., 2016). Plasmatocytes and granulocytes are the most important haemocytes due to their role in phagocytosis, nodulation, and encapsulation. Nodulation is an affective process to eliminate a large number of pathogens by making a layer of cells around the foreign target (Tsai et al., 2016, Pereira et al., 2018). Encapsulation begins with granular cell recognition of the target-releasing material that promotes the attachment of plasmatocytes around the pathogens. Phagocytosis begins with releasing enzymes from haemocytes towards the foreign target (Pereira et al., 2018). The humoral response is regulated by molecules that have a toxic effect on pathogens, complement-like proteins, melanin, and antimicrobial peptide (AMP) (Harding et al., 2013). Complement-like proteins are plasma proteins acting as opsonins that attach to the conserved microbial components. Apolipophorin-III, as an example, can bind to bacterial lipopolysaccharide and lipoteichoic acid effectively (Tsai et al., 2016). Melanin formation is catalysed by phenoloxidase, which is released in haemocytes. This enzyme converts monophenols and phenols to quinines, and polymerisation of quinines forms melanin towards the pathogens (Tsai et al., 2016). About 20 AMPs have been identified in *G. mellonela*. AMPs are hydrophobic membrane active peptides. Different AMPs are released against different

pathogens (Pereira et al., 2018). Cecropins and moricin peptides were observed to form pores on bacterial cells. Moricin-like peptides were shown to work against filamentous fungi. Proline-rich peptides have an inhibition activity towards yeast (Tsai et al., 2016).

By using this model, the impact of the mutation on virulence relative to the wild-type was evaluated by monitoring the changes in the larva viability. This model was able to differentiate between levels of virulence in bacteria (Wand et al., 2013). Although the features of *G. mellonella* make it easy to use, there is a need for larvae homogenisation, serial dilution and plating. These can lead to additional errors in the results and can be time-consuming. Luminescent bacteria overcame these steps and facilitated the follow-up of infection and treatment without needing to process the larvae. In this study, I developed the model by constructing the luminescent *S. pneumoniae* containing the P*phrA*::*luc* construct and tested it with IVIS. Using real-time bioluminescence imaging for tracking the infection and testing of the antimicrobial agents in *G. mellonella,* the model was reported by using a *lux* reporter system (Meir et al., 2018, La Rosa et al., 2012) but not with CBRluc. Herein, I established the *G. mellonella* model of pneumococcal infection by using CBRluc-expressing *S. pneumoniae*. Larvae were inoculated with the bioluminescent *S. pneumoniae* via injection. This method is more suited for *S. pneumoniae* with the microbe injected directly into the larvae hemocoel and therefore, a known amount of pathogen is delivered. By using *G. mellonella*, I was able to demonstrate that *S. pneumoniae* proliferates in and kills *G. mellonella* larvae in a reproducible manner. This finding was also supported by Evans and Rozen (2012) study, where a *G. mellonella* model was able to differentiate *S. pneumoniae* serotypes that are different in virulence.

By analysing larvae using IVIS, I demonstrated that the infection could be detected and imaged in live larvae, and the luminescence could be used as a substitute for a CFU count. I showed a good correlation between the bioluminescence intensity and CFU counts in infected larvae by measuring photon flux and different inoculum sizes of *S. pneumoniae*. A linear relation between the CFU and the expression of light was shown and can, therefore, be used as a reporter system for real-time growth assessment. These results are consistent with the findings of Meir et al. (2018) and La Rosa et al. (2012), which were generated from a study of *Mycobacterium abscessus* and *Enterococcus faecalis* infection, but with the *lux* system. I demonstrated the non-toxic effects of luciferin on the viability of bacteria in larvae by using three different concentrations (15 mg/ larva, 30 mg/ larva and 60 mg/ larva). The non-toxicity

effect of luciferin previously had been shown only on mice (Contag et al., 1997). The bioluminescence intensity of the three concentrations was considerably similar. The viability of bacteria recovered from the group injected with different luciferin concentrations (15 mg/ ml, 30 mg/ ml or 60 mg/ ml) showed no significant difference in bacterial load among the groups using one-way ANOVA, demonstrating the non-toxic effect of luciferin. Bioluminescent *S. pneumoniae* may allow multiple assessments of infection over time in the same larvae and is less time- and effort-consuming; however, the need for addition of exogenous substrate could limit the use of this system in *G. mellonella.* Multiple injections of luciferin to the small model can cause trauma leading to larvae death. To overcome this issue with multiple injections, a new injection site must be used (Fuchs et al., 2010).

There are some limitations associated with the use of this model. The lack of a genome sequence for Galleria makes it difficult to establish a method for generating mutant strains. In addition, there are no stock centres for *G. mellonella*, which can provide specific genotypes under standard conditions. Variations in genotypes, suppliers, and maintenance, handling and housing temperatures of the insects may affect their susceptibility to infection. The *Streptococcus pyogenes* serotype M3 strain, for example, has been used in US larvae and New Zealand larvae showing different mortality rates. These variations have been attributed to the different suppliers, and housing temperatures. It was shown that the pre-incubation temperature of larvae prior to infection influence the insects' immune response. It was found that pre-incubation at 37C^{o} led to an increase in the haemocyte density and the expression of a number of antimicrobial peptides, which are associated with the protection of larvae from microbial pathogens (Mowlds and Kavanagh, 2008). Starvation was also observed to affect the Galleria's susceptibility to the infection. Banville et al. (2012) showed starvation results in a reduction in the cellular and immune responses and an increased susceptibility to infection.

Lange et al. (2018) provided the first draft of the sequenced genome of Galleria which may overcome some of the previous limitations, and thus stock centres are needed to provide well-defined *G. mellonella* genotypes. In this work, the mortality rate was used to monitor the infection, however, additional signs can be included to improve the use of this model such as melanisation and histopathological effects. In conclusion, by using larvae in this study I demonstrate that *G. mellonella* is a simply powerful model and an attractive option to understand the pathogenesis process and respective immune response.

Concluding remarks

Streptococcus pneumoniae is a human respiratory tract pathogen and is responsible for most of the community-acquired pneumonia. To study the pathogenesis of pneumococcal infections in detail, the murine model is widely used. Construction and use of bioluminescent strains have streamlined *in vivo* studies on infection models. Bioluminescence imaging is a non-invasive technology that allows the visualising and tracking infection progression in animals in real time. This technology also reduces the animal numbers used. *S. pneumoniae* D39 Tn*4001 luxABCDE* transposant is a bioluminescent strain previously constructed for use in the *in vivo* imaging of infections in animal models. This construct has been used successfully in previous studies; however, a decrease in light detection was associated with an increase in depth tissues because of the low penetrating power of the shorter wavelengths light emitted by *lux* operon (peak 490 nm).

In this study, the findings that CBRluc can be detected at a relatively low dose non-invasively in live mice is a significant step for using this bioluminescent strain to study the pathogenesis of *S. pneumoniae.* I constructed a system for the stable chromosomal integration of expressed CBR luciferase in *S. pneumoniae*. I showed that using CBRluc increased bioluminescent signals *in vitro*, which has deeper tissue penetration for improved *in vivo* BLI imaging to monitor the progression of pneumoniae in mice. I showed that in comparison to the *S. pneumoniae* strain expressing bacterial luciferase lux, CBRluc provides a greater luminescence signal during the stationary phase of growth. Further, I established the *G. mellonella* for *S. pneumoniae* infection with CBRluc and I demonstrate that *G. mellonella* is a simply powerful model and an attractive tool to study the progression of bacterial infection.

In conclusion, this study demonstrates the power of using genetically-engineered bioluminescent bacteria to gain new insights into the infectious process of bacteria and the response to antibiotics.

Future work

Using the CBRluc system is a significant step forward in studying *S. pneumoniae* biology in mammalian hosts in real time. BLI provides useful information during the course of infection from the same animal in real time, pertinent for the process of disease and the evaluation of potential therapies. In addition to a reduction in the animals used, this technology can be utilised to refine the existing models. For example, at an early stage of infection, mice not showing bioluminescence can be eliminated to decrease experimental variation and unnecessary suffering. The features of BLI can contribute to create a highly informative model of pneumonia.

The sensitivity of bioluminescence imaging is dependent on longer wavelength signals and the number of photons emitted by luciferase enzyme. These signals are limited due to the absorption by haemoglobin and other tissue components. In this study, I used luciferin as a substrate. In future, alternative substrates can be used to improve *in vivo* BLI signals to enhance tissue penetration and thus detection of low bacterial CFU in pneumonia models of *S. pneumoniae* infection. These luciferin substrate analogues include alkylaminoluciferins and aminoluciferins, which emit longer wavelengths (Sun et al., 2012) . In addition, some targeted mutation can be made to alter certain codons in the CBRluc amino acid sequence. It has been observed that such modifications can improve enzyme efficiency and provide the ability to utilise luciferin derivatives (Woodroofe et al., 2008). In addition, by modification of the molecular structure in *in vivo* biodistribution can be affected and the availability of the substrate within living cells for the reaction can be increased and imaging studies would benefit as a result.

In addition, in future, the environmental conditions affecting the inducibility of promoters that drives the expression of CBRluc can be studied in detail, for example, different sugars and acidity to identify the optimal conditions for *luc* expression. The resulting data then can be utilised to induce the *in vivo* expression of CBRluc.

S. pneumoniae strains vary considerably in phenotypic outcomes, such as the ability to cause disease and response to antibiotics, due to loss or gene acquisition through genetic competence and horizontal gene transfer. To provide new insights into cooperative interactions between the different pneumococcal lineages with respect to growth and virulence, the bioluminescent strains created in this study can be utilised. Other work that

may be done in future includes *in vivo* testing of pneumococcal therapeutic compounds using bioluminescent strains in the *G. mellonella* model. The innate immune system of *G. mellonella* shares a structural similarity and functional homology to the innate immune systems of mammals. *G. mellonella* shows a powerful resistance to microbial infections, although it does not have an adaptive immune system. It has cellular and humoral defences (Tsai et al., 2016). *G. mellonella* use is not subject to ethical limitations. It is cheap and easy to handle and maintain, and there is no need for anaesthesia or special training to use it (Cools et al., 2019, Harding et al., 2013). Bioluminescence imaging could be used to assess the bacterial load of luminescent *S. pneumoniae* after treatment with various antibiotics. The antimicrobial efficacy can be demonstrated by using this technology in this model. Bioluminescence imaging for different size inocula of *S. pneumoniae* in the *G. mellonella* model was investigated in this study. It would be interesting to study antimicrobial agents against *S. pneumoniae* in this model through the treatment of infected larvae with standard antibiotics such as amoxicillin. Bioluminescence imaging would be used to assess the bacterial load of luminescent *S. pneumoniae* after treatment comparing to the untreated larvae.

It would be also interesting to further modify the specific *S. pneumoniae* CBRluc constructs developed in this study with species-specific promoters to use it in other Gram-positive bacteria to provide an alternative to *lux*-expressing strains for improving *in vivo* BLI detection in animal models of infection.

Appendix

Insertion site of lux cassette into pPP3 sequence is highlighted

CTAGCGCTATATGCGTTGATGCAATTTCTATGCGCACCCGTTCTCGGAGCACTGTCCGACCGCTTTGGCCGCCGCCCAGT
CCTGCTCGCTTCGCTACTTGGAGCCACTATCGACTACGCGATCATGGCGACCACACCCGTCCTGTGGATCTATCGATGCATGCATCGGTA
CCTGC*GAATTC*TAGTCTAGAATCGGATCCG*CCATGG* AA*GGAGG*CACTCACGATGGTCAAGCGGGAAAAAAA
CGTTATTTACGGTCCAGAACCCCTCCACCCGCTAGAAGACTTAACGGCTGGAGAAATGTTATTCCGTGCCCTCCGTAAGC
ACAGCCACTTACCACAG GCCTTAGTTGATGTAGTTGGTGACGAAAGCTTGTCATATAAA*GAATTC*TTTGAAGCTACAGTC
CTTTTGGCACAATCATTGCACAACTGTGGGTATAAGATGAATGACGTCGTTTCAATTTGTGCAGAAAACAATACCCGTTT
TTTCATCCCAGTTATTGCTGCTTGGTACATCGGCATGATTGTCGCTCCTGTAAACGAATCATATATCCCAGATGAATTAT
GCAAGGTCATGGGAATCTCTAAGCCTCAAATTGTTTTTACGACTAAGAACATTTTGAACAAGGTTTTAGAAGTGCAAAGC
CGCACCAACTTCATTAAACGGATCATTATTTTGGACACCGTTGAAAACATTCATGGGTGTGAATCATTACCAAACTTCAT
CAGTCGTTACAGTGATGGTAATATTGCAAACTTCAAGCCATTACATTTTGACCCTGTGGAACAAGTTGCTGCTATCTTGT
GTAGTTCAGGCACAACTGGTTTGCCTAAAGGTGTTATGCAAACGCATCAAAACATTTGTGTCCGGTTAATCCATGCTTTA
GATCCTCGGTATGGTACGCAATTAATTCCGGGCGTTACTGTGTTAGTTTATCTGCCATTCTTTCACGCATTTGGCTTCCA
CATTACGCTCGGTTACTTTATGGTTGGCCTTCGTGTTATTATGTTCCGTCGTTTCGACCAAGAGGCCTTTTTAAAGGCTA
TTCAAGACTACGAAGTGCGGAGTGTTATTAATGTTCCAAGTGTTATCTTATTTTTAAGTAAGTCACCATTAGTTGATAAG
TATGACTTGTCATCTCTTCGTGAATTGTGTTGTGGTGCTGCACCATTAGCCAAGGAAGTTGCCGAAGTTGCTGCCAAGCG
GCTTAACTTACCAGGTATTCGTTGCGGTTTTGGACTCACGGAGTCAACTTCTGCTATCATCCAAACCCTGGGTGACGAAT
TCAAATCCGGCAGTTTAGGCCGTGTCACGCCTTTAATGGCTGCTAAGATCGCTGATCGTGAAACAGGCAAGGCTTTGGGA
CCTAACCAAGTGGGCGAATTATGTATCAAAGGTCCAATGGTTAGTAAAGGCTACGTTAATAACGTTGAAGCTACTAAAGA
GGCCATTGATGATGATGGTTGGTTACACTCTGGCGATTTCGGGTACTACGACGAAGATGAACATTTTTACGTTGTTGATC
GCTATAAAGAATTAATTAAATACAAGGGCTCTCAGGTTGCTCCGGCAGAATTGGAAGAAATTTTGTTAAAGAACCCTTGT
ATTCGTGATGTTGCGGTTGTTGGCATCCCAGACTTGGAAGCCGGAGAATTGCCATCAGCTTTTGTTGTAAAGCAACCAGG
TACTGAAATTACTGCTAAGGAAGTTTACGACTACTTAGCAGAACGTGTTAGTCACACTAAGTATTTACGGGGTGGTGTTC
GTTTTGTCGAC TCAATTCCACGGAACGTAACCGGAAAAAT TACGCGCAAGGAACTCTTGAAGCAATTATTAGTTAAAGCT
GGTGGTTAGGCTCAGCGCCGGTCGCTACCATTACCAGTTGGTCTGGTGTCAAAAATAATAATAACCGGGCAGGCCATGTC
TGCCCGTATTTCGCGTAAGGAAATCCATTATGTACTATTTCTGGTGATGAAATCAACGTAACATTTAAAGCTGTCAAAGC
CAAAGTCATGAGATGGCGTATGGAGCGTAAAGCTGACAAGAGCGGTGTTGCGATGATTGAGATGACCTTCCTTGCACCAA
GTGAATTGCCTCAAGAAAGCACTCAATCAAAGATTCTTGTAGATGGAAAAGAACTTGCTGATTTCGCTGAAAATCGTCAA
GACTATCAAATTACCTATAAAGGTCAACGGCCAAAAGTCTCAGTTGAAGAAAACAATCAAGTAGCTTCAACTGTGGTAGA
TAGTGGAGAAGATAGCCTTCCAGTACTTGTTCGCCTCGTTTCAGAAAGTGGAAAACAAGTCAAGGAATACCGTATCCAGT
TGACTAAGGAAAAACCAGTTTCTGCTGTACAAGAAGATCTTCCAAAACTCGAATTTGTTGAAAAAGATTTGGCCTACAAG
ACAGTTGAGAAAAAAGATTCAACACTGTATCTAGGTGAAACTCGTGTAGAACAAGAAGGAAAAGTTGGAAAAGAACGTAT
CTTTACAGTGATTAATCCTGATGGAAGTAAGGAAGAAAAACTCCGTGAAGTGGTAGAAGTTCCGACAGACCGCATCGTCT
TGGTTGGAACCAAACCAGTAGCTCAAGAAGCTAAAAAACCACAAGTGTCAGAAAAAGCAGATACAAAACCAATTGATTCA
AGTGAAGCTGATCAAACTAATAAAGCCCAGTTACCAAATACAGGTAGTGCGGCAAGCCAAGCAGCAGTAGCAGCAGGTTT
AGCCTGCCTCGCGCGTTTCGGTGATGACGGTGAAAACCTCTGACACATGCAGCTCCCGGAGACGGTCACAGCTTGTCTGT
AAGCGGATGCCGGGAGCAGACAAGCCCGTCAGGGCGCGTCAGCGGGTGTTGGCGGGTGTCGGGGCGCAGCCATGACCCAG
TCACGTAGCGATAGCGGAGTGTATACTGGCTTAACTATGCGGCATCAGAGCAGATTGTACTGAGAGTGCACCATATGCGG
TGTGAAATACCGCACAGATGCGTAAGGAGAAAATACCGCATCAGGCGCTCTTCCGCTTCCTCGCTCACTGACTCGCTGCG
CTCGGTCGTTCGGCTGCGGCGAGCGGTATCAGCTCACTCAAAGGCGGTAATACGGTTATCCACAGAATCAGGGGATAACG
CAGGAAAGAACATGTGAGCAAAAGGCCAGCAAAAGGCCAGGAACCGTAAAAAGGCCGCGTTGCTGGCGTTTTTCCATAGG
CTCCGCCCCCCTGACGAGCATCACAAAAATCGACGCTCAAGTCAGAGGTGGCGAAACCCGACAGGACTATAAAGATACCA
GGCGTTTCCCCCTGGAAGCTCCCTCGTGCGCTCTCCTGTTCCGACCCTGCCGCTTACCGGATACCTGTCCGCCTTTCTCC
CTTCGGGAAGCGTGGCGCTTTCTCATAGCTCACGCTGTAGGTATCTCAGTTCGGTGTAGGTCGTTCGCTCCAAGCTGGGC
TGTGTGCACGAACCCCCCGTTCAGCCCGACCGCTGCGCCTTATCCGGTAACTATCGTCTTGAGTCCAACCCGGTAAGACA
CGACTTATCGCCACTGGCAGCAGCCACTGGTAACAGGATTAGCAGAGCGAGGTATGTAGGCGGTGCTACAGAGTTCTTGA
AGTGGTGGCCTAACTACGGCTACACTAGAAGGACAGTATTTGGTATCTGCGCTCTGCTGAAGCCAGTTACCTTCGGAAAA
AGAGTTGGTAGCTCTTGATCCGGCAAACAAACCACCGCTGGTAGCGGTGGTTTTTTTGTTTGCAAGCAGCAGATTACGCG
CAGAAAAAAAGGATCTCAAGAAGATCCTTTGATCTTTTCTACGGGGTCTGACGCTCAGTGGAACGAAAACTCACGTTAAG
GGATTTTGGTCATGAGATTATCAAAAAGGATCTTCACCTAGATCCTTTTAAATTAAAAATGAAGTTTTAAATCAATCTAA
AGTATATATGAGTAAACTTGGTCTGACAGTTACCAATGCTTAATCAGTGAGGCACCTATCTCAGCGATCTGTCTATTTCG
TTCATCCATAGTTGCCTGACTCCCCGTCGTGTAGATAACTACGATACGGGAGGGCTTACCATCTGGCCCCAGTGCTGCAA

TGATACCGCGAGACCCACGCTCACCGGCTCCAGATTTATCAGCAATAAACCAGCCAGCCGGAAGGGCCGAGCGCAGAAGT
GGTCCTGCAACTTTATCCGCCTCCATCCAGTCTATTAATTGTTGCCGGGAAGCTAGAGTAAGTAGTTCGCCAGTTAATAG
TTTGCGCAACGTTGTTGCCATTGCTGCAGGCATCGTGGTGTCACGCTCGTCGTTTGGTATGGCTTCATTCAGCTCCGGTT
CCCAACGATCAAGGCGAGTTACATGATCCCCCATGTTGTGCAAAAAAGCGGTTAGCTCCTTCGGTCCTCCGATCGTTGTC
AGAAGTAAGTTGGCCGCAGTGTTATCACTCATGGTTATGGCAGCACTGCATAATTCTCTTACTGTCATGCCATCCGTAAG
ATGCTTTTCTGTGACTGGTGAGTACTCAACCAAGTCATTCTGAGAATAGTGTATGCGGCGACCGAGTTGCTCTTGCCCGG
CGTCAACACGGGATAATACCGCGCCACATAGCAGAACTTTAAAAGTGCTCATCATTGGAAAACGTTCTTCGGGGCGAAAA
CTCTCAAGGATCTTACCGCTGTTGAGATCCAGTTCGATGTAACCCACTCGTGCACCCAACTGATCTTCAGCATCTTTTAC
TTTCACCAGCGTTTCTGGGTGAGCAAAAACAGGAAGGCAAAATGCCGCAAAAAAGGGAATAAGGGCGACACGGAAATGTT
GAATACTCATACTCTTCCTTTTTCAATATTATTGAAGCATTTATCAGGGTTATTGTCTCATGAGCGGATACATATTTGAA
TGTATTTAGAAAAATAAACAAATAGGGGTTCCGCGCACATTTCCCCGAAAAGTGCCACCTGACGTCTAAGAAACCATTAT
TATCATGACATTAACCTATAAAAATAGGCGTATCACGAGGCCCTTTCGTCTTCAAGAATTAATTCCTTCTTAACGCCCCA
AGTTCATCACCAATGACATCAACTCACATGAACTACATGATGAACCCAGTTATCATGGTTTTGGATAAGATTTTTGAAAA
ATTCTTCCCAGGCCTTGATAAATATGACTTTGATGCTGCTAAATTGAACAAGAAAATCGGTTTCTGGGGATCTAAATTCT
TCATCGGTTTCATCCTTGGTATCGTTATCGGTATTATGGGAACTCCACATCCAATTGCAGGTGTTGCAGATGCAGATAAA
TGGCGTCTTGTTATCAAAGGATGGTTGTCTCTTGGTTTGACTGCCGGTGTATCTTTGGAACTCTTCTCACTTATCGGTTC
ATGGTTCATCGCAGCCGTAGAACCACTATCACAAGGTATTACAAACGTTGCTACTAAACGTCTTCAAGGACGTAAATTCA
ATATCGGTCTTGACTGGCCATTCATCGCTGGTCGTGCTGAAATCTGGGCTTGTGCCAACGTACTTGCACCAATCATGTTG
ATTGAAGCAGTGCTTCTTTCAAAAGTTGGAAATGGTATCTTGCCACTTGCAGGTATCATCGCTATGGGTGTTACTCCAGC
TCTCTTGGTTGTAACTCGTGGTAAATTGCTCCGTATGATTATCTTCGGAACACTCTTGTTGCCACTCTTCCTTCTTTCAG
GTACACTTATTGCACCATTTGCAACAGAACTTGCTAAAGGTGTAGGTGCCTTCCCAGAAGGTGTGAGCCAAACTCAATTG
ATTACTCACTCTACTCTTGAAGGACCAATCGAAAAACTTCTTGGTTGGACAATTGGTAACACTACAACTGGTGATATCAA
AGCAATCCTTGGTGCAGTAGCCTTCCTTGTATTCTATATCGGTATCTTTGCTTGGTACAGAAAACAAATGATCAAACGTA
ACGAAGAGTACGCAGCAAAAGCAAAATAATGCGCTCCGCTAGCTTTACAGACAAAGAACTATCCTTAATGGAAGCACTAG
CAAAAGGTATCAATGAAGCAAGAAATATTGAAGGCTAGTCAGTAAAATTCAGATAAACAAAAAGAGCCGATAAGATGAGA
GTTTCATTTCTCAAATTATCGGCTCTGCGTCTTGGCGTCTGGCTCTTTGATTGTTATTATATTCATTTTTTGAACATTAA
TTAAAGTTTCGTTCTTACATTTGGGGCAGTATAAAGGGAAATTTTTAAGTATAGTATCCACTCGTATTCGTAGTCTTGTT
TTATTTCCACAAATAGGACACAATATCCACTTGTAGTTTATAATAACAATCTCCTCCTTTCCACTTTAATTCAAATCTAT
ATTAAAGAATATTTCATCTTATTTAATAAGAAACCATATTTATATAACAACATAAAACGCACTAAGTTATTTTATTGAAC
ATATATCTTACTTTATCTATCTGACTATTTAGACGACGGGTCTGGCAAACAGGTTCGCCAGTGGTAACCTGATATCCTTT
TAGCTCTGCTAAACAAACACTAAGCCCATTTGTAAAAAAAGTTAAATCATTGCGATAATCTTGAATACATCGAGCAGGAA
TTTCTCCAATAATAATGACCTCATTATTTTTCAGTTGAGTATTTACGATATTTGCACAATATTTGGGAGCATCGTTATAT
GCCCGTGAAAGATATTCCTGTGGTGCATAAACTTTAAAACTAAGATATGGCTCTAACAATTCTGTTCCAGCTTTTCTAAA
GGCTTGCTCCAATACAATAGGAGCAAGCATCCGAAAATCTGCTGGGGTACTAACAGGGCTATAGTATAAGCCATACTTAA
AACAGATTTTACAGTCCGTCACATTCCAACCATACAATCCTTGTTCACAACCATAGCGTATCCCTTCCATAACTGCATTT
TGAAATGATTGATTTAAGTATCCAAGAGAAACCGAGCTCTCATACTGCATTCCACTTCCCAACGGAAGCGGTGATACAGA
TAAACCAATGGAAGCCCAGAAAGGATTTGGCGGCACTTCGATGTGAATGGTATATTCTGCATTTTTTAACGGTCTCTCCA
TATAAATGACTGTAGGCTCTTTTAGTTCTATCTCCACATGATACTTTTCTTGCAACAGTGCACTAATCACTTCCATTTGT
ACTTTCCCTAAGAAAGAAAGTATAATTTCATGTGTCGTAGAATCCACGTAATATCGTAGAAGCGGATCACTATCTGAGAT
TTCCAAAAGGGCATCAAGCAACATTTCTCTCTGTTCAGGTTTACTCGGTTCAACAGTTGTTTGTAGTAGAGGGTGCGGAT
TTTCAATCTTTTTTCTCTGTGGCAATAGTTTTGTATCTCCAAGAACACTATTTAACTTCAAAAACTCATTTTGCAAAATA
ACAATTTCTCCAGAATAAGCTCTATCAATCTTACATAATTCACCATTTATTGAAGTATACATTTCTGTAACTTTTATTTT
TTCTTTTTCTGATACTCTAACCGAATCTCGTAAATGTAGTACTCCACTATAAAGGCGTATATATGCAAGACGTTGTCTTT
TTTTTGTATATTCAATTTTGAAAACATTTCCGCAAAGTTCAGACGGACCTCGATGTGTTGATGAATAAAATTTATTAGTA
ATAACTTCTATAAGGTTATCAATCCCTATATTACTTTTTGCACTTCCATGATAAAGAGGGAACAGAGAACAATTCTGAAA
TCTTATGCTTTCCTCTTGTTCGAGTTCCAATGCTTCTAATGATTTACCGGACATATATTTCTCTAAAAGGTCATCGTTTC
CCTCTATTACCGTATCCCATTGTTCAGATTCGGTAAAGTTCGTCACACACACATTAGGATACAGTTCTACCTTCTGTTTG
ATTACAATTTCGGCAGAAAGTTTCTCTTTAATATCCTGATAAACCGTTGATAAATCAATTCCATTTTGGTCAATCTTATT
GATAAAAAAGATTGTGGGAATCCCCATTTTCCTAAGTGCATGAAATAATATACGAGTTTGTGCTTGTACGCCATCTTTTG
CAGAAATCAGTAGAATTGCCCCATCTAAAACTGATAATGAACGATATACTTCTGCTAAGAAATCCATATGTCCTGGCGTG
TCTATGATGTTCACCTTCGTATTTTCCCACTGAAAAGAGGTTATTCCTGTCTGAATTGTAATTCCTCTCTGACGTTCTAA
AAGCGTATTATCCGTCCTCGTTGTACCTTTGTCCACGCTTCCTAATTCTGTAATCGCTCCACTGTTATATAATAAGCTTT
CTGTTAAGGTAGTTTTTCCTGCATCAACATGAGCTAAAACTCCAATATTAATAATTTTCATGTGATTTTCCTCCATTCAA
AAGCCCAAAAGGGCATAAAAATCCCAGTGATAAATACTCTTATCACTGGGATTTTTATGCATAACCATAGGCATACAAAG
CATACAGATATTCTCCGGATACTTTAGAATCACATGATAAAGGTATTCTTAAACTGGGTACAAAAAACTAAGCCCTCCTA
AAAAAGGACATCCAATTATTTGTTCCCGCTATCAAATTGACAGTTTATTTAAGAATACCTTGCCGCATATTTATTAACTC
CTTTTAAATAGATACTTAAATTATAGCACGTAAGAGCATATTTGTAAAGGAATCTCCAATTTTTTATCAAAAAGAGTACA
TGATTACAAAGTATCTGTAATCATGTACCAATATTTGTTATTTTACAATCTTCCAATTATCTTGTTTTTCTAATATCAAC
TCAAATTGCGAGATTTGGGTTGCCTTTGTTTCTTGATCTAAATATTTCACAGCGACATTCACGATTACTTGG

References

AL-BAYATI, F. A., KAHYA, H. F., DAMIANOU, A., SHAFEEQ, S., KUIPERS, O. P., ANDREW, P. W. & YESILKAYA, H. 2017. Pneumococcal galactose catabolism is controlled by multiple regulators acting on pyruvate formate lyase. *Scientific reports,* 7**,** 1-17.

ALARI, A., CHAUSSADE, H., DE CELLÈS, M. D., LE FOULER, L., VARON, E., OPATOWSKI, L., GUILLEMOT, D. & WATIER, L. 2016. Impact of pneumococcal conjugate vaccines on pneumococcal meningitis cases in France between 2001 and 2014: a time series analysis. *BMC medicine,* 14**,** 211.

ANDRE, G. O., CONVERSO, T. R., POLITANO, W. R., FERRAZ, L. F., RIBEIRO, M. L., LEITE, L. C. & DARRIEUX, M. 2017. Role of *Streptococcus pneumoniae* proteins in evasion of complement-mediated immunity. *Frontiers in microbiology,* 8**,** 224.

ANDREU, N., ZELMER, A., FLETCHER, T., ELKINGTON, P. T., WARD, T. H., RIPOLL, J., PARISH, T., BANCROFT, G. J., SCHAIBLE, U. & ROBERTSON, B. D. 2010. Optimisation of bioluminescent reporters for use with *mycobacteria*. *PloS one,* 5**,** e10777.

ANDREU, N., ZELMER, A. & WILES, S. 2011. Noninvasive biophotonic imaging for studies of infectious disease. *FEMS microbiology reviews,* 35**,** 360-394.

APPELBAUM, P. C. 2002. Resistance among *Streptococcus pneumoniae*: implications for drug selection. *Clinical infectious diseases,* 34**,** 1613-1620.

APRIANTO, R., SLAGER, J., HOLSAPPEL, S. & VEENING, J.-W. 2018. High-resolution analysis of the pneumococcal transcriptome under a wide range of infection-relevant conditions. *Nucleic acids research,* 46**,** 9990-10006.

ARBIQUE, J. C., POYART, C., TRIEU-CUOT, P., QUESNE, G., MARIA DA GLÓRIA, S. C., STEIGERWALT, A. G., MOREY, R. E., JACKSON, D., DAVIDSON, R. J. & FACKLAM, R. R. 2004. Accuracy of Phenotypic and Genotypic Testing for Identification of *Streptococcus pneumoniae* and Description of *Streptococcus pseudopneumoniae* sp. nov. *Journal of Clinical Microbiology,* 42**,** 4686-4696.

AUZAT, I., CHAPUY-REGAUD, S., LE BRAS, G., DOS SANTOS, D., OGUNNIYI, A. D., LE THOMAS, I., GAREL, J. R., PATON, J. C. & TROMBE, M. C. 1999. The NADH oxidase of *Streptococcus pneumoniae*: its involvement in competence and virulence. *Molecular microbiology,* 34**,** 1018-1028.

BADR, C. E. 2014. Bioluminescence imaging: basics and practical limitations. *Bioluminescent Imaging.* Springer.

BALMER, P., BORROW, R. & ARKWRIGHT, P. D. 2007. The 23-valent pneumococcal polysaccharide vaccine does not provide additional serotype antibody protection in children who have been primed with two doses of heptavalent pneumococcal conjugate vaccine. *Vaccine,* 25**,** 6321-6325.

BANVILLE, N., BROWNE, N. & KAVANAGH, K. 2012. Effect of nutrient deprivation on the susceptibility of *Galleria mellonella* larvae to infection. *Virulence,* 3**,** 497-503.

BAQUERO, F., BELTRÉN, J. M. & LOZA, E. 1991. A review of antibiotic resistance patterns of *Streptococcus pneumoniae* in Europe. *Journal of Antimicrobial Chemotherapy,* 28**,** 31-38.

BARMAN, T. K., RAO, M., BHATI, A., KISHORE, K., SHUKLA, G., KUMAR, M., MATHUR, T., PANDYA, M. & UPADHYAY, D. J. 2011. Non invasive real-time monitoring of bacterial infection & therapeutic effect of anti-microbials in five mouse models. *The Indian journal of medical research,* 134**,** 688.

BAROCCHI, M., RIES, J., ZOGAJ, X., HEMSLEY, C., ALBIGER, B., KANTH, A., DAHLBERG, S., FERNEBRO, J., MOSCHIONI, M. & MASIGNANI, V. 2006. A pneumococcal pilus influences virulence and host inflammatory responses. *Proceedings of the National Academy of Sciences,* 103**,** 2857-2862.

BEARD, S., SALISBURY, V., LEWIS, R., SHARPE, J. & MACGOWAN, A. 2002. Expression of lux genes in a clinical isolate of *Streptococcus pneumoniae*: using bioluminescence to monitor gemifloxacin activity. *Antimicrobial agents and chemotherapy,* 46**,** 538-542.
BERRY, A., YOTHER, J., BRILES, D., HANSMAN, D. & PATON, J. 1989. Reduced virulence of a defined pneumolysin-negative mutant of *Streptococcus pneumoniae*. *Infection and immunity,* 57**,** 2037-2042.
BERTHOLD, F., HERICK, K. & SIEWE, R. M. 2000. Luminometer design and low light detection.
BLUE, C. E. & MITCHELL, T. J. 2003. Contribution of a response regulator to the virulence of *Streptococcus pneumoniae* is strain dependent. *Infection and immunity,* 71**,** 4405-4413.
BOGAERT, D., DE GROOT, R. & HERMANS, P. 2004a. *Streptococcus pneumoniae* colonisation: the key to pneumococcal disease. *The Lancet infectious diseases,* 4**,** 144-154.
BOGAERT, D., HERMANS, P., ADRIAN, P., RÜMKE, H. & DE GROOT, R. 2004b. Pneumococcal vaccines: an update on current strategies. *Vaccine,* 22**,** 2209-2220.
BOURGOIS, J.-J., SLUSE, F., BAGUET, F. & MALLEFET, J. 2001. Kinetics of light emission and oxygen consumption by bioluminescent bacteria. *Journal of bioenergetics and biomembranes,* 33**,** 353-363.
BRICKER, A. L. & CAMILLI, A. 1999. Transformation of a type 4 encapsulated strain of *Streptococcus pneumoniae*. *FEMS microbiology letters,* 172**,** 131-135.
BRITTAN, J., BUCKERIDGE, T., FINN, A., KADIOGLU, A. & JENKINSON, H. 2012. Pneumococcal neuraminidase A: an essential upper airway colonization factor for *Streptococcus pneumoniae*. *Molecular oral microbiology,* 27**,** 270-283.
BROCK, M. 2011. Application of bioluminescence imaging for in vivo monitoring of fungal infections. *International Journal of Microbiology,* 2012.
BRODL, E., WINKLER, A. & MACHEROUX, P. 2018. Molecular mechanisms of bacterial bioluminescence. *Computational and structural biotechnology journal,* 16**,** 551-564.
BROWN, J. S., OGUNNIYI, A. D., WOODROW, M. C., HOLDEN, D. W. & PATON, J. C. 2001. Immunization with components of two iron uptake ABC transporters protects mice against systemic *Streptococcus pneumoniae* infection. *Infection and immunity,* 69**,** 6702-6706.
BRUMBAUGH, C. D., KIM, H. J., GIOVACCHINI, M. & POURMAND, N. 2011. NanoStriDE: normalization and differential expression analysis of NanoString nCounter data. *BMC bioinformatics,* 12**,** 479.
BUIS, J. M. & BRODERICK, J. B. 2005. Pyruvate formate-lyase activating enzyme: elucidation of a novel mechanism for glycyl radical formation. *Archives of biochemistry and biophysics,* 433**,** 288-296.
CADEDDU, C., DE WAURE, C., GUALANO, M. R., DI NARDO, F. & RICCIARDI, G. W. 2012. 23-valent pneumococcal polysaccharide vaccine (PPV23) for the prevention of invasive pneumococcal diseases (IPDs) in the elderly: is it really effective? *Journal of Preventive Medicine and Hygiene,* 53.
CANVIN, J. R., MARVIN, A. P., SIVAKUMARAN, M., PATON, J. C., BOULNOIS, G. J., ANDREW, P. W. & MITCHELL, T. J. 1995. The role of pneumolysin and autolysin in the pathology of pneumonia and septicemia in mice infected with a type 2 pneumococcus. *Journal of Infectious Diseases,* 172**,** 119-123.
CARVALHO, S. M., KLOOSTERMAN, T. G., KUIPERS, O. P. & NEVES, A. R. 2011. CcpA ensures optimal metabolic fitness of *Streptococcus pneumoniae*. *PloS one,* 6.
CERCA, F., FRANÇA, Â., PÉREZ-CABEZAS, B., CARVALHAIS, V., RIBEIRO, A., AZEREDO, J., PIER, G., CERCA, N. & VILANOVA, M. 2014. Dormant bacteria within *Staphylococcus epidermidis* biofilms have low inflammatory properties and maintain tolerance to vancomycin and penicillin after entering planktonic growth. *Journal of medical microbiology,* 63**,** 1274.
CHANG, M., ANTTONEN, K. P., CIRILLO, S. L., FRANCIS, K. P. & CIRILLO, J. D. 2014. Real-time bioluminescence imaging of mixed mycobacterial infections. *PLoS One,* 9**,** e108341.
CHARPENTIER, E. & TUOMANEN, E. 2000. Mechanisms of antibiotic resistance and tolerance in *Streptococcus pneumoniae*. *Microbes and infection,* 2**,** 1855-1864.
CHIAVOLINI, D., POZZI, G. & RICCI, S. 2008. Animal models of *Streptococcus pneumoniae* disease. *Clinical microbiology reviews,* 21**,** 666-685.

CLOSE, D. M., XU, T., SAYLER, G. S. & RIPP, S. 2011. In vivo bioluminescent imaging (BLI): noninvasive visualization and interrogation of biological processes in living animals. *Sensors,* 11**,** 180-206.

CONTAG, C. H., CONTAG, P. R., MULLINS, J. I., SPILMAN, S. D., STEVENSON, D. K. & BENARON, D. A. 1995. Photonic detection of bacterial pathogens in living hosts. *Molecular microbiology,* 18**,** 593-603.

CONTAG, C. H., SPILMAN, S. D., CONTAG, P. R., OSHIRO, M., EAMES, B., DENNERY, P., STEVENSON, D. K. & BENARON, D. A. 1997. Visualizing gene expression in living mammals using a bioluminescent reporter. *Photochemistry and photobiology,* 66**,** 523-531.

CONTAG, P. R. 2008. Bioluminescence imaging to evaluate infections and host response in vivo. *Innate Immunity.* Springer.

COOLS, F., TORFS, E., AIZAWA PORTO DE ABREU, J., VANHOUTTE, B., MAES, L., CALJON, G., DELPUTTE, P., CAPPOEN, D. & COS, P. 2019. Optimization and Characterization of a *Galleria mellonella* Larval Infection Model for Virulence Studies and the Evaluation of Therapeutics against Streptococcus pneumoniae. *Frontiers in microbiology,* 10**,** 311.

COOPER, D., YU, X., SIDHU, M., NAHM, M. H., FERNSTEN, P. & JANSEN, K. U. 2011. The 13-valent pneumococcal conjugate vaccine (PCV13) elicits cross-functional opsonophagocytic killing responses in humans to *Streptococcus pneumoniae* serotypes 6C and 7A. *Vaccine,* 29**,** 7207-7211.

CROUCHER, N. J., HARRIS, S. R., BARQUIST, L., PARKHILL, J. & BENTLEY, S. D. 2012. A high-resolution view of genome-wide pneumococcal transformation. *PLoS pathogens,* 8.

CUEVAS, R. A., EBRAHIMI, E. E., GAZIOGLU, O., YESILKAYA, H. & HILLER, N. L. 2019. Pneumococcal attachment to epithelial cells is enhanced by the secreted peptide VP1 via its control of hyaluronic acid processing. *bioRxiv***,** 788430.

CUEVAS, R. A., EUTSEY, R., KADAM, A., WEST-ROBERTS, J. A., WOOLFORD, C. A., MITCHELL, A. P., MASON, K. M. & HILLER, N. L. 2017. A novel streptococcal cell–cell communication peptide promotes pneumococcal virulence and biofilm formation. *Molecular microbiology,* 105**,** 554-571.

DALIA, A. B., STANDISH, A. J. & WEISER, J. N. 2010. Three surface exoglycosidases from *Streptococcus pneumoniae*, NanA, BgaA, and StrH, promote resistance to opsonophagocytic killing by human neutrophils. *Infection and immunity,* 78**,** 2108-2116.

DANIEL, C., POIRET, S., DENNIN, V., BOUTILLIER, D., LACORRE, D. A., FOLIGNÉ, B. & POT, B. 2015. Dual-color bioluminescence imaging for simultaneous monitoring of the intestinal persistence of *Lactobacillus plantarum* and *Lactococcus lactis* in living mice. *Appl. Environ. Microbiol.,* 81**,** 5344-5349.

DANIEL, C., POIRET, S., DENNIN, V., BOUTILLIER, D. & POT, B. 2012. Bioluminescent *Lactobacillus plantarum* and *Lactococcus lactis* to study spatial and temporal persistence in living mice. *Applied and Environmental Microbiology*.

DANIEL, C., POIRET, S., DENNIN, V., BOUTILLIER, D. & POT, B. 2013. Bioluminescence imaging study of spatial and temporal persistence of *Lactobacillus plantarum* and *Lactococcus lactis* in living mice. *Appl. Environ. Microbiol.,* 79**,** 1086-1094.

DAVE, S., CARMICLE, S., HAMMERSCHMIDT, S., PANGBURN, M. K. & MCDANIEL, L. S. 2004. Dual roles of PspC, a surface protein of *Streptococcus pneumoniae*, in binding human secretory IgA and factor H. *The Journal of Immunology,* 173**,** 471-477.

DELUCA, M. & MCELROY, W. 1978. [1] purification and properties of firefly luciferase. *Methods in enzymology.* Elsevier.

DEMIDOVA, T. N., GAD, F., ZAHRA, T., FRANCIS, K. P. & HAMBLIN, M. R. 2005. Monitoring photodynamic therapy of localized infections by bioluminescence imaging of genetically engineered bacteria. *Journal of Photochemistry and Photobiology B: Biology,* 81**,** 15-25.

DENNIS, A., KUDO, T., KRUIDENIER, L., GIRARD, F., CREPIN, V. F., MACDONALD, T. T., FRANKEL, G. & WILES, S. 2008. The p50 subunit of NF-κB is critical for in vivo clearance of the noninvasive enteric pathogen Citrobacter rodentium. *Infection and immunity,* 76**,** 4978-4988.

DIAVATOPOULOS, D. A., SHORT, K. R., PRICE, J. T., WILKSCH, J. J., BROWN, L. E., BRILES, D. E., STRUGNELL, R. A. & WIJBURG, O. L. 2010. Influenza A virus facilitates *Streptococcus pneumoniae* transmission and disease. *The FASEB Journal,* 24**,** 1789-1798.

DINTILHAC, A., ALLOING, G., GRANADEL, C. & CLAVERYS, J. P. 1997. Competence and virulence of *Streptococcus pneumoniae*: Adc and PsaA mutants exhibit a requirement for Zn and Mn resulting from inactivation of putative ABC metal permeases. *Molecular microbiology,* 25**,** 727-739.

DOERN, G. V., BRUEGGEMANN, A., HOLLEY, H. P. & RAUCH, A. M. 1996. Antimicrobial resistance of *Streptococcus pneumoniae* recovered from outpatients in the United States during the winter months of 1994 to 1995: results of a 30-center national surveillance study. *Antimicrobial Agents and Chemotherapy,* 40**,** 1208-1213.

DOERN, G. V., RICHTER, S. S., MILLER, A., MILLER, N., RICE, C., HEILMANN, K. & BEEKMANN, S. 2005. Antimicrobial resistance among *Streptococcus pneumoniae* in the United States: have we begun to turn the corner on resistance to certain antimicrobial classes? *Clinical infectious diseases,* 41**,** 139-148.

DOYLE, T. C., BURNS, S. M. & CONTAG, C. H. 2004. Technoreview: In vivo bioluminescence imaging for integrated studies of infection. *Cellular microbiology,* 6**,** 303-317.

DUNCAN, S., GLOVER, L. A., KILLHAM, K. & PROSSER, J. I. 1994. Luminescence-based detection of activity of starved and viable but nonculturable bacteria. *Appl. Environ. Microbiol.,* 60**,** 1308-1316.

DWORKIN, M. S., WARD, J. W., HANSON, D. L., JONES, J. L., KAPLAN, J. E., ADULT & PROJECT, A. S. O. H. D. 2001. Pneumococcal disease among human immunodeficiency virus-infected persons: incidence, risk factors, and impact of vaccination. *Clinical infectious diseases,* 32**,** 794-800.

EVANS, B. & ROZEN, D. 2012. A *Streptococcus pneumoniae* infection model in larvae of the wax moth *Galleria mellonella*. *European journal of clinical microbiology & infectious diseases,* 31**,** 2653-2660.

FAHY, J. V. & DICKEY, B. F. 2010. Airway mucus function and dysfunction. *New England Journal of Medicine,* 363**,** 2233-2247.

FELMINGHAM, D. 2004. Comparative antimicrobial susceptibility of respiratory tract pathogens. *Chemotherapy,* 50**,** 3-10.

FRANCIS, K. P., YU, J., BELLINGER-KAWAHARA, C., JOH, D., HAWKINSON, M. J., XIAO, G., PURCHIO, T. F., CAPARON, M. G., LIPSITCH, M. & CONTAG, P. R. 2001. Visualizing Pneumococcal Infections in the Lungs of Live Mice Using Bioluminescent *Streptococcus pneumoniae* Transformed with a Novel Gram-Positive luxTransposon. *Infection and immunity,* 69**,** 3350-3358.

FU, X., FU, N., GUO, S., YAN, Z., XU, Y., HU, H., MENZEL, C., CHEN, W., LI, Y. & ZENG, R. 2009. Estimating accuracy of RNA-Seq and microarrays with proteomics. *BMC genomics,* 10**,** 161.

FUCHS, B. B., O'BRIEN, E., EL KHOURY, J. B. & MYLONAKIS, E. 2010. Methods for using *Galleria mellonella* as a model host to study fungal pathogenesis. *Virulence,* 1**,** 475-482.

GARDAM, M. & MILLER, M. 1998. Optochin revisited: defining the optimal type of blood agar for presumptive identification of *Streptococcus pneumoniae*. *Journal of clinical microbiology,* 36**,** 833-834.

GAY, K., BAUGHMAN, W., MILLER, Y., JACKSON, D., WHITNEY, C. G., SCHUCHAT, A., FARLEY, M. M., TENOVER, F. & STEPHENS, D. S. 2000. The emergence of *Streptococcus pneumoniae* resistant to macrolide antimicrobial agents: a 6-year population-based assessment. *The Journal of infectious diseases,* 182**,** 1417-1424.

GEISS, G. K., BUMGARNER, R. E., BIRDITT, B., DAHL, T., DOWIDAR, N., DUNAWAY, D. L., FELL, H. P., FERREE, S., GEORGE, R. D. & GROGAN, T. 2008. Direct multiplexed measurement of gene expression with color-coded probe pairs. *Nature biotechnology,* 26**,** 317-325.

GHAFFAR, F., FRIEDLAND, I. R. & GEORGE H MCCRACKEN, J. 1999. Dynamics of nasopharyngeal colonization by *Streptococcus pneumoniae*. *The Pediatric infectious disease journal,* 18**,** 638-646.

GLOMSKI, I. J., CORRE, J.-P., MOCK, M. & GOOSSENS, P. L. 2007. Noncapsulated toxinogenic *Bacillus anthracis* presents a specific growth and dissemination pattern in naive and protective antigen-immune mice. *Infection and immunity,* 75**,** 4754-4761.

GOLOS, M., ELIAKIM-RAZ, N., STERN, A., LEIBOVICI, L. & PAUL, M. 2016. Conjugated pneumococcal vaccine versus polysaccharide pneumococcal vaccine for prevention of pneumonia and invasive pneumococcal disease in immunocompetent and immunocompromised adults and children. *Cochrane Database of Systematic Reviews*.

GOULD, J. M. & WEISER, J. N. 2002. The Inhibitory Effect of C-Reactive Protein on Bacterial Phosphorylcholine Platelet-Activating Factor Receptor–Mediated Adherence Is Blocked by Surfactant. *The Journal of infectious diseases,* 186**,** 361-371.

HAKKILA, K., MAKSIMOW, M., KARP, M. & VIRTA, M. 2002. Reporter genes lucFF, luxCDABE, gfp, and dsred have different characteristics in whole-cell bacterial sensors. *Analytical biochemistry,* 301**,** 235-242.

HALFMANN, A., HAKENBECK, R. & BRÜCKNER, R. 2007. A new integrative reporter plasmid for *Streptococcus pneumoniae*. *FEMS microbiology letters,* 268**,** 217-224.

HAMMERSCHMIDT, S., WOLFF, S., HOCKE, A., ROSSEAU, S., MÜLLER, E. & ROHDE, M. 2005. Illustration of pneumococcal polysaccharide capsule during adherence and invasion of epithelial cells. *Infection and immunity,* 73**,** 4653-4667.

HARDING, C. R., SCHROEDER, G. N., COLLINS, J. W. & FRANKEL, G. 2013. Use of *Galleria mellonella* as a model organism to study Legionella pneumophila infection. *JoVE (Journal of Visualized Experiments)***,** e50964.

HASTINGS, J. W. 1996. Chemistries and colors of bioluminescent reactions: a review. *Gene,* 173**,** 5-11.

HAYWARD, S., THOMPSON, L. A. & MCEACHERN, A. 2016. Is 13-valent pneumococcal conjugate vaccine (PCV13) combined with 23-valent pneumococcal polysaccharide vaccine (PPSV23) superior to PPSV23 alone for reducing incidence or severity of pneumonia in older adults? A Clin-IQ. *Journal of patient-centered research and reviews,* 3**,** 111.

HENKEN, S., BOHLING, J., OGUNNIYI, A. D., PATON, J. C., SALISBURY, V. C., WELTE, T. & MAUS, U. A. 2010. Evaluation of biophotonic imaging to estimate bacterial burden in mice infected with highly virulent compared to less virulent *Streptococcus pneumoniae* serotypes. *Antimicrobial agents and chemotherapy,* 54**,** 3155-3160.

HENRICHSEN, J. 1995. Six newly recognized types of *Streptococcus pneumoniae*. *Journal of clinical microbiology,* 33**,** 2759.

HERBERT, J. A., MITCHELL, A. M., RITCHIE, R., MA, J., ROSS-HUTCHINSON, K. & MITCHELL, T. J. 2018. Expression of the lux genes in *Streptococcus pneumoniae* modulates pilus expression and virulence. *PloS one,* 13.

HOBAN, D., DOERN, G., FLUIT, A., ROUSSEL-DELVALLEZ, M. & JONES, R. 2001. Worldwide prevalence of antimicrobial resistance in *Streptococcus pneumoniae*, *Haemophilus influenzae*, and *Moraxella catarrhalis* in the SENTRY Antimicrobial Surveillance Program, 1997–1999. *Clinical Infectious Diseases,* 32**,** S81-S93.

HOOVER, S. E., PEREZ, A. J., TSUI, H. C. T., SINHA, D., SMILEY, D. L., DIMARCHI, R. D., WINKLER, M. E. & LAZAZZERA, B. A. 2015. A new quorum-sensing system (TprA/PhrA) for *Streptococcus pneumoniae* D 39 that regulates a lantibiotic biosynthesis gene cluster. *Molecular microbiology,* 97**,** 229-243.

HUTCHENS, M. & LUKER, G. D. 2007. Applications of bioluminescence imaging to the study of infectious diseases. *Cellular microbiology,* 9**,** 2315-2322.

HYAMS, C., YUSTE, J., BAX, K., CAMBERLEIN, E., WEISER, J. N. & BROWN, J. S. 2010. *Streptococcus pneumoniae* resistance to complement-mediated immunity is dependent on the capsular serotype. *Infection and immunity,* 78**,** 716-725.

IBRAHIM, Y. M., KERR, A. R., MCCLUSKEY, J. & MITCHELL, T. J. 2004. Role of HtrA in the virulence and competence of *Streptococcus pneumoniae*. *Infection and immunity,* 72**,** 3584-3591.

IGNASIAK, K. & MAXWELL, A. 2017. *Galleria mellonella* (greater wax moth) larvae as a model for antibiotic susceptibility testing and acute toxicity trials. *BMC research notes,* 10**,** 428.

INOUE, Y., KIRYU, S., IZAWA, K., WATANABE, M., TOJO, A. & OHTOMO, K. 2009. Comparison of subcutaneous and intraperitoneal injection of D-luciferin for in vivo bioluminescence imaging. *European journal of nuclear medicine and molecular imaging,* 36**,** 771-779.

IYER, R., BALIGA, N. S. & CAMILLI, A. 2005. Catabolite control protein A (CcpA) contributes to virulence and regulation of sugar metabolism in *Streptococcus pneumoniae*. *Journal of bacteriology,* 187**,** 8340-8349.

JACOBS, M. R. 2004. *Streptococcus pneumoniae*: epidemiology and patterns of resistance. *The American Journal of Medicine Supplements,* 117**,** 3-15.

JACOBS, M. R., GOOD, C. E., BAJAKSOUZIAN, S. & WINDAU, A. R. 2008. Emergence of *Streptococcus pneumoniae* serotypes 19A, 6C, and 22F and serogroup 15 in Cleveland, Ohio, in relation to introduction of the protein-conjugated pneumococcal vaccine. *Clinical Infectious Diseases,* 47**,** 1388-1395.

JANOFF, E. N. & RUBINS, J. B. 1997. Invasive pneumococcal disease in the immunocompromised host. *Microbial Drug Resistance,* 3**,** 215-232.

JANOFF, E. N. & RUBINS, J. B. 2004. Immunodeficiency and invasive pneumococcal disease. *The pneumococcus.* American Society of Microbiology.

JENKINS, D. E., OEI, Y., HORNIG, Y. S., YU, S.-F., DUSICH, J., PURCHIO, T. & CONTAG, P. R. 2003. Bioluminescent imaging (BLI) to improve and refine traditional murine models of tumor growth and metastasis. *Clinical & experimental metastasis,* 20**,** 733-744.

JENSCH, I., GÁMEZ, G., ROTHE, M., EBERT, S., FULDE, M., SOMPLATZKI, D., BERGMANN, S., PETRUSCHKA, L., ROHDE, M. & NAU, R. 2010. PavB is a surface-exposed adhesin of *Streptococcus pneumoniae* contributing to nasopharyngeal colonization and airways infections. *Molecular microbiology,* 77**,** 22-43.

JOHNSON, A. W., SIDMAN, J. D. & LIN, J. 2013. Bioluminescent imaging of pneumococcal otitis media in chinchillas. *Annals of Otology, Rhinology & Laryngology,* 122**,** 344-352.

JORGENSEN, J., DOERN, G., MAHER, L. A., HOWELL, A. & REDDING, J. 1990. Antimicrobial resistance among respiratory isolates of *Haemophilus influenzae*, *Moraxella catarrhalis*, and *Streptococcus pneumoniae* in the United States. *Antimicrobial Agents and Chemotherapy,* 34**,** 2075-2080.

JOYCE, S. A. & GAHAN, C. G. 2010. Molecular pathogenesis of *Listeria monocytogenes* in the alternative model host *Galleria mellonella*. *Microbiology,* 156**,** 3456-3468.

KADIOGLU, A. & ANDREW, P. W. 2005. Susceptibility and resistance to pneumococcal disease in mice. *Briefings in Functional Genomics,* 4**,** 241-247.

KADIOGLU, A., WEISER, J. N., PATON, J. C. & ANDREW, P. W. 2008. The role of *Streptococcus pneumoniae* virulence factors in host respiratory colonization and disease. *Nature Reviews Microbiology,* 6**,** 288.

KADURUGAMUWA, J. L., SIN, L., ALBERT, E., YU, J., FRANCIS, K., DEBOER, M., RUBIN, M., BELLINGER-KAWAHARA, C., PARR JR, T. & CONTAG, P. R. 2003. Direct continuous method for monitoring biofilm infection in a mouse model. *Infection and immunity,* 71**,** 882-890.

KALTOFT, M. S., SØRENSEN, U. B. S., SLOTVED, H.-C. & KONRADSEN, H. B. 2008. An easy method for detection of nasopharyngeal carriage of multiple *Streptococcus pneumoniae* serotypes. *Journal of microbiological methods,* 75**,** 540-544.

KAPITAN, M., EICHHOF, I., LAGADEC, Q. & ERNST, J. F. 2016. Click beetle luciferases as dual reporters of gene expression in *Candida albicans*. *Microbiology,* 162**,** 1310-1320.

KARLIN, S., THERIOT, J. & MRÁZEK, J. 2004. Comparative analysis of gene expression among low G+ C gram-positive genomes. *Proceedings of the National Academy of Sciences,* 101**,** 6182-6187.

KELLY, M., SURETTE, M., SMIEJA, M., ROSSI, L., LUINSTRA, K., STEENHOFF, A., GOLDFARB, D., ARSCOTT-MILLS, T., BOIDITSWE, S. & RULAGANYANG, I. Pneumococcal Colonization and the Nasopharyngeal Microbiota of Children in Botswana. Open Forum Infectious Diseases, 2017. Oxford University Press US, S233-S233.

KING, S. 2010. Pneumococcal modification of host sugars: a major contributor to colonization of the human airway? *Molecular oral microbiology,* 25**,** 15-24.

KLOOSTERMAN, T. G., BIJLSMA, J. J., KOK, J. & KUIPERS, O. P. 2006. To have neighbour's fare: extending the molecular toolbox for *Streptococcus pneumoniae*. *Microbiology,* 152**,** 351-359.

KONG, I. G., SATO, A., YUKI, Y., NOCHI, T., TAKAHASHI, H., SAWADA, S., MEJIMA, M., KUROKAWA, S., OKADA, K. & SATO, S. 2013. Nanogel-based PspA intranasal vaccine prevents invasive disease and nasal colonization by *Streptococcus pneumoniae*. *Infection and immunity,* 81**,** 1625-1634.

LA ROSA, S. L., DIEP, D. B., NES, I. F. & BREDE, D. A. 2012. Construction and application of a luxABCDE reporter system for real-time monitoring of gene expression and growth of *Enterococcus faecalis*. *Applied and Environmental Microbiology***,** AEM. 02018-12.

LACKS, S. A. 1997. Cloning and expression of pneumococcal genes in *Streptococcus pneumoniae*. *Microbial drug resistance,* 3**,** 327-337.

LANE, M. C., ALTERI, C. J., SMITH, S. N. & MOBLEY, H. L. 2007. Expression of flagella is coincident with uropathogenic *Escherichia coli* ascension to the upper urinary tract. *Proceedings of the National Academy of Sciences,* 104**,** 16669-16674.

LANGE, A., BEIER, S., HUSON, D., PARUSEL, R., IGLAUER, F. & FRICK, J. 2018. Genome sequence of *Galleria mellonella* (greater wax moth). Genome Announc 6 (2): e01220–e01317.

LEEGAARD, T. M., BOOTSMA, H. J., CAUGANT, D. A., ELEVELD, M. J., MANNSÅKER, T., FRØHOLM, L. O., GAUSTAD, P., HØIBY, E. A. & HERMANS, P. W. 2010. Phenotypic and genomic characterization of pneumococcus-like streptococci isolated from HIV-seropositive patients. *Microbiology,* 156**,** 838-848.

LEMESSURIER, K. S., OGUNNIYI, A. D. & PATON, J. C. 2006. Differential expression of key pneumococcal virulence genes in vivo. *Microbiology,* 152**,** 305-311.

LIPSITCH, M., DYKES, J., JOHNSON, S., ADES, E., KING, J., BRILES, D. & CARLONE, G. 2000. Competition among *Streptococcus pneumoniae* for intranasal colonization in a mouse model. *Vaccine,* 18**,** 2895-2901.

LOVING, C. L., KHURANA, T., OSORIO, M., LEE, G. M., KELLY, V. K., STIBITZ, S. & MERKEL, T. J. 2009. Role of anthrax toxins in dissemination, disease progression, and induction of protective adaptive immunity in the mouse aerosol challenge model. *Infection and immunity,* 77**,** 255-265.

MANCO, S., HERNON, F., YESILKAYA, H., PATON, J. C., ANDREW, P. W. & KADIOGLU, A. 2006. Pneumococcal neuraminidases A and B both have essential roles during infection of the respiratory tract and sepsis. *Infection and immunity,* 74**,** 4014-4020.

MARÍN, M., CERCENADO, E., SÁNCHEZ-CARRILLO, C., RUIZ, A., GÓMEZ GONZÁLEZ, Á., RODRÍGUEZ-SÁNCHEZ, B. & BOUZA, E. 2017. Accurate differentiation of *Streptococcus pneumoniae* from other species within the Streptococcus mitis group by peak analysis using MALDI-TOF MS. *Frontiers in microbiology,* 8**,** 698.

MARINCS, F. 2000. On-line monitoring of growth of *Escherichia coli* in batch cultures by bioluminescence. *Applied microbiology and biotechnology,* 53**,** 536-541.

MARION, C., STEWART, J. M., TAZI, M. F., BURNAUGH, A. M., LINKE, C. M., WOODIGA, S. A. & KING, S. J. 2012. *Streptococcus pneumoniae* can utilize multiple sources of hyaluronic acid for growth. *Infection and immunity,* 80**,** 1390-1398.

MCAVIN, J. C., REILLY, P. A., ROUDABUSH, R. M., BARNES, W. J., SALMEN, A., JACKSON, G. W., BENINGA, K. K., ASTORGA, A., MCCLESKEY, F. K. & HUFF, W. B. 2001. Sensitive and specific method for rapid identification of *Streptococcus pneumoniae* using real-time fluorescence PCR. *Journal of clinical microbiology,* 39**,** 3446-3451.

MCCOOL, T. L., CATE, T. R., MOY, G. & WEISER, J. N. 2002. The immune response to pneumococcal proteins during experimental human carriage. *The Journal of experimental medicine,* 195**,** 359-365.

MCCULLERS, J. A., KARLSTRÖM, Å., IVERSON, A. R., LOEFFLER, J. M. & FISCHETTI, V. A. 2007. Novel strategy to prevent otitis media caused by colonizing *Streptococcus pneumoniae*. *PLOS pathogens,* 3.

MEIR, M., GROSFELD, T. & BARKAN, D. 2018. Establishment and validation of *Galleria mellonella* as a novel model organism to study *Mycobacterium abscessus* infection, pathogenesis, and treatment. *Antimicrobial agents and chemotherapy,* 62**,** e02539-17.
MELEGARO, A., EDMUNDS, W., PEBODY, R., MILLER, E. & GEORGE, R. 2006. The current burden of pneumococcal disease in England and Wales. *Journal of Infection,* 52**,** 37-48.
MILES, A. A., MISRA, S. & IRWIN, J. 1938. The estimation of the bactericidal power of the blood. *Epidemiology & Infection,* 38**,** 732-749.
MILLER, M. B. & BASSLER, B. L. 2001. Quorum sensing in bacteria. *Annual Reviews in Microbiology,* 55**,** 165-199.
MILLER, R. J., CROSBY, H. A., SCHILCHER, K., WANG, Y., ORTINES, R. V., MAZHAR, M., DIKEMAN, D. A., PINSKER, B. L., BROWN, I. D. & JOYCE, D. P. 2019. Development of a *Staphylococcus aureus* reporter strain with click beetle red luciferase for enhanced in vivo imaging of experimental bacteremia and mixed infections. *Scientific reports,* 9**,** 1-19.
MILOUD, T., HENRICH, C. & HAMMERLING, G. J. 2007. Quantitative comparison of click beetle and firefly luciferases for in vivo bioluminescence imaging. *Journal of biomedical optics,* 12**,** 054018.
MIZUGUCHI, Y. 1998. Single photon counting. *Free Radical and Antioxidant Protocols.* Springer.
MOTIB, A. S., AL-BAYATI, F. A., MANZOOR, I., SHAFEEQ, S., KADAM, A., KUIPERS, O. P., HILLER, N. L., ANDREW, P. W. & YESILKAYA, H. 2019. TprA/PhrA quorum sensing system has a major effect on pneumococcal survival in respiratory tract and blood, and its activity is controlled by CcpA and GlnR. *Frontiers in cellular and infection microbiology,* 9**,** 326.
MOWLDS, P. & KAVANAGH, K. 2008. Effect of pre-incubation temperature on susceptibility of *Galleria mellonella* larvae to infection by *Candida albicans*. *Mycopathologia,* 165**,** 5-12.
MUKERJI, R., MIRZA, S., ROCHE, A. M., WIDENER, R. W., CRONEY, C. M., RHEE, D.-K., WEISER, J. N., SZALAI, A. J. & BRILES, D. E. 2012. Pneumococcal surface protein A inhibits complement deposition on the pneumococcal surface by competing with the binding of C-reactive protein to cell-surface phosphocholine. *The Journal of Immunology,* 189**,** 5327-5335.
NEVES, A. R., RAMOS, A., COSTA, H., VAN SWAM, I. I., HUGENHOLTZ, J., KLEEREBEZEM, M., DE VOS, W. & SANTOS, H. 2002. Effect of different NADH oxidase levels on glucose metabolism by *Lactococcus lactis*: kinetics of intracellular metabolite pools determined by in vivo nuclear magnetic resonance. *Appl. Environ. Microbiol.,* 68**,** 6332-6342.
NUNES, M. C., VON GOTTBERG, A., DE GOUVEIA, L., COHEN, C., KUWANDA, L., KARSTAEDT, A. S., KLUGMAN, K. P. & MADHI, S. A. 2011. Persistent high burden of invasive pneumococcal disease in South African HIV-infected adults in the era of an antiretroviral treatment program. *PloS one,* 6**,** e27929.
O'BRIEN, K. L., WOLFSON, L. J., WATT, J. P., HENKLE, E., DELORIA-KNOLL, M., MCCALL, N., LEE, E., MULHOLLAND, K., LEVINE, O. S. & CHERIAN, T. 2009. Burden of disease caused by *Streptococcus pneumoniae* in children younger than 5 years: global estimates. *The Lancet,* 374**,** 893-902.
OBARO, S. K. 1996. Carriage of pneumococci after pneumococcal vaccination. *Lancet,* 348**,** 271-272.
ORIHUELA, C. J., GAO, G., MCGEE, M., YU, J., FRANCIS, K. P. & TUOMANEN, E. 2003. Organ-specific models of *Streptococcus pneumoniae* disease. *Scandinavian journal of infectious diseases,* 35**,** 647-652.
ORIHUELA, C. J., RADIN, J. N., SUBLETT, J. E., GAO, G., KAUSHAL, D. & TUOMANEN, E. I. 2004. Microarray analysis of pneumococcal gene expression during invasive disease. *Infection and immunity,* 72**,** 5582-5596.
OWEN, R. H., BOULNOIS, G. J., ANDREW, P. W. & MITCHELL, T. J. 1994. A role in cell-binding for the C-terminus of pneumolysin, the thiol-activated toxin of *Streptococcus pneumoniae*. *FEMS microbiology letters,* 121**,** 217-221.
OZAWA, T., YOSHIMURA, H. & KIM, S. B. 2013. Advances in fluorescence and bioluminescence imaging. *Analytical chemistry,* 85**,** 590-609.

PARKER, D., SOONG, G., PLANET, P., BROWER, J., RATNER, A. J. & PRINCE, A. 2009. The NanA neuraminidase of *Streptococcus pneumoniae* is involved in biofilm formation. *Infection and immunity,* 77**,** 3722-3730.
PATERSON, G. K. & MITCHELL, T. J. 2006. The role of *Streptococcus pneumoniae* sortase A in colonisation and pathogenesis. *Microbes and infection,* 8**,** 145-153.
PELTOLA, V. T., BOYD, K. L., MCAULEY, J. L., REHG, J. E. & MCCULLERS, J. A. 2006. Bacterial sinusitis and otitis media following influenza virus infection in ferrets. *Infection and immunity,* 74**,** 2562-2567.
PEREIRA, T. C., DE BARROS, P. P., FUGISAKI, L. R. D. O., ROSSONI, R. D., RIBEIRO, F. D. C., DE MENEZES, R. T., JUNQUEIRA, J. C. & SCORZONI, L. 2018. Recent advances in the use of *Galleria mellonella* model to study immune responses against human pathogens. *Journal of Fungi,* 4**,** 128.
PETERS, C. & PATERSON, Y. 2003. Enhancing the immunogenicity of bioengineered *Listeria monocytogenes* by passaging through live animal hosts. *Vaccine,* 21**,** 1187-1194.
QAZI, S. N., COUNIL, E., MORRISSEY, J., REES, C. E., COCKAYNE, A., WINZER, K., CHAN, W. C., WILLIAMS, P. & HILL, P. J. 2001. agr Expression Precedes Escape of Internalized *Staphylococcus aureus* from the Host Endosome. *Infection and immunity,* 69**,** 7074-7082.
RAI, P., HE, F., KWANG, J., ENGELWARD, B. P. & CHOW, V. T. 2016. Pneumococcal pneumolysin induces DNA damage and cell cycle arrest. *Scientific reports,* 6**,** 22972.
RAJASHEKARA, G., GLOVER, D. A., KREPPS, M. & SPLITTER, G. A. 2005. Temporal analysis of pathogenic events in virulent and avirulent *Brucella melitensis* infections. *Cellular microbiology,* 7**,** 1459-1473.
RAMOS-MONTAÑEZ, S., KAZMIERCZAK, K. M., HENTCHEL, K. L. & WINKLER, M. E. 2010. Instability of ackA (acetate kinase) mutations and their effects on acetyl phosphate and ATP amounts in *Streptococcus pneumoniae* D39. *Journal of bacteriology,* 192**,** 6390-6400.
READ, H. M., MILLS, G., JOHNSON, S., TSAI, P., DALTON, J., BARQUIST, L., PATRICK, W. M. & WILES, S. 2016. The in vitro and in vivo effects of constitutive light expression on the mouse enteropathogen Citrobacter rodentium. PeerJ Preprints.
RICE, B. W., CABLE, M. D. & NELSON, M. B. 2001. In vivo imaging of light-emitting probes. *Journal of biomedical optics,* 6**,** 432-441.
RIEDEL, C. U., MONK, I. R., CASEY, P. G., MORRISSEY, D., O'SULLIVAN, G. C., TANGNEY, M., HILL, C. & GAHAN, C. G. 2007. Improved luciferase tagging system for *Listeria monocytogenes* allows real-time monitoring in vivo and in vitro. *Appl. Environ. Microbiol.,* 73**,** 3091-3094.
ROCCHETTA, H., BOYLAN, C., FOLEY, J., IVERSEN, P., LETOURNEAU, D., MCMILLIAN, C., CONTAG, P., JENKINS, D. & PARR, T. 2001. Validation of a noninvasive, real-time imaging technology using bioluminescent *Escherichia coli* in the neutropenic mouse thigh model of infection. *Antimicrobial agents and chemotherapy,* 45**,** 129-137.
ROCHE, A., RICHARD, A., RAHKOLA, J., JANOFF, E. & WEISER, J. 2014. Antibody blocks acquisition of bacterial colonization through agglutination. Mucosal Immunol 8: 176–185.
RUDAN, I., BOSCHI-PINTO, C., BILOGLAV, Z., MULHOLLAND, K. & CAMPBELL, H. 2008. Epidemiology and etiology of childhood pneumonia. *Bulletin of the world health organization,* 86**,** 408-416B.
SADIKOT, R. T. & BLACKWELL, T. S. 2008. Bioluminescence: imaging modality for in vitro and in vivo gene expression. *Advanced Protocols in Oxidative Stress I.* Springer.
SAITO, H. & MIURA, K.-I. 1963. Preparation of transforming deoxyribonucleic acid by phenol treatment. *Biochimica et Biophysica Acta (BBA)-Specialized Section on Nucleic Acids and Related Subjects,* 72**,** 619-629.
SANDGREN, A., ALBIGER, B., ORIHUELA, C. J., TUOMANEN, E., NORMARK, S. & HENRIQUES-NORMARK, B. 2005. Virulence in mice of pneumococcal clonal types with known invasive disease potential in humans. *The Journal of infectious diseases,* 192**,** 791-800.
SAXENA, A., SRIVASTAVA, V., SRIVASTAVA, R. & SRIVASTAVA, B. S. 2008. Identification of genes of *Mycobacterium tuberculosis* upregulated during anaerobic persistence by fluorescence and kanamycin resistance selection. *Tuberculosis,* 88**,** 518-525.

SCHOLZ, C. F., POULSEN, K. & KILIAN, M. 2012. Novel molecular method for identification of *Streptococcus pneumoniae* applicable to clinical microbiology and 16S rRNA sequence-based microbiome studies. *Journal of clinical microbiology,* 50**,** 1968-1973.

SCHRAG, S. J., BEALL, B., DOWELL, S. & ORGANIZATION, W. H. 2001. Resistant pneumococcal infections: the burden of disease and challenges in monitoring and controlling antimicrobial resistance. World Health Organization.

SEBERT, M., PALMER, L., ROSENBERG, M. & WEISER, J. 2002. Microarray-based identification of htrA, a *Streptococcus pneumoniae* gene that is regulated by the CiaRH two-component system and contributes to nasopharyngeal colonization. *Infection and immunity,* 70**,** 4059-4067.

SHAPER, M., HOLLINGSHEAD, S. K., BENJAMIN, W. H. & BRILES, D. E. 2004. PspA protects *Streptococcus pneumoniae* from killing by apolactoferrin, and antibody to PspA enhances killing of pneumococci by apolactoferrin. *Infection and immunity,* 72**,** 5031-5040.

SHORT, K. R. & DIAVATOPOULOS, D. A. 2015. Nasopharyngeal colonization with *Streptococcus pneumoniae*. *Streptococcus pneumoniae.* Elsevier.

SHORT, K. R., DIAVATOPOULOS, D. A., READING, P. C., BROWN, L. E., ROGERS, K. L., STRUGNELL, R. A. & WIJBURG, O. L. 2011. Using bioluminescent imaging to investigate synergism between *Streptococcus pneumoniae* and influenza A virus in infant mice. *JoVE (Journal of Visualized Experiments)***,** e2357.

SIGNORE, A., MATHER, S., PIAGGIO, G., MALVIYA, G. & DIERCKX, R. 2010. Molecular imaging of inflammation/infection: nuclear medicine and optical imaging agents and methods. *Chemical reviews,* 110**,** 3112-3145.

SNEWIN, V. A., GARES, M.-P., ÓGAORA, P., HASAN, Z., BROWN, I. N. & YOUNG, D. B. 1999. Assessment of immunity to mycobacterial infection with luciferase reporter constructs. *Infection and immunity,* 67**,** 4586-4593.

STEINHUBER, A., LANDMANN, R., GOERKE, C., WOLZ, C. & FLÜCKIGER, U. 2008. Bioluminescence imaging to study the promoter activity of hla of *Staphylococcus aureus* in vitro and in vivo. *International Journal of Medical Microbiology,* 298**,** 599-605.

SUN, Y. Q., LIU, J., WANG, P., ZHANG, J. & GUO, W. 2012. D-Luciferin Analogues: a Multicolor Toolbox for Bioluminescence Imaging. *Angewandte Chemie International Edition,* 51**,** 8428-8430.

SZITTNER, R., JANSEN, G., THOMAS, D. Y. & MEIGHEN, E. 2003. Bright stable luminescent yeast using bacterial luciferase as a sensor. *Biochemical and biophysical research communications,* 309**,** 66-70.

SZITTNER, R. & MEIGHEN, E. 1990. Nucleotide sequence, expression, and properties of luciferase coded by lux genes from a terrestrial bacterium. *Journal of Biological Chemistry,* 265**,** 16581-16587.

TANIAI, H., IIDA, K.-I., SEKI, M., SAITO, M., SHIOTA, S., NAKAYAMA, H. & YOSHIDA, S.-I. 2008. Concerted action of lactate oxidase and pyruvate oxidase in aerobic growth of *Streptococcus pneumoniae*: role of lactate as an energy source. *Journal of bacteriology,* 190**,** 3572-3579.

TANNOUS, B. A., KIM, D.-E., FERNANDEZ, J. L., WEISSLEDER, R. & BREAKEFIELD, X. O. 2005. Codon-optimized Gaussia luciferase cDNA for mammalian gene expression in culture and in vivo. *Molecular Therapy,* 11**,** 435-443.

TROY, T., JEKIC-MCMULLEN, D., SAMBUCETTI, L. & RICE, B. 2004. Quantitative comparison of the sensitivity of detection of fluorescent and bioluminescent reporters in animal models. *Molecular imaging,* 3**,** 15353500200403196.

TSAI, C., LOH, J. & PROFT, T. 2016. *Galleria mellonella* infection models for the study of bacterial diseases and for antimicrobial drug testing. Virulence 7: 214–229.

TUOMANEN, E. I. 1996. Molecular and cellular mechanisms of pneumococcal meningitis. *Annals of the New York Academy of Sciences,* 797**,** 42-52.

UR RAHMAN, S., STANTON, M., CASEY, P. G., SPAGNUOLO, A., BENSI, G., HILL, C., FRANCIS, K. P., TANGNEY, M. & GAHAN, C. G. 2017. Development of a Click Beetle luciferase reporter system for enhanced bioluminescence imaging of *Listeria monocytogenes*: analysis in cell culture and murine infection models. *Frontiers in microbiology,* 8**,** 1797.

VAHIDY, R., WASEEM, M. & KHALID, S. 1996. A comparative study of unpassaged and animal passaged cultures of *Listeria monocytogenes* in rabbits. *Annals of the Academy of Medicine, Singapore,* 25**,** 139-142.
VAN DER LINDEN, M., AL-LAHHAM, A., NICKLAS, W. & REINERT, R. R. 2009. Molecular characterization of pneumococcal isolates from pets and laboratory animals. *PloS one,* 4.
VAN DER POLL, T. & OPAL, S. M. 2009. Pathogenesis, treatment, and prevention of pneumococcal pneumonia. *The Lancet,* 374**,** 1543-1556.
VAN REET, N., VAN DE VYVER, H., PYANA, P. P., VAN DER LINDEN, A. M. & BÜSCHER, P. 2014. A panel of *Trypanosoma brucei* strains tagged with blue and red-shifted luciferases for bioluminescent imaging in murine infection models. *PLoS neglected tropical diseases,* 8.
VEMURI, G. N., ALTMAN, E., SANGURDEKAR, D., KHODURSKY, A. B. & EITEMAN, M. A. 2006. Overflow metabolism in *Escherichia coli* during steady-state growth: transcriptional regulation and effect of the redox ratio. *Appl. Environ. Microbiol.,* 72**,** 3653-3661.
VUONG, C., KOCIANOVA, S., YU, J., KADURUGAMUWA, J. L. & OTTO, M. 2008. Development of real-time in vivo imaging of device-related *Staphylococcus epidermidis* infection in mice and influence of animal immune status on susceptibility to infection. *The Journal of infectious diseases,* 198**,** 258-261.
WAIDMANN, M. S., BLEICHRODT, F. S., LASLO, T. & RIEDEL, C. U. 2011. Bacterial luciferase reporters: the Swiss army knife of molecular biology. *Bioengineered bugs,* 2**,** 8-16.
WALSH, F. M. & AMYES, S. G. 2004. Microbiology and drug resistance mechanisms of fully resistant pathogens. *Current opinion in microbiology,* 7**,** 439-444.
WAND, M. E., MCCOWEN, J. W., NUGENT, P. G. & SUTTON, J. M. 2013. Complex interactions of *Klebsiella pneumoniae* with the host immune system in a *Galleria mellonella* infection model. *Journal of medical microbiology,* 62**,** 1790-1798.
WANG, Z., GERSTEIN, M. & SNYDER, M. 2009. RNA-Seq: a revolutionary tool for transcriptomics. *Nature reviews genetics,* 10**,** 57-63.
WEISER, J. N., FERREIRA, D. M. & PATON, J. C. 2018. *Streptococcus pneumoniae*: transmission, colonization and invasion. *Nature Reviews Microbiology,* 16**,** 355.
WILSON, T. & HASTINGS, J. W. 1998. Bioluminescence. *Annual review of cell and developmental biology,* 14**,** 197-230.
WOOD, K. V., LAM, Y. A., SELIGER, H. H. & MCELROY, W. D. 1989. Complementary DNA coding click beetle luciferases can elicit bioluminescence of different colors. *Science,* 244**,** 700-702.
WOODROOFE, C. C., SHULTZ, J. W., WOOD, M. G., OSTERMAN, J., CALI, J. J., DAILY, W. J., MEISENHEIMER, P. L. & KLAUBERT, D. H. 2008. N-Alkylated 6′-aminoluciferins are bioluminescent substrates for Ultra-Glo and QuantiLum luciferase: new potential scaffolds for bioluminescent assays. *Biochemistry,* 47**,** 10383-10393.
WORLD HEALTH ORGANIZATION. 2012. *Estimated Hib and pneumococcal deaths for children under 5 years of age, 2008* [Online]. Available: https://www.who.int/immunization/monitoring_surveillance/burden/estimates/Pneumo_hib/en/ [Accessed 14/01 2020].
WYLLIE, A. L. 2016. *Molecular surveillance of pneumococcal carriage in all ages.* Utrecht University.
YADAV, M. K., CHAE, S.-W., PARK, K. & SONG, J.-J. 2013. Hyaluronic acid derived from other streptococci supports *Streptococcus pneumoniae* in vitro biofilm formation. *BioMed research international,* 2013.
YESILKAYA, H., MANCO, S., KADIOGLU, A., TERRA, V. S. & ANDREW, P. W. 2008. The ability to utilize mucin affects the regulation of virulence gene expression in *Streptococcus pneumoniae*. *FEMS microbiology letters,* 278**,** 231-235.
YESILKAYA, H., SPISSU, F., CARVALHO, S. M., TERRA, V. S., HOMER, K. A., BENISTY, R., PORAT, N., NEVES, A. R. & ANDREW, P. W. 2009. Pyruvate formate lyase is required for pneumococcal fermentative metabolism and virulence. *Infection and immunity,* 77**,** 5418-5427.

ZHAO, H., DOYLE, T. C., COQUOZ, O., KALISH, F., RICE, B. W. & CONTAG, C. H. 2005. Emission spectra of bioluminescent reporters and interaction with mammalian tissue determine the sensitivity of detection in vivo. *Journal of biomedical optics,* 10**,** 041210.